5-2018

Cancer-Induced Muscle Wasting

Jacob Levi Brown
University of Arkansas, Fayetteville

Cancer-Induced Muscle Wasting

A dissertation submitted in partial fulfillment
of the requirements for the degree of
Doctor of Philosophy in Cell and Molecular Biology

by

Jacob Levi Brown
Missouri Southern State University
Bachelor of Science in Biology, 2014

May 2018
University of Arkansas

This dissertation is approved for recommendation to the Graduate Council.

_____

Nicholas Greene, Ph.D.
Dissertation Director

_____

Tyrone Washington, Ph.D.
Committee Member

_____

Jeffrey Wolchok, Ph.D.
Committee Member

_____

Sami Dridi, Ph.D.
Committee Member

Abstract

Cancer-induced muscle wasting, otherwise known as cancer-cachexia, is a wasting syndrome that occurs in approximately 80% of cancer patients that is the primary cause of death for 22%-30% of cancer cases. Cancer-cachexia may be metabolically induced; therefore, the central hypothesis of this dissertation is mitochondrial degeneration occurs before cancer-cachexia, and increased oxidative stress because of mitochondrial degeneration in muscle may instigate cancer-cachexia. Lewis Lung Carcinoma cells (LLC) or PBS (control) were injected into the hind-flank of C57Bl6/J mice at 8 wks age, and tumor allowed to develop for 1, 2, 3 or 4 wks. Mitochondrial quality, function, ROS emission, protein synthesis and protein breakdown were assessed. LLC Conditioned Media (LCM) treatment of C2C12 myotubes was used to analyze cancer-cachexia *in-vitro*. Data were analyzed by one-way (animal experiments) or two-way (cell culture experiments) ANOVA with Student-Newman Kuels post hoc test. Cachectic muscle loss and decreased oxidative capacity was evident only at 4 wks post-tumor implantation. Mitochondrial function decreased by ~25% by 3wks after tumor implantation. Mitochondrial degeneration (MitoTimer) was evident by 2 weeks LLC compared to PBS control. Mitochondrial ROS production was elevated by ~50% to ~100% when compared to PBS at 1-3 wks post-tumor implantation. Mixed FSR Protein synthesis was ~40% lower in 4 wk tumor-bearing mice when compared to PBS controls. Mitochondrial quality control and protein turnover signaling were dysregulated throughout the progression of cancer-cachexia. Ubiquitin content was elevated by ~50% 4wks after tumor implantation. ERK and p38 MAPK phosphorylation was 4 and 3 fold greater than control muscle 4 wks following tumor implantation, respectively. MitoT treatment and inhibition of p38 MAPK ameliorated LCM-induced loss of myotube diameter. These data provide novel insight into mechanisms which may induce cancer-cachexia.

Dissertation formatted for submission to *Journal of Cachexia, Sarcopenia and Muscle*

Acknowledgements

Special thanks to Integrative Muscle Metabolism Laboratory colleagues, David E. Lee and Megan Rosa, Exercise Muscle Biology Laboratory collaborators, Lemuel A. Brown, Richard A. Perry Jr., and Dr. Tyrone Washington. Also thanks to my advisor Dr. Nicholas P. Greene and our collaborators.

Dedication

This dissertation is dedicated to my wife Katie Stephenson-Brown.

Table of Contents

I. Review of Literature 1

a. Cancer-cachexia: Mechanisms of Muscle Atrophy 2

b. Cancer-cachexia: Role of Mitochondria in Muscle Wasting 14

c. Mitochondrial ROS in Cancer-cachexia 19

d. Models to Study Cancer-cachexia 23

e. Gaps in Cancer-cachexia Literature 26

f. Summary 27

g. References 29

II. Proposal 48

a. References 65

III. Mitochondrial Degeneration Precedes Cancer-Cachexia 69

a. Citation: Brown JL, Rosa-Caldwell ME, Lee DE, Blackwell TA, Brown LA, Perry RA et al. Mitochondrial degeneration precedes the development of muscle atrophy in progression of cancer cachexia in tumour-bearing mice. Journal of cachexia, sarcopenia and muscle. 2017. doi:10.1002/jcsm.12232.

b. Tables and Figures 91

c. References 99

IV. Protein Imbalance in the Development of Cancer-Cachexia 105

a. Figures 123

b. References 131

V. Mitochondrial Oxidative Stress and p38 MAPK Signaling 135

a. Figures 151

b. References 158

VI. Concluding Statements 162

a. References 166

VII. Appendices 169

a. IACUC and IBC Approval Letter 167

b. MitoTimer Protocol 167

c. Protein Synthesis Protocol 174

d. Respiration and Reactive Oxygen Species Protocol 194

List of Published Papers

Chapter 3 citation:

Brown JL, Rosa-Caldwell ME, Lee DE, Blackwell TA, Brown LA, Perry RA et al. Mitochondrial degeneration precedes the development of muscle atrophy in progression of cancer cachexia in tumour-bearing mice. Journal of cachexia, sarcopenia and muscle. 2017. doi:10.1002/jcsm.12232.

Chapter 4 and 5:

Submitted to the Journal of Cachexia, Sarcopenia and Muscle

Chapter 1

Review of Literature

Cancer is one of the leading causes of death with the World Health Organization reporting 8.2 million deaths and 14.1 million new cancer cases in 2008 worldwide [1]. Moreover, half of the people that are affected by cancer will die as a result of the condition [2]. In fact, between 1970 and 2008, mortality rates from heart disease, cerebrovascular disease, and accidents declined 62%, 73%, and 38%, respectively [3], but in the same period, cancer mortality rates declined just 12%, mostly since 1990 [3]. One problem associated with cancer is cancer-cachexia, a wasting syndrome that occurs in approximately 80% of cancer patients [4, 5]. Cancer-cachexia is the primary cause of death for 22%-30% of cancer patients [4, 5]. Not only is cancer-cachexia behind an escalation in cancer associated mortality, it also increases the cost of health care [6]. Based on these findings, it is clear that cancer-cachexia is a major health care concern that lacks adequate therapies.

The syndrome of cancer-cachexia is multifactorial, cannot be fully reversed by nutritional support and is triggered by a combination of reduced food intake and abnormal metabolism, seemingly induced by tumor- and host-derived factors [4]. Skeletal muscle atrophy is instigated by an imbalance of protein turnover favoring protein degradation over protein synthesis; however, mechanisms behind this imbalance of protein turnover vary depending on the (patho)physiological circumstance [7, 8]. Overall, metabolic derangements inducing cancer-cachexia are not fully elucidated in scientific literature; however, mitochondrial degeneration may contribute [9]. This review of literature will outline cellular processes that contribute to cancer-cachexia [10].

Cancer-Cachexia: Mechanisms of Muscle Atrophy

Cancer-cachexia is a prevalent problem which lacks adequate therapies. Current therapies for cancer-cachexia are focused on increasing energy intake of patients whether from pharmacological interventions or diet modifications [11]. While hypophagia may influence skeletal muscle loss, other cellular processes contribute to cancer-cachexia [4]. Cancer-cachexia is associated with reduced muscle protein synthesis and increased muscle protein breakdown [7, 8] which promotes loss of skeletal muscle mass [10]. Numerous molecular substrates and mechanisms underlie the dysregulation of skeletal muscle protein turnover associated with cancer-cachexia [12, 11]. These pathways/molecules include protein synthetic pathways, autophagy pathways, proteasome pathways, inflammatory cytokines, myostatin pathways and myogenesis [11-14].

A. Protein Synthesis

Protein Synthesis is a highly controled process that is predominantly regulated at the stage of initiation [15]. Translation initiation can be divided into three stages: the binding of initiator methionyl-tRNA (met-tRNA) to the 40S ribosomal subunit to form the 43S preinitiation complex, the binding of mRNA to the 43S preinitiation complex to form the 48S preinitiation complex, and the binding of the 60S ribosomal subunit to the 48S preinitiation complex to form the active 80S initiation complex [15]. Translation initiation is predominantly regulated by signal transduction [16] (Figure 1). Many factors regulate signal transduction pathways that influence skeletal muscle's ability to synthesize protein. This includes energy status, anabolic hormones, catabolic hormones and mechanical stimuli [17]. The most important signal transduction event involved in the regulation of protein synthesis is the Akt/mTOR pathway [18]. Insulin and IGF-1 are both major activators of the Akt/mTOR pathway [18]. mTOR regulates translation initiation

primarily through the inhibition of eIF4E-BP1 (hereafter 4EBP1) via hyper phosphorylation and the activation of p70S6K via phosphorylation [19, 20].

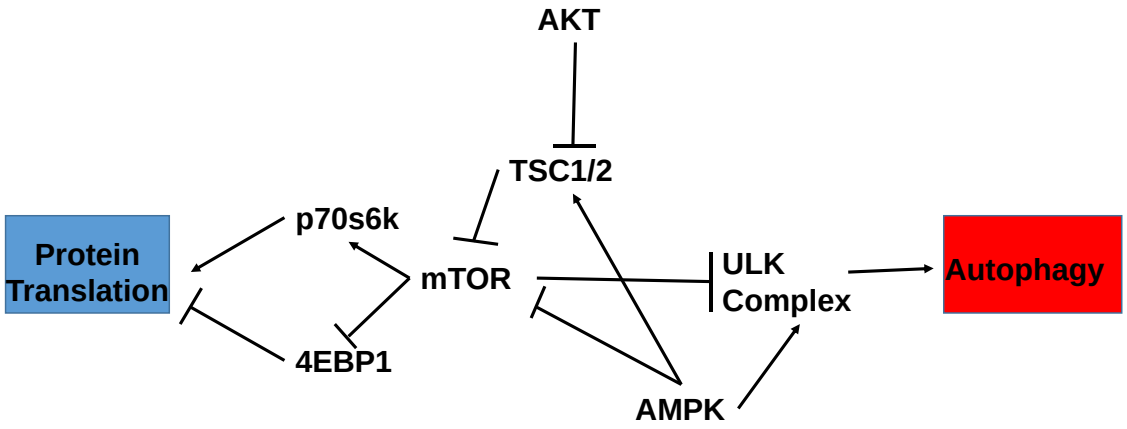

Figure 1-1: Schematic of mTOR and AMPK regulation of protein synthesis and autophagy.

In cancer-cachexia literature, there is an ongoing debate as to whether a decrease in protein synthesis, upregulated protein degradation or both play a bigger role in the onset of cancer-induced muscle wasting [21]. There appears to be discrepancies based on both the type of model used and the methodology for measuring protein synthesis [21-25]. Current measurements of protein synthesis in cancer-cachexia literature use acute measurement techniques (3 hours or less); therefore, there is a key need to explore protein synthesis over a larger range of time.

Protein synthesis may be decreased in cancer-cachexia through a variety of mechanisms [26, 27]. Both circulating IGF-1 and IGF-1 expression from skeletal muscle is impaired in cancer-cachexia [28]. Furthermore, both early and late stage cancer-cachexia exhibit diminished mTOR activation [29, 30]. Many cellular processes can inhibit mTOR activation; however, in cancer-cachexia both 5′-adenosine monophosphate-activated protein kinase (AMPK) and inflammation are likely candidates [31, 26]. AMPK becomes active when cellular energy levels are reduced and upon skeletal muscle contraction [32]. AMPK directly and indirectly through

TSC2 activation inhibits mTOR signaling (Figure 1). Specifically, AMPK prevents interactions between mTOR and 4EBP1 and p70S6K1 [33]. In the early stages of cancer-cachexia, muscle protein synthesis has been reported to be suppressed by 19% [27]. As cancer-cachexia progresses, muscle protein synthesis is further decreased by ~50% [27]. Cancer induces a pro-inflammatory environment which alters skeletal muscle protein turnover. Inflammatory molecules such as IL-6 reduce phosphorylation of mTOR and 4EBP1 in a dose dependent manner while increasing the phosphorylation of AMPK [26]. Glycoprotein 130 (GP130) is critical for fascillitating IL-6 signaling [24]. While GP130 knockout (KO) mice attenuated cancer-cachexia by ~15%, GP130 KO did not prevent increased AMPK expression and reduced mTOR phosphorylation which suggests that GP130 is responsible for these alterations in cancer-cachexia [24]. This suggests that IL-6 partially suppresses protein synthesis in cancer-cachexia through pathways that are not mediated by GP130.

B. Autophagy

Autophagy is another mechanism which influences protein turnover that appears to be dysregulated in cancer-cachexia [14]. Autophagy is a process involving the formation of an autophagosome in order to facilitate lysosomal clearance of proteins and organelles in response to stress [34-36]. Autophagy in most cases is inversely regulated from protein synthesis [35]. More specifically, autophagy is induced by lack of nutrients, hormones, oxidative stress and energy balance [36], while mTOR activation inhibits autophagy [37, 35] (Figure 1). Recent evidence has revealed autophagy may be dysregulated in cancer-cachexia [14]. Promotion of autophagy via cancer-cachexia related stimuli is evidenced by increased LC3 II: LC3 I ratio; however, lysosomal clearance may be impaired indicated by increased p62, an autophagy cargo protein [14]. Likely mechanisms for the induction of autophagy as it relates to cancer-cachexia

are mTOR inhibition and AMPK activation [36, 38, 9]. Excess oxidative stress may also upregulate autophagy in cancer cachexia; however, skeletal muscle reactive oxygen species (ROS) production has not been adequately examined [36, 38]. Autophagy is one of many processes that influence protein breakdown. To current knowledge, other cellular processes such as proteasomal degradation are likely more involved in cancer-cachexia than autophagy; however, autophagy enables the cell to remove damaged organelles such as the mitochondria which may influence cancer-cachexia. Autophagic removal of mitochondria will be discussed at a later section in this literature review.

C. E3 Ligases and Proteasome

The proteasome is essential for cellular function as demonstrated by the onset of oxidative stress and apoptotic cellular death following the administration of proteasome inhibitors [39]. Despite the proteasome's essential function for cellular health, in skeletal muscle over-activation of proteasomes induces skeletal muscle wasting [40]. In late stage cancer-cachexia, proteasome-induced muscle atrophy is clearly prevalent [7, 41].

The ubiquitin proteasome system works via a complex series of reactions which transfer activated ubiquitin to protein substrate via E1, E2 and E3 ligases. The 26S proteasome which consists of a 20S catalytic core and 19S regulatory subunits [42] will then degrade the ubiquitin tagged proteins. Specifically, the 19S subunits are responsible for recognizing ubiquitin-tagged proteins, while the 20S catalytic core is responsible for protein degradation [42]. In order to load ubiquitin onto a protein substrate, ubiquitin-activating enzymes (E1s), ubiquitin-conjugating enzymes (E2s), and ubiquitin-protein ligases (E3s) perform a series of high energy reactions [43] (Figure 2). Briefly, the process begins with the ATP-dependent activation of ubiquitin (Ub) by an E1, which results in a high-energy thioester linkage between the COOH terminus of ubiquitin

and the active site cysteine of the E1 [44, 45]. The activated ubiquitin is then transferred to an E2, again forming a thioester bond [44, 45]. The final step is the transfer of the ubiquitin from the E2 to a substrate via an E3 ligase [44, 45]. E3 ligases facilitate poly-ubiquitination in order to tag a protein for the proteasome by the formation of isopeptide bonds on lysine residues [46, 47, 45] [48, 45].

In skeletal muscle, there are two muscle specific E3 ligases that are particularly involved in the induction of skeletal muscle wasting [49]. Specifically these ligases are Muscle Atrophy F-Box Protein-1 (Atrogin-1) and Muscle Specific RING Finger-1 (MuRF-1) [49] (Figure 2). Under normal conditions, Atrogin-1 and MuRF are scarcely expressed; however, expression rapidly increases following atrophic stressors [50]. Atrogin-1 and MuRF facilitate the ubiquitination of many proteins involved in hypertrophic programing including proteins involved in ATP generation, protein synthesis, myogenic regulatory factors and myofibrillar proteins [51-54]. Both Atrogin-1 and MuRF-1 are regulated by FOX-O1/3, members of the fork head family of transcription factors, in skeletal muscle [55, 56]. Fork head family of transcription factors have the ability to be translocated into the nucleus upon phosphorylation and bind to a distinct fork head DNA binding domain to influence transcriptional activity [56]. FOX-O1/3 signaling appears to interact with protein synthetic signaling demonstrated by the inhibition of FOX-O1/3 activation via AKT phosphorylation [57, 58]. Cellular stress seems to promote FOX-O1/3 signaling [59]. FOX-O1/3 signaling upregulates the process of autophagy as well [59, 60]. Intriguingly, FOX-O1/3 promotes cellular ROS detoxification by increasing the transcription of the antioxidant enzymes MnSOD and Catalase which will be discussed in subsequent sections in the literature review [61].

When cancer-cachexia occurs, the expression of both Atrogin-1 and MuRF dramatically increase mediated by FOX-O1/3 signaling [27]. Chronically elevated cytokines such as IL-6 are involved in promoting the upregulation of both Atrogin-1 and MuRF [7]. Considering the regulation of Atrogin-1 and MuRF is multifaceted, multiple cellular signals other than inflammation stimulate increased expression of these E3 ligases. Pathways associated with energy levels and stress related signaling which induce Atrogin-1 and MuRF are likely behind the induction of these E3 ligases in cancer-cachexia [62, 63].

D. Pro-inflammatory Cytokines

Cachexia is a systemic problem with the presence of an inflammatory response and profound metabolic derangements in not only muscle and fat, but in hypothalamus, liver, heart, blood, spleen and likely other organs [64]. This global response is orchestrated in part through circulating cytokines that rise in conditions of cachexia [9, 65, 66, 64]. Cytokines implicated to induce negative metabolic effects in cancer cachexia are IL-6 and TNFα [67].

Exogenous IL-6 and related cytokines can induce most cachexia symptomatology, including muscle and fat wasting, the acute phase response and anemia, while IL-6 inhibition reduces muscle loss in cancer [64]. In tumor bearing mice, there is a dramatic increase in plasma IL-6 [68]. Downstream of IL-6, GP130 KO mice exhibit attenuated cancer-induced muscle and fat loss and reduced pathological phosphorylations of STAT3, p38 and FOX-O3 [24]. Moreover, IL-6 reduces protein synthesis by indirectly inhibiting mTOR [26], a key regulator of protein synthesis [69], signaling likely mediated through upregulated AMPK expression and induces cellular proteolysis [70, 66]. Furthermore, recent evidence suggests IL-6 represses *Pgc-1α4* mRNA, a regulator of skeletal muscle hypertrophy [71], content by signaling through ERK-MAPK [72]. STAT3 signaling is causally linked to phenotypes of cancer-cachexia including

skeletal muscle wasting, cardiac dysfunction and hypothalamic inflammation [64, 9, 26, 73]. Intriguingly, the induction of cancer-cachexia is IL-6 independent in female mice [74].

TNF-α is an inflammatory mediator present in the tumor microenvironment that has been implicated in carcinogenesis, especially in the early stages, including angiogenesis and invasion [75]. As far as muscle atrophy is concerned, TNF-α is involved in the promotion of apoptotic signaling of Type II muscle fibers, which can induce muscle atrophy [76]. Furthermore, TNF-α has been shown to increase the expression of ubiquitin and key E3 ligases (Atrogin-1 and MuRF-1) leading to an accumulation of ubiquitin tagged proteins which will prompt skeletal muscle atrophy [77, 78]. This is mediated through the activation and translocation of transcription factor NFκB [79]. Intriguingly, TNF-α also decreases food intake by acting on the hypothalamus to modulate expression of neurotransmitters dealing with energy balance [80]. TNF-α further modulates energy balance by increasing the gene expression of uncoupling proteins 2 and 3 in skeletal muscle, leading to inefficient mitochondrial energy production [81].

E. Myostatin

Myostatin (Mstn) is another heavily researched target for the promotion and prevention of cancer-cachexia. Mstn is a highly conserved member of the TGF-β superfamily of proteins, and is considered to be a master regulator of skeletal muscle mass that promotes/inhibits many protein turnover processes [82]. Mstn acts in an autocrine/paracrine manner by binding to type-II activing receptors ActRIIA and ActRIIB, which then recruit and activate type-I activin receptors, also known as activin receptor-like kinase (Alk) 4 and 5 [83]. This, in turn, causes phosphorylation of Smad2 and Smad3, the association with Smad4 into a Smad2/3/4 complex, which then enters into the nucleus to trigger gene transcription [83]. Smad 2/3/4 complex stimulates FoxO-dependent transcription and enhanced muscle protein breakdown via the

ubiquitin-proteasome system and autophagy [83]. In addition, Smad activation inhibits muscle protein synthesis by suppressing Akt signaling [83]. Due to Mstn's vast role in the regulation of skeletal muscle mass, it has garnered attention in the prevention of cancer cachexia [84]. Intriguingly, cancerous Mstn KO mice live longer than cancerous wildtype mice [84]. Mstn KO mice also exhibit the ability to repress tumor growth [84]. These mice prevent atrophy inducing pathways such as FOXO3 mediated induction of Atrogin-1 and MuRF-1 and autophagy [84]. Moreover, Mstn KO mice prevent cancer-cachexia associated reduction of protein synthesis [84]. Also, inhibitors for myostatin pathways appear to diminish cancer-cachexia [85, 22]. Though Mstn exhibits these effects, tumor burden does not appear to alter myostatin expression and signaling in skeletal muscle, therefore cancer-cachexia is likely mediated through other mechanisms [84].

F. Myogenesis

Myogenesis is the formation of muscular tissue and is especially important for postnatal skeletal muscle regeneration that is necessary for muscle repair. Myogenesis is primarily regulated by four myogenic regulatory factors (MRF): MyoD, Myf5, Myf 6 and myogenin [86]. Muscle repair coincides with injury induced inflammation, and the induction of some pro-inflammatory cytokines [87]. Satellite cells, which lie under the basal lamina of muscle fibers and are marked by the expression of Pax7, also provide a crucial role in skeletal muscle regeneration [88]. In certain diseased states such as aging, muscular dystrophy and cancer, satellite cell numbers and proliferative potential decreases, which may induce a failure to maintain muscle homeostasis [89, 90]. In the process of skeletal muscle regeneration, satellite cells become activated and shift from expressing Pax7 to MyoD and Myf5 [91]. Upon activation, satellite cells transmigrate through the Extra Cellular Matrix (ECM) to the outside of the muscle

fiber [91]. Progenitor cells within the satellite cell pool proliferate into myoblasts stimulated by signals induced from MyoD and Myf5 [92, 91]. The accretion of myoblasts to preexisting myofibers is essential for hypertrophic muscle growth [73]. These myoblasts will then differentiate into myotubes from signals induced from Myogenin [92, 91].

It is clear that myogenesis is involved in the regulation of muscle mass [73]. It is postulated that impaired myogenesis does not directly influence muscle atrophy; however, this may be due to a compensation by protein synthetic programing that is not present in cancer-cachexia [93, 94]. In cancer, the sarcolemma becomes damaged due to factors secreted by the tumor. This is problematic because cancer is associated with impaired myogenesis in skeletal muscle, which is linked to dysregulated differentiation and muscle loss [95]. NFκB is activated in muscle progenitor cells during cachexia leading to sustained Pax7 expression [94]. In turn, a self-renewing signal in myogenic cells is likely propagated that results in their inability to progress through a differentiation programing (Figure 3) [94]. NFκB mediated Pax 7 expression has been linked to impaired MyoD synthesis [96]. In fact, cancer decreases the expression of MRFs despite the induction of satellite cells or other resident progenitor cells in skeletal muscle [97, 94]. Furthermore, the process of myogenesis may have a more direct effect on promoting skeletal muscle atrophy [98, 99]. Myogenin seems to upregulate both Atrogin-1 and MuRF-1 to elicit a proteolytic response [99, 98].

G. *Apoptosis*

It is theorized that there is a linear relationship between the link between cell volume and DNA content of cells [100]. Muscle fibers are the largest volume animal cell requiring multiple nuclei to support the amount of tissue [101]. There is a correlation between the nuclei present and the size of the muscle tissue in young (less than 2 months of age) and old mice (greater than

23 months of age), but not middle aged mice [102]. Based on this principle, a loss of myonuclei could lead to smaller muscle fibers.

It has not been proven that myonuclear apoptosis does occur in permanent fibres undergoing atrophy [102]. Using TUNEL staining, nuclear apoptosis appears to occur in atrophic conditions [103]; however, it is not clear whether the myonuclear apoptosis occurs in satellite cells or myonuclei [102]. In cancer-induced muscle wasting, severe cachectic phenotype shows an increase of up to 1.5% tunel + nuclei [104]. Moreover, prior literature showed a 9.8 fold increase in skeletal muscle DNA fragmentation of LLC tumor-bearing mice when compared to control mice utilizing scanning densitometry [105]. Also in more severe cachectic phenotypes, literature suggests that cleaved caspase 3 may be upregulated in LLC tumor-bearing mice [106]. It is still not clear whether myonuclear apoptosis has a role in the onset of cancer-cachexia due to lack of data.

MAPK signaling in cancer-cachexia.

A mitogen-activated protein kinases (MAPKs) are involved in directing cellular responses that promote survival [107]. Specifically, MAPKs coordinately regulate proliferation, gene expression, differentiation, mitosis, cell survival, and apoptosis among other things [107]. MAPK family of proteins includes extracellular signal-regulated kinases 1 and 2 (ERK1/2), c-Jun amino-terminal kinases 1 to 3 (JNK1-3), p38 (α, β, γ, and δ), and ERK5 families [108]. Typically, MAPKs are activated by a number of phosphorylation events on both threonine and tyrosine residues, and are inactivated by a variety of phosphatases [109, 110]. MAPK literature indicates a wide array of regulatory functions; however, future research needs to further elucidate MAPKs role in the regulation of skeletal muscle mass in atrophic conditions.

Recently, MAPKs have been implicated as critical controllers of skeletal muscle mass [111, 112], and are potential theraputic targets for multiple muscle wasting conditions [113-117]. MAPKs regulate skeletal muscle programs such as ubiquitin proteasome system [118], extra cellular matrix processes, myogenic programing [119], fibrosis, lipid accumulation, inflammation [112], and morphological changes [64] all of which are involved in the maintenance of skeletal muscle mass. A few specific examples of MAPK inhibition attenuating muscle loss include models of endotoxin, musclular dystrophy, inflammation and chemotherapy mediated muscle wasting [115, 114, 120, 121]. Both p38 MAPK and ERK MAPK seem to be the major controllers of processes which regulate proteostasis in these studies.

In models of cancer-cachexia, it appears that p38 MAPK expression is induced in response to tumor burden [113], which may be from associated inflammation [122]. Furthermore, there is evidence that inhibition of p38 MAPK in myotubes and skeletal muscle prevents upregulation of E3 ligases [117, 123, 124]. Moreover, experimental evidence suggests inhibition of ERK MAPK signaling may help prevent cancer-induced muscle wasting [116]. Furthermore, pharmacological inhibition of both p38 and ERK 1/2 MAPK may attenuate cancer-induced muscle loss [123]. Based on these reports, p38 and ERK 1/2 MAPK could be potential targets for new therapeutic strategies to treat cancer-cachexia.

Denervation in Skeletal Muscle

A neuromuscular junction is a synapse formed by the contact between a motor neuron and a muscle fiber [125]. The neuron releases acetycholine into the synaptic cleft using microvesicles which fuse to the neuronal membrane [125]. The acetylcholine then travels down the acetylcholine receptor (AChR) enriched synaptic cleft to bind to AChR and elicit a contractile response in skeletal muscle [125]. Normally AChR density is higher than needed for

efficient capture of the acetylcholine released [126]. In fact, blockade or removal of ~80% of receptors is required to reduce the response to acetylcholine by 50% [126]. Therefore, it is unlikely that downregulation of AChR results in functional denervation. The expression of AChR is partially mediated through ERK 1/2 [127]. AChRs are concentrated at the synaptic cleft, with a receptor density of ~10,000–20,000 AChRs/μm2 [128].

It is well established that denervation will induce skeletal muscle wasting by both the downregulating protein synthesis and the upregulation of rates of protein breakdown. Denervation downregulates mTOR complexes thus decreasing capacity for protein synthesis [129]. Moreover, denervation is associated with upregulated atrogenes (Atrogin1 and MuRF1), which are heavily involved in proteasome mediated muscle wasting [130]. Also autophagy genes are upregulated in response to denervation [60]. To my knowledge denervation has never been examined in cancer-cachexia; therefore, it is worthwhile for future research to examine this considering its role in inducing numerous factors regulating protein turnover.

Cancer-Cachexia: The Role of Mitochondria in Muscle Wasting

It is clear that mechanisms related to muscle wasting may also be related to muscle metabolism since glycolytic muscle fibers have greater wasting susceptibility with several

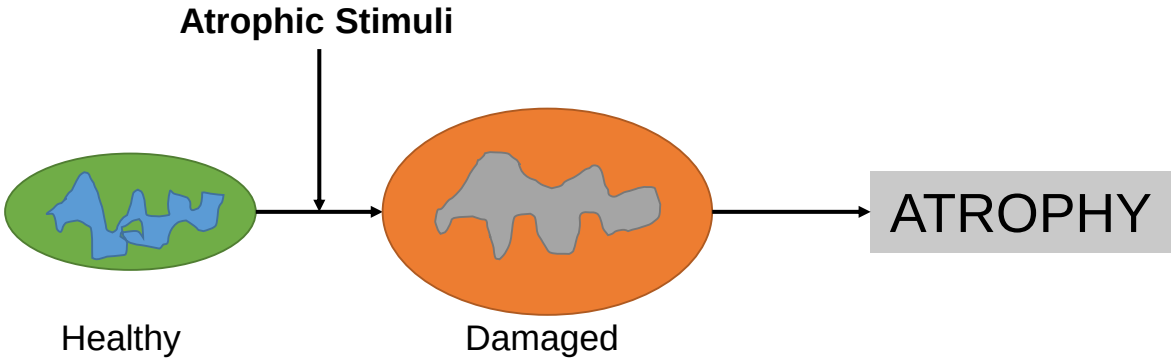

Figure 1-3: Schematic of mitochondrial damage leading to skeletal muscle atrophy.

diseases [70, 131, 132]. In fact, mitochondrial induced mechanisms of skeletal muscle atrophy are a common feature across numerous models of skeletal muscle atrophy [133]. Mitochondrial degeneration may instigate skeletal muscle atrophy through mechanisms such as reduced protein synthesis, increased autophagy, an upregulation of skeletal muscle atrogenes, produce inflammation and alter myogenesis all of which are altered in cancer-cachexia [134-140] (Figure 3). This may be due to reduced energy production and/or excess mitochondrial ROS production [137-140]. In cancer, there are dysregulations in mitochondrial quality control mechanisms which may instigate mitochondrial degeneration [9, 141]. These quality control mechanisms include mitochondrial biogenesis, mitochondrial dynamics and mitochondrial specific autophagy [142]. Because of this, the mitochondria may be a potential therapeutic target to treat cancer-cachexia.

In order to prevent mitochondrial degeneration, several regulatory processes must be implemented to ensure that the mitochondria are able to perform oxidative metabolism. These processes include the biogenesis of new mitochondrial components, fusion and fission of new and damaged mitochondrial regions with the network (dynamics), and the selective degradation of damaged mitochondrial regions through the process of autophagy (mitophagy) [142]. These mitochondrial regulatory processes aid in the maintenance of the mitochondrial network that and ensures that the mitochondria does not emit excess toxic substances such as reactive oxygen species. In cancer-cachexia, many of these mitochondrial regulatory processes appear to be disrupted, which may induce mitochondrial degeneration [9, 141, 38]. Mitochondrial degeneration quickly leads to a loss of mitochondrial function, which is commonly associated with skeletal muscle atrophy [143]. Disrupted mitochondrial function leads to an upregulation of

cellular catabolic affects such as reduced protein synthesis, increased autophagy and increased proteasome induced atrophy [144, 140].

A. Mitochondrial Biogenesis and Dynamics

PGC-1α is a transcriptional co-activator that coordinates the transcription factors critical for the addition of mitochondrial components [145]; therefore, PGC-1α is critical for optimal metabolic function [146, 147]. In fact, PGC-1α may even regulate protein turnover processes [148]. PGC-1α can actually inhibit FOXO3 and thereby reduce the expression of both Atrogin1 and MuRF1 [148]. Cancer-cachexia seems to dysregulate the expression of PGC-1α [147, 38]. This altered expression of PGC-1α will likely have drastic affects in cellular oxidative metabolism, which if PGC-1α signaling becomes disrupted, may instigate a loss of mitochondrial function which induces catabolic effects [149].

PGC-1α appears to perform an important role in promoting mitochondrial quality through other mitochondrial regulatory factors such as mitochondrial dynamics and mitophagy [150, 142] (Figure 4). Non-functioning mitochondria are often fragmented and removed from the central network resulting in the inability to share mitochondrial components which

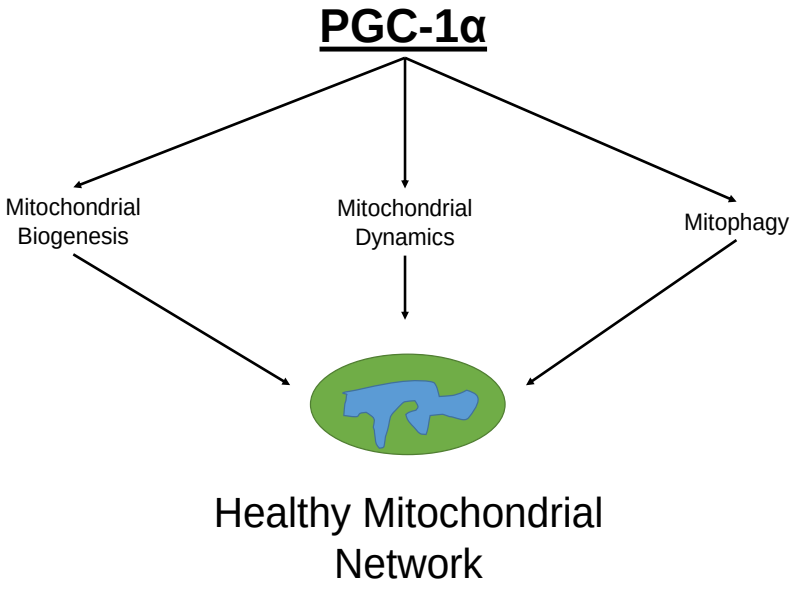

Figure 1-4: Schematic of regulators of the mitochondrial network.

exacerbates mitochondrial dysfunction [142]. Mitochondrial dynamics is the process in which the mitochondrial network is enzymatically divided (fission) or merged (fusion) [142]. Mitochondrial division is mediated by a single dynamin-related protein, DRP1, whereas fusion requires two families of dynamin-like proteins, Mitofusin 1/2 (MFN1/MFN2) and OPA1. Evidence suggests that Dynamin Related Protein 1 (DRP1) divides mitochondria by forming helical structures that wrap around mitochondria [151-154]. The process of mitochondrial dynamics is highly regulated. Proteins such as FIS1 or Mitochondria Fission Factor (MFF) are involved in coordinating the recruitment of fission factors to the mitochondrial membranes [155]. Moreover, kinase activity will promote interaction of fission factors to fission regulators [155]. It is clear regulators of mitochondrial dynamics are involved in mitochondrial function. Specifically, MFN2 regulates critical co-factors for oxidative metabolism [156].

Dysregulation in mitochondrial dynamics may instigate skeletal muscle atrophy [157, 158]. Dysregulation in mitochondrial dynamics favoring an upregulation of mitochondrial fission proteins and a downregulation of mitochondrial fusion proteins will promote atrophic stimuli [159]. Recent evidence suggests an increase in mitochondrial fission is a required signal that promotes AMPK-FOXO3 signaling promoting increased expression of Atrogin-1 and MuRF [158]. In cancer-cachexia, like other (patho)physiological stimuli, there is a dysregulation in mitochondrial dynamics [9].

B. Mitochondrial Specific Autophagy

Mitochondrial specific autophagy (mitophagy) is another mitochondria quality control process that when disrupted appears to exacerbate (patho) physiological conditions such as aging and diabetes [160, 161]. Mitophagy is the selective engulfment of mitochondria by autophagosomes and their subsequent catabolism by lysosomes [162]. Mitophagy is highly

selective in nature [160]. This selectivity initially was found associated with a loss in mitochondrial membrane potential at the inner membrane [163]; however, recently other factors such as Uth1p and Cyclophilin D seem to be involved [164, 165]. This process of mitophagy is crucial for the maintenance of a healthy mitochondrial network [166].

Mitophagy regulation appears to be multifaceted. The PINK-Parkin pathway appears to be a key regulator of mitophagy [162]. Parkin is a cytosolic E3 ligase that translocates to the mitochondria upon depolarization [167, 168]. Parkin will then ubiquitinate mitochondrial outer membrane proteins in order to initiate the process of mitophagy [169]. Intriguingly, Parkin also inhibits mitochondrial fusion by triggering the degradation of MFN 1/2 [170]. Furthermore PINK-1 can act as a molecular sensor for damaged mitochondria which will then aid in the recruitment of Parkin to the mitochondrial membrane [171]. It appears PINK-1 will directly phosphorylate Parkin in order to aid in the recruitment to the mitochondria [172]. BNIP3 is another protein involved in the process of regulating the accumulation of PINK-1 to the outer membrane of the mitochondria [173]. BNIP3 is a stress-induced molecular adaptor that directly interacts with the mitochondria and LC3 to promote the process of mitophagy [174].

Cancer-cachexia appears to increase susceptibility for mitophagy in skeletal muscle [175, 14]. In cachectic human patients, markers for autophagasome formation are elevated along with elevated p62 protein content [14]. Considering p62 is a cargo protein that becomes degraded once autophagy occurs, this data suggests that there may be impaired autophagy clearance in individuals with cancer-cachexia. Protein contents of both BNIP3 and Nix/BNIP3L tend to increase in human cachectic patients [14]. There are mixed results in the expression of PINK-1 mRNA in cachectic cancer patients [14]. Taken together, this data suggests that the process of mitophagy appears to be upregulated in cancer-cachexia; however, autophagosome clearance

may be impaired. This failure for autophagosome clearance may result in excess damaged mitochondria in the cytosol of the cell.

It is clear that cancer-cachexia induces dysregulation of mitochondrial quality control processes which most likely results in degeneration of the mitochondrial network. It is well established that cancer cells utilize a glycolytic metabolism; however, due to impairments in muscle oxidative metabolism associated with cancer glycolytic metabolism may also be utilized in muscle [176]. This is termed the Warburg effect [176]. Mechanisms for the induction of the Warburg effect in skeletal muscle are not understood.

C. Mitochondrial Super Complex

The electron transport chain is a multi-protein system organized into 4 respiratory chain complexes (complex 1-4) used to create a chemiosmotic gradient from reducing NADH and $FADH_2$. Complex 5 then uses this chemiosmotic gradient to generate ATP. The structure of these electron transport complexes will change from freely moving along the inner membrane of the mitochondria to a multi-protein oligomerization called the supercomplex [177]. Briefly, subunits of complex 1 in the mitochondrial electron transport chain contribute to the oligomerization of complex 1, complex 3 and complex 4 [178]. Also, COX7C and COX7A subunits of complex 4 attach to complex 3 and complex 1 [178]. This supercomplex formation has been theorized to be critical for the transport of electrons through the electron transport chain [178]. Mitochondrial supercomplex formation has been shown to reduce the diffusion distance required for the transfer of electrons [179, 180]. This increases the efficiency of electron transfer between complexes and limits the opportunity for ROS production [179, 180].

Recently exercise was shown to be a key contributor to mitochondrial supercomplex formation [181]. Increased mitochondrial supercomplex formation likely increases energy production efficiency, which is needed during exercise [181]. The importance of supercomplex formation has recently become clinically relevant. Disease states such as aging [182, 183] and diabetes [184] have impaired mitochondrial supercomplex formation in skeletal muscle.

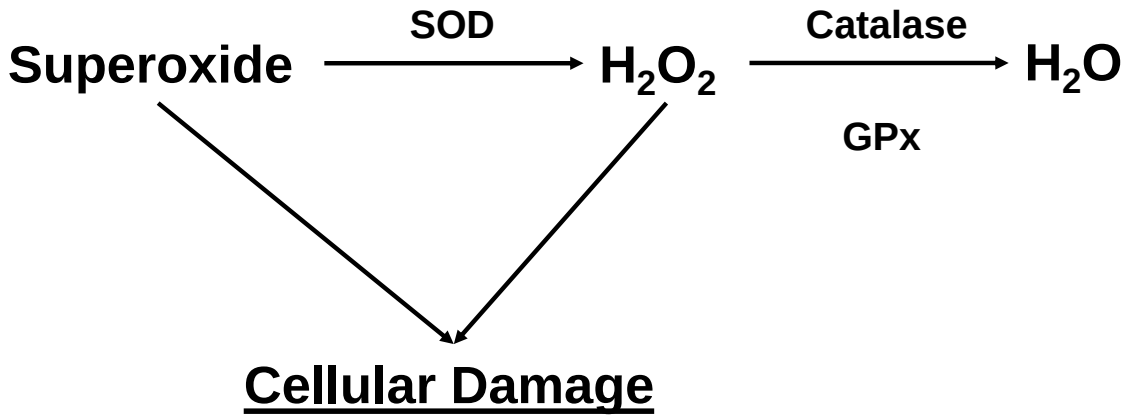

Figure 1-5: Schematic of Mechanisms to neutralize ROS.

Mitochondrial ROS in Cancer-Cachexia

Multiple lines of evidence suggest that cancer-cachexia may lead to mitochondrial degeneration [141, 9]. Mitochondrial degeneration leads to a robust decrease in mitochondrial oxygen consumption and diminished ATP production from metabolic substrates [185]. Furthermore, mitochondrial degeneration leads to excess mitochondrial ROS production which disrupts cellular health [186, 187]. Because of this, mitochondrial ROS may induce cancer-cachexia.

Mitochondrial ROS is neutralized in a two-step process starting with SOD 2/3 in the conversion of superoxide molecules to H_2O_2 [188] followed by catalase converting H_2O_2 into H_2O [186]. H_2O_2 is problematic for cellular responses as it can freely pass through the

mitochondrial membrane; while other forms of ROS that are more reactive per se (superoxide) typically need a channel to cross the mitochondrial membrane [188]. Superoxide will likely exacerbate normal mitochondrial processes.

A. ROS Signaling

It is clear that in many cases ROS and RNS can play a double role in organisms [189]. At elevated levels free radicals induce oxidative damage and tissue dysfunction; however, free radicals may also elicit a stress response beneficial to the cell [189]. It is currently accepted that all cellular sources of ROS provide significant contribution to processes that damage tissues. Cells assure their survival, through mechanisms such as autophagy and apoptosis [189]. Elevated

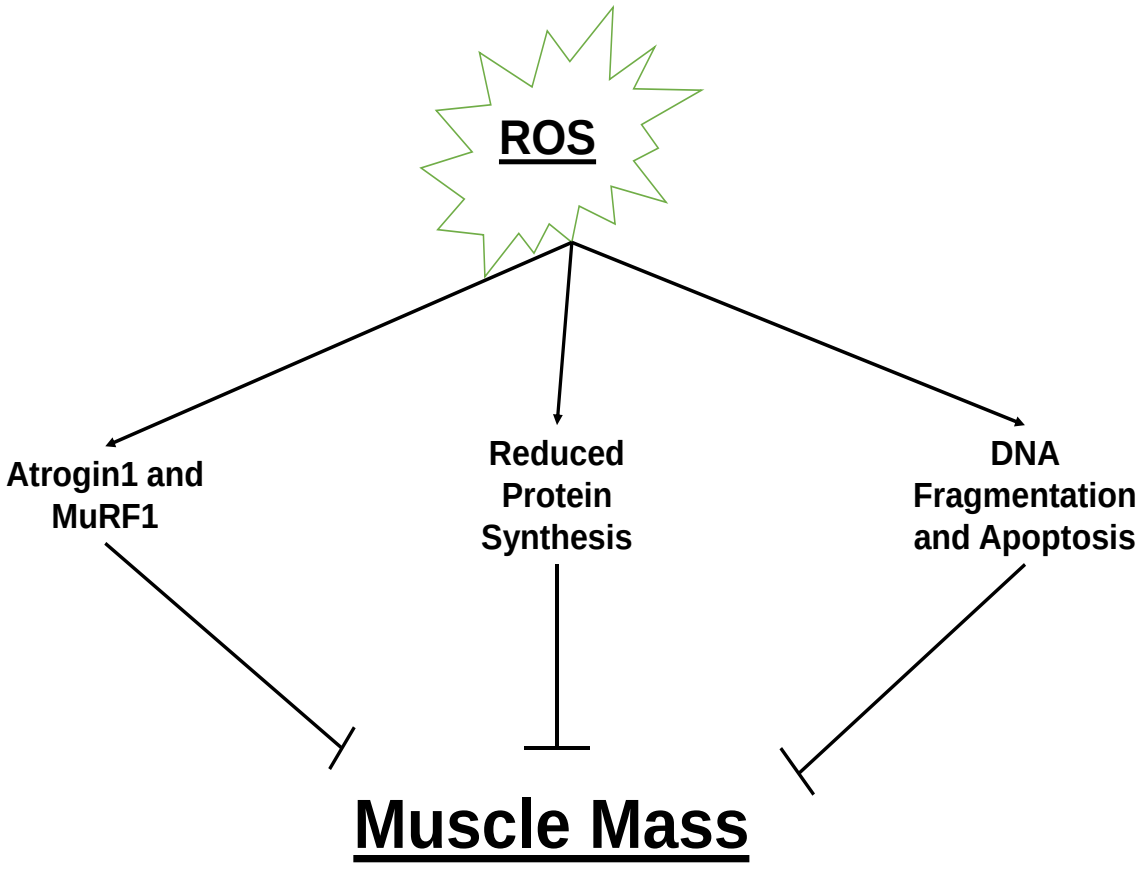

Figure 1-6: Mechanisms in which ROS induces atrophy.

ROS is widely studied in a variety of (patho)physiological conditions, and is associated with impaired skeletal muscle function [190]. Excess ROS is associated with elevated skeletal muscle inflammation as well as apoptotic signaling, promoting skeletal muscle atrophy [191-194]. The first reported incident of oxidative stress inducing skeletal muscle atrophy was identified approximately 2 decades ago in a hindlimb unloading model [195]. Since this early observation, numerous animal studies have confirmed that prolonged skeletal muscle inactivity promotes oxidative stress and a growing number of studies reveal that "select" antioxidants can delay disuse muscle atrophy [191, 192]. ROS significantly decreases the content of proteins associated with muscle health and function, including myosin, alpha-actinin, desmin, talin, and troponin I [193]. The mechanisms in which ROS impairs skeletal muscle health are through apoptotic signaling, promoting increased protein breakdown, reducing protein synthesis and oxidizing cellular proteins [194].

B. ROS and Apoptosis

Apoptotic signaling is involved in the induction of skeletal muscle atrophy by inducing nuclear and myofilament degradation [196]. ROS activates both caspase 3 and calpain which is responsible for nuclear and myofilament degradation [196]. Futhermore, ROS may be responsible for the loss of myonuclei which has been observed in many atrophic conditions [197, 198]. This loss of myonuclei decreases the skeletal muscle myonuclear domain [197]. It has been shown that the number of nuclei in skeletal muscle is relatively stable; which implies that loss of nuclei may not be involved in the induction of skeletal muscle atrophy [197]. This myonuclear loss leads to a decrease in the amount of skeletal muscle tissue that muscle cells can support [198]. This myonuclear loss may be the result of satellite cell apoptosis which prevents the addition of additional myonuclei [199]. ROS has been shown to induce apoptosis of satellite

cells, which may reduce satellite cell pool and prevent the addition of new myonuclei [200]. Apoptotic signaling is the only thing that can degrade actinomyosin complexes which makes it a clear mechanism for the induction of skeletal muscle atrophy [196].

C. ROS and Protein Turnover

Apoptosis is not the only mechanism of muscle atrophy that ROS induces. Exposing skeletal muscle myotubes to ROS activates proteases leading to protein degradation [201]. Specifically H_2O_2 upregulates expression of specific E3 and E2 proteins that are thought to regulate muscle catabolism, including atrogin1, MuRF1, and E214k [201]. Furthermore, ROS can impede cell signaling pathways that promote skeletal muscle protein synthesis [202, 203]. Specifically ROS disrupts the assembly of the mTOR complex [203] and reduces phosphorylation of 4EBP1 [202]. Furthermore, ROS increases the expression of Calpain1. Calpain1, a calcium activated protease, seems to be required for muscle atrophy as displayed in C2C12 cells and evidenced by the use of small interfering RNA's against Calpain1 [193]. Calpain1 is involved in the regulation of numerous protein turnover pathways including the ubiquitin proteasome pathway and anabolic processes mediated by Akt-mTOR-p70S6K and ERK-MAPK [204].Taken together, excess ROS imbalances protein turnover towards protein degradation.

ROS may potentially be a key instigator of cancer-cachexia; however, it has not been directly measured in cancer-cachexia. Some researchers have implicated excess oxidative stress as a potential mechanism for inducing cancer-cachexia and have successfully attenuated cachexia progression with antioxidant treatments such as quercetin [205]. Utilizing antioxidants to specifically treat cancer-cachexia is challenging because antioxidants may influence tumor growth as well [206]. ROS exerts a dual role within the tumor itself, as it either promotes

proliferation and vascularization of the tumor or induces senescence and apoptosis [206]. Currently it is postulated that antioxidants may only be helpful for individuals with a compromised antioxidant defense status due to the inability to specifically target skeletal muscle ROS production [206].

Models to Study Cancer-Cachexia

Cachexia is a wasting disease that is associated with the course of multiple underlying disease processes, including cancer, chronic kidney disease, chronic heart failure, AIDS and other chronic diseases [207]; therefore, animal models to successfully study cachexia are crucial to gain a greater understanding of the condition. Intriguingly, each of these disease states produces clinical symptoms of cachexia that are strikingly similar such as increased energy expenditure, loss of lean body mass and fat mass and a loss of appetite [208]. Of utmost importance is identifying models to study cancer-cachexia given that cachexia affects up to 80% of individuals with certain types of cancer [209]. Despite the gravity of cachexia, there have only been a few clinical trials to attempt to treat the condition; therefore, a reliable animal model to study cachexia is critical to provide insight to potential therapies that could be utilized to treat cachexia [210].

Patients with cancer-cachexia, like other diseases/disorders that induce muscle wasting, are exposed to a high inflammatory environment. This high inflammatory environment may be the root cause behind the hypophagia seen in many cachectic individuals [210]. In order to mimic inflammatory responses induced by cancer animals can be injected with cytokines such as TNFα, IL-1β or IL-6 [211, 212]. These inflammatory cytokines are often injected directly into skeletal muscle to induce a quick response to inflammation [213]. This method for inducing cachexia has its draw backs. While it is easy to isolate specific cytokines to examine direct

signaling responses elicited by them, there are many other tumor properties that are not going to be examined.

Animal models that simulate human cancer-cachexia most commonly use implanted tumor cell lines such as Lewis Lung Carcinoma (LLC) and C26 model, colorectal tumors, syngeneic sarcomas and other types of stable, cachectogenic neoplasms [214-217]. Other models for the study of cancer-cachexia include methylcholanthrene-induced sarcomas [218], prostate tumors [219], Yoshida AH-130 hepatoma (rats only) [220], EHS chondrosarcomas (mice only) [6], MAC16 colon adenocarcinoma [221], and Walker 256 carcinosarcomas [222]. In implantation models, the rate in which cancer-cachexia occurs is largely dependent on the amount of tumor cells injected into the mouse and the location of the injection of tumor cells. If $1X10^7$ tumor cells are implanted into the hind flank of a mouse than cachexia occurs around 30 days after implantation [217, 24].

LLC is considered the most commonly used and best characterized model of cancer cachexia [223, 210]. These cell lines are implanted subcutaneously into experimental animals and are allowed to grow to a particular burden at which point they cause symptoms of cachexia. The implanted cell lines do not metastasize significantly, a key difference from cachexia-causing neoplasms in humans, but implanted tumors have been demonstrated to be similar in many other ways to human cancer [210]. The commonly used tumor lines induce cachexia through release of cachexia-inducing factors and stimulation of host-tumor interactions [210]. Many of these implanted tumor cells express or induce inflammatory cytokines or prostaglandins, which is similar to human cancer [210]. Moreover, implanted tumors have been reported to result in key features of cachexia, including anorexia, weight loss and increased energy expenditure which is similar to human cancer [224]. A key advantage of the LLC model to study cancer-cachexia is

the ease of monitoring tumor growth and proliferation and knowing the exact time frame in which the animal has cancer.

Genetic models such as the *APC*$^{Min+}$ mouse are also commonly used in order to study cachexia. The *APC*$^{Min+}$ mouse will sporatically have a mutation that will lead to colorectal cancer. The *APC*$^{Min+}$ model of cancer-cachexia has been shown to be largely IL-6 dependent [225]. The rate in which muscle loss occurs in *APC*$^{Min+}$ may vary. Typically this model will exhibit mild cancer-cachexia by 16 weeks of age and will continue to a severe form of cancer-cachexia after that [7]. These mice typically do not live much longer than 20 weeks of age. These mice have a distinct advantage of not being hypophagic, so cachexia can be attributed to factors secreted by cancer or cancer proliferation. However, most human cancer patients are hypophagic; therefore, the *APC*$^{Min+}$ mouse may not accurately reflect human cancer. Another disadvantage is the inability to pinpoint when the mouse is cancerous.

Different models used for the analysis of cancer-cachexia often have vastly different results. For example, rates of protein synthesis are different based on the model and the number of tumor cells injected. Because of this, it is of utmost importance to specify details of the specific model used to induce cachexia. The tumor microenvironment may be dramatically different for each line of tumor and therefore, may contribute to the differences observed with each cell line. Future research should use an omics approach to compare muscle wasting of different models of cancer-cachexia order to identify differences between models of cancer-cachexia.

Gaps in Cancer-Cachexia Literature

Considerable progress has been made behind mechanisms of cancer-cachexia; however, the process of cancer-cachexia is not fully understood. Specifically, progression of cancer-cachexia has not been well examined and ROS as a potential mechanism for the onset of cancer-cachexia has not been studied.

First, studies do not examine the progression of cancer-cachexia. In cancer-cachexia literature, studies tend to only examine end point cachexia [9, 27, 24]. This can provide valuable information about the atrophic pathways that are elevated when the muscle is cachectic; however, it does not address signaling that instigated cancer-cachexia. Recent literature calls for research investigating modalities that could be used to prevent cancer-cachexia [226]. Understanding signaling that leads to the induction of cancer-cachexia will provide valuable information that could be used to develop therapies to prevent cancer-cachexia. Using a time course experiment will provide this information.

Second, ROS has been implicated as a possible mechanism leading to cancer-cachexia; however, it has yet to be measured in cancer-cachexia. Moreover, antioxidant therapies have been utilized with mixed results because they fail to specifically target skeletal muscle. In fact, antioxidants may progress tumor proliferation leading to a worsened prognosis. Utilizing muscle specific ROS neutralizing agents may prove to be a valuable treatment for cancer-cachexia.

A few other gaps in literature include the study of cancer-cachexia in aged animals and chemotherapy mediated muscle wasting. In the clinic, cancer normally occurs in older individuals; therefore, studies should focus on the progression of cancer-cachexia in aged animals. It is possible that pre-existing sarcopenia may speed up the onset of cancer-cachexia.

Also, chemotherapy agents may induce muscle wasting. Therefore, it is important to study cancer-cachexia in conjunction with chemotherapy treatment.

Summary of Literature Review.

Cancer is one of the leading causes of death worldwide with over half of the people affected by cancer dying as a result of the condition [1, 2]. Cancer-cachexia is a wasting syndrome that occurs in approximately 80% of cancer patients [4, 5]. In fact, cancer-cachexia is the primary cause of death for 22%-30% of all individuals with cancer [4, 5]. Cancer-cachexia is multifactorial and cannot be fully reversed by nutritional support with a combination of reduced food intake and abnormal metabolism, seemingly induced by tumor- and host-derived factors [4].

Cancer-cachexia is associated with reduced muscle protein synthesis and increased muscle protein breakdown [7, 8], which leads to a loss of skeletal muscle mass [10]. There are many factors that influence this dysregulation of protein turnover including reduced protein synthesis, elevated autophagy, elevated proteasome activity and impaired myogenesis. Cancer-cachexia is likely metabolically induced; therefore, mitochondrial degeneration may prompt cancer-cachexia. Mitochondrial degeneration results in inefficient ATP production and excess mitochondrial reactive oxygen species (ROS) production. Mitochondrial degeneration results in reduced protein synthesis and the upregulation of atrophic signaling. Furthermore, mitochondrial degeneration results in excess mitochondrial ROS production. Elevated levels of ROS reduces protein synthesis and promotes protein breakdown. Furthermore, ROS upregulates apoptosis in skeletal muscle.

Mitochondrial degeneration may be behind the induction of signaling contributing to cancer-cachexia. Future cancer-cachexia experiments should focus on mechanisms that lead to the onset of cancer-cachexia in order develop adequate therapies.

References

1. Ferlay J, Soerjomataram I, Dikshit R, Eser S, Mathers C, Rebelo M et al. Cancer incidence and mortality worldwide: sources, methods and major patterns in GLOBOCAN 2012. International journal of cancer. 2015;136(5):E359-86. doi:10.1002/ijc.29210.

2. Fitzmaurice C, Dicker D, Pain A, Hamavid H, Moradi-Lakeh M, MacIntyre MF et al. The Global Burden of Cancer 2013. JAMA oncology. 2015;1(4):505-27. doi:10.1001/jamaoncol.2015.0735.

3. Jemal A, Ward E, Hao Y, Thun M. Trends in the leading causes of death in the United States, 1970-2002. Jama. 2005;294(10):1255-9. doi:10.1001/jama.294.10.1255.

4. Fearon Kenneth CH, Glass David J, Guttridge Denis C. Cancer Cachexia: Mediators, Signaling, and Metabolic Pathways. Cell metabolism. 2012;16(2):153-66. doi:http://dx.doi.org/10.1016/j.cmet.2012.06.011.

5. Onesti JK, Guttridge DC. Inflammation based regulation of cancer cachexia. BioMed research international. 2014;2014:168407. doi:10.1155/2014/168407.

6. Janssen I, Shepard DS, Katzmarzyk PT, Roubenoff R. The healthcare costs of sarcopenia in the United States. Journal of the American Geriatrics Society. 2004;52(1):80-5.

7. Narsale AA, Puppa MJ, Hardee JP, VanderVeen BN, Enos RT, Murphy EA et al. Short-term pyrrolidine dithiocarbamate administration attenuates cachexia-induced alterations to muscle and liver in ApcMin/+ mice. Oncotarget. 2016. doi:10.18632/oncotarget.10699.

8. Oliveira AG, Gomes-Marcondes MC. Metformin treatment modulates the tumour-induced wasting effects in muscle protein metabolism minimising the cachexia in tumour-bearing rats. BMC cancer. 2016;16:418. doi:10.1186/s12885-016-2424-9.

9. White JP, Puppa MJ, Sato S, Gao S, Price RL, Baynes JW et al. IL-6 regulation on skeletal muscle mitochondrial remodeling during cancer cachexia in the ApcMin/+ mouse. Skeletal muscle. 2012;2:14. doi:10.1186/2044-5040-2-14.

10. Bonaldo P, Sandri M. Cellular and molecular mechanisms of muscle atrophy. Disease Models & Mechanisms. 2013;6(1):25-39. doi:10.1242/dmm.010389.

11. Suzuki H, Asakawa A, Amitani H, Nakamura N, Inui A. Cancer cachexia—pathophysiology and management. Journal of Gastroenterology. 2013;48(5):574-94. doi:10.1007/s00535-013-0787-0.

12. Miyamoto Y, Hanna DL, Zhang W, Baba H, Lenz HJ. Molecular Pathways: Cachexia Signaling-A Targeted Approach to Cancer Treatment. Clinical cancer research : an official journal of the American Association for Cancer Research. 2016;22(16):3999-4004. doi:10.1158/1078-0432.ccr-16-0495.

13. Tisdale MJ. The ubiquitin-proteasome pathway as a therapeutic target for muscle wasting. The journal of supportive oncology. 2005;3(3):209-17.

14. Aversa Z, Pin F, Lucia S, Penna F, Verzaro R, Fazi M et al. Autophagy is induced in the skeletal muscle of cachectic cancer patients. Scientific reports. 2016;6:30340. doi:10.1038/srep30340.

15. Pain VM. Initiation of protein synthesis in eukaryotic cells. European journal of biochemistry / FEBS. 1996;236(3):747-71.

16. Svitkin YV, Herdy B, Costa-Mattioli M, Gingras AC, Raught B, Sonenberg N. Eukaryotic translation initiation factor 4E availability controls the switch between cap-dependent and internal ribosomal entry site-mediated translation. Molecular and cellular biology. 2005;25(23):10556-65. doi:10.1128/mcb.25.23.10556-10565.2005.

17. Kimball SR, Farrell PA, Jefferson LS. Invited Review: Role of insulin in translational control of protein synthesis in skeletal muscle by amino acids or exercise. Journal of applied physiology (Bethesda, Md : 1985). 2002;93(3):1168-80. doi:10.1152/japplphysiol.00221.2002.

18. Sekulic A, Hudson CC, Homme JL, Yin P, Otterness DM, Karnitz LM et al. A direct linkage between the phosphoinositide 3-kinase-AKT signaling pathway and the mammalian target of rapamycin in mitogen-stimulated and transformed cells. Cancer research. 2000;60(13):3504-13.

19. Gingras AC, Raught B, Gygi SP, Niedzwiecka A, Miron M, Burley SK et al. Hierarchical phosphorylation of the translation inhibitor 4E-BP1. Genes & development. 2001;15(21):2852-64. doi:10.1101/gad.912401.

20. Burnett PE, Barrow RK, Cohen NA, Snyder SH, Sabatini DM. RAFT1 phosphorylation of the translational regulators p70 S6 kinase and 4E-BP1. Proceedings of the National Academy of Sciences of the United States of America. 1998;95(4):1432-7.

21. Johns N, Stephens NA, Fearon KC. Muscle wasting in cancer. The international journal of biochemistry & cell biology. 2013;45(10):2215-29. doi:10.1016/j.biocel.2013.05.032.

22. Toledo M, Busquets S, Penna F, Zhou X, Marmonti E, Betancourt A et al. Complete reversal of muscle wasting in experimental cancer cachexia: Additive effects of activin type II receptor inhibition and beta-2 agonist. International journal of cancer. 2016;138(8):2021-9. doi:10.1002/ijc.29930.

23. Lima M, Sato S, Enos RT, Baynes JW, Carson JA. Development of an UPLC mass spectrometry method for measurement of myofibrillar protein synthesis: application to analysis of murine muscles during cancer cachexia. Journal of Applied Physiology. 2013;114(6):824-8. doi:10.1152/japplphysiol.01141.2012.

24. Puppa MJ, Gao S, Narsale AA, Carson JA. Skeletal muscle glycoprotein 130's role in Lewis lung carcinoma-induced cachexia. FASEB journal : official publication of the Federation of American Societies for Experimental Biology. 2014;28(2):998-1009. doi:10.1096/fj.13-240580.

25. Llovera M, Garcia-Martinez C, Lopez-Soriano J, Agell N, Lopez-Soriano FJ, Garcia I et al. Protein turnover in skeletal muscle of tumour-bearing transgenic mice overexpressing the soluble TNF receptor-1. Cancer letters. 1998;130(1-2):19-27.

26. White JP, Puppa MJ, Gao S, Sato S, Welle SL, Carson JA. Muscle mTORC1 suppression by IL-6 during cancer cachexia: a role for AMPK. American Journal of Physiology - Endocrinology and Metabolism. 2013;304(10):E1042-E52. doi:10.1152/ajpendo.00410.2012.

27. White JP, Baynes JW, Welle SL, Kostek MC, Matesic LE, Sato S et al. The regulation of skeletal muscle protein turnover during the progression of cancer cachexia in the Apc(Min/+) mouse. PloS one. 2011;6(9):e24650. doi:10.1371/journal.pone.0024650.

28. Attard-Montalto SP, Camacho-Hubner C, Cotterill AM, D'Souza-Li L, Daley S, Bartlett K et al. Changes in protein turnover, IGF-I and IGF binding proteins in children with cancer. Acta paediatrica (Oslo, Norway : 1992). 1998;87(1):54-60.

29. Russell ST, Siren PM, Siren MJ, Tisdale MJ. Attenuation of skeletal muscle atrophy in cancer cachexia by D-myo-inositol 1,2,6-triphosphate. Cancer chemotherapy and pharmacology. 2009;64(3):517-27. doi:10.1007/s00280-008-0899-z.

30. Eley HL, Russell ST, Tisdale MJ. Effect of branched-chain amino acids on muscle atrophy in cancer cachexia. The Biochemical journal. 2007;407(1):113-20. doi:10.1042/bj20070651.

31. Bolster DR, Crozier SJ, Kimball SR, Jefferson LS. AMP-activated protein kinase suppresses protein synthesis in rat skeletal muscle through down-regulated mammalian target of rapamycin (mTOR) signaling. The Journal of biological chemistry. 2002;277(27):23977-80. doi:10.1074/jbc.C200171200.

32. Hardie DG. Energy sensing by the AMP-activated protein kinase and its effects on muscle metabolism. The Proceedings of the Nutrition Society. 2011;70(1):92-9. doi:10.1017/s0029665110003915.

33. Gwinn DM, Shackelford DB, Egan DF, Mihaylova MM, Mery A, Vasquez DS et al. AMPK phosphorylation of raptor mediates a metabolic checkpoint. Molecular cell. 2008;30(2):214-26. doi:10.1016/j.molcel.2008.03.003.

34. Kobayashi S. Choose Delicately and Reuse Adequately: The Newly Revealed Process of Autophagy. Biological & pharmaceutical bulletin. 2015;38(8):1098-103. doi:10.1248/bpb.b15-00096.

35. Chang YY, Neufeld TP. An Atg1/Atg13 complex with multiple roles in TOR-mediated autophagy regulation. Molecular biology of the cell. 2009;20(7):2004-14. doi:10.1091/mbc.E08-12-1250.

36. He C, Klionsky DJ. Regulation Mechanisms and Signaling Pathways of Autophagy. Annual review of genetics. 2009;43:67-93. doi:10.1146/annurev-genet-102808-114910.

37. Fritzen AM, Madsen AB, Kleinert M, Treebak JT, Lundsgaard AM, Jensen TE et al. Regulation of autophagy in human skeletal muscle: effects of exercise, exercise training and insulin stimulation. The Journal of physiology. 2016;594(3):745-61. doi:10.1113/jp271405.

38. Carson JA, Hardee JP, VanderVeen BN. The emerging role of skeletal muscle oxidative metabolism as a biological target and cellular regulator of cancer-induced muscle wasting. Seminars in cell & developmental biology. 2016;54:53-67. doi:10.1016/j.semcdb.2015.11.005.

39. Mehdad A, Brumana G, Souza AA, Barbosa J, Ventura MM, de Freitas SM. A Bowman-Birk inhibitor induces apoptosis in human breast adenocarcinoma through mitochondrial impairment and oxidative damage following proteasome 20S inhibition. Cell death discovery. 2016;2:15067. doi:10.1038/cddiscovery.2015.67.

40. Abrigo J, Rivera JC, Aravena J, Cabrera D, Simon F, Ezquer F et al. High Fat Diet-Induced Skeletal Muscle Wasting Is Decreased by Mesenchymal Stem Cells Administration: Implications on Oxidative Stress, Ubiquitin Proteasome Pathway Activation, and Myonuclear Apoptosis. Oxidative medicine and cellular longevity. 2016;2016:9047821. doi:10.1155/2016/9047821.

41. Rom O, Reznick AZ. The role of E3 ubiquitin-ligases MuRF-1 and MAFbx in loss of skeletal muscle mass. Free radical biology & medicine. 2016;98:218-30. doi:10.1016/j.freeradbiomed.2015.12.031.

42. Smith DM, Chang SC, Park S, Finley D, Cheng Y, Goldberg A. Docking of the Proteasomal ATPases' C-termini in the 20S Proteasomes alpha Ring Opens the Gate for Substrate Entry. Molecular cell. 2007;27(5):731-44. doi:10.1016/j.molcel.2007.06.033.

43. Metzger MB, Hristova VA, Weissman AM. HECT and RING finger families of E3 ubiquitin ligases at a glance. Journal of cell science. 2012;125(Pt 3):531-7. doi:10.1242/jcs.091777.

44. Navon A, Ciechanover A. The 26 S proteasome: from basic mechanisms to drug targeting. The Journal of biological chemistry. 2009;284(49):33713-8. doi:10.1074/jbc.R109.018481.

45. Passmore LA, Barford D. Getting into position: the catalytic mechanisms of protein ubiquitylation. The Biochemical journal. 2004;379(Pt 3):513-25. doi:10.1042/bj20040198.

46. Haas AL, Warms JV, Hershko A, Rose IA. Ubiquitin-activating enzyme. Mechanism and role in protein-ubiquitin conjugation. The Journal of biological chemistry. 1982;257(5):2543-8.

47. Thrower JS, Hoffman L, Rechsteiner M, Pickart CM. Recognition of the polyubiquitin proteolytic signal. The EMBO journal. 2000;19(1):94-102. doi:10.1093/emboj/19.1.94.

48. Hershko A, Ciechanover A. The ubiquitin system. Annual review of biochemistry. 1998;67:425-79. doi:10.1146/annurev.biochem.67.1.425.

49. Attaix D, Ventadour S, Codran A, Bechet D, Taillandier D, Combaret L. The ubiquitin-proteasome system and skeletal muscle wasting. Essays in biochemistry. 2005;41:173-86. doi:10.1042/eb0410173.

50. Bodine SC, Baehr LM. Skeletal muscle atrophy and the E3 ubiquitin ligases MuRF1 and MAFbx/atrogin-1. American Journal of Physiology - Endocrinology and Metabolism. 2014;307(6):E469-E84. doi:10.1152/ajpendo.00204.2014.

51. Lagirand-Cantaloube J, Offner N, Csibi A, Leibovitch MP, Batonnet-Pichon S, Tintignac LA et al. The initiation factor eIF3-f is a major target for Atrogin1/MAFbx function in skeletal muscle atrophy. The EMBO journal. 2008;27(8):1266-76. doi:10.1038/emboj.2008.52.

52. Csibi A, Leibovitch MP, Cornille K, Tintignac LA, Leibovitch SA. MAFbx/Atrogin-1 controls the activity of the initiation factor eIF3-f in skeletal muscle atrophy by targeting multiple C-terminal lysines. The Journal of biological chemistry. 2009;284(7):4413-21. doi:10.1074/jbc.M807641200.

53. Hirner S, Krohne C, Schuster A, Hoffmann S, Witt S, Erber R et al. MuRF1-dependent regulation of systemic carbohydrate metabolism as revealed from transgenic mouse studies. Journal of molecular biology. 2008;379(4):666-77. doi:10.1016/j.jmb.2008.03.049.

54. Clarke BA, Drujan D, Willis MS, Murphy LO, Corpina RA, Burova E et al. The E3 Ligase MuRF1 degrades myosin heavy chain protein in dexamethasone-treated skeletal muscle. Cell metabolism. 2007;6(5):376-85. doi:10.1016/j.cmet.2007.09.009.

55. Kavazis AN, Smuder AJ, Powers SK. Effects of short-term endurance exercise training on acute doxorubicin-induced FoxO transcription in cardiac and skeletal muscle. Journal of applied physiology (Bethesda, Md : 1985). 2014;117(3):223-30. doi:10.1152/japplphysiol.00210.2014.

56. Brunet A, Bonni A, Zigmond MJ, Lin MZ, Juo P, Hu LS et al. Akt promotes cell survival by phosphorylating and inhibiting a Forkhead transcription factor. Cell. 1999;96(6):857-68.

57. O'Neill BT, Lee KY, Klaus K, Softic S, Krumpoch MT, Fentz J et al. Insulin and IGF-1 receptors regulate FoxO-mediated signaling in muscle proteostasis. The Journal of clinical investigation. 2016;126(9):3433-46. doi:10.1172/jci86522.

58. Ouyang W, Li MO. Foxo: in command of T lymphocyte homeostasis and tolerance. Trends in immunology.32(1):26-33. doi:10.1016/j.it.2010.10.005.

59. Milan G, Romanello V, Pescatore F, Armani A, Paik JH, Frasson L et al. Regulation of autophagy and the ubiquitin-proteasome system by the FoxO transcriptional network during muscle atrophy. Nature communications. 2015;6:6670. doi:10.1038/ncomms7670.

60. Zhao J, Brault JJ, Schild A, Cao P, Sandri M, Schiaffino S et al. FoxO3 coordinately activates protein degradation by the autophagic/lysosomal and proteasomal pathways in atrophying muscle cells. Cell metabolism. 2007;6(6):472-83. doi:10.1016/j.cmet.2007.11.004.

61. Greer EL, Brunet A. FOXO transcription factors at the interface between longevity and tumor suppression. Oncogene. 2005;24(50):7410-25. doi:10.1038/sj.onc.1209086.

62. Lee K, Ochi E, Song H, Nakazato K. Activation of AMP-activated protein kinase induce expression of FoxO1, FoxO3a, and myostatin after exercise-induced muscle damage.

Biochemical and biophysical research communications. 2015;466(3):289-94. doi:10.1016/j.bbrc.2015.08.126.

63. Wilhelm K, Happel K, Eelen G, Schoors S, Oellerich MF, Lim R et al. FOXO1 couples metabolic activity and growth state in the vascular endothelium. Nature. 2016;529(7585):216-20. doi:10.1038/nature16498.

64. Zimmers TA, Fishel ML, Bonetto A. STAT3 in the systemic inflammation of cancer cachexia. Seminars in cell & developmental biology. 2016;54:28-41. doi:10.1016/j.semcdb.2016.02.009.

65. Inácio Pinto N, Carnier J, Oyama LM, Otoch JP, Alcântara PS, Tokeshi F et al. Cancer as a Proinflammatory Environment: Metastasis and Cachexia. Mediators of inflammation. 2015;2015:791060. doi:10.1155/2015/791060.

66. Lenk K, Schuler G, Adams V. Skeletal muscle wasting in cachexia and sarcopenia: molecular pathophysiology and impact of exercise training. Journal of cachexia, sarcopenia and muscle. 2010;1(1):9-21. doi:10.1007/s13539-010-0007-1.

67. Seelaender MC, Batista ML. Adipose tissue inflammation and cancer cachexia: the role of steroid hormones. Hormone molecular biology and clinical investigation. 2014;17(1):5-12. doi:10.1515/hmbci-2013-0040.

68. Puppa MJ, White JP, Sato S, Cairns M, Baynes JW, Carson JA. Gut barrier dysfunction in the Apc(Min/+) mouse model of colon cancer cachexia. Biochimica et biophysica acta. 2011;1812(12):1601-6. doi:10.1016/j.bbadis.2011.08.010.

69. Dobashi Y, Watanabe Y, Miwa C, Suzuki S, Koyama S. Mammalian target of rapamycin: a central node of complex signaling cascades. International Journal of Clinical and Experimental Pathology. 2011;4(5):476-95.

70. Baltgalvis KA, Berger FG, Peña MMO, Davis JM, White JP, Carson JA. Muscle Wasting and Interleukin-6-Induced Atrogin-I Expression in the Cachectic Apc(Min/+) Mouse. Pflugers Archiv : European journal of physiology. 2009;457(5):989-1001. doi:10.1007/s00424-008-0574-6.

71. Ruas JL, White JP, Rao RR, Kleiner S, Brannan KT, Harrison BC et al. A PGC-1alpha isoform induced by resistance training regulates skeletal muscle hypertrophy. Cell. 2012;151(6):1319-31. doi:10.1016/j.cell.2012.10.050.

72. Brown JL, Rosa-Caldwell ME, Lee DE, Brown LA, Perry RA, Shimkus KL et al. PGC-1alpha4 gene expression is suppressed by the IL-6-MEK-ERK 1/2 MAPK signalling axis and altered by resistance exercise, obesity and muscle injury. Acta physiologica (Oxford, England). 2016. doi:10.1111/apha.12826.

73. Serrano AL, Baeza-Raja B, Perdiguero E, Jardi M, Munoz-Canoves P. Interleukin-6 is an essential regulator of satellite cell-mediated skeletal muscle hypertrophy. Cell metabolism. 2008;7(1):33-44. doi:10.1016/j.cmet.2007.11.011.

74. Hetzler KL, Hardee JP, Puppa MJ, Narsale AA, Sato S, Davis JM et al. Sex differences in the relationship of IL-6 signaling to cancer cachexia progression. Biochimica et biophysica acta. 2015;1852(5):816-25. doi:10.1016/j.bbadis.2014.12.015.

75. Landskron G, De la Fuente M, Thuwajit P, Thuwajit C, Hermoso MA. Chronic inflammation and cytokines in the tumor microenvironment. Journal of immunology research. 2014;2014:149185. doi:10.1155/2014/149185.

76. Phillips T, Leeuwenburgh C. Muscle fiber specific apoptosis and TNF-alpha signaling in sarcopenia are attenuated by life-long calorie restriction. FASEB journal : official publication of the Federation of American Societies for Experimental Biology. 2005;19(6):668-70. doi:10.1096/fj.04-2870fje.

77. Melstrom LG, Melstrom KA, Jr., Ding XZ, Adrian TE. Mechanisms of skeletal muscle degradation and its therapy in cancer cachexia. Histology and histopathology. 2007;22(7):805-14.

78. Zhang L, Tang H, Kou Y, Li R, Zheng Y, Wang Q et al. MG132-mediated inhibition of the ubiquitin-proteasome pathway ameliorates cancer cachexia. Journal of cancer research and clinical oncology. 2013;139(7):1105-15. doi:10.1007/s00432-013-1412-6.

79. Argiles JM, Lopez-Soriano FJ, Busquets S. Counteracting inflammation: a promising therapy in cachexia. Critical reviews in oncogenesis. 2012;17(3):253-62.

80. Amaral ME, Barbuio R, Milanski M, Romanatto T, Barbosa HC, Nadruz W et al. Tumor necrosis factor-alpha activates signal transduction in hypothalamus and modulates the expression of pro-inflammatory proteins and orexigenic/anorexigenic neurotransmitters. Journal of neurochemistry. 2006;98(1):203-12. doi:10.1111/j.1471-4159.2006.03857.x.

81. Busquets S, Sanchis D, Alvarez B, Ricquier D, Lopez-Soriano FJ, Argiles JM. In the rat, tumor necrosis factor alpha administration results in an increase in both UCP2 and UCP3 mRNAs in skeletal muscle: a possible mechanism for cytokine-induced thermogenesis? FEBS letters. 1998;440(3):348-50.

82. McPherron AC, Lawler AM, Lee SJ. Regulation of skeletal muscle mass in mice by a new TGF-beta superfamily member. Nature. 1997;387(6628):83-90. doi:10.1038/387083a0.

83. Han HQ, Zhou X, Mitch WE, Goldberg AL. Myostatin/activin pathway antagonism: molecular basis and therapeutic potential. The international journal of biochemistry & cell biology. 2013;45(10):2333-47. doi:10.1016/j.biocel.2013.05.019.

84. Gallot YS, Durieux AC, Castells J, Desgeorges MM, Vernus B, Plantureux L et al. Myostatin gene inactivation prevents skeletal muscle wasting in cancer. Cancer research. 2014;74(24):7344-56. doi:10.1158/0008-5472.can-14-0057.

85. Marino FE, Risbridger G, Gold E. Activin-betaC modulates cachexia by repressing the ubiquitin-proteasome and autophagic degradation pathways. Journal of cachexia, sarcopenia and muscle. 2015;6(4):365-80. doi:10.1002/jcsm.12031.

86. Zanou N, Gailly P. Skeletal muscle hypertrophy and regeneration: interplay between the myogenic regulatory factors (MRFs) and insulin-like growth factors (IGFs) pathways. Cellular and molecular life sciences : CMLS. 2013;70(21):4117-30. doi:10.1007/s00018-013-1330-4.

87. Tidball JG. Inflammatory processes in muscle injury and repair. American journal of physiology Regulatory, integrative and comparative physiology. 2005;288(2):R345-53. doi:10.1152/ajpregu.00454.2004.

88. Buckingham M. Skeletal muscle progenitor cells and the role of Pax genes. Comptes rendus biologies. 2007;330(6-7):530-3. doi:10.1016/j.crvi.2007.03.015.

89. Jejurikar SS, Kuzon WM, Jr. Satellite cell depletion in degenerative skeletal muscle. Apoptosis : an international journal on programmed cell death. 2003;8(6):573-8. doi:10.1023/a:1026127307457.

90. Luz MA, Marques MJ, Santo Neto H. Impaired regeneration of dystrophin-deficient muscle fibers is caused by exhaustion of myogenic cells. Brazilian journal of medical and biological research = Revista brasileira de pesquisas medicas e biologicas / Sociedade Brasileira de Biofisica [et al]. 2002;35(6):691-5.

91. Karalaki M, Fili S, Philippou A, Koutsilieris M. Muscle regeneration: cellular and molecular events. In vivo (Athens, Greece). 2009;23(5):779-96.

92. Hettmer S, Wagers AJ. Muscling in: Uncovering the origins of rhabdomyosarcoma. Nature medicine. 2010;16(2):171-3.

93. McCarthy JJ, Mula J, Miyazaki M, Erfani R, Garrison K, Farooqui AB et al. Effective fiber hypertrophy in satellite cell-depleted skeletal muscle. Development (Cambridge, England). 2011;138(17):3657-66. doi:10.1242/dev.068858.

94. He WA, Berardi E, Cardillo VM, Acharyya S, Aulino P, Thomas-Ahner J et al. NF-κB–mediated Pax7 dysregulation in the muscle microenvironment promotes cancer cachexia. The Journal of clinical investigation. 2013;123(11):4821-35. doi:10.1172/JCI68523.

95. Penna F, Costamagna D, Fanzani A, Bonelli G, Baccino FM, Costelli P. Muscle wasting and impaired myogenesis in tumor bearing mice are prevented by ERK inhibition. PloS one. 2010;5(10):e13604. doi:10.1371/journal.pone.0013604.

96. Guttridge DC, Mayo MW, Madrid LV, Wang CY, Baldwin AS, Jr. NF-kappaB-induced loss of MyoD messenger RNA: possible role in muscle decay and cachexia. Science (New York, NY). 2000;289(5488):2363-6.

97. Ramamoorthy S, Donohue M, Buck M. Decreased Jun-D and myogenin expression in muscle wasting of human cachexia. American journal of physiology Endocrinology and metabolism. 2009;297(2):E392-401. doi:10.1152/ajpendo.90529.2008.

98. Macpherson PC, Wang X, Goldman D. Myogenin regulates denervation-dependent muscle atrophy in mouse soleus muscle. Journal of cellular biochemistry. 2011;112(8):2149-59. doi:10.1002/jcb.23136.

99. Moresi V, Williams AH, Meadows E, Flynn JM, Potthoff MJ, McAnally J et al. Myogenin and class II HDACs control neurogenic muscle atrophy by inducing E3 ubiquitin ligases. Cell. 2010;143(1):35-45. doi:10.1016/j.cell.2010.09.004.

100. Gregory TR. Coincidence, coevolution, or causation? DNA content, cell size, and the C-value enigma. Biological reviews of the Cambridge Philosophical Society. 2001;76(1):65-101.

101. Bruusgaard JC, Liestol K, Ekmark M, Kollstad K, Gundersen K. Number and spatial distribution of nuclei in the muscle fibres of normal mice studied in vivo. The Journal of physiology. 2003;551(Pt 2):467-78. doi:10.1113/jphysiol.2003.045328.

102. Gundersen K, Bruusgaard JC. Nuclear domains during muscle atrophy: nuclei lost or paradigm lost? The Journal of physiology. 2008;586(Pt 11):2675-81. doi:10.1113/jphysiol.2008.154369.

103. Dupont-Versteegden EE, Murphy RJ, Houle JD, Gurley CM, Peterson CA. Activated satellite cells fail to restore myonuclear number in spinal cord transected and exercised rats. The American journal of physiology. 1999;277(3 Pt 1):C589-97.

104. Murphy KT, Chee A, Gleeson BG, Naim T, Swiderski K, Koopman R et al. Antibody-directed myostatin inhibition enhances muscle mass and function in tumor-bearing mice. American journal of physiology Regulatory, integrative and comparative physiology. 2011;301(3):R716-26. doi:10.1152/ajpregu.00121.2011.

105. Carbó N, Busquets S, van Royen M, Alvarez B, López-Soriano FJ, Argilés JM. TNF-α is involved in activating DNA fragmentation in skeletal muscle. British Journal of Cancer. 2002;86(6):1012-6. doi:10.1038/sj.bjc.6600167.

106. Silva KA, Dong J, Dong Y, Dong Y, Schor N, Tweardy DJ et al. Inhibition of Stat3 activation suppresses caspase-3 and the ubiquitin-proteasome system, leading to preservation of muscle mass in cancer cachexia. The Journal of biological chemistry. 2015;290(17):11177-87. doi:10.1074/jbc.M115.641514.

107. Pearson G, Robinson F, Beers Gibson T, Xu BE, Karandikar M, Berman K et al. Mitogen-activated protein (MAP) kinase pathways: regulation and physiological functions. Endocrine reviews. 2001;22(2):153-83. doi:10.1210/edrv.22.2.0428.

108. Cargnello M, Roux PP. Activation and function of the MAPKs and their substrates, the MAPK-activated protein kinases. Microbiology and molecular biology reviews : MMBR. 2011;75(1):50-83. doi:10.1128/mmbr.00031-10.

109. Coulombe P, Meloche S. Atypical mitogen-activated protein kinases: structure, regulation and functions. Biochimica et biophysica acta. 2007;1773(8):1376-87. doi:10.1016/j.bbamcr.2006.11.001.

110. Deleris P, Trost M, Topisirovic I, Tanguay PL, Borden KL, Thibault P et al. Activation loop phosphorylation of ERK3/ERK4 by group I p21-activated kinases (PAKs) defines a novel PAK-ERK3/4-MAPK-activated protein kinase 5 signaling pathway. The Journal of biological chemistry. 2011;286(8):6470-8. doi:10.1074/jbc.M110.181529.

111. Porter JD, Khanna S, Kaminski HJ, Rao JS, Merriam AP, Richmonds CR et al. A chronic inflammatory response dominates the skeletal muscle molecular signature in dystrophin-deficient mdx mice. Human molecular genetics. 2002;11(3):263-72.

112. Wilde JM, Gumucio JP, Grekin JA, Sarver DC, Noah AC, Ruehlmann DG et al. Inhibition of p38 mitogen-activated protein kinase signaling reduces fibrosis and lipid accumulation after rotator cuff repair. Journal of shoulder and elbow surgery. 2016;25(9):1501-8. doi:10.1016/j.jse.2016.01.035.

113. Verzola D, Bonanni A, Sofia A, Montecucco F, D'Amato E, Cademartori V et al. Toll-like receptor 4 signalling mediates inflammation in skeletal muscle of patients with chronic kidney disease. Journal of cachexia, sarcopenia and muscle. 2017;8(1):131-44. doi:10.1002/jcsm.12129.

114. Wissing ER, Boyer JG, Kwong JQ, Sargent MA, Karch J, McNally EM et al. P38alpha MAPK underlies muscular dystrophy and myofiber death through a Bax-dependent mechanism. Human molecular genetics. 2014;23(20):5452-63. doi:10.1093/hmg/ddu270.

115. Morales MG, Olguin H, Di Capua G, Brandan E, Simon F, Cabello-Verrugio C. Endotoxin-induced skeletal muscle wasting is prevented by angiotensin-(1-7) through a p38 MAPK-dependent mechanism. Clinical science (London, England : 1979). 2015;129(6):461-76. doi:10.1042/cs20140840.

116. Fermoselle C, Garcia-Arumi E, Puig-Vilanova E, Andreu AL, Urtreger AJ, de Kier Joffe ED et al. Mitochondrial dysfunction and therapeutic approaches in respiratory and limb muscles of cancer cachectic mice. Experimental physiology. 2013;98(9):1349-65. doi:10.1113/expphysiol.2013.072496.

117. Zhang G, Lin R-K, Kwon YT, Li Y-P. Signaling mechanism of tumor cell-induced up-regulation of E3 ubiquitin ligase UBR2. The FASEB Journal. 2013;27(7):2893-901. doi:10.1096/fj.12-222711.

118. Leestemaker Y, de Jong A, Witting KF, Penning R, Schuurman K, Rodenko B et al. Proteasome Activation by Small Molecules. Cell chemical biology. 2017;24(6):725-36.e7. doi:10.1016/j.chembiol.2017.05.010.

119. Obradovic H, Krstic J, Kukolj T, Trivanovic D, Dordevic IO, Mojsilovic S et al. Doxycycline Inhibits IL-17-Stimulated MMP-9 Expression by Downregulating ERK1/2 Activation: Implications in Myogenic Differentiation. Mediators of inflammation. 2016;2016:2939658. doi:10.1155/2016/2939658.

120. Girven M, Dugdale HF, Owens DJ, Hughes DC, Stewart CE, Sharples AP. l-glutamine Improves Skeletal Muscle Cell Differentiation and Prevents Myotube Atrophy After Cytokine

(TNF-alpha) Stress Via Reduced p38 MAPK Signal Transduction. Journal of cellular physiology. 2016;231(12):2720-32. doi:10.1002/jcp.25380.

121. Barreto R, Waning DL, Gao H, Liu Y, Zimmers TA, Bonetto A. Chemotherapy-related cachexia is associated with mitochondrial depletion and the activation of ERK1/2 and p38 MAPKs. Oncotarget. 2016;7(28):43442-60. doi:10.18632/oncotarget.9779.

122. Belizario JE, Fontes-Oliveira CC, Borges JP, Kashiabara JA, Vannier E. Skeletal muscle wasting and renewal: a pivotal role of myokine IL-6. SpringerPlus. 2016;5:619. doi:10.1186/s40064-016-2197-2.

123. Chacon-Cabrera A, Fermoselle C, Urtreger AJ, Mateu-Jimenez M, Diament MJ, de Kier Joffe ED et al. Pharmacological strategies in lung cancer-induced cachexia: effects on muscle proteolysis, autophagy, structure, and weakness. Journal of cellular physiology. 2014;229(11):1660-72. doi:10.1002/jcp.24611.

124. Zhang G, Jin B, Li YP. C/EBPbeta mediates tumour-induced ubiquitin ligase atrogin1/MAFbx upregulation and muscle wasting. The EMBO journal. 2011;30(20):4323-35. doi:10.1038/emboj.2011.292.

125. Tintignac LA, Brenner H-R, Rüegg MA. Mechanisms Regulating Neuromuscular Junction Development and Function and Causes of Muscle Wasting. Physiological Reviews. 2015;95(3):809-52. doi:10.1152/physrev.00033.2014.

126. Pennefather P, Quastel DM. Relation between subsynaptic receptor blockade and response to quantal transmitter at the mouse neuromuscular junction. The Journal of General Physiology. 1981;78(3):313-44. doi:10.1085/jgp.78.3.313.

127. Seaberg B, Henslee G, Wang S, Paez-Colasante X, Landreth GE, Rimer M. Muscle-Derived Extracellular Signal-Regulated Kinases 1 and 2 Are Required for the Maintenance of Adult Myofibers and Their Neuromuscular Junctions. Molecular and cellular biology. 2015;35(7):1238-53. doi:10.1128/MCB.01071-14.

128. Fertuck HC, Salpeter MM. Localization of Acetylcholine Receptor by 125I-Labeled α-Bungarotoxin Binding at Mouse Motor Endplates. Proceedings of the National Academy of Sciences. 1974;71(4):1376-8.

129. Laplante M, Sabatini DM. mTOR signaling in growth control and disease. Cell. 2012;149(2):274-93. doi:10.1016/j.cell.2012.03.017.

130. Gomes MD, Lecker SH, Jagoe RT, Navon A, Goldberg AL. Atrogin-1, a muscle-specific F-box protein highly expressed during muscle atrophy. Proceedings of the National Academy of Sciences. 2001;98(25):14440-5. doi:10.1073/pnas.251541198.

131. Li P, Waters RE, Redfern SI, Zhang M, Mao L, Annex BH et al. Oxidative phenotype protects myofibers from pathological insults induced by chronic heart failure in mice. The American journal of pathology. 2007;170(2):599-608. doi:10.2353/ajpath.2007.060505.

132. Yu Z, Li P, Zhang M, Hannink M, Stamler JS, Yan Z. Fiber type-specific nitric oxide protects oxidative myofibers against cachectic stimuli. PloS one. 2008;3(5):e2086. doi:10.1371/journal.pone.0002086.

133. Kandarian SC, Jackman RW. Intracellular signaling during skeletal muscle atrophy. Muscle & nerve. 2006;33(2):155-65. doi:10.1002/mus.20442.

134. Cannavino J, Brocca L, Sandri M, Bottinelli R, Pellegrino MA. PGC1-alpha over-expression prevents metabolic alterations and soleus muscle atrophy in hindlimb unloaded mice. The Journal of physiology. 2014;592(20):4575-89. doi:10.1113/jphysiol.2014.275545.

135. Ji LL. Redox signaling in skeletal muscle: role of aging and exercise. Advances in physiology education. 2015;39(4):352-9. doi:10.1152/advan.00106.2014.

136. Bijland S, Mancini SJ, Salt IP. Role of AMP-activated protein kinase in adipose tissue metabolism and inflammation. Clinical science (London, England : 1979). 2013;124(8):491-507. doi:10.1042/cs20120536.

137. Debold EP. Potential molecular mechanisms underlying muscle fatigue mediated by reactive oxygen and nitrogen species. Frontiers in physiology. 2015;6:239. doi:10.3389/fphys.2015.00239.

138. Lamb GD, Westerblad H. Acute effects of reactive oxygen and nitrogen species on the contractile function of skeletal muscle. The Journal of physiology. 2011;589(Pt 9):2119-27. doi:10.1113/jphysiol.2010.199059.

139. Sivakumar AS, Hwang I. Effects of Sunphenon and Polyphenon 60 on proteolytic pathways, inflammatory cytokines and myogenic markers in H2O2-treated C2C12 cells. Journal of biosciences. 2015;40(1):53-9.

140. Liu J, Peng Y, Wang X, Fan Y, Qin C, Shi L et al. Mitochondrial Dysfunction Launches Dexamethasone-Induced Skeletal Muscle Atrophy via AMPK/FOXO3 Signaling. Molecular pharmaceutics. 2016;13(1):73-84. doi:10.1021/acs.molpharmaceut.5b00516.

141. White JP, Baltgalvis KA, Puppa MJ, Sato S, Baynes JW, Carson JA. Muscle oxidative capacity during IL-6-dependent cancer cachexia. American journal of physiology Regulatory, integrative and comparative physiology. 2011;300(2):R201-11. doi:10.1152/ajpregu.00300.2010.

142. Yan Z, Lira VA, Greene NP. Exercise training-induced regulation of mitochondrial quality. Exercise and sport sciences reviews. 2012;40(3):159-64. doi:10.1097/JES.0b013e3182575599.

143. Spendiff S, Vuda M, Gouspillou G, Aare S, Perez A, Morais JA et al. Denervation drives mitochondrial dysfunction in skeletal muscle of octogenarians. The Journal of physiology. 2016. doi:10.1113/jp272487.

144. Dirks ML, Wall BT, van de Valk B, Holloway TM, Holloway GP, Chabowski A et al. One Week of Bed Rest Leads to Substantial Muscle Atrophy and Induces Whole-Body Insulin

Resistance in the Absence of Skeletal Muscle Lipid Accumulation. Diabetes. 2016;65(10):2862-75. doi:10.2337/db15-1661.

145. Puigserver P, Wu Z, Park CW, Graves R, Wright M, Spiegelman BM. A cold-inducible coactivator of nuclear receptors linked to adaptive thermogenesis. Cell. 1998;92(6):829-39.

146. Iacovelli J, Rowe GC, Khadka A, Diaz-Aguilar D, Spencer C, Arany Z et al. PGC-1alpha Induces Human RPE Oxidative Metabolism and Antioxidant Capacity. Investigative ophthalmology & visual science. 2016;57(3):1038-51. doi:10.1167/iovs.15-17758.

147. Puigserver P, Rhee J, Lin J, Wu Z, Yoon JC, Zhang CY et al. Cytokine stimulation of energy expenditure through p38 MAP kinase activation of PPARgamma coactivator-1. Molecular cell. 2001;8(5):971-82.

148. Brault JJ, Jespersen JG, Goldberg AL. Peroxisome proliferator-activated receptor gamma coactivator 1alpha or 1beta overexpression inhibits muscle protein degradation, induction of ubiquitin ligases, and disuse atrophy. The Journal of biological chemistry. 2010;285(25):19460-71. doi:10.1074/jbc.M110.113092.

149. Kuo YT, Shih PH, Kao SH, Yeh GC, Lee HM. Pyrroloquinoline Quinone Resists Denervation-Induced Skeletal Muscle Atrophy by Activating PGC-1alpha and Integrating Mitochondrial Electron Transport Chain Complexes. PloS one. 2015;10(12):e0143600. doi:10.1371/journal.pone.0143600.

150. Greene NP, Lee DE, Brown JL, Rosa ME, Brown LA, Perry RA et al. Mitochondrial quality control, promoted by PGC-1α, is dysregulated by Western diet-induced obesity and partially restored by moderate physical activity in mice. vol 7. 2015.

151. Hoppins S, Lackner L, Nunnari J. The machines that divide and fuse mitochondria. Annual review of biochemistry. 2007;76:751-80. doi:10.1146/annurev.biochem.76.071905.090048.

152. Ingerman E, Perkins EM, Marino M, Mears JA, McCaffery JM, Hinshaw JE et al. Dnm1 forms spirals that are structurally tailored to fit mitochondria. The Journal of cell biology. 2005;170(7):1021-7. doi:10.1083/jcb.200506078.

153. Labrousse AM, Zappaterra MD, Rube DA, van der Bliek AM. C. elegans dynamin-related protein DRP-1 controls severing of the mitochondrial outer membrane. Molecular cell. 1999;4(5):815-26.

154. Yoon Y, Pitts KR, McNiven MA. Mammalian dynamin-like protein DLP1 tubulates membranes. Molecular biology of the cell. 2001;12(9):2894-905.

155. Zhang Z, Liu L, Wu S, Xing D. Drp1, Mff, Fis1, and MiD51 are coordinated to mediate mitochondrial fission during UV irradiation-induced apoptosis. FASEB journal : official publication of the Federation of American Societies for Experimental Biology. 2016;30(1):466-76. doi:10.1096/fj.15-274258.

156. Ramos ES, Larsson NG, Mourier A. Bioenergetic roles of mitochondrial fusion. Biochimica et biophysica acta. 2016. doi:10.1016/j.bbabio.2016.04.002.

157. Cannavino J, Brocca L, Sandri M, Grassi B, Bottinelli R, Pellegrino MA. The role of alterations in mitochondrial dynamics and PGC-1alpha over-expression in fast muscle atrophy following hindlimb unloading. The Journal of physiology. 2015;593(8):1981-95. doi:10.1113/jphysiol.2014.286740.

158. Powers SK, Wiggs MP, Duarte JA, Zergeroglu AM, Demirel HA. Mitochondrial signaling contributes to disuse muscle atrophy. American journal of physiology Endocrinology and metabolism. 2012;303(1):E31-9. doi:10.1152/ajpendo.00609.2011.

159. Iqbal S, Ostojic O, Singh K, Joseph AM, Hood DA. Expression of mitochondrial fission and fusion regulatory proteins in skeletal muscle during chronic use and disuse. Muscle & nerve. 2013;48(6):963-70. doi:10.1002/mus.23838.

160. Lemasters JJ. Selective mitochondrial autophagy, or mitophagy, as a targeted defense against oxidative stress, mitochondrial dysfunction, and aging. Rejuvenation research. 2005;8(1):3-5. doi:10.1089/rej.2005.8.3.

161. Romanello V, Sandri M. Mitochondrial Quality Control and Muscle Mass Maintenance. Frontiers in physiology. 2015;6:422. doi:10.3389/fphys.2015.00422.

162. Jin SM, Youle RJ. PINK1- and Parkin-mediated mitophagy at a glance. Journal of cell science. 2012;125(4):795-9. doi:10.1242/jcs.093849.

163. Lemasters JJ, Nieminen AL, Qian T, Trost LC, Elmore SP, Nishimura Y et al. The mitochondrial permeability transition in cell death: a common mechanism in necrosis, apoptosis and autophagy. Biochimica et biophysica acta. 1998;1366(1-2):177-96.

164. Kissova I, Deffieu M, Manon S, Camougrand N. Uth1p is involved in the autophagic degradation of mitochondria. The Journal of biological chemistry. 2004;279(37):39068-74. doi:10.1074/jbc.M406960200.

165. Kramer P, Jung AT, Hamann A, Osiewacz HD. Cyclophilin D Is Involved in the Regulation of Autophagy and Affects the Lifespan of P. anserina in Response to Mitochondrial Oxidative Stress. Frontiers in genetics. 2016;7:165. doi:10.3389/fgene.2016.00165.

166. Wu JJ, Quijano C, Chen E, Liu H, Cao L, Fergusson MM et al. Mitochondrial dysfunction and oxidative stress mediate the physiological impairment induced by the disruption of autophagy. Aging. 2009;1(4):425-37. doi:10.18632/aging.100038.

167. Kitada T, Asakawa S, Hattori N, Matsumine H, Yamamura Y, Minoshima S et al. Mutations in the parkin gene cause autosomal recessive juvenile parkinsonism. Nature. 1998;392(6676):605-8. doi:10.1038/33416.

168. Narendra D, Tanaka A, Suen DF, Youle RJ. Parkin is recruited selectively to impaired mitochondria and promotes their autophagy. The Journal of cell biology. 2008;183(5):795-803. doi:10.1083/jcb.200809125.

169. Chan NC, Salazar AM, Pham AH, Sweredoski MJ, Kolawa NJ, Graham RL et al. Broad activation of the ubiquitin-proteasome system by Parkin is critical for mitophagy. Human molecular genetics. 2011;20(9):1726-37. doi:10.1093/hmg/ddr048.

170. Gegg ME, Cooper JM, Chau KY, Rojo M, Schapira AH, Taanman JW. Mitofusin 1 and mitofusin 2 are ubiquitinated in a PINK1/parkin-dependent manner upon induction of mitophagy. Human molecular genetics. 2010;19(24):4861-70. doi:10.1093/hmg/ddq419.

171. Matsuda N, Sato S, Shiba K, Okatsu K, Saisho K, Gautier CA et al. PINK1 stabilized by mitochondrial depolarization recruits Parkin to damaged mitochondria and activates latent Parkin for mitophagy. The Journal of cell biology. 2010;189(2):211-21. doi:10.1083/jcb.200910140.

172. Sha D, Chin LS, Li L. Phosphorylation of parkin by Parkinson disease-linked kinase PINK1 activates parkin E3 ligase function and NF-kappaB signaling. Human molecular genetics. 2010;19(2):352-63. doi:10.1093/hmg/ddp501.

173. Zhang T, Xue L, Li L, Tang C, Wan Z, Wang R et al. BNIP3 Suppresses PINK1 Proteolytic Cleavage to Promote Mitophagy. The Journal of biological chemistry. 2016. doi:10.1074/jbc.M116.733410.

174. Springer MZ, Macleod KF. In Brief: Mitophagy: mechanisms and role in human disease. The Journal of pathology. 2016. doi:10.1002/path.4774.

175. Vitorino R, Moreira-Goncalves D, Ferreira R. Mitochondrial plasticity in cancer-related muscle wasting: potential approaches for its management. Current opinion in clinical nutrition and metabolic care. 2015;18(3):226-33. doi:10.1097/mco.0000000000000161.

176. Vander Heiden MG, Cantley LC, Thompson CB. Understanding the Warburg effect: the metabolic requirements of cell proliferation. Science (New York, NY). 2009;324(5930):1029-33. doi:10.1126/science.1160809.

177. Lapuente-Brun E, Moreno-Loshuertos R, Acin-Perez R, Latorre-Pellicer A, Colas C, Balsa E et al. Supercomplex assembly determines electron flux in the mitochondrial electron transport chain. Science (New York, NY). 2013;340(6140):1567-70. doi:10.1126/science.1230381.

178. Wu M, Gu J, Guo R, Huang Y, Yang M. Structure of Mammalian Respiratory Supercomplex I1III2IV1. Cell. 2016;167(6):1598-609.e10. doi:10.1016/j.cell.2016.11.012.

179. Genova ML, Lenaz G. Functional role of mitochondrial respiratory supercomplexes. Biochimica et Biophysica Acta (BBA) - Bioenergetics. 2014;1837(4):427-43. doi:http://dx.doi.org/10.1016/j.bbabio.2013.11.002.

180. Cogliati S, Enriquez JA, Scorrano L. Mitochondrial Cristae: Where Beauty Meets Functionality. Trends in Biochemical Sciences. 2016;41(3):261-73. doi:http://dx.doi.org/10.1016/j.tibs.2016.01.001.

181. Greggio C, Jha P, Kulkarni SS, Lagarrigue S, Broskey NT, Boutant M et al. Enhanced Respiratory Chain Supercomplex Formation in Response to Exercise in Human Skeletal Muscle. Cell metabolism. 2017;25(2):301-11. doi:10.1016/j.cmet.2016.11.004.

182. López-Lluch G, Santos-Ocaña C, Sánchez-Alcázar JA, Fernández-Ayala DJM, Asencio-Salcedo C, Rodríguez-Aguilera JC et al. Mitochondrial responsibility in ageing process: innocent, suspect or guilty. Biogerontology. 2015;16(5):599-620. doi:10.1007/s10522-015-9585-9.

183. Lombardi A, Silvestri E, Cioffi F, Senese R, Lanni A, Goglia F et al. Defining the transcriptomic and proteomic profiles of rat ageing skeletal muscle by the use of a cDNA array, 2D- and Blue native-PAGE approach. Journal of Proteomics. 2009;72(4):708-21. doi:http://dx.doi.org/10.1016/j.jprot.2009.02.007.

184. Antoun G, McMurray F, Thrush AB, Patten DA, Peixoto AC, Slack RS et al. Impaired mitochondrial oxidative phosphorylation and supercomplex assembly in rectus abdominis muscle of diabetic obese individuals. Diabetologia. 2015;58(12):2861-6. doi:10.1007/s00125-015-3772-8.

185. Liu R, Jin P, Yu L, Wang Y, Han L, Shi T et al. Impaired mitochondrial dynamics and bioenergetics in diabetic skeletal muscle. PloS one. 2014;9(3):e92810. doi:10.1371/journal.pone.0092810.

186. Anderson EJ, Lustig ME, Boyle KE, Woodlief TL, Kane DA, Lin CT et al. Mitochondrial H2O2 emission and cellular redox state link excess fat intake to insulin resistance in both rodents and humans. The Journal of clinical investigation. 2009;119(3):573-81. doi:10.1172/jci37048.

187. Koves TR, Ussher JR, Noland RC, Slentz D, Mosedale M, Ilkayeva O et al. Mitochondrial overload and incomplete fatty acid oxidation contribute to skeletal muscle insulin resistance. Cell metabolism. 2008;7(1):45-56. doi:10.1016/j.cmet.2007.10.013.

188. Flynn JM, Melov S. SOD2 in mitochondrial dysfunction and neurodegeneration. Free radical biology & medicine. 2013;62:4-12. doi:10.1016/j.freeradbiomed.2013.05.027.

189. Di Meo S, Reed TT, Venditti P, Victor VM. Role of ROS and RNS Sources in Physiological and Pathological Conditions. Oxidative medicine and cellular longevity. 2016;2016:1245049. doi:10.1155/2016/1245049.

190. Loehr JA, Stinnett GR, Hernandez-Rivera M, Roten WT, Wilson LJ, Pautler RG et al. Eliminating Nox2 reactive oxygen species production protects dystrophic skeletal muscle from pathological calcium influx assessed in vivo by manganese-enhanced magnetic resonance imaging. The Journal of physiology. 2016. doi:10.1113/jp272907.

191. Appell HJ, Duarte JA, Soares JM. Supplementation of vitamin E may attenuate skeletal muscle immobilization atrophy. International journal of sports medicine. 1997;18(3):157-60.

192. Whidden MA, Smuder AJ, Wu M, Hudson MB, Nelson WB, Powers SK. Oxidative stress is required for mechanical ventilation-induced protease activation in the diaphragm. Journal of applied physiology (Bethesda, Md : 1985). 2010;108(5):1376-82. doi:10.1152/japplphysiol.00098.2010.

193. McClung JM, Judge AR, Talbert EE, Powers SK. Calpain-1 is required for hydrogen peroxide-induced myotube atrophy. American journal of physiology Cell physiology. 2009;296(2):C363-71. doi:10.1152/ajpcell.00497.2008.

194. Powers SK, Morton AB, Ahn B, Smuder AJ. Redox control of skeletal muscle atrophy. Free radical biology & medicine. 2016;98:208-17. doi:10.1016/j.freeradbiomed.2016.02.021.

195. Kondo H, Miura M, Itokawa Y. Oxidative stress in skeletal muscle atrophied by immobilization. Acta physiologica Scandinavica. 1991;142(4):527-8. doi:10.1111/j.1748-1716.1991.tb09191.x.

196. Powers SK, Smuder AJ, Criswell DS. Mechanistic links between oxidative stress and disuse muscle atrophy. Antioxidants & redox signaling. 2011;15(9):2519-28. doi:10.1089/ars.2011.3973.

197. Schwartz LM, Brown C, McLaughlin K, Smith W, Bigelow C. The myonuclear domain is not maintained in skeletal muscle during either atrophy or programmed cell death. American journal of physiology Cell physiology. 2016;311(4):C607-c15. doi:10.1152/ajpcell.00176.2016.

198. Brooks NE, Myburgh KH. Skeletal muscle wasting with disuse atrophy is multi-dimensional: the response and interaction of myonuclei, satellite cells and signaling pathways. Frontiers in physiology. 2014;5:99. doi:10.3389/fphys.2014.00099.

199. Pallafacchina G, Blaauw B, Schiaffino S. Role of satellite cells in muscle growth and maintenance of muscle mass. Nutrition, metabolism, and cardiovascular diseases : NMCD. 2013;23 Suppl 1:S12-8. doi:10.1016/j.numecd.2012.02.002.

200. Fei F, Zhu DL, Tao LJ, Huang BZ, Zhang HH. Protective effect of ATP on skeletal muscle satellite cells damaged by H(2)O(2). Journal of Huazhong University of Science and Technology Medical sciences = Hua zhong ke ji da xue xue bao Yi xue Ying De wen ban = Huazhong keji daxue xuebao Yixue Yingdewen ban. 2015;35(1):76-81. doi:10.1007/s11596-015-1392-7.

201. Li YP, Chen Y, Li AS, Reid MB. Hydrogen peroxide stimulates ubiquitin-conjugating activity and expression of genes for specific E2 and E3 proteins in skeletal muscle myotubes. American journal of physiology Cell physiology. 2003;285(4):C806-12. doi:10.1152/ajpcell.00129.2003.

202. O'Loghlen A, Perez-Morgado MI, Salinas M, Martin ME. N-acetyl-cysteine abolishes hydrogen peroxide-induced modification of eukaryotic initiation factor 4F activity via distinct signalling pathways. Cellular signalling. 2006;18(1):21-31. doi:10.1016/j.cellsig.2005.03.013.

203. Zhang L, Kimball SR, Jefferson LS, Shenberger JS. Hydrogen peroxide impairs insulin-stimulated assembly of mTORC1. Free radical biology & medicine. 2009;46(11):1500-9. doi:10.1016/j.freeradbiomed.2009.03.001.

204. Shenkman BS, Belova SP, Lomonosova YN, Kostrominova TY, Nemirovskaya TL. Calpain-dependent regulation of the skeletal muscle atrophy following unloading. Archives of biochemistry and biophysics. 2015;584:36-41. doi:10.1016/j.abb.2015.07.011.

205. Velazquez KT, Enos RT, Narsale AA, Puppa MJ, Davis JM, Murphy EA et al. Quercetin supplementation attenuates the progression of cancer cachexia in ApcMin/+ mice. The Journal of nutrition. 2014;144(6):868-75. doi:10.3945/jn.113.188367.

206. Assi M, Rebillard A. The Janus-Faced Role of Antioxidants in Cancer Cachexia: New Insights on the Established Concepts. Oxidative medicine and cellular longevity. 2016;2016:9579868. doi:10.1155/2016/9579868.

207. Tisdale MJ. Biology of cachexia. Journal of the National Cancer Institute. 1997;89(23):1763-73.

208. Laviano A, Meguid MM, Inui A, Muscaritoli M, Rossi-Fanelli F. Therapy insight: Cancer anorexia-cachexia syndrome--when all you can eat is yourself. Nature clinical practice Oncology. 2005;2(3):158-65. doi:10.1038/ncponc0112.

209. Tan BH, Fearon KC. Cachexia: prevalence and impact in medicine. Current opinion in clinical nutrition and metabolic care. 2008;11(4):400-7. doi:10.1097/MCO.0b013e328300ecc1.

210. DeBoer MD. Animal models of anorexia and cachexia. Expert opinion on drug discovery. 2009;4(11):1145-55. doi:10.1517/17460440903300842.

211. DeBoer MD, Scarlett JM, Levasseur PR, Grant WF, Marks DL. Administration of IL-1beta to the 4th ventricle causes anorexia that is blocked by agouti-related peptide and that coincides with activation of tyrosine-hydroxylase neurons in the nucleus of the solitary tract. Peptides. 2009;30(2):210-8. doi:10.1016/j.peptides.2008.10.019.

212. Plata-Salaman CR, Oomura Y, Kai Y. Tumor necrosis factor and interleukin-1 beta: suppression of food intake by direct action in the central nervous system. Brain research. 1988;448(1):106-14.

213. Acharyya S, Ladner KJ, Nelsen LL, Damrauer J, Reiser PJ, Swoap S et al. Cancer cachexia is regulated by selective targeting of skeletal muscle gene products. Journal of Clinical Investigation. 2004;114(3):370-8. doi:10.1172/JCI200420174.

214. Weyermann P, Dallmann R, Magyar J, Anklin C, Hufschmid M, Dubach-Powell J et al. Orally available selective melanocortin-4 receptor antagonists stimulate food intake and reduce cancer-induced cachexia in mice. PloS one. 2009;4(3):e4774. doi:10.1371/journal.pone.0004774.

215. DeBoer MD, Zhu XX, Levasseur P, Meguid MM, Suzuki S, Inui A et al. Ghrelin treatment causes increased food intake and retention of lean body mass in a rat model of cancer cachexia. Endocrinology. 2007;148(6):3004-12. doi:10.1210/en.2007-0016.

216. Chen C, Tucci FC, Jiang W, Tran JA, Fleck BA, Hoare SR et al. Pharmacological and pharmacokinetic characterization of 2-piperazine-alpha-isopropyl benzylamine derivatives as melanocortin-4 receptor antagonists. Bioorganic & medicinal chemistry. 2008;16(10):5606-18. doi:10.1016/j.bmc.2008.03.072.

217. Guo D, Wang C, Wang Q, Qiao Z, Tang H. Pantoprazole blocks the JAK2/STAT3 pathway to alleviate skeletal muscle wasting in cancer cachexia by inhibiting inflammatory response. Oncotarget. 2017;8(24):39640-8. doi:10.18632/oncotarget.17387.

218. Wang Z, Wang W, Qiu W, Fan Y, Zhao J, Wang Y et al. Involvement of ghrelin-growth hormone secretagogue receptor system in pathoclinical profiles of digestive system cancer. Acta biochimica et biophysica Sinica. 2007;39(12):992-8.

219. Wisse BE, Frayo RS, Schwartz MW, Cummings DE. Reversal of cancer anorexia by blockade of central melanocortin receptors in rats. Endocrinology. 2001;142(8):3292-301. doi:10.1210/endo.142.8.8324.

220. Hanada T, Toshinai K, Date Y, Kajimura N, Tsukada T, Hayashi Y et al. Upregulation of ghrelin expression in cachectic nude mice bearing human melanoma cells. Metabolism: clinical and experimental. 2004;53(1):84-8.

221. Beck SA, Tisdale MJ. Production of lipolytic and proteolytic factors by a murine tumor-producing cachexia in the host. Cancer research. 1987;47(22):5919-23.

222. Piffar PM, Fernandez R, Tchaikovski O, Hirabara SM, Folador A, Pinto GJ et al. Naproxen, clenbuterol and insulin administration ameliorates cancer cachexia and reduce tumor growth in Walker 256 tumor-bearing rats. Cancer letters. 2003;201(2):139-48.

223. Markison S, Foster AC, Chen C, Brookhart GB, Hesse A, Hoare SR et al. The regulation of feeding and metabolic rate and the prevention of murine cancer cachexia with a small-molecule melanocortin-4 receptor antagonist. Endocrinology. 2005;146(6):2766-73. doi:10.1210/en.2005-0142.

224. Marks DL, Ling N, Cone RD. Role of the central melanocortin system in cachexia. Cancer research. 2001;61(4):1432-8.

225. Carson JA, Baltgalvis KA. Interleukin-6 as a Key Regulator of Muscle Mass during Cachexia. Exercise and sport sciences reviews. 2010;38(4):168-76. doi:10.1097/JES.0b013e3181f44f11.

226. Maddocks M, Hopkinson J, Conibear J, Reeves A, Shaw C, Fearon KC. Practical multimodal care for cancer cachexia. Current opinion in supportive and palliative care. 2016;10(4):298-305. doi:10.1097/spc.0000000000000241.

Chapter 2

Doctoral Dissertation Proposal

Cancer is one of the leading causes of death worldwide with over half of the people affected by cancer dying as a result of the condition [2, 3]. Cancer-cachexia is a wasting syndrome that occurs in approximately 80% of cancer patients [4-6]. In fact, cancer-cachexia is the primary cause of death for 22%-30% of all individuals with cancer [4-6]. Cancer-cachexia is defined as a multifactorial syndrome which displays an ongoing loss of skeletal muscle mass (with or without loss of fat mass) that cannot be fully reversed by conventional nutritional support and leads to progressive functional impairment [4, 6]. Underlying mechanisms of cancer-cachexia are not fully understood.

Cancer-cachexia is associated with reduced muscle protein synthesis and increased muscle protein breakdown [7, 8], which leads to a loss of skeletal muscle mass [9]. The progression of signaling which induces cancer-cachexia is not understood. Cancer-cachexia is likely metabolically induced; therefore, mitochondrial degeneration may prompt cancer-cachexia. Mitochondrial degeneration results in inefficient ATP production and excess mitochondrial reactive oxygen species (ROS) production. Therefore, the central hypothesis of this proposal is mitochondrial degeneration occurs before the onset of measurable cancer-cachexia and aiding cellular capacity to neutralize mitochondrial ROS prevents cancer induced muscle wasting (Fig. 1).

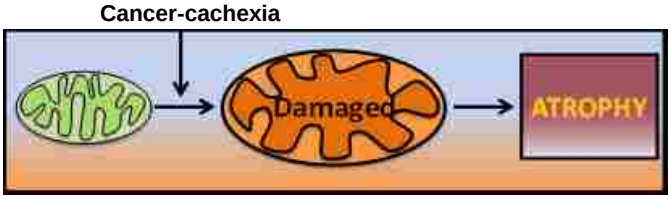

Figure 2-1. Schematic of the central hypothesis.

Specific Aim 1: ***Analyzed degeneration of the mitochondrial network throughout the progression of cancer-cachexia.*** Phosphate Buffered Saline (PBS) or Lewis Lung Carcinoma was implanted to the hind flank of C57Bl/6J mice at 8 weeks of age. The tumor was allowed to develop for 1, 2, 3 or 4 weeks. Reporter gene Mitotimer was utilized to directly assess mitochondrial quality. Mitotimer shifts from a green to a red fluorescent spectra when the mitochondrial network is damaged. Mitotimer was electroporated into C57Bl/6J mice at 6 weeks of age (2 weeks prior to tumor implantation). A 30% increase in mitotimer's red/green fluorescent ratio was considered severe mitochondrial degeneration in accordance to previous literature [10]. Mitochondrial degeneration can lead to a loss of mitochondrial function and excess mitochondrial ROS production; therefore, mitochondrial respiration and reactive oxygen species production were measured throughout the progression of cancer-cachexia. Succinate Dehydrogenase staining was used to assess the amount of oxidative and non-oxidative muscle fibers. Immunoblot was utilized to analyze regulators of the mitochondrial network and antioxidant enzymes.

Specific Aim 2: ***Utilized a time course of the progression of Cancer-cachexia to analyze dysregulation in protein turnover signaling.*** Muscle atrophy was assessed by muscle wet weights and cross sectional area (CSA). Groups with 10% decrease in muscle wet weights and/or a mean decrease of 30% in the CSA of the Tibialis Anterior muscle when compared to PBS control injection was considered cachectic in accordance to previous literature [11-14] . 24-hour protein synthesis was measured using deuterium oxide labelling followed by GC-MS based assessment. Immunoblot and RT-PCR was used to measure the expression and signaling of key enzymes in muscle wasting pathways (denervation, myogenesis, protein synthesis, autophagy, E3 ligase/proteasome). TUNEL assay was utilized to assess apoptotic nuclei.

Specific Aim 3: ***Determined enhanced mitochondrial ROS scavenging is sufficient to attenuate cancer-cachexia In-Vitro and examine the role of MAPK in the onset of cancer-cachexia In-Vitro.*** Myotubes were treated with either control (Con, Low serum media: 25% volume of 10% fetal bovine serum growth media diluted in serum free media) or LLC conditioned media (LCM, 25% volume of LLC conditioned 10% fetal bovine serum diluted in serum free media). Mito-TEMPO (MitoT, a mitochondrial specific antioxidant) was given to a subset of myotubes in each group. Myotube diameter was assessed in all experimental conditions. Inhibitors specific to p38 and ERK 1/2 MAPK were used in Con and LCM conditions were used to assess the role of MAPK in the loss of myotube diameter. Immunoblot and RT-PCR were used to measure dependent variables specific to protein breakdown.

These experiments gave insight to mechanisms behind cancer-cachexia and will open doors to new therapeutic treatments to combat cancer-cachexia.

Research Strategy

A.Significance

A1. Cancer-cachexia is a major health care problem. While skeletal muscle atrophy is common to many chronic disease conditions [15-17], it is especially problematic in cancer [6, 4]. Cancer-cachexia is defined as a multifactorial syndrome which displays an ongoing loss of skeletal muscle mass (with or without loss of fat mass) that cannot be fully reversed by conventional nutritional support and leads to progressive functional impairment [4, 6]. Cancer-cachexia has been linked to increase mortality during hospital visits [18] and increases likelihood of death [15]. In fact, cancer-cachexia is the primary cause of death for 22%-30% of all individuals with cancer [4, 5]. Moreover, cancer-cachexia is costly to treat [19]. **Current therapies to prevent muscle wasting are not fully efficacious; therefore, a critical need**

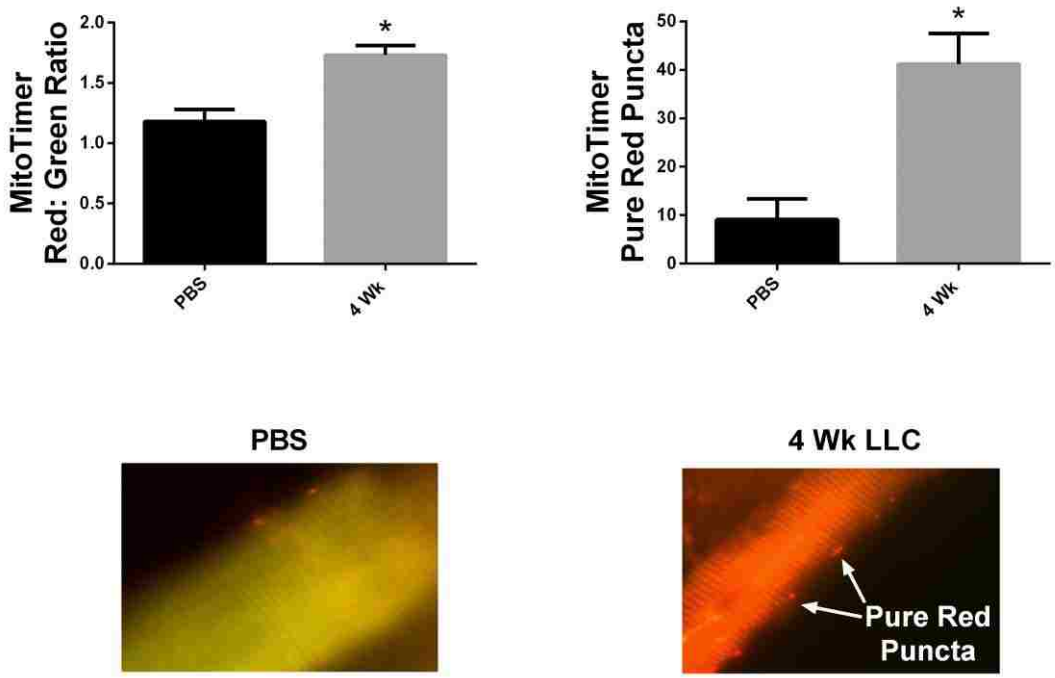

Figure 2-2. Two weeks prior to LLC implantation the fluorescent reporter pMitoTimer[1] was transfected into contralateral flexor digitorum brevis muscles. MitoTimer is a mitochondrially targeted variant of DsRed, validated by Laker et al.[1] to emit green fluorescence when mitochondria are "healthy" and shift to red when mitochondria are "damaged". Construct quantified by calculation of the ratio of red:green fluorescence whereby a greater red:green ratio signifies degenerated mitochondria. Locations of pure red puncta colocalize with LC3 and appear to represent completely degenerated mitochondria targeted for autophagy[1].

remains to identify mechanisms and potential therapeutic targets to prevent muscle atrophy in disease states.

Cancer-cachexia is a result of an imbalance of protein turnover favoring protein degradation; however, underlying mechanisms are not clear. In cancer-cachexia, it is apparent muscle atrophy is metabolically induced [20-22]. Energy stress instigated from tumor derived factors induces increased protein breakdown and a reduction in protein synthesis [7, 8]. The mitochondria is responsible for the majority of cellular energy production. A potential mechanism behind the cellular energy stress induced by tumor burden is mitochondrial

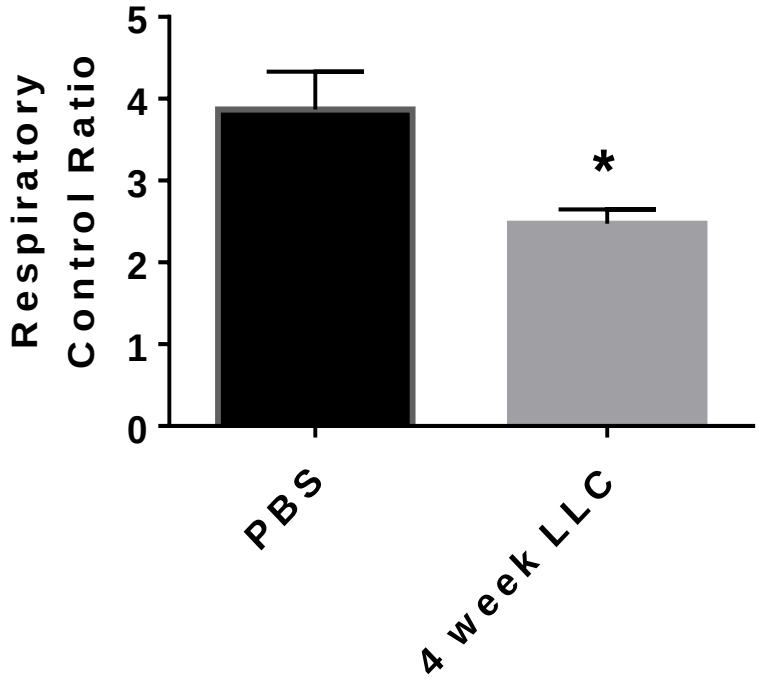

Figure 2-3. Mitochondrial dysfunction in Cancer-Cachexia. Respiratory control ratio measured in plantaris muscle of C57BL/6J mice 4 weeks following implantation of $1X10^6$ Lewis Lung Carcinoma cells in the hind flank. Mitochondrial function in permeabilized plantaris muscle.

degeneration. Mitochondrial degeneration results in inefficient ATP production and excess mitochondrial ROS production.

A2. Mitochondrial degeneration is apparent in cancer-cachexia. Development of mitochondrial dysfunction and derangements in response to tumor burden may instigate skeletal muscle atrophy. Mitochondrial degeneration leads to skeletal muscle atrophy through a number of different mechanisms including impaired ATP production and excess mitochondrial ROS excretion which reduces protein synthesis and promotes protein breakdown [23]. Due to the mitochondria's central role in cellular metabolism, mitochondrial degeneration may instigate cancer-cachexia [24, 22, 25]. Furthermore, we have more recently acquired preliminary evidence of mitochondrial degeneration utilizing Mitotimer (a mitochondrially targeted plasmid which

shifts from green to red fluorescence upon mitochondrial damage [1], Fig 2). This suggests that tumor burden elicits mitochondrial degeneration, which may induce cancer-cachexia.

Experiments will identify if mitochondrial degeneration precedes cancer-cachexia. Mitochondrial degeneration inevitably leads to a loss of mitochondrial function which results in reduced ATP production leading to skeletal muscle wasting. I have preliminary evidence that suggests mitochondrial function is impaired 4 wks following tumor implantation (Fig 3).

A3. Cancer-cachexia is associated with impaired regulation of the mitochondrial network. In order to effectively perform oxidative metabolism, several regulatory processes must be implemented to ensure mitochondrial health. These processes include the biogenesis of new mitochondrial components, fusion and fission of new and damaged mitochondrial regions with the network (dynamics), and the selective degradation of damaged mitochondrial regions through the process of autophagy (mitophagy) [26]. Cancer-cachexia appears to be associated with dysregulation of mitochondrial quality controllers according to our data (Fig 4). Intriguingly it appears dysregulation of mitochondrial biogenesis and dynamics occurs prior to severe cachexia (Fig 4). Therefore, *evidence exists that mitochondrial degeneration precedes cancer-cachexia and may be the instigation event.*

A4. Aiding in mitochondrial ROS neutralization may attenuate cancer-cachexia. Mitochondrial degeneration is prevalent in many atrophic conditions; however, whether alleviating atrophy by neutralizing mitochondrial ROS is less certain. Additionally, mitochondrial degeneration is associated with excess ROS leak from the mitochondria which may provide the primary mechanism of muscle atrophy via ROS-induced damage to other

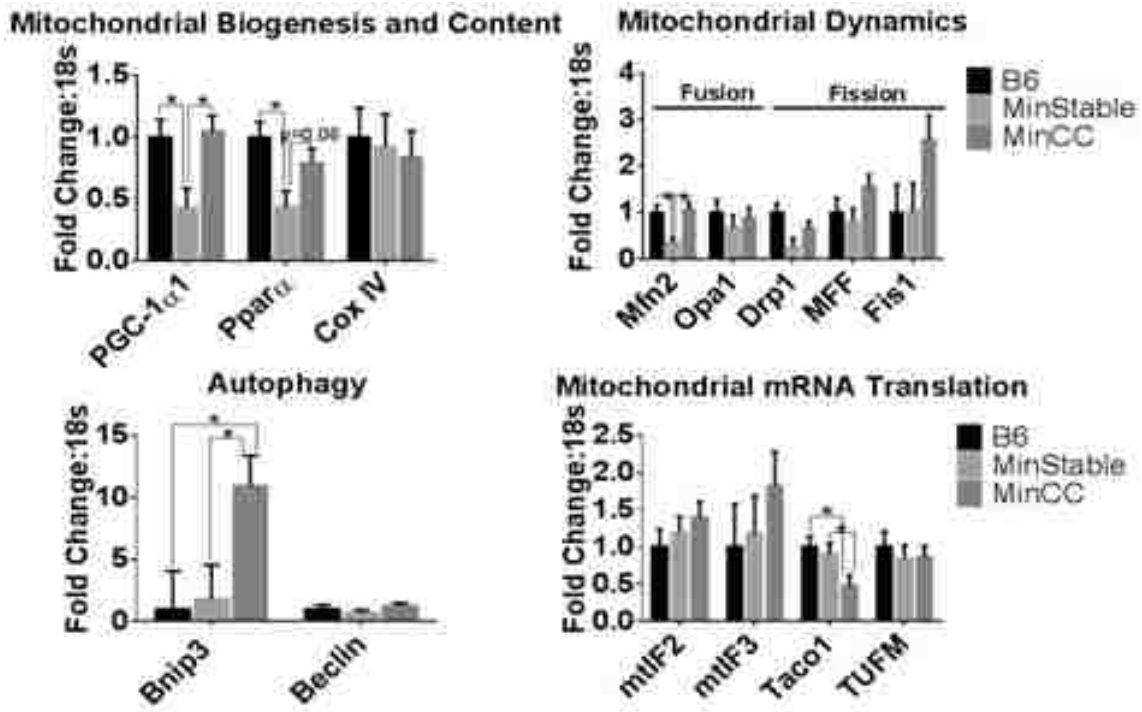

Figure 2-4: Mitochondrial quality control regulators are disrupted prior to wasting in a colorectal cancer model to study cancer-cachexia.

cellular mechanisms (i.e., protein accretion)[25]. Recent studies suggest: genetic enhancement of mitochondrial antioxidant defense through transgenic overexpression of mitochondrial catalase (MCAT) improves muscle function in aging [27] and inhibition of the ROS producer NADPH Oxidase may attenuate Duchenne Muscular Dystrophy [28].; therefore, aiding in the capacity to neutralize mitochondrial ROS may prevent cancer-cachexia. Mitotimer is a reporter gene that shifts from green to red fluorescence upon oxidation of a handful of amino acids [10] ;therefore, preliminary evidence suggests that ROS is elevated due to tumor burden (Fig 2). However, these data do not elucidate if mitochondrial ROS scavenging protects against muscle atrophy. Therefore, ***it is likely that promoting mitochondrial quality by mitochondrial antioxidant defense mechanisms may prevent cancer-cachexia.***

A5. MAPK involvement in cancer-mediated muscle wasting. In models to study cancer-cachexia, it appears that p38 MAPK expression is induced in response to tumor burden [29], and experimental evidence suggests inhibition of both p38 and ERK 1/2 MAPK may attenuate cancer-induced muscle loss [30]. Other literature indicates this may be mediated through the ubiquitin proteasome system [31, 30, 32]. Furthermore, ROS is a mediator for the induction of p38 MAPK and inhibition of p38 MAPK partially prevents loss of myotube diameter *In-Vitro* [33]. Therefore, p38 and ERK 1/2 MAPK may be potential therapeutic targets to treat cancer-cachexia.

The central hypothesis of this proposal was mitochondrial degeneration occurs before the onset of measurable cancer-cachexia and aiding cellular capacity to neutralize mitochondrial ROS prevents cancer induced muscle wasting (Fig. 1).

B. Innovation

The proposed study was *innovative in observing atrophic signaling during the progression of the development of cancer-cachexia and used innovative methodologies to target the primary research questions*. The approach of assessing the timecourse of cancer-cachexia to identify and compare the onset of muscle mitochondrial derangements and atrophy mechanisms was novel and provided greater understanding of the pathogenesis of cancer-cachexia. We utilized multiple approaches to identify mechanisms of muscle atrophy as well as mitochondrial degeneration. This represented a first of its kind encompassing approach to understand the progression of cancer-cachexia. While prior evidence suggests that oxidative stress may be involved in the onset of cancer-cachexia, no study has attempted to prevent cancer-cachexia by specifically neutralizing ROS in skeletal muscle. Therefore, the study was *innovative in the proposed hypothesis* for underlying mechanisms for cancer-cachexia. Additionally, we used

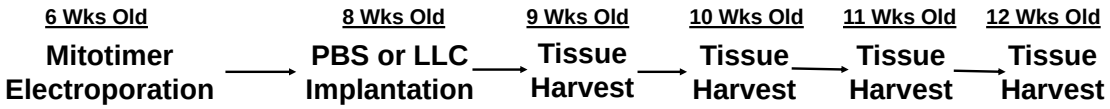

Figure 2-5: Schematic of Experimental Design for Aim 1 and 2.

innovative methodologies to examine multiple modalities of muscle atrophy and determine the role of mitochondrial degeneration in atrophy. This study was the first to use Mitotimer to measure mitochondrial degeneration in cancer-cachexia. Moreover, mitochondrial function and mitochondrial ROS production were not examined in cancer-cachexia.

C. Approach

Overall approach. In order to test the central hypothesis, I perfomed a series of experiments designed to reveal if mitochondrial degeneration precedes cancer-cachexia and uncover if ROS is involved in the onset of cancer-cachexia. I performed timecourse assessments of muscle atrophy and mitochondrial quality throughout the progression of cancer-cachexia using the Lewis Lung Carcinoma (LLC) tumor implantation model in order to determine atrophic signaling that leads to cancer-cachexia and examine mitochondrial degeneration throughout the progression of cancer-cachexia. These experiments gave valuable insight into metabolic aspects which induce cancer-cachexia. We utilized MitoT to ameliorate cancer-cachexia *in-vitro* by increasing cellular capacity to neutralize mitochondrial ROS production, a negative by-product of damaged mitochondria. These experiments provided novel information for mechanisms which will induce cancer-cachexia and provided novel therapeutic targets for the treatment of cancer-cachexia.

Specific Aim 1.Determined if mitochondrial network degeneration preceded cancer-cachexia. Hypothesis and Rationale. We hypothesized mitochondrial derangements precede the development of cancer-cachexia and may instigate muscle wasting. Preliminary data

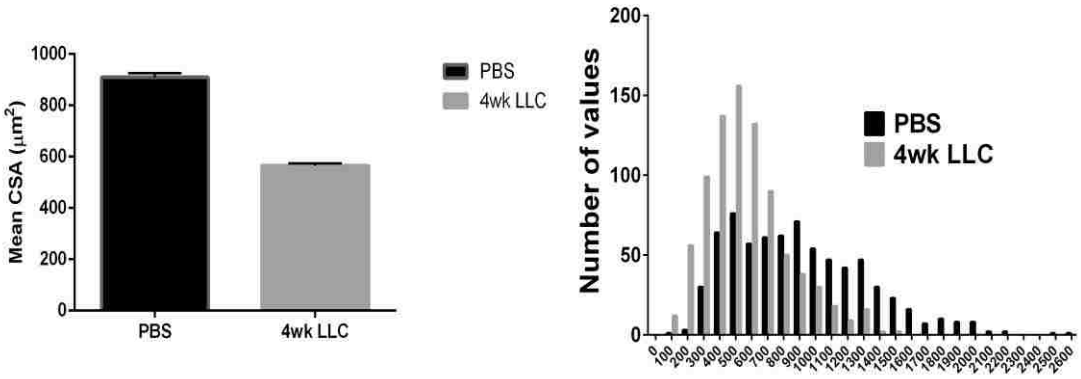

Figure 2-6. Mean CSA and a histogram of values in PBS and 4 wk LLC animals. There is a dramatic decrease in mean CSA and an increase in the number of small muscle fibers in the 4wk LLC group.

suggested dysregulation of proteins which aid in the maintenance of the mitochondrial network (Fig 4). These mitochondrial impairments may present before cancer-cachexia . To test this hypothesis, we proposed to examine mitochondrial quality and function throughout the development of cancer-cachexia.

Culturing of LLC Cells: LLC cells were cultured in 10% Fetal Bovine Serum Growth Media with 1% Penicillin and Streptomycin added. Once confluent, cells will be trypsinized, counted and diluted in PBS for implantation.

Induction of muscle atrophy by cancer-cachexia. For tumor implantation we performed LLC implantation. Briefly, LLC was implanted to the hind flank of anesthetized mice at $1X10^6$ cells in a 100 µL suspension in sterile PBS. Atrophy was allowed to develop for up to 4 wks, similar to prior reports, and cohorts harvested weekly.

Model confirmation. To confirm atrophy and validate models we examined hindlimb muscle wet weights and cross-sectional area (CSA) of TA myofibers. Groups with 10% decrease in muscle wet weights and/or a mean decrease of 30% in the CSA of the Tibialis Anterior muscle

when compared to PBS control injection was considered cachectic (Fig 6). These numbers were consistent with previous literature [11, 12, 34].

Fluorescent reporter. MitoTimer was delivered by electric pulse-mediated gene transfer to flexor digitorum brevis muscles 2 wks prior to tumor implantation. To assure data quality MitoTimer fluorescence was assessed day of tissue harvest and microscopy acquisition parameters were carefully controlled using the Nikon TiS fluorescent microscope. We measured the ratio of red:green fluorescence and number of pure red puncta (completely degenerated mitochondria) (Fig 2).

Mitochondrial respiration and ROS emission: Small strips, ~10 mg, of muscle were teased to near-single fibers and permeabilized with saponin to open small pores in the membrane. Mitochondrial oxygen consumption (VO_2) of a permeabilized fiber bundle was measured as described. Mitochondria were primed with malate and glutamate. Maximal respiration (ADP-stimulated, state 3) and state 4 respiration were measured. The respiratory control ratio (RCR) was calculated by dividing state 3 by state 4. The dry weight of the permeabilized mitochondria was used to normalize the results. ROS emission was measured using amplex red hydrogen peroxide detection kit. In the presence of horse radish peroxidase, the Amplex Red reagent reacts with H_2O_2 in a 1:1 stoichiometry to produce the red-fluorescent oxidation product, resorufin.

Succinate Dehydrogenase Staining: Tibialis Anterior (TA) muscles were embedded in optimal cutting temperature (OCT) compound and frozen in liquid nitrogen cooled isopentane. Sections were cut at 10 µm using a cryostat and stained for Succinate Dehydrogenase (SDH). Sections were placed in incubation solution (50 mM Soduim succinate, 50 mM phosphate buffer, 0.12M KH2PO4 & 0.88M Na2HPO4), 0.5 mg/ml Nitroblue tetrazolium for 40 min in a 37o C

water bath. Slides were washed 3 min with dH2O and imaged. Images were collected with Nikon Sight DS-Vi1 camera mounted on an Olympus CKX41 inverted microscope. SDH+ (purple) and SDH– fibers were counted, cross-validated by two independent and blinded investigators, and circled for cross sectional area analysis using Nikon Basic Research Imaging Software.

Analysis of Mitochondrial Regulatory Proteins: Immunoblot and RT-PCR were performed in order to measure the protein content of key proteins involved in mitochondrial regulatory processes. Immunoblot targets included are PGC-1α, COX IV, CYT C, TFAM, PPARα/γ, NRF2, MFN 1/2, DRP1, FIS1, OPA1 and BNIP3.

*Statistics and Sample Size Determination***.** To determine differences among conditions, a One-way ANOVA with a factor of tumor progression between groups was used for the global analysis. To delineate differences among means, the Student Newman Keuls post hoc test was used. I estimated that 8 animals/group were needed to achieve statistical significance at $\alpha = 0.05$ and $\beta = 0.20$ (power = 0.80).

Anticipated Results and Interpretation of Findings. We expected mitochondrial degeneration to precede cancer-cachexia suggesting mitochondrial degeneration may instigate cancer-cachexia. The use of directly measuring mitochondrial quality by Mitotimer as well as functional measurements and ROS assays provided significant insight into mechanisms of mitochondrial dysfunction. Multiple modes of muscle wasting are present in cancer-cachexia, and *mitochondrial degeneration may be behind the induction of all modes of muscle wasting in cancer based on our data*.

Potential Problems and Contingency Plans. While preliminary evidence is clear that mitochondrial degeneration takes place in cancer-cachexia, we were not sure if it preceded muscle wasting and instead occured concomitantly. Loss of mitochondrial function in a muscle

wasting state will not only induce skeletal muscle atrophy, but it will make it difficult to recover from atrophy; therefore, mitochondrial degeneration may still play a significate role in cancer-cachexia. Furthermore, I collaborated with Dr. Michael P. Wiggs in order to successfully complete these assays.

Specific Aim 2.Utilized a time course of the progression of Cancer-cachexia to analyze dysregulation in of protein turnover. Hypothesis and Rationale. We hypothesized cancer-cachexia will occur 4 weeks following tumor implantation demonstrated by a loss of muscle mass and fiber size. Furthermore, we hypothesized that skeletal muscle wasting will be brought on by increased protein breakdown and reduced protein synthesis. Our time frame for inducing cancer-cachexia was based off of prior research from our laboratory and other laboratories [11](Fig.6). To test this hypothesis we proposed to examine muscle atrophy over the course of cancer-cachexia progression (Fig 5).

Culturing LLC cells. Was performed as in Aim 1.

Induction of Muscle Atrophy by Cancer-Cachexia and conformation of model. Was performed as in Aim 1.

Measurement of Protein Synthesis: A bolus of deuterium oxide was injected intraperitoneally in the mouse approximately 24 hours before tissue collection. Each mouse was then given 4% deuterated drinking water in order to maintain the levels of deuterium oxide in the blood [35-37]. The deuterium is transferred to amino acids inside the cell before the amino acid is incorporated in the protein chain. GC-MS was used to detect the deuterium levels in the skeletal muscle to measure 24 hour protein synthesis via the amount of deuterium taken up by the muscle[35-37]. Myofibrillar fraction of muscle was used in order to assess protein synthesis.

This method has been validated in mouse models to give an accurate measurement of protein synthesis [35, 36].

Analysis of Protein Turnover Signaling: Immunoblot and RT-PCR were used to understand alterations in the expression in proteolytic signaling of various pathways. Targets included to AKT, 4EBP1, p70S6K, FOXO 1/3, p62, LC3 A/B, Ubiquitin, Atrogin-1, MuRF and Caspace 3. Post translational modifications such as phosphorylation of targets were measured as necessary to delineate activation of pathways.

TUNEL Assay to measure apoptotic nuclei: 10 μm sections were fixed in 4% paraformaldehyde. Roche Diagnostics (Indianapolis, IN) *In Situ* cell death detection Fluorescein (11684795910) was used to detect damaged DNA. Manufacturer's protocols were used. Slides were mounted with DAPI mounting media. Nikon Ti-S inverted epiflourescent microscope with LED-based light source was used to image total nuclei (DAPI) and TUNEL + nuclei (FITC). Total nuclei and TUNEL + nuclei were then counted using Nikon Basic Research Imaging Software.

*Statistics and Sample Size Determination***.** To determine differences among conditions, a One-way ANOVA with a factor of tumor progression between groups was used for the global analysis. To delineate differences among means, the Student Newman Keuls post hoc test was used. I estimated that 8 animals/group were needed to achieve statistical significance at $\alpha = 0.05$ and $\beta = 0.20$ (power = 0.80).

Anticipated Results and Interpretation of Findings. We anticipated that LLC implantation induced cancer-cachexia after 4 wks tumor growth based off of a reduction of mean CSA and a decrease in muscle wet weight. Furthermore, we anticipated that protein turnover signaling favored catabolic pathways. We hypothesized protein synthesis was decreased by 4 wk LLC.

These data provided novel evidence for mechanisms of cancer-cachexia as well as a time frame in which atrophic pathways are enhanced.

Potential Problems and Contingency. With the tumor implantation model it was possible that not all animals will be able to reach the 4 wk timepoint. To account for this, twice as many animals were utilized than what would be needed to account for premature animal death due to tumor burden. In order to ensure I was able to successfully measure protein synthesis I worked with Dr. Michael Wiggs, an expert on this technique to measure protein synthesis.

Specific Aim 3.Demonstrated that improving ROS scavenging attenuated cancer-cachexia *In-Vitro*. Hypothesis and Rationale. I hypothesized promoting cellular capacity to neutralize mitochondrial ROS by using MitoT was sufficient to attenuate loss of myotube diameter in cells treated with LLC conditioned media. Cancer is associated with an increase in bloodborne factors likely secreted from tumor cells including inflammatory cytokines that induce excess ROS production in skeletal muscle. Damaged mitochondria, are the greatest cellular ROS emitter [38], thereby removal of mitochondrial ROS (MitoT) was likely to prevent such ROS-induced cell damage. This experiment provided evidence for mechanisms of mitochondrial degeneration in cancer-cachexia and demonstrated efficacy of ameliorating cancer-cachexia through promotion of mitochondrial ROS scavenging.

LLC conditioned media. LLC cells were grown to 100% confluence. Media was then filtered and diluted to 25% total volume in serum free media. For the Control group, 10% fetal bovine serum growth media was diluted to 25% total volume with serum free media.

LLC conditioned media decreases myotube diameter. Myotube diameter was assessed ~24 hours after treating C2C12 cells with either Control or LLC conditioned media. Myotube diameter decreased by ~40%.

Drug Treatments. 2 μM of MitoT suspended in DMSO was given to a subset of cell culture wells in both Con and LCM. The DMSO vehicle was administered to cell culture wells in equal volume as the MitoT treatment. SB202190 (p38 MAPK inhibitor) was given to both Con and LCM cells at a concentration of 20 μM. PD098059 (MEK inhibitor upstream of ERK 1/2 MAPK) was administered to both Con and LCM treated cells at a concentration of 20 μM.

Analysis of Protein Breakdown. Immunoblot and RT-PCR were used to understand alterations in the expression in proteolytic signaling of various pathways. Targets included FOXO 1/3, Ubiquitin, Atrogin-1 and MuRF. Post translational modifications such as phosphorylation of targets were measured when it was necessary to delineate activation of pathways.

*Statistics and Sample Size Determination***.** To determine differences among conditions, a two-way ANOVA with factors of tumor (Control Media vs. LLC Conditioned Media) and treatment (Vehicle vs. MitoT) were used for the global analysis. To delineate differences among means, the Student Newman Kuels post hoc test was used. I estimated that an n of 6 in each group was needed to achieve statistical significance at $\alpha = 0.05$ and $\beta = 0.20$ (power = 0.80).

Anticipated Results and Interpretation of Findings. I anticipated that aiding in the scavenging of mitochondrial ROS with MitoT attenuated loss of myotube diameter. I have shown that mitochondrial degeneration is present in cancer-cachexia. Excess mitochondrial ROS production is associated with degeneration, induced skeletal muscle atrophy by a variety of mechanisms. *These findings provided valuable insight to mechanisms that promote cancer-cachexia.*

Potential Problems and Contingency. While our laboratory had vast experience with cell culture experiments, we had only utilized MitoT for a brief period of time. In order to compensate for our inexperience with MitoT, we allotted additional time to troubleshoot cell culture protocols. It was possible that MitoT could have had no effect on myotube diameter; however, this information was still valuable and gave insight to therapies to treat cancer-cachexia.

Timeline. Animal work for Aims 1 and 2 was completed December 2016. Analysis of dependent variables for aims 1 and 2 were completed by December 2017. Writing Aims 1 and 2 was complete by January 2018. Dependent variable analysis for aim 3 was complete by January 2018. Writing for Aim 3 and dissertation overview was complete by February 2018. My dissertation defense was completed by March 2018. By following this plan I was able to graduate with my dissertation by May 2018.

Summary. Cancer is one of the leading causes of death worldwide with over half of the people affected by cancer dying as a result of the condition [2, 3]. Cancer-cachexia is a wasting syndrome that occurs in approximately 80% of cancer patients causing the death of 20-30% of the cancer patients [4, 5]. Cancer-cachexia is multifactorial and cannot be fully reversed by nutritional support [4]; therefore, **understanding underlying mechanisms of cancer-cachexia is critical to the development of adequate therapies.**

These experiments provided novel insight towards mechanisms behind cancer-cachexia. Moreover, this was the first study which focuses on the progression of cancer-cachexia. Utilizing MitoT in order to aid in cellular capacity handle ROS gave mechanistic insight towards the role of mitochondrial ROS in cancer-cachexia. The data from these experiments could lead to novel therapies to treat cancer-cachexia.

References

1. Laker RC, Xu P, Ryall KA, Sujkowski A, Kenwood BM, Chain KH et al. A novel MitoTimer reporter gene for mitochondrial content, structure, stress and damage in vivo. Journal of Biological Chemistry. 2014. doi:10.1074/jbc.M113.530527.

2. Ferlay J, Soerjomataram I, Dikshit R, Eser S, Mathers C, Rebelo M et al. Cancer incidence and mortality worldwide: sources, methods and major patterns in GLOBOCAN 2012. International journal of cancer. 2015;136(5):E359-86. doi:10.1002/ijc.29210.

3. Fitzmaurice C, Dicker D, Pain A, Hamavid H, Moradi-Lakeh M, MacIntyre MF et al. The Global Burden of Cancer 2013. JAMA oncology. 2015;1(4):505-27. doi:10.1001/jamaoncol.2015.0735.

4. Fearon Kenneth CH, Glass David J, Guttridge Denis C. Cancer Cachexia: Mediators, Signaling, and Metabolic Pathways. Cell metabolism. 2012;16(2):153-66. doi:http://dx.doi.org/10.1016/j.cmet.2012.06.011.

5. Onesti JK, Guttridge DC. Inflammation based regulation of cancer cachexia. BioMed research international. 2014;2014:168407. doi:10.1155/2014/168407.

6. Fearon K, Strasser F, Anker SD, Bosaeus I, Bruera E, Fainsinger RL et al. Definition and classification of cancer cachexia: an international consensus. The Lancet Oncology. 2011;12(5):489-95. doi:10.1016/s1470-2045(10)70218-7.

7. Narsale AA, Puppa MJ, Hardee JP, VanderVeen BN, Enos RT, Murphy EA et al. Short-term pyrrolidine dithiocarbamate administration attenuates cachexia-induced alterations to muscle and liver in ApcMin/+ mice. Oncotarget. 2016. doi:10.18632/oncotarget.10699.

8. Oliveira AG, Gomes-Marcondes MC. Metformin treatment modulates the tumour-induced wasting effects in muscle protein metabolism minimising the cachexia in tumour-bearing rats. BMC cancer. 2016;16:418. doi:10.1186/s12885-016-2424-9.

9. Bonaldo P, Sandri M. Cellular and molecular mechanisms of muscle atrophy. Disease Models & Mechanisms. 2013;6(1):25-39. doi:10.1242/dmm.010389.

10. Laker RC, Xu P, Ryall KA, Sujkowski A, Kenwood BM, Chain KH et al. A novel MitoTimer reporter gene for mitochondrial content, structure, stress, and damage in vivo. The Journal of biological chemistry. 2014;289(17):12005-15. doi:10.1074/jbc.M113.530527.

11. Puppa MJ, Gao S, Narsale AA, Carson JA. Skeletal muscle glycoprotein 130's role in Lewis lung carcinoma-induced cachexia. FASEB journal : official publication of the Federation of American Societies for Experimental Biology. 2014;28(2):998-1009. doi:10.1096/fj.13-240580.

12. Carson JA, Hardee JP, VanderVeen BN. The emerging role of skeletal muscle oxidative metabolism as a biological target and cellular regulator of cancer-induced muscle wasting. Seminars in cell & developmental biology. 2016;54:53-67. doi:10.1016/j.semcdb.2015.11.005.

13. White JP, Puppa MJ, Sato S, Gao S, Price RL, Baynes JW et al. IL-6 regulation on skeletal muscle mitochondrial remodeling during cancer cachexia in the ApcMin/+ mouse. Skeletal muscle. 2012;2:14. doi:10.1186/2044-5040-2-14.

14. Velazquez KT, Enos RT, Narsale AA, Puppa MJ, Davis JM, Murphy EA et al. Quercetin supplementation attenuates the progression of cancer cachexia in ApcMin/+ mice. The Journal of nutrition. 2014;144(6):868-75. doi:10.3945/jn.113.188367.

15. Egerman MA, Glass DJ. Signaling pathways controlling skeletal muscle mass. Critical reviews in biochemistry and molecular biology. 2014;49(1):59-68. doi:10.3109/10409238.2013.857291.

16. Koopman R, Ryall JG, Church JE, Lynch GS. The role of beta-adrenoceptor signaling in skeletal muscle: therapeutic implications for muscle wasting disorders. Current opinion in clinical nutrition and metabolic care. 2009;12(6):601-6. doi:10.1097/MCO.0b013e3283318a25.

17. Polge C, Heng AE, Combaret L, Bechet D, Taillandier D, Attaix D. Recent progress in elucidating signalling proteolytic pathways in muscle wasting: potential clinical implications. Nutrition, metabolism, and cardiovascular diseases : NMCD. 2013;23 Suppl 1:S1-5. doi:10.1016/j.numecd.2012.08.008.

18. Moisey LL, Mourtzakis M, Cotton BA, Premji T, Heyland DK, Wade CE et al. Skeletal muscle predicts ventilator-free days, ICU-free days, and mortality in elderly ICU patients. Critical care (London, England). 2013;17(5):R206. doi:10.1186/cc12901.

19. Janssen I, Shepard DS, Katzmarzyk PT, Roubenoff R. The healthcare costs of sarcopenia in the United States. Journal of the American Geriatrics Society. 2004;52(1):80-5.

20. Baltgalvis KA, Berger FG, Peña MMO, Davis JM, White JP, Carson JA. Muscle Wasting and Interleukin-6-Induced Atrogin-I Expression in the Cachectic Apc(Min/+) Mouse. Pflugers Archiv : European journal of physiology. 2009;457(5):989-1001. doi:10.1007/s00424-008-0574-6.

21. Li P, Waters RE, Redfern SI, Zhang M, Mao L, Annex BH et al. Oxidative phenotype protects myofibers from pathological insults induced by chronic heart failure in mice. The American journal of pathology. 2007;170(2):599-608. doi:10.2353/ajpath.2007.060505.

22. Yu Z, Li P, Zhang M, Hannink M, Stamler JS, Yan Z. Fiber type-specific nitric oxide protects oxidative myofibers against cachectic stimuli. PloS one. 2008;3(5):e2086. doi:10.1371/journal.pone.0002086.

23. Alleman RJ, Katunga LA, Nelson MA, Brown DA, Anderson EJ. The "Goldilocks Zone" from a redox perspective-Adaptive vs. deleterious responses to oxidative stress in striated muscle. Frontiers in physiology. 2014;5:358. doi:10.3389/fphys.2014.00358.

24. Okutsu M, Call JA, Lira VA, Zhang M, Donet JA, French BA et al. Extracellular superoxide dismutase ameliorates skeletal muscle abnormalities, cachexia, and exercise intolerance in mice

with congestive heart failure. Circulation Heart failure. 2014;7(3):519-30. doi:10.1161/circheartfailure.113.000841.

25. Gilliam LA, Moylan JS, Patterson EW, Smith JD, Wilson AS, Rabbani Z et al. Doxorubicin acts via mitochondrial ROS to stimulate catabolism in C2C12 myotubes. American journal of physiology Cell physiology. 2012;302(1):C195-202. doi:10.1152/ajpcell.00217.2011.

26. Yan Z, Lira VA, Greene NP. Exercise training-induced regulation of mitochondrial quality. Exercise and sport sciences reviews. 2012;40(3):159-64. doi:10.1097/JES.0b013e3182575599.

27. Umanskaya A, Santulli G, Xie W, Andersson DC, Reiken SR, Marks AR. Genetically enhancing mitochondrial antioxidant activity improves muscle function in aging. Proc Natl Acad Sci U S A. 2014;111(42):15250-5. doi:10.1073/pnas.1412754111.

28. Pal R, Palmieri M, Loehr JA, Li S, Abo-Zahrah R, Monroe TO et al. Src-dependent impairment of autophagy by oxidative stress in a mouse model of Duchenne muscular dystrophy. Nat Commun. 2014;5. doi:10.1038/ncomms5425.

29. Verzola D, Bonanni A, Sofia A, Montecucco F, D'Amato E, Cademartori V et al. Toll-like receptor 4 signalling mediates inflammation in skeletal muscle of patients with chronic kidney disease. Journal of cachexia, sarcopenia and muscle. 2017;8(1):131-44. doi:10.1002/jcsm.12129.

30. Chacon-Cabrera A, Fermoselle C, Urtreger AJ, Mateu-Jimenez M, Diament MJ, de Kier Joffe ED et al. Pharmacological strategies in lung cancer-induced cachexia: effects on muscle proteolysis, autophagy, structure, and weakness. Journal of cellular physiology. 2014;229(11):1660-72. doi:10.1002/jcp.24611.

31. Zhang G, Lin R-K, Kwon YT, Li Y-P. Signaling mechanism of tumor cell-induced up-regulation of E3 ubiquitin ligase UBR2. The FASEB Journal. 2013;27(7):2893-901. doi:10.1096/fj.12-222711.

32. Zhang G, Jin B, Li YP. C/EBPbeta mediates tumour-induced ubiquitin ligase atrogin1/MAFbx upregulation and muscle wasting. The EMBO journal. 2011;30(20):4323-35. doi:10.1038/emboj.2011.292.

33. McClung JM, Judge AR, Powers SK, Yan Z. p38 MAPK links oxidative stress to autophagy-related gene expression in cachectic muscle wasting. American journal of physiology Cell physiology. 2010;298(3):C542-9. doi:10.1152/ajpcell.00192.2009.

34. White JP, Puppa MJ, Gao S, Sato S, Welle SL, Carson JA. Muscle mTORC1 suppression by IL-6 during cancer cachexia: a role for AMPK. American Journal of Physiology - Endocrinology and Metabolism. 2013;304(10):E1042-E52. doi:10.1152/ajpendo.00410.2012.

35. Gasier HG, Riechman SE, Wiggs MP, Previs SF, Fluckey JD. A comparison of 2H2O and phenylalanine flooding dose to investigate muscle protein synthesis with acute exercise in rats. American journal of physiology Endocrinology and metabolism. 2009;297(1):E252-9. doi:10.1152/ajpendo.90872.2008.

36. Nilsson MI, Dobson JP, Greene NP, Wiggs MP, Shimkus KL, Wudeck EV et al. Abnormal protein turnover and anabolic resistance to exercise in sarcopenic obesity. FASEB journal : official publication of the Federation of American Societies for Experimental Biology. 2013;27(10):3905-16. doi:10.1096/fj.12-224006.

37. Hudson MB, Smuder AJ, Nelson WB, Wiggs MP, Shimkus KL, Fluckey JD et al. Partial Support Ventilation and Mitochondrial-Targeted Antioxidants Protect against Ventilator-Induced Decreases in Diaphragm Muscle Protein Synthesis. PloS one. 2015;10(9):e0137693. doi:10.1371/journal.pone.0137693.

38. Zhdanov AV, Aviello G, Knaus UG, Papkovsky DB. Cellular ROS imaging with hydro-Cy3 dye is strongly influenced by mitochondrial membrane potential. Biochimica et biophysica acta. 2016;1861(2):198-204. doi:10.1016/j.bbagen.2016.10.023.

Chapter 3

Mitochondrial Degeneration Precedes the Development of Muscle Atrophy in Progression of Cancer-Cachexia in Tumor-Bearing Mice.

Jacob L. Brown[1], Megan E. Rosa-Caldwell[1], David E. Lee[1], Thomas A. Blackwell[1], Lemuel A. Brown[2], Richard A. Perry[2], Wesley S. Haynie[2], Justin P. Hardee[3], James A. Carson[3], Michael P. Wiggs[4], Tyrone A. Washington[2], Nicholas P. Greene[1]

[1] Integrative Muscle Metabolism Laboratory, Human Performance Laboratory, Department of Health, Human Performance and Recreation, University of Arkansas, Fayetteville, AR 72701

[2] Exercise Muscle Biology Laboratory, Human Performance Laboratory, Department of Health, Human Performance and Recreation, University of Arkansas, Fayetteville, AR 72701

[3] Integrative Muscle Biology Laboratory, Department of Exercise Science, University of South Carolina, Columbia, SC 29208

[4] Integrated Physiology and Nutrition Laboratory, Department of Health and Kinesiology, University of Texas at Tyler, TX 75799

Corresponding Author: Nicholas P. Greene

Human Performance Laboratory

University of Arkansas

155 Stadium Dr, 321Q HPER

Fayetteville, AR 72701

E-mail: npgreene@uark.edu

Phone: 479-575-6638

Fax: 479-575-2853

Running Title: Mitochondrial Degeneration Precedes Cancer-Cachexia

Abstract

Background: Cancer-cachexia is largely irreversible, at least via nutritional means, and responsible for 20-40% of cancer-related deaths. Therefore, preventive measures are of primary importance, however little is known about muscle perturbations prior to onset of cachexia. Cancer-cachexia is associated with mitochondrial degeneration; yet, it remains to be determined if mitochondrial degeneration precedes muscle wasting in cancer-cachexia. Therefore, our purpose was to determine if mitochondrial degeneration precedes cancer-induced muscle atrophy wasting in tumor bearing mice.

Methods: First, weight stable (MinStable) and cachectic (MinCC) $Apc^{Min/+}$ mice were compared to C57Bl6/J controls for mRNA contents of mitochondrial quality regulators in quadriceps muscle. Next, Lewis Lung Carcinoma cells (LLC) or PBS (control) were injected into the hind-flank of C57Bl6/J mice at 8 wks age, and tumor allowed to develop for 1, 2, 3 or 4 wks to examine timecourse of cachectic development. SDH stain was used to measure oxidative phenotype in TA muscle. Mitochondrial quality and function were assessed using the reporter MitoTimer by transfection to flexor digitorum brevis and mitochondrial function/ROS emission in permeabilized adult myofibers from plantaris. RT-qPCR and Immunoblot measured the expression of mitochondrial quality control and antioxidant proteins. Data were analyzed by one-way ANOVA with Student-Newman Kuels post hoc test.

Results: MinStable mice displayed ~50% lower *Pgc-1α*, *Pparα*, and *Mfn2* compared to C57Bl6/J controls; whereas MinCC exhibited 10-fold greater *Bnip3* content compared to C57Bl6/J controls. In LLC, cachectic muscle loss was evident only at 4 wks post-tumor implantation. Oxidative capacity and mitochondrial content decreased by ~40% 4 wks post-tumor

implantation. Mitochondrial function decreased by ~25% by 3wks after tumor implantation. Mitochondrial degeneration was evident by 2 weeks LLC compared to PBS control, indicated by Mitotimer Red/Green ratio and number of pure red puncta. Mitochondrial ROS production was elevated by ~50% to ~100% when compared to PBS at 1-3 wks post-tumor implantation. Mitochondrial quality control was dysregulated throughout the progression of cancer-cachexia in tumor-bearing mice. In contrast, antioxidant proteins were not altered in cachectic muscle wasting.

Conclusions: Functional mitochondrial degeneration is evident in LLC tumor-bearing mice prior to muscle atrophy. Contents of mitochondrial quality regulators across *Apc*$^{Min/+}$ and LLC mice suggest impaired mitochondrial quality control as a commonality among pre-clinical models of cancer-cachexia. Our data provide novel evidence for impaired mitochondrial health prior to cachectic muscle loss and provides a potential therapeutic target to prevent cancer-cachexia.

Key Words

Cancer, Cachexia, MitoTimer, ROS, muscle wasting, mitochondrial quality

Introduction

Cancer is one of the leading causes of death worldwide [1, 2]. Moreover, therapies to prevent mortality from cancer are inadequate [3]. Cancer-cachexia is a wasting syndrome which occurs in up to 80% of cancer cases and is directly attributable for up to 40% of cancer-related deaths [4-6]. Cancer-cachexia is primarily defined by an ongoing loss of skeletal muscle mass and function, which nutritional therapies currently lack sufficient efficacy to reverse [4, 6]. Therefore, prevention remains a substantial goal of cachexia research, and recent literature calls for a focus on therapies to prevent cachexia [7]. Prior evidence suggests skeletal muscle oxidative capacity may influence atrophy in cancer-cachexia and other forms of muscle wasting [8-11]. Mitochondria are organelles critical for muscle oxidative metabolism. In fact, mitochondrial quality may be critical to the maintenance of skeletal muscle mass [12]. We recently acquired evidence in $Apc^{Min/+}$ mice, a genetic model of colorectal cancer, suggesting impaired mitochondrial quality control in quadriceps muscle of weight stable (not yet cachectic) mice (Fig 1). These data suggest impaired mitochondrial quality may precede development of cachexia and thus be a critical step in development of this condition, which has recently been discussed in detail [13]. Therefore, to better define such impacts, we have sought to investigate development of mitochondrial impairments across a time course of cachectic development in tumor-bearing mice.

Mitochondrial quality can be defined as the general health and function of the mitochondrial network [14]. When the mitochondrial network is impaired, degeneration of the network structure occurs leading to a loss of mitochondrial function (impaired ATP production) [15] and excess mitochondrial reactive oxygen species (ROS) production, disrupting cellular health [16, 17]. These related but distinct events result in impaired mitochondrial health and may

initiate skeletal muscle atrophy [18-24]. Cancer appears to impair the mitochondrial network in skeletal muscle [25], which may lead to cancer-cachexia. In addition to mitochondrial degeneration in cancer-cachexia, a decreased content of ROS eliminating enzymes has been reported [26]. Antioxidants may attenuate the progression of cancer-cachexia by aiding in the elimination of cellular ROS [27], suggesting ROS as an instigator for cancer-cachexia. Considering these points, there is a clear need to understand if mitochondrial degeneration, associated with mitochondrial ROS production and impaired energy production, may be the initiating event behind the onset of cancer-cachexia.

Skeletal muscle has a series of processes involved in mitochondrial quality control to aid in the maintenance of the mitochondrial network [28, 14]. These processes are the biogenesis of new mitochondrial components, fusion and fission of new and damaged mitochondrial regions within the network (dynamics), and the selective degradation of damaged mitochondrial regions through the process of autophagy (mitophagy) [28]. Mitochondrial biogenesis is primarily regulated by PGC-1α, a transcriptional co-activator that coordinates the transcription factors critical for the addition of mitochondrial components [29]. Mitochondrial dynamics is a highly regulated process in which components of the mitochondrial network are enzymatically divided (fission) or merged (fusion) [28]. Mitophagy is a highly selective engulfment of mitochondria by autophagosomes and their subsequent catabolism by lysosomes [30, 31]. Many of these mitochondrial regulatory processes are impaired in cancer-cachectic muscle [32, 25, 13], which may directly promote skeletal muscle atrophy [33-35]; however, current literature predominantly only measures mitochondrial quality control regulators at late stage cancer-cachexia. It is possible this mitochondrial degeneration occurs only after development of cancer-induced

muscle wasting; however, currently it is not known if such mitochondrial degeneration may precede and potentially instigate the muscle wasting in cancer-cachexia.

To our knowledge, mitochondrial degeneration during the progression of cancer-cachexia has not been examined over a time course protocol; therefore, the purpose of this study was to examine mitochondrial quality throughout the progression of cancer-cachexia in tumor-bearing mice. We hypothesized that impaired mitochondrial quality would be evident prior to the onset of cachexia. To test this hypothesis, we measured multiple functional (ROS emission, respiratory function, degeneration via pMitoTimer reporter gene) and signaling aspects of the mitochondria across time course progression of cancer-cachexia in tumor bearing mice. Utilizing direct and functional measurements of the mitochondrial network over time course progression, we now highlight a potential mechanism behind the onset of cancer-cachexia. We additionally provide evidence that signaling for mitochondrial quality control is impaired in pre-cachectic mice from each of two pre-clinical models of cancer-cachexia. Our study provides a novel insight into mitochondrial perturbations prior to development of the cachectic phenotype.

Methods

Animals and Interventions. Animal experiments were performed at two major institutions. All procedures were approved by the Institutional Animal Care and Use Committees of the University of Arkansas, Fayetteville (LLC experiments) and University of South Carolina ($Apc^{Min/+}$ experiments). A subset of the mice used for the LLC experiment have previously been reported on [36].

In the current study we have utilized two pre-clinical models of cancer-cachexia – the $Apc^{Min/+}$ mouse, a genetic model of colorectal cancer, and LLC implantation. Initial observations

were made at the level of mRNA contents in the $Apc^{Min/+}$ and followed by functional assessments of mitochondrial quality through time course of tumor development using the LLC implantation model. As pre-clinical models of cancer-cachexia often exhibit inherent differences the utilization of two models additionally was utilized to add surety that observations were not unique to any one model.

$Apc^{Min/+}$ mice. $Apc^{Min/+}$ mice used in this study were on a C57BL/6 (B6) background and were originally purchased from Jackson Laboratories. All mice used in the present study were obtained from the investigator's breeding colony (JAC) within the Center for Colon Cancer Research Mouse Core at the University of South Carolina. Experimental mice were group housed, kept on a 12:12-h light-dark cycle, and had access to standard rodent chow (no. 8604 Rodent Diet; Harlan Teklad, Madison, WI) and water *ad libitum*. Male $Apc^{Min/+}$ and B6 mice were aged to 18-20 wks of age, and stratified based on cachexia severity at sacrifice as previously described [25]. Experimental Groups included (B6 [control]), weight stable $Apc^{Min/+}$ mice (MinStable; no weight loss) and cachectic $Apc^{Min/+}$ mice (MinCC; 11.3% body weight loss). Phenotypic description of $Apc^{Min/+}$ mice in Table 1.

LLC Growth and Tumor Implantation. Lewis Lung Carcinoma (LLC) cells (ATCC CRL-1642) were plated in 250 mL culture flasks in DMEM supplemented with 10% Fetal Bovine Serum plus 1% Penicillin and Streptomycin. Once confluent, cells were trypsinized, counted and diluted in PBS for implantation. LLC cells were plated at passage 2.

Male C57BL/6J (Stock 000664) mice were purchased from Jackson Laboratories. The mice were kept on a 12:12-h light-dark cycle with *ad libitum* access to normal rodent chow and water. At 6 wks of age, MitoTimer [15] (a reporter gene that directly measures mitochondrial

quality) was delivered by electric pulse-mediated gene transfer to the flexor digitorum brevis (FDB) muscle on one foot of each mouse (described below). $1X10^6$ LLC cells suspended in 100 µL sterile PBS were implanted to the hind flank of mice at 8 wks of age as described [37, 36]. The tumor was allowed to develop for 1, 2, 3 or 4 wks in separate cohorts of animals. For sham control one group of mice received a bolus injection of 100 µL sterile PBS. PBS controls were age-matched to the most cachectic group (4 wk post-implantation, 12 weeks of age at tissue collection). Animal tissues were quickly collected under isoflurane anesthesia prior to euthanasia. Tissues were weighed and snap-frozen in liquid nitrogen for further processing and stored at -80°C. Body weights between the PBS and 4 wk group were not different; however, the 4 wk group lost a significant amount of muscle mass. According to Fearon et al., loss of skeletal muscle mass is an effective diagnostic criteria for cancer-cachexia [6]. Phenotypic description of LLC tumor-bearing mice in Table 2.

Plasmid DNA Amplification and Electroporation. DH5-α Escherichia coli containing pMitoTimer plasmid [15] were amplified and plasmid DNA isolated using PureLink HiPure Plasmid Filter Maxiprep kit (Life Technologies, K210017). Plasmid transfection to FDB muscle was performed as described by Laker et al. [15]. Briefly, 10 µL of 0.36 mg/mL hyaluronidase (in saline) was injected with insulin syringe with a 30 gauge needle subcutaneously above the FDB muscle prior to plasmid DNA injection. One hour after hyaluronidase injection, 20 µg of DNA was injected into the FDB muscle. 10 minutes following DNA injection, the mice were anesthetized, and an electrical field was delivered through gold-plated acupuncture needles placed at the heel of the foot and at the base of the toes. 10 pulses were delivered at 20 ms duration/pulse and 1 Hz at 75V using an S88 Stimulator (Grass Telefactor).

Mitochondrial Function and ROS production. This methodology was adapted from Kisuk Min et al. 2015 [38]. Briefly, small strips of plantaris muscle, ~10 mg, of muscle were teased to near-single fibers and permeabilized with saponin to open small pores in the membrane. Mitochondrial oxygen consumption (VO_2) of a permeabilized fiber bundle was measured. Briefly, mitochondria were primed with malate and glutamate. Maximal respiration (ADP-stimulated, state 3) and state 4 respiration (ADP depleted respiration) was measured. The respiratory control ratio (RCR) was calculated by dividing state 3 by state 4 respiration. The dry weight of the permeabilized mitochondria was used to normalize the results.

Mitochondrial ROS was measured in permeabilized plantaris fibers. All forms of ROS were converted to hydrogen peroxide by the addition of Superoxide Dismutase 1. ROS emission was measured using amplex red hydrogen peroxide detection kit. In the presence of peroxidase, the Amplex Red reagent reacts with H_2O_2 in a 1:1 stoichiometry to produce the red-fluorescent oxidation product, resorufin. Plantaris muscle was utilized for mitochondrial respiration and ROS analyses because it is a mixed fiber type and as a smaller muscle more easily teased apart into near single fiber bundles, which is required for the assay.

Fluorescence microscopy for MitoTimer. For MitoTimer, freshly harvested FDB muscles were fixed for 20 min in 4% PFA at room temperature and washed 5 min in PBS. Muscles were then whole mounted on gelatin-coated glass slides using 50% glycerol in PBS as mounting media and cover slipped. MitoTimer images were acquired at 100X magnification using the FITC (green, excitation/emission 488/518 nm) and TRITC (red, excitation/emission 543/572 nm) channels on a Nikon Ti-S inverted epiflourescent microscope (Melville, NY) with LED-based light source with controlled acquisition parameters as described by Laker et al. [15]. All slides were imaged the day of tissue harvest. Acquisition parameters were set using a pilot study of

cachectic and control animals and maintained consistent throughout all experiments. A specially written MATLAB program was a generous gift from Dr. Z. Yan (U. Virginia) and was used to analyze MitoTimer red: green ratio and pure red puncta as described by Laker et al. [15]. The assay is best performed on freshly dissected muscles as time *ex vivo* impacts the fluorescent indicator of MitoTimer. Therefore we transfected and utilized the FDB which can be dissected, whole mounted to microscope slide and imaged within 30 min of the initial dissection.

Cryosectioning. Tibialis Anterior (TA) muscles were embedded in optimal cutting temperature (OCT) compound and frozen in liquid nitrogen cooled isopentane. Sections were cut at 10 μm using a Leica CM1859 cryostat (Leica Biosystems, Buffalo Grove, IL) and stained for Succinate Dehydrogenase (SDH). Sections were placed in incubation solution (50 mM Soduim succinate, 50 mM phosphate buffer, 0.12M KH2PO4 & 0.88M Na2HPO4), 0.5 mg/ml Nitroblue tetrazolium for 40 min in a 37^{o} C water bath. Slides were washed 3 min with dH_2O and imaged. Images were collected with Nikon Sight DS-Vi1 camera mounted on an Olympus CKX41 inverted microscope. SDH+ (purple) and SDH– fibers were counted, cross-validated by two independent and blinded investigators, and circled for cross sectional area analysis using Nikon Basic Research Imaging Software (Melville, NY). There was no difference between the measurements across two blinded researchers. TA muscle was utilized because it is a bigger muscle, which minimizes freezer damage to fibers to centrally located muscle fibers. Other muscles suitable for cryosectioning such as the gastrocnemius were utilized for other analyses.

RNA isolation, cDNA synthesis and quantitative real-time PCR. RNA isolation, cDNA synthesis and quantitative real-time PCR were performed as we have previously described [39-41, 14]. Taqman probes or SYBR primers specific to *Pgc-1α1, Cox4, Pparα, Mfn2, Opa1, Drp1,*

MFF, Fis1, Bnip3 and Beclin1. Taqman probes and SYBR primers have previously been reported in Greene et al. [14].

Immunoblotting. Immunoblotting performed as we have previously described [41, 14, 42, 40, 43]. Membranes were probed overnight for primary antibodies. Protein targets were selected based upon prior literature to encompass key components of each of the mitochondrial quality control systems [28, 14] and ROS protection [44, 26] as previously described. Primary antibodies were specific to mitochondrial content and biogenesis proteins: COX-IV (Cell Signaling 4844S), VDAC (Cell Signaling 4866S), PGC-1α (Santa Cruz sc-13067), PPARα (Santa Cruz sc-9000), PPARδ (Santa Cruz sc-7197), TFAM (Cell Signaling 7495). Mitochondrial dynamics proteins: MFN1 (Santa Cruz sc-50330), MFN2 (Santa Cruz sc-50331), OPA1 (Santa Cruz sc-367890), DRP1 (Cell Signaling 14647), Fis1 (Novus NB100-56646). Mitophagy proteins: BNIP3 (Cell Signaling 3769), PINK 1 (Santa Cruz sc-33796), p-PARKIN (Ser65, Abcam ab154995), PARKIN (Cell Signaling 42115). Antioxidant proteins: SOD1 (Genetex GTX100554), SOD2 (Cell Signaling 131945), SOD3 (R and D Systems AF4817), GPx7 (Genetex GTX117516), GPx3 (Genetex GTX89142) and Catalase (Cell Signaling 140975). Primary antibodies were isolated from rabbit, mouse and goat. Antibodies were diluted in TBST with 5% milk. Membranes were imaged on Protein Simple FluorChem (Minneapolis, MN) and analyzed using Alpha View software. All bands were normalized to the 45 kDa Actin band of Ponceau S stain as a loading control. There was no difference detected between the 45 kDa Actin band of Ponceau S stain across experimental groups. Powdered gastrocnemius muscle (mixed fiber type) was utilized to represent both type I and II fibers for immunoblot analysis.

Statistical Analysis. For $Apc^{Min/+}$ independent variables were B6 control, weight stable $Apc^{Min/+}$ mice (MinStable) and cachectic $Apc^{Min/+}$ mice (MinCC). For LLC, independent

variables were PBS and number of weeks tumor progressed. A One-way ANOVA was employed as the global analysis for each dependent variable in both experiments. Differences among means were determined by Student Newman-Keuls post hoc test. For all experiments, the comparison-wise error rate, α, was set at 0.05 for all statistical tests. All data were analyzed using the Statistical Analysis System (SAS, version 9.3, Cary, NC, USA), figures were compiled using GraphPad Prism (La Jolla, CA, USA) and data expressed as mean ± standard error of the mean (SEM).

Results

Mitochondrial quality control is dysregulated before severe cancer-cachexia in $Apc^{Min/+}$ mice. $Apc^{Min/+}$ mice were stratified into experimental groups based on % total body weight loss from peak body weight as an estimate of cachectic development as previously described [25]. Cachectic mice (MinCC) lost on average 11.3% body weight by time of tissue harvest, while no loss was seen in B6 or weight stable (MinStable) controls (Table 1). Loss of body weight coincided with reduction in quadriceps muscle mass. While no significant differences in muscle mass were observed between B6 (118 ± 4.6) and MinStable (103 ± 3.6), MinCC (67 ± 5.5) quadriceps mass was reduced compared to both B6 and MinStable (Table 1). Intriguingly, the process of mitochondrial biogenesis was dysregulated in MinStable mice indicated by a ~50% decrease in mRNA content of both *Pgc-1α* and *Pparα* (Figure 1 a). Furthermore, a ~50% decrease in *Mfn2* mRNA in weight stable $Apc^{Min/+}$ mice indicated alterations in mitochondrial fusion before cancer-cachexia occurred (Figure 1 b). *Bnip3* mRNA was increased by 10-fold in MinCC only, which indicates an upregulation of mitophagy in mice with cancer-cachexia (Figure 1 c).

Characterization of the progression of LLC-induced cancer-cachexia. Body weights (Body weight with tumor weight subtracted) of the C57Bl/6J mice were not different between groups throughout the 4 wk progression of cancer-cachexia; however, muscle wet weights of TA, gastrocnemius, plantaris, quadriceps and soleus were ~15-20% lower 4 wks following tumor implantation compared to PBS, with no significant differences in muscle weights between PBS, 1, 2, and 3 wk animals (Table 2). Furthermore, epididymal fat decreased by ~35% in mice with 4 wks tumor growth compared to PBS. Spleen weight, a surrogate marker for inflammatory state, was 270% and 450% greater 3 and 4 wks, respectively, following tumor implantation when compared to PBS control (Table 2).

Oxidative phenotype is diminished 4 wks following tumor implantation. The percentage of SDH+ fibers in the Tibialis Anterior muscle was ~20% lower in mice 4 wks following tumor implantation (Figure 2 a/b), indicating a loss of muscle oxidative phenotype. Furthermore, there was a greater number of small muscle fibers that are SDH- 4 wks following tumor implantation compared to PBS control while little difference was observed in SDH+ suggesting specific atrophy of non-oxidative muscle fibers (Figure 2 c/d). There was a lower mitochondrial content 4 wks following tumor implantation compared to PBS indicated by a ~50% decrease in both COX-IV and VDAC protein contents (Figure 2 e-g). No significant changes in SDH or mitochondrial content (COX-IV/VDAC) were observed prior to 4 wk tumor development.

Mitochondrial degeneration occurs before cancer-cachexia. Mitochondrial network degeneration is evident 2 wks following tumor implantation. Examining the MitoTimer fluorescence spectra we observed a ~50% and 4 fold greater MitoTimer Red:Green ratio and number of pure red puncta, respectively (Figure 3 a-c). These measures were previously validated by Laker et al. [15] to directly indicate impaired mitochondrial quality. Furthermore,

mitochondrial function (indicated by the RCR, the ratio of State 3: State 4 respiration) was ~25% and 45% lower 3 and 4 wks following tumor implantation compared to PBS (Figure 3 d). Moreover, mitochondrial ROS production, indicated by H_2O_2 emission, was two-fold greater 1 wk following tumor implantation and remained elevated through 3 wks post tumor implantation compared to PBS (Figure 3 e).

LLC impairs mitochondrial quality control before development of cancer-cachexia. LLC implantation did not affect the mitochondrial biogenesis proteins PGC-1α, PPARα or TFAM; however, one week following tumor implantation, PPARδ protein content was ~40% lower compared to PBS, but not significantly different from control in other experimental groups (2-4 wks post tumor implantation) (Figure 4 a/b). Mitochondrial dynamics was dysregulated as soon as 1 wk following tumor implantation. Opa1 (a protein critical for mitochondrial inner membrane fusion) content was ~45% lower than PBS control in all LLC tumor-bearing groups (Figure 4 c/d). Intriguingly, mitochondrial fission proteins Drp1 and Fis1 were differentially expressed throughout the progression of cancer-cachexia. Drp1 protein content was ~ 45% lower 4 wks following tumor implantation compared to PBS, an apparent lower Drp1 content in 1-3 wk tumor groups did not reach significance (Figure 4 c/d). In contrast, Fis1 protein content was elevated ~80% in 4 week cachectic animals compared to PBS only (Figure 4 c/d). Mitophagy regulator BNIP3 protein content was ~2-fold greater in 3 wks following tumor implantation compared to PBS (Figure 4 e/f). In contrast, PINK1, p-PARKIN and PARKIN protein content were not significantly different among groups (Figure 4 e/f).

Antioxidant enzymes are unchanged despite increased mitochondrial ROS production. Protein contents of SOD1, SOD2, SOD3, GPx3, GPx7 and Catalase were not different among experimental groups (Figure 5).

Discussion

Current literature is clear that mitochondria are dysregulated in cachectic skeletal muscle [32, 25, 45]. However, our findings are the first to demonstrate mitochondrial network deterioration and dysfunction occurs before the onset of cancer-induced loss of muscle mass in tumor-bearing mice. Recently, mitochondria have been implicated as critical controllers of skeletal muscle mass [46]; therefore, mitochondrial degeneration may be a key promotor of cancer-cachexia. Initial observations presented here and by White et al. [25], compared mitochondrial quality control regulators across degrees of cachexia in $Apc^{Min/+}$ mice suggesting impaired mitochondrial quality precedes cachectic phenotype which have herein been built upon via time course and functional assessments in LLC tumor-bearing mice. The current study demonstrates increased mitochondrial oxidative stress within the muscle one week post tumor implantation, followed by mitochondrial network degeneration and lost mitochondrial function 2 and 3 weeks post tumor implantation, respectively. Moreover, mitochondrial quality control regulators are altered throughout the progression of cancer-cachexia in both $Apc^{Min/+}$ and Lewis Lung Carcinoma pre-clinical models suggesting early mitochondrial degenerations are a common alteration in development of muscle wasting in cancer-cachexia across pre-clinical models. Our findings clearly present functional mitochondrial degeneration as an early event preceding muscle wasting in the development of cancer-cachexia in both LLC tumor-bearing and $Apc^{Min/+}$ mice. Furthermore, to our knowledge we are the first to examine progression of cancer-cachexia by time course design. The data presented herein demonstrate the imperative nature to elucidate intramyofibrillar alterations prior to the onset of the cachectic phenotype.

Cancer-cachexia alters mitochondrial quality control signaling in $Apc^{Min/+}$ mice. In our examination of the $Apc^{Min/+}$ mouse we note that mRNA contents of regulators of mitochondrial

biogenesis (*Pgc-1α* and *Pparα*) and fusion (*Mfn2*) occur in the MinStable condition, that is in tumor bearing mice who do not present signs of the cachectic phenotype. In contrast, the mRNA content of mitophagy marker *Bnip3* was elevated only in cachectic mice. These signaling data are similar to White et al. [25] and suggested that mitochondrial quality control is impaired prior to signs of cachexia beginning with downregulations of biogenic and fusion regulators and progressing to elevated markers of mitophagy in cachectic mice. Considering these data, we next elected to tease the mitochondrial degenerations in progression of cancer-cachexia induced muscle wasting using a tumor implantation model (LLC) to allow time course assessments of the functional mitochondrial alterations in development of this condition.

Cancer-cachexia impairs oxidative phenotype and mitochondrial content in skeletal muscle in LLC tumor bearing mice. Using this model ($1X10^6$ LLC cells implanted into the hind flank) of LLC-induced cancer cachexia it takes 4 weeks for the cachectic phenotype (muscle wasting) to develop [36, 37, 47]. While, our mice did not lose total body weight after 4 weeks following tumor implantation, significant muscle and fat mass was lost along with an increased spleen mass indicative of an inflammatory state [48], which is an effective diagnostic criteria [6]. Loss of oxidative phenotype in late stage cancer-cachexia has commonly been observed in the literature [25, 13, 49]; however, oxidative phenotype throughout the progression of cancer-cachexia is understudied. Our data indicates loss of oxidative phenotype (SDH stain) and mitochondrial content (COX-IV/VDAC) occur concomitantly with cancer-induced muscle loss. Furthermore, when cancer-cachexia develops, our data indicates oxidative muscle fibers may be resistant to atrophy during the initial stages of wasting (CSA distribution by SDH stain). Based on our data and prior reports cancer-cachexia preferentially impacts glycolytic muscle fibers; however, oxidative fibers have superior antioxidant defenses when compared to glycolytic fibers

[50, 51], which may slow cancer-cachexia. This is commonly observed in cancer-cachexia literature [49], and indicates that oxidative metabolism is an important factor for the maintenance of muscle size. Therefore, muscle mitochondria may be a primary target of the cancer environment, and may be a contributor to cancer-induced muscle wasting [13].

Mitochondrial degeneration occurs prior to the onset of cancer-induced muscle loss. To determine functional mitochondrial degeneration we examined multiple functional parameters including respiratory function, ROS emission and fluorescence-based measures of network degeneration. We measured a 2-fold increase in ROS production 1-wk post tumor implantation. Chronically elevated ROS may be an instigating factor for the muscle wasting observed in tumor-bearing mice as it has been shown to promote protein catabolic functions [16, 17]. We do note that mitochondrial ROS production appeared to normalize at 4 wk post tumor implantation, however these data are normalized to tissue mass and it must also be noted that at this timepoint mitochondrial density is ~50% reduced by COX-IV and VDAC markers. Next, utilizing the reporter pMitotimer [15], we observed signs of network degeneration 2 wks following tumor implantation along with the sudden and dramatic appearance of pure red puncta which by prior reports appear to be completely degenerated mitochondria tagged for autophagic degradation [15]. Degeneration of the mitochondrial network then leads to impaired mitochondrial respiratory function, which we observed 3 wks following tumor implantation. These combined findings suggest early and progressive derangements in mitochondrial health during the development of cancer-cachexia in tumor-bearing mice (Figure 6).

The mitochondrial aberrations described herein may induce LLC mediated cancer-cachexia considering damaged mitochondria have been shown to directly promote atrophic signaling in skeletal muscle in other models [21-24]. Furthermore, cellular energy stress induced

by mitochondrial dysfunction leads to skeletal muscle wasting [52]. Our data demonstrates clear evidence that mitochondrial degeneration occurs before the development of cancer-induced muscle wasting in tumor-bearing mice. Critically, these aberrations are most likely due to influences of the tumor microenvironment as mitochondrial disruptions are observed only one week following tumor implant when the animal presents as otherwise healthy.

To provide insight to how these mitochondrial derangements occur we next examined mechanisms of the mitochondrial quality control system in the LLC mice as mitochondrial degeneration observed in cancer-induced muscle wasting may be attributed to disruptions to these processes. While not all measured markers of mitochondrial quality control were altered we note that when impacts were observed in mitochondrial biogenic (PPARδ) and fusion (Opa1) proteins these alterations were via downregulation and occurred shortly after tumor implantation (1 wk). Intriguingly, $Apc^{Min/+}$ mice exhibit a significant reduction in *Pgc-1α* mRNA content in MinStable mice, while PGC-1α protein content is not altered throughout the progression of cancer-cachexia in the LLC pre-clinical model. This may be explained by differences in the tumor microenvironment between the pre-clinical models. Moreover, *Pgc-1α* mRNA content is not different between MinCC and B6 control. At this time we are unable to be certain as the reason behind reduced *Pgc-1α* mRNA in MinStable mice, however, differences in the inflammatory environment between the MinStable and MinCC group may explain this [53], however this is only speculative. Similar to $Apc^{Min/+}$ mice, in LLC mice the mitochondrial fission regulator Fis1 and mitophagy protein BNIP3 were both met with induced expression and both only impacted later in cachectic development. These observations in mitochondrial quality control are similar to those presented here in the $Apc^{Min/+}$ mouse, and congruent with prior literature in cancer-cachexia [32], whereby early downregulations in biogenic and fusion

regulators followed by strong induction of *Bnip3* mRNA content is observed. These combined data suggest early stage mitochondrial degeneration as a commonality in two otherwise distinct pre-clinical models of cancer-cachexia.

These observations may directly tie to the development of cachectic wasting. First, Opa1 has recently been identified as a key controller of muscle size [54]. Second, the induction of Fis1 suggests an upregulation in the amount of fragmented mitochondria, which are typically inefficient at generating ATP [55] leading to cellular energy stress and loss of muscle mass. Furthermore, a decrease in content of these controllers of mitochondrial dynamics may indicate alterations in the balance of fusion and fission of the mitochondria [56]. Finally, mitophagy is regulated by two distinct processes: BNIP3-mediated mitophagy and PINK1-PARKIN-mediated mitophagy [57, 58]. While we have observed induction of BNIP3, such an impact on PINK1-PARKIN expression was not seen. This suggests differential regulation of BNIP3 compared to PINK1-PARKIN whereby alterations present in cancer-cachexia selectively induce BNIP3-mediated mitophagy.

Considering the 2-fold increase of mitochondrial ROS production and the shift in MitoTimer fluorescence spectra, we next examined how cellular anti-oxidant defense mechanisms might be impacted in development of cancer-cachexia. Multiple lines of evidence suggest excess ROS induces skeletal muscle atrophy [59-64]. Intriguingly, we examined protein contents of 6 anti-oxidant components all of which are unchanged despite an increase in mitochondrial ROS production, suggesting a failure of the system to adequately respond to mitochondrial oxidative stress which may exacerbate free radical-induced proteolysis during cancer-cachexia. Unfortunately, we were unable to perform functional enzyme activity assays of anti-oxidant proteins to further elucidate the cellular response to oxidative stress due to lack of

tissue. Further experiments should be performed to test these enzymatic activities to determine any alterations in function of anti-oxidant proteins.

Relationship between mitochondrial degeneration and cancer-cachexia. Mitochondrial degeneration is a common feature across numerous models of skeletal muscle atrophy [12, 65, 66], including cancer-cachexia. In fact, mitochondrial degeneration may instigate skeletal muscle atrophy through mechanisms including reduced protein synthesis, increased autophagic and ubiquitin-proteasome mediated protein catabolism, inflammation and altered myogenesis all of which are perturbed in cancer-cachexia [18-24]. In this study, we have clearly shown aberrations in the mitochondrial network, beginning with increased ROS production and leading to loss of mitochondrial function in cancer-cachexia (Figure 6). Intriguingly, these alterations occur before cancer-induced loss of muscle mass occurs (Figure 6) and while animals would otherwise appear healthy suggesting mitochondrial degeneration in cancer-cachexia is largely resultant of the tumor microenvironment. Functional data presented herein across time course with LLC-induced muscle wasting coupled with signaling data presented from the $Apc^{Min/+}$ and LLC experiments suggest that early onset mitochondrial degeneration is likely a common factor in development of cancer-induced muscle loss across pre-clinical models which otherwise display distinct mechanistic traits.

Conclusions and future direction. In summary, this is the first experiment to investigate mitochondrial degeneration and dysfunction throughout a time course development of cancer-cachexia in tumor-bearing mice. While altered signaling of mitochondrial regulatory processes (biogenesis, dynamics and mitophagy) provides important insight into potential mechanisms behind mitochondrial degeneration, the current study directly measures mitochondrial quality (MitoTimer), mitochondrial ROS emission and respiratory function (RCR) in order to fully

assess mitochondrial aberrations that occur throughout the progression of cancer-cachexia in a pre-clinical model. Intriguingly, mitochondrial aberrations such as increased ROS production occur as soon as 1 wk after tumor implantation (Figure 6), which is likely instigated by the tumor microenvironment however at this time we cannot rule out denervation, hypoxia and/or apoptosis. Data from the current study implicate the importance of early cancer detection as well as preventive measures for cancer-cachexia. However, cancer-cachexia is often not treated before stage IV of cancer is reached [67]. These data suggest targeting of mitochondrial quality may be vital for the treatment and prevention of cancer-cachexia whether pharmacologically or through exercise [28, 15]. Though future studies will need to validate promotion of mitochondrial quality as an efficacious modality. To accomplish this, future experiments should be performed to determine if promoting maintenance of mitochondrial quality may prevent cancer-induced muscle wasting. We now see a clear need for further study of the early-stage progression of cancer-cachexia as well as early-stage impacts of the tumor microenvironment.

Acknowledgements

Support for LLC experiments has been provided in part by the Arkansas Biosciences Institute, the major research component of the Arkansas Tobacco Settlement Proceeds Act of 2000 (NPG) and National Institutes of Health under Award Number R15AR069913 from the National Institute Of Arthritis And Musculoskeletal And Skin Diseases and the National Institute Of General Medical Sciences. *Apc*$^{Min/+}$ experiments were partially supported by National Institutes of Health grant # R01CA121249A501 (JAC) from the National Cancer Institute, and the National Institutes of Health grant # 5P30GM103336 from the National Institute of General Medicine. Contents of this publication are solely the responsibility of the authors and do not necessarily represent the official views of the ABI, NIGMS or NIH. The authors would like to thank Drs. Sami Dridi, Elizabeth Greene and Jeffrey Wolchok (U. Arkansas), as well as Mr. Connor Benson (UT Tyler), Ms. Haley McCarver and Mrs. Katie Stephenson-Brown for their contributions. We would like to thank the Cell and Molecular Biology program at the University of Arkansas, Fayetteville for supporting Jacob L. Brown's graduate education. We would also like to extend our gratitude to the numerous other faculty, staff and students of the Integrative Muscle Biology Laboratory at the University of South Carolina and the Exercise Science Research Center at the University of Arkansas.

The authors certify that they comply with the ethical guidelines for publishing in the Journal of Cachexia, Sarcopenia and Muscle [68].

Conflict of Interest.

All authors declare no conflicts of interest.

Tables

Table 1

Variable	B6	MinStable	MinCC
Peak BW (g)	27.4±0.4	25.34±0.7	25.5±0.9
Sac BW (g)	27.4±0.4 **a**	25.34±0.7 **a**	22.7±0.8 **b**
BW Loss (g)	0±0 **a**	0±0 **a**	11.3±1.1 **b**
Quadriceps (mg)	111.7±4.7 **a**	103.5±3.1 **a**	67±5.5 **b**
Tibia (mm)	17.5±0.1	17.06±0.1	17.2±0.1

Table 1: Body and tissue weights in B6 and *Apc*$^{Min/+}$ mice . Tibia length was measured as an estimate of total body size which did not differ between experimental groups, therefore all tissue weights are presented as non-normalized wet weights. Lettering denotes statistical significance at an alpha set at $p<0.05$.

Table 2

Variable (LLC)	PBS (n=24)	1 Week (n=16)	2 Week (n=16)	3 Week (n=12)	4 Week (n=14)
Body Weight (g)	24.9±0.3 **a**	23.9±0.3 **a**	23.8±0.6 **a**	24.4±0.8 **a**	27.0±0.6 **b**
Tumor Weight (g)	N/A	0.03±0.007 **a**	0.2±0.03 **a**	0.8±0.1 **b**	3.5±0.4 **c**
BW - Tumor (g)	24.9±0.3	23.9±0.3	23.7±0.6	23.6±0.7	23.5±0.6
TA (mg)	45.1±0.9 **a**	43.8±1.2 **a**	44.5±1.2 **a**	42.9±1.6 **a**	38.3±1.3 **b**
Gastroc (mg)	134.6±2.1 **a**	129.5±2.5 **a**	130.0±4.1 **a**	125.2±3.5 **a,b**	118.4±4.1 **b**
Plantaris (mg)	18.3±0.4 **a**	18.3±0.3 **a**	18.1±0.6 **a**	17.7±0.7 **a**	15.9±0.6 **b**
EDL (mg)	9.9±0.4	9.4±0.3	9.9±0.3	9.6±0.4	8.6±0.5
Soleus (mg)	8.7±0.2 **a**	8.2±0.2 **a,b**	8.1±0.2 **a,b**	8.1±0.3 **a,b**	7.7±0.2 **b**
Spleen (mg)	81.1±3.2 **a**	81.9±2.8 **a**	85.7±2.6 **a**	222.8±31.1 **b**	366.5±31.8 **c**
Lungs (mg)	151.2±6.8	173.0±8.9	161.7±3.9	173.2±8.9	156.8±10.0
EpiFat (mg)	367.5±12.9 **a**	332.5±22.6 **a**	348.2±12.8 **a**	316.7±33.6 **a**	240.4±19.2 **b**
Quadriceps (mg)	152.3±6.7	149.2±5.7	147.8±8.8	148.5±7.6	127.1±7.2
Tibia (mm)	17.4±0.1	17.4±0.1	17.3±0.1	17.4±0.1	17.3±0.1

Table 2: Body and tissue weights at the time of harvest in LLC tumor-bearing mice. N of 12-24/group as indicated on table was utilized. Tibia length was measured as an estimate of total body size which did not differ between experimental groups, therefore all tissue weights are presented as non-normalized wet weights. Lettering denotes statistical significance at an alpha set at $p<0.05$.

Figures

Figure 1

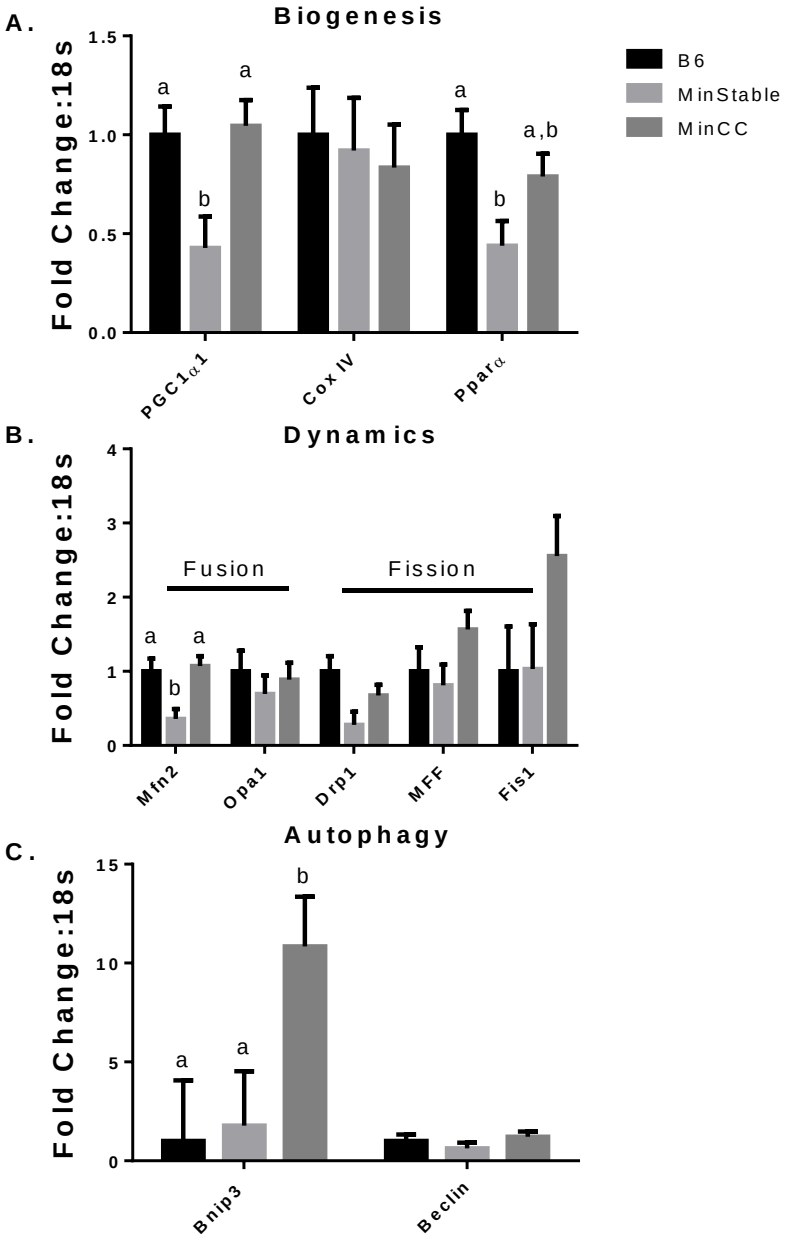

Figure 1. mRNA content of mitochondrial quality controllers in **quadriceps muscle of B6** and APC/Min+ mice. A: mRNA content of mitochondrial biogenesis controllers. B: mRNA content of mitochondrial dynamics controllers. C: mRNA content of mitophagy regulators. N of 5-6 was utilized for each group. Lettering denotes statistical significance at an alpha set at $p<0.05$.

Figure 2

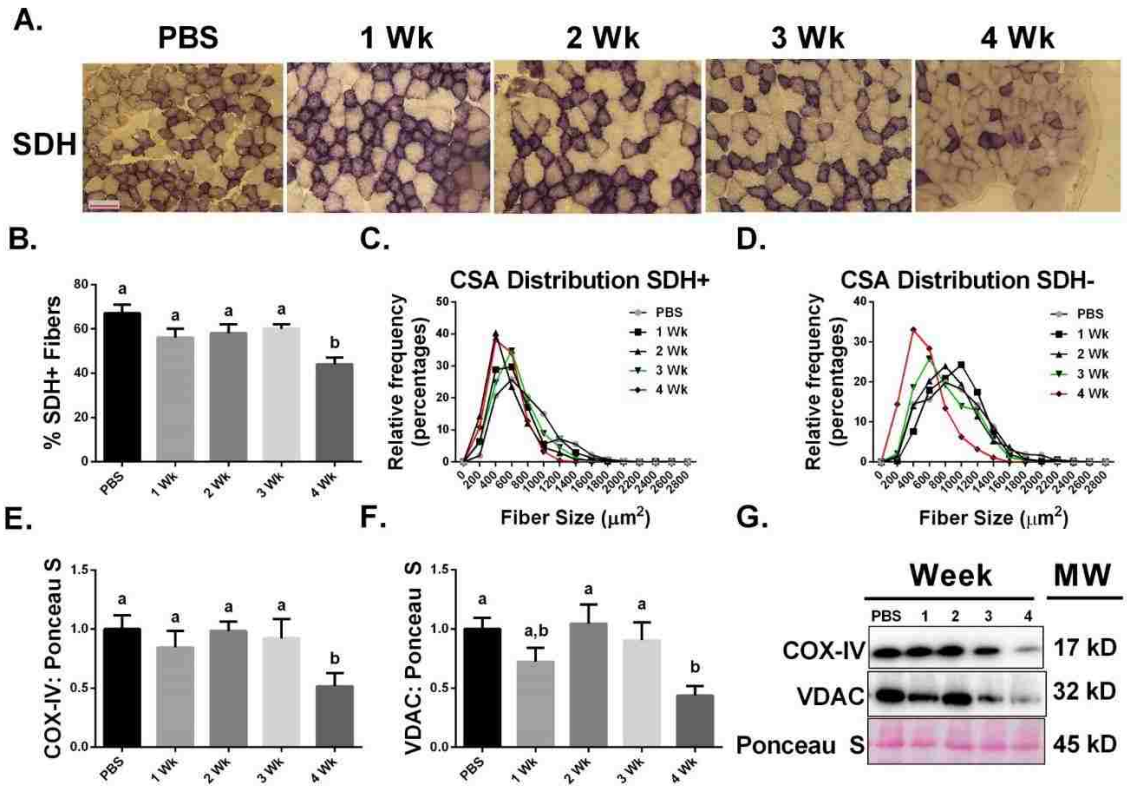

Figure 2. Oxidative muscle fibers and mitochondrial content across a time course progression of cancer-cachexia in LLC tumor-bearing mice. A-D: SDH staining performed in TA muscle. A: Representative images for SDH stain across the different experimental groups. Scale bar is 50 μM long. B: % SDH+ fibers throughout the progression of cancer-cachexia. C: Cross Sectional Area distribution of SDH+ fibers. D: Cross Sectional Area distribution of SDH- fibers. E-G: Immunoblotting in gastrocnemius muscle. E and F: Immunoblot quantification of mitochondrial content markers COX-IV (E) and VDAC (F). G: Representative immunoblot images. N of 10 for each group was used for SDH analysis and N of 8 for each group was utilized for immunoblot analysis. Lettering denotes statistical significance at an alpha set at $p<0.05$.

Figure 3

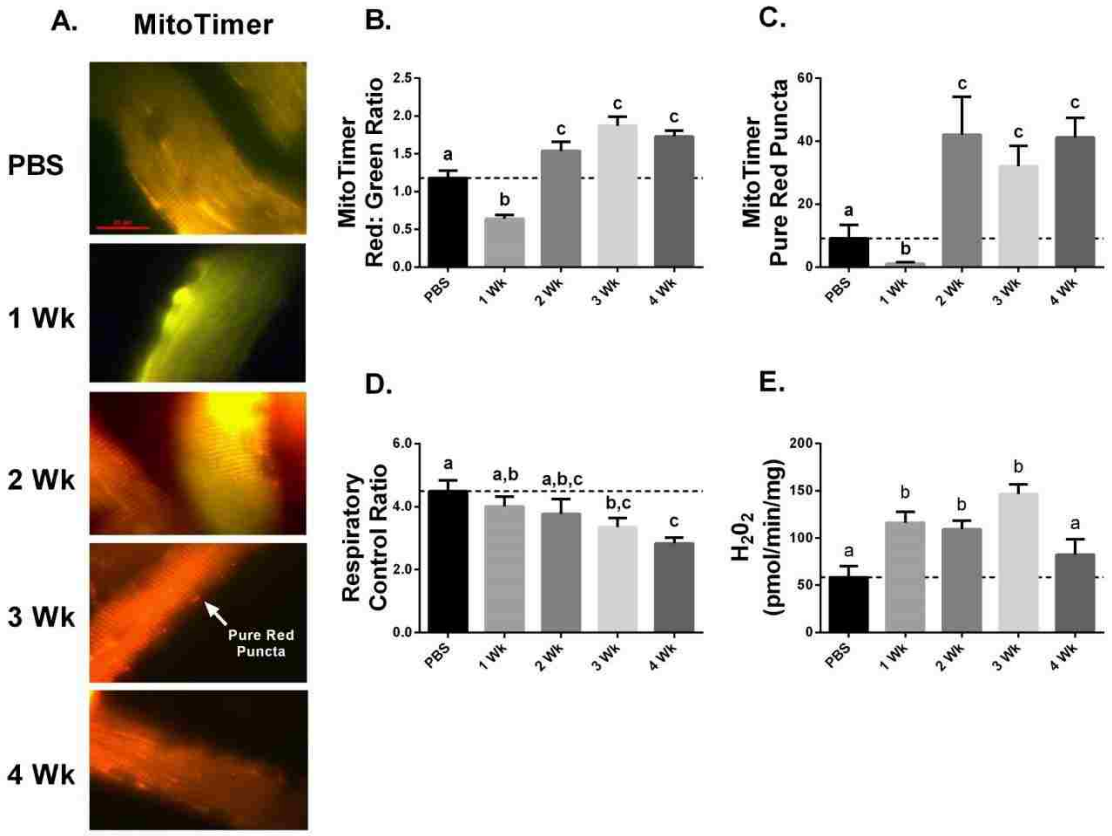

Figure 3. Mitochondrial degeneration precedes muscle wasting in cancer-cachexia in LLC tumor-bearing mice. MitoTimer is a mitochondrially targeted variant of DsRed validated by Laker et al., 2014 [15] to emit green fluorescence when mitochondria are healthy and shift to red when mitochondria are damaged. A-C: MitoTimer in FDB muscle. A: Representative MitoTimer images taken at 100X magnification. Scale bar is 20 µM in length. B: Quantification of MitoTimer Red: Green ratio. C: Quantification of pure red puncta in MitoTimer. Locations of pure red puncta co-localize with LC3 and appear to represent completely degenerated mitochondria targeted for autophagy [15]. D-E mitochondrial function and ROS emission in plantaris muscle. D: Respiratory control ratio (Ratio of State 3: State 4 respiration) of permeabilized plantaris muscle. E: Mitochondrial H_2O_2 production in permeabilized plantaris muscle. N of 12-24 per group was utilized for MitoTimer, while n of 12/group was utilized for respiration and ROS production analysis. Lettering denotes statistical significance at an alpha set at $p<0.05$.

Figure 4

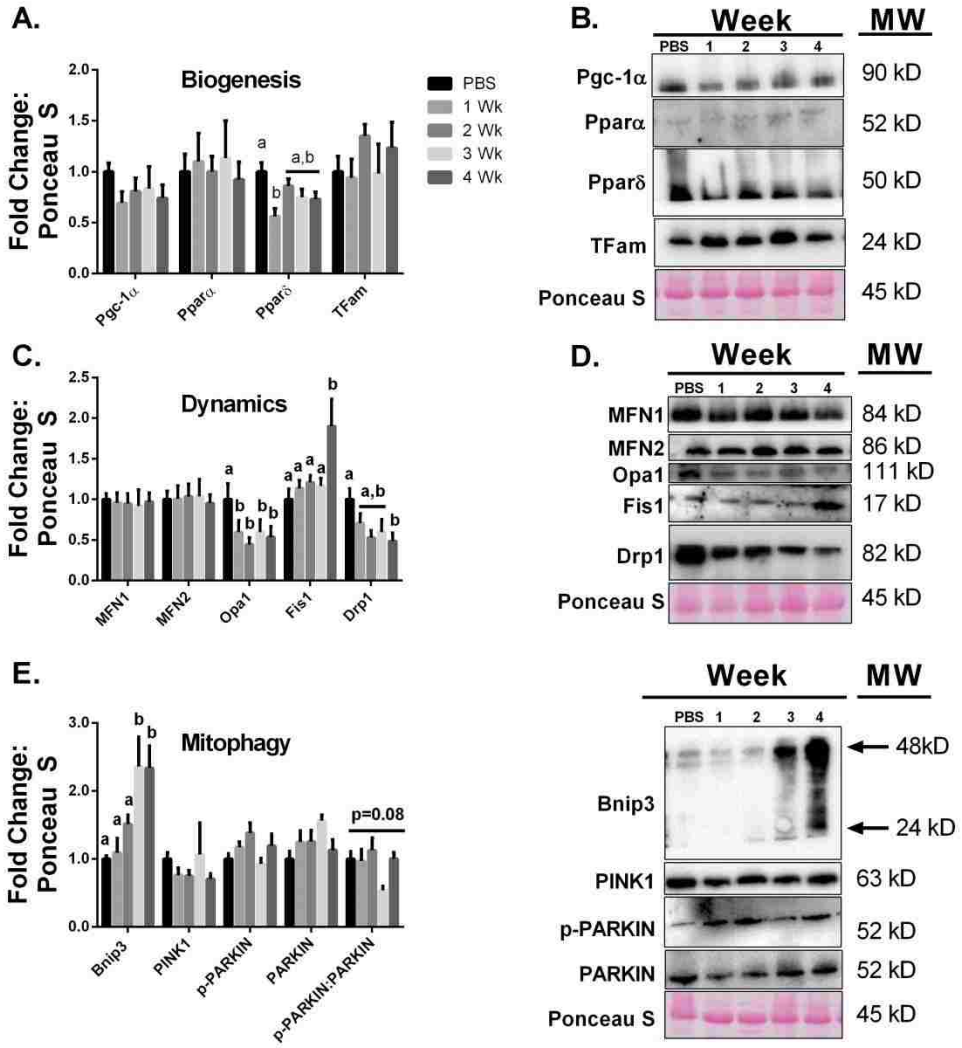

Figure 4. Immunoblot analysis of mitochondrial quality control regulators during progression of cancer-cachexia in **gastrocnemius muscle** of LLC tumor-bearing mice. A and B: Immunoblot quantification (A) and representative immunoblots (B) of mitochondrial biogenesis regulators PGC-1α, PPARα, PPARδ and TFAM. c and d: Immunoblot quantification (C) and representative immunoblots (D) of mitochondrial dynamics regulators MFN1, MFN2, OPA1, DRP1 and Fis1. E and F: Immunoblot quantification (E) and representative immunoblots (F) of mitophagy regulators BNIP3, PINK1, p-PARKIN and PARKIN. N of 7-8 per group was utilized for immunoblot analysis. Lettering denotes statistical significance at an alpha set at $p<0.05$.

Figure 5

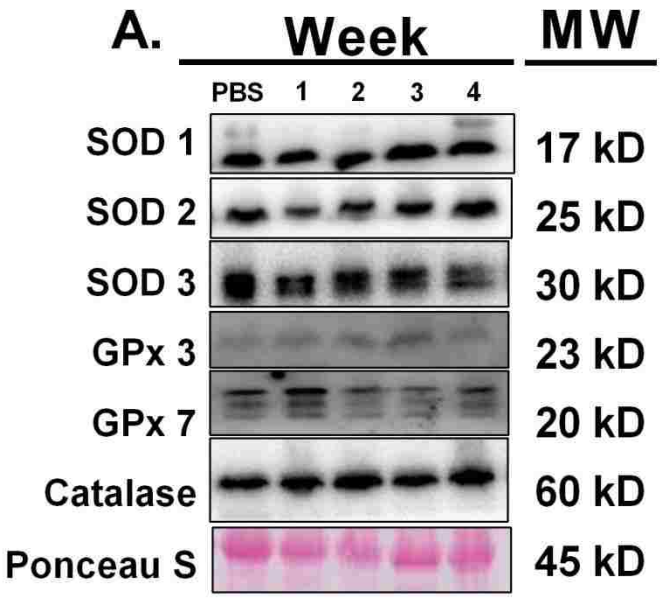

Figure 5. Content of antioxidant enzymes during progression of cancer-cachexia in gastrocnemius muscle of LLC tumor-bearing mice. A: Representative images of antioxidant enzymes. No statistically significant findings were found. N of 7-8 per group was utilized for immunoblot analysis.

Figure 6

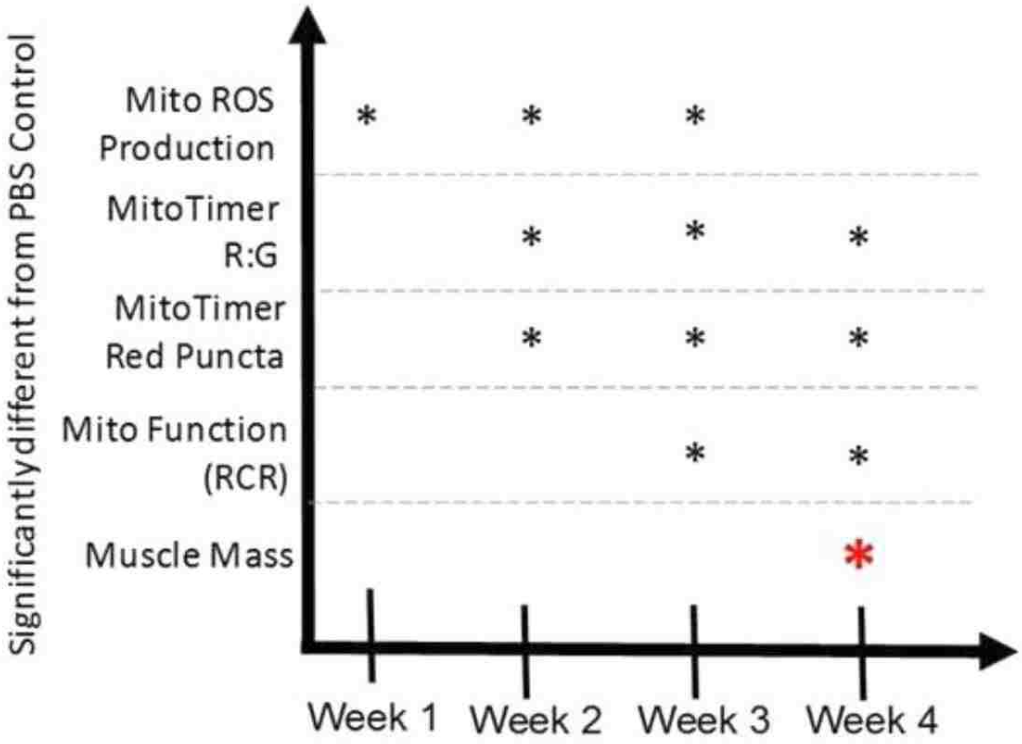

Figure 6. Summary of functional mitochondrial derangements preceding cachectic muscle wasting in tumor-bearing mice.

References

1. Ferlay J, Soerjomataram I, Dikshit R, Eser S, Mathers C, Rebelo M et al. Cancer incidence and mortality worldwide: sources, methods and major patterns in GLOBOCAN 2012. International journal of cancer. 2015;136(5):E359-86. doi:10.1002/ijc.29210.

2. Fitzmaurice C, Dicker D, Pain A, Hamavid H, Moradi-Lakeh M, MacIntyre MF et al. The Global Burden of Cancer 2013. JAMA oncology. 2015;1(4):505-27. doi:10.1001/jamaoncol.2015.0735.

3. Jemal A, Ward E, Hao Y, Thun M. Trends in the leading causes of death in the United States, 1970-2002. Jama. 2005;294(10):1255-9. doi:10.1001/jama.294.10.1255.

4. Fearon Kenneth CH, Glass David J, Guttridge Denis C. Cancer Cachexia: Mediators, Signaling, and Metabolic Pathways. Cell metabolism. 2012;16(2):153-66. doi:http://dx.doi.org/10.1016/j.cmet.2012.06.011.

5. Onesti JK, Guttridge DC. Inflammation based regulation of cancer cachexia. Biomed Res Int. 2014;2014:168407. doi:10.1155/2014/168407.

6. Fearon K, Strasser F, Anker SD, Bosaeus I, Bruera E, Fainsinger RL et al. Definition and classification of cancer cachexia: an international consensus. The Lancet Oncology. 2011;12(5):489-95. doi:10.1016/s1470-2045(10)70218-7.

7. Fearon K. Cachexia: Treat wasting illness on multiple fronts. Nature. 2016;529(7585):156. doi:10.1038/529156b.

8. Baltgalvis KA, Berger FG, Peña MMO, Davis JM, White JP, Carson JA. Muscle Wasting and Interleukin-6-Induced Atrogin-I Expression in the Cachectic Apc(Min/+) Mouse. Pflugers Archiv : European journal of physiology. 2009;457(5):989-1001. doi:10.1007/s00424-008-0574-6.

9. Li P, Waters RE, Redfern SI, Zhang M, Mao L, Annex BH et al. Oxidative phenotype protects myofibers from pathological insults induced by chronic heart failure in mice. The American journal of pathology. 2007;170(2):599-608. doi:10.2353/ajpath.2007.060505.

10. Yu Z, Li P, Zhang M, Hannink M, Stamler JS, Yan Z. Fiber type-specific nitric oxide protects oxidative myofibers against cachectic stimuli. PloS one. 2008;3(5):e2086. doi:10.1371/journal.pone.0002086.

11. Acharyya S, Ladner KJ, Nelsen LL, Damrauer J, Reiser PJ, Swoap S et al. Cancer cachexia is regulated by selective targeting of skeletal muscle gene products. J Clin Invest. 2004;114(3):370-8. doi:10.1172/jci20174.

12. Kandarian SC, Jackman RW. Intracellular signaling during skeletal muscle atrophy. Muscle & nerve. 2006;33(2):155-65. doi:10.1002/mus.20442.

13. Carson JA, Hardee JP, VanderVeen BN. The emerging role of skeletal muscle oxidative metabolism as a biological target and cellular regulator of cancer-induced muscle wasting. Seminars in cell & developmental biology. 2016;54:53-67. doi:10.1016/j.semcdb.2015.11.005.

14. Greene NP, Lee DE, Brown JL, Rosa ME, Brown LA, Perry RA et al. Mitochondrial quality control, promoted by PGC-1alpha, is dysregulated by Western diet-induced obesity and partially restored by moderate physical activity in mice. Physiol Rep. 2015;3(7). doi:10.14814/phy2.12470.

15. Laker RC, Xu P, Ryall KA, Sujkowski A, Kenwood BM, Chain KH et al. A novel MitoTimer reporter gene for mitochondrial content, structure, stress, and damage in vivo. The Journal of biological chemistry. 2014;289(17):12005-15. doi:10.1074/jbc.M113.530527.

16. Anderson EJ, Lustig ME, Boyle KE, Woodlief TL, Kane DA, Lin CT et al. Mitochondrial H2O2 emission and cellular redox state link excess fat intake to insulin resistance in both rodents and humans. J Clin Invest. 2009;119(3):573-81. doi:10.1172/jci37048.

17. Koves TR, Ussher JR, Noland RC, Slentz D, Mosedale M, Ilkayeva O et al. Mitochondrial overload and incomplete fatty acid oxidation contribute to skeletal muscle insulin resistance. Cell metabolism. 2008;7(1):45-56. doi:10.1016/j.cmet.2007.10.013.

18. Cannavino J, Brocca L, Sandri M, Bottinelli R, Pellegrino MA. PGC1-alpha over-expression prevents metabolic alterations and soleus muscle atrophy in hindlimb unloaded mice. J Physiol. 2014;592(20):4575-89. doi:10.1113/jphysiol.2014.275545.

19. Ji LL. Redox signaling in skeletal muscle: role of aging and exercise. Advances in physiology education. 2015;39(4):352-9. doi:10.1152/advan.00106.2014.

20. Bijland S, Mancini SJ, Salt IP. Role of AMP-activated protein kinase in adipose tissue metabolism and inflammation. Clinical science (London, England : 1979). 2013;124(8):491-507. doi:10.1042/cs20120536.

21. Debold EP. Potential molecular mechanisms underlying muscle fatigue mediated by reactive oxygen and nitrogen species. Frontiers in physiology. 2015;6:239. doi:10.3389/fphys.2015.00239.

22. Lamb GD, Westerblad H. Acute effects of reactive oxygen and nitrogen species on the contractile function of skeletal muscle. The Journal of physiology. 2011;589(Pt 9):2119-27. doi:10.1113/jphysiol.2010.199059.

23. Sivakumar AS, Hwang I. Effects of Sunphenon and Polyphenon 60 on proteolytic pathways, inflammatory cytokines and myogenic markers in H2O2-treated C2C12 cells. Journal of biosciences. 2015;40(1):53-9.

24. Liu J, Peng Y, Wang X, Fan Y, Qin C, Shi L et al. Mitochondrial Dysfunction Launches Dexamethasone-Induced Skeletal Muscle Atrophy via AMPK/FOXO3 Signaling. Molecular pharmaceutics. 2016;13(1):73-84. doi:10.1021/acs.molpharmaceut.5b00516.

25. White JP, Baltgalvis KA, Puppa MJ, Sato S, Baynes JW, Carson JA. Muscle oxidative capacity during IL-6-dependent cancer cachexia. American journal of physiology Regulatory, integrative and comparative physiology. 2011;300(2):R201-11. doi:10.1152/ajpregu.00300.2010.

26. Sullivan-Gunn MJ, Campbell-O'Sullivan SP, Tisdale MJ, Lewandowski PA. Decreased NADPH oxidase expression and antioxidant activity in cachectic skeletal muscle. Journal of cachexia, sarcopenia and muscle. 2011;2(3):181-8. doi:10.1007/s13539-011-0037-3.

27. Velazquez KT, Enos RT, Narsale AA, Puppa MJ, Davis JM, Murphy EA et al. Quercetin supplementation attenuates the progression of cancer cachexia in ApcMin/+ mice. The Journal of nutrition. 2014;144(6):868-75. doi:10.3945/jn.113.188367.

28. Yan Z, Lira VA, Greene NP. Exercise training-induced regulation of mitochondrial quality. Exercise and sport sciences reviews. 2012;40(3):159-64. doi:10.1097/JES.0b013e3182575599.

29. Puigserver P, Wu Z, Park CW, Graves R, Wright M, Spiegelman BM. A cold-inducible coactivator of nuclear receptors linked to adaptive thermogenesis. Cell. 1998;92(6):829-39.

30. Jin SM, Youle RJ. PINK1- and Parkin-mediated mitophagy at a glance. Journal of cell science. 2012;125(4):795-9. doi:10.1242/jcs.093849.

31. Lemasters JJ. Selective mitochondrial autophagy, or mitophagy, as a targeted defense against oxidative stress, mitochondrial dysfunction, and aging. Rejuvenation research. 2005;8(1):3-5. doi:10.1089/rej.2005.8.3.

32. White JP, Puppa MJ, Sato S, Gao S, Price RL, Baynes JW et al. IL-6 regulation on skeletal muscle mitochondrial remodeling during cancer cachexia in the ApcMin/+ mouse. Skeletal muscle. 2012;2:14. doi:10.1186/2044-5040-2-14.

33. Cannavino J, Brocca L, Sandri M, Grassi B, Bottinelli R, Pellegrino MA. The role of alterations in mitochondrial dynamics and PGC-1alpha over-expression in fast muscle atrophy following hindlimb unloading. J Physiol. 2015;593(8):1981-95. doi:10.1113/jphysiol.2014.286740.

34. Powers SK, Wiggs MP, Duarte JA, Zergeroglu AM, Demirel HA. Mitochondrial signaling contributes to disuse muscle atrophy. American journal of physiology Endocrinology and metabolism. 2012;303(1):E31-9. doi:10.1152/ajpendo.00609.2011.

35. Kuo YT, Shih PH, Kao SH, Yeh GC, Lee HM. Pyrroloquinoline Quinone Resists Denervation-Induced Skeletal Muscle Atrophy by Activating PGC-1alpha and Integrating Mitochondrial Electron Transport Chain Complexes. PloS one. 2015;10(12):e0143600. doi:10.1371/journal.pone.0143600.

36. Lee DE, Brown JL, Rosa-Caldwell ME, Blackwell TA, Perry RA, Jr., Brown LA et al. Cancer Cachexia-Induced Muscle Atrophy: Evidence for Alterations in microRNAs important for Muscle Size. Physiological genomics. 2017:physiolgenomics.00006.2017. doi:10.1152/physiolgenomics.00006.2017.

37. Puppa MJ, Gao S, Narsale AA, Carson JA. Skeletal muscle glycoprotein 130's role in Lewis lung carcinoma-induced cachexia. FASEB journal : official publication of the Federation of American Societies for Experimental Biology. 2014;28(2):998-1009. doi:10.1096/fj.13-240580.

38. Min K, Kwon O-S, Smuder AJ, Wiggs MP, Sollanek KJ, Christou DD et al. Increased mitochondrial emission of reactive oxygen species and calpain activation are required for doxorubicin-induced cardiac and skeletal muscle myopathy. The Journal of physiology. 2015;593(Pt 8):2017-36. doi:10.1113/jphysiol.2014.286518.

39. Brown LA, Lee DE, Patton JF, Perry RA, Brown JL, Baum J et al. Diet-induced obesity alters anabolic signaling in mice at the onset of muscle regeneration. Acta Physiologica. 2015:n/a-n/a. doi:10.1111/apha.12537.

40. Lee DE, Brown JL, Rosa ME, Brown LA, Perry RA, Jr., Washington TA et al. Translational machinery of mitochondrial mRNA is promoted by physical activity in Western diet-induced obese mice. Acta physiologica (Oxford, England). 2016. doi:10.1111/apha.12687.

41. Brown JL, Rosa-Caldwell ME, Lee DE, Brown LA, Perry RA, Shimkus KL et al. PGC-1alpha4 gene expression is suppressed by the IL-6-MEK-ERK 1/2 MAPK signalling axis and altered by resistance exercise, obesity and muscle injury. Acta physiologica (Oxford, England). 2016. doi:10.1111/apha.12826.

42. Rosa-Caldwell ME, Lee DE, Brown JL, Brown LA, Perry RA, Jr., Greene ES et al. Moderate physical activity promotes basal hepatic autophagy in diet-induced obese mice. Applied physiology, nutrition, and metabolism = Physiologie appliquee, nutrition et metabolisme. 2017;42(2):148-56. doi:10.1139/apnm-2016-0280.

43. Perry RA, Jr., Brown LA, Lee DE, Brown JL, Baum JI, Greene NP et al. Differential effects of leucine supplementation in young and aged mice at the onset of skeletal muscle regeneration. Mechanisms of ageing and development. 2016;157:7-16. doi:10.1016/j.mad.2016.05.007.

44. Powers SK, Lennon SL. Analysis of cellular responses to free radicals: focus on exercise and skeletal muscle. The Proceedings of the Nutrition Society. 1999;58(4):1025-33.

45. Constantinou C, Fontes De Oliveira CC, Mintzopoulos D, Busquets S, He J, Kesarwani M et al. Nuclear magnetic resonance in conjunction with functional genomics suggests mitochondrial dysfunction in a murine model of cancer cachexia. International journal of molecular medicine. 2011;27(1):15-24. doi:10.3892/ijmm.2010.557.

46. Romanello V, Sandri M. Mitochondrial biogenesis and fragmentation as regulators of muscle protein degradation. Current hypertension reports. 2010;12(6):433-9. doi:10.1007/s11906-010-0157-8.

47. Pin F, Busquets S, Toledo M, Camperi A, Lopez-Soriano FJ, Costelli P et al. Combination of exercise training and erythropoietin prevents cancer-induced muscle alterations. Oncotarget. 2015;6(41):43202-15. doi:10.18632/oncotarget.6439.

48. Anderson LJ, Albrecht ED, Garcia JM. Update on Management of Cancer-Related Cachexia. Current oncology reports. 2017;19(1):3. doi:10.1007/s11912-017-0562-0.

49. Ciciliot S, Rossi AC, Dyar KA, Blaauw B, Schiaffino S. Muscle type and fiber type specificity in muscle wasting. The international journal of biochemistry & cell biology. 2013;45(10):2191-9. doi:10.1016/j.biocel.2013.05.016.

50. Charles AL, Guilbert AS, Guillot M, Talha S, Lejay A, Meyer A et al. Muscles Susceptibility to Ischemia-Reperfusion Injuries Depends on Fiber Type Specific Antioxidant Level. Frontiers in physiology. 2017;8:52. doi:10.3389/fphys.2017.00052.

51. Okutsu M, Call JA, Lira VA, Zhang M, Donet JA, French BA et al. Extracellular superoxide dismutase ameliorates skeletal muscle abnormalities, cachexia, and exercise intolerance in mice with congestive heart failure. Circulation Heart failure. 2014;7(3):519-30. doi:10.1161/circheartfailure.113.000841.

52. Max SR. Disuse atrophy of skeletal muscle: loss of functional activity of mitochondria. Biochemical and biophysical research communications. 1972;46(3):1394-8.

53. White JP, Baynes JW, Welle SL, Kostek MC, Matesic LE, Sato S et al. The regulation of skeletal muscle protein turnover during the progression of cancer cachexia in the Apc(Min/+) mouse. PloS one. 2011;6(9):e24650. doi:10.1371/journal.pone.0024650.

54. Varanita T, Soriano Maria E, Romanello V, Zaglia T, Quintana-Cabrera R, Semenzato M et al. The Opa1-Dependent Mitochondrial Cristae Remodeling Pathway Controls Atrophic, Apoptotic, and Ischemic Tissue Damage. Cell metabolism. 2015;21(6):834-44. doi:10.1016/j.cmet.2015.05.007.

55. Benard G, Bellance N, James D, Parrone P, Fernandez H, Letellier T et al. Mitochondrial bioenergetics and structural network organization. Journal of cell science. 2007;120(Pt 5):838-48. doi:10.1242/jcs.03381.

56. Wada J, Nakatsuka A. Mitochondrial Dynamics and Mitochondrial Dysfunction in Diabetes. Acta medica Okayama. 2016;70(3):151-8.

57. Pickrell AM, Youle RJ. The roles of PINK1, parkin, and mitochondrial fidelity in Parkinson's disease. Neuron. 2015;85(2):257-73. doi:10.1016/j.neuron.2014.12.007.

58. Youle RJ, Narendra DP. Mechanisms of mitophagy. Nat Rev Mol Biol. 2011;12.

59. Appell HJ, Duarte JA, Soares JM. Supplementation of vitamin E may attenuate skeletal muscle immobilization atrophy. International journal of sports medicine. 1997;18(3):157-60.

60. Whidden MA, Smuder AJ, Wu M, Hudson MB, Nelson WB, Powers SK. Oxidative stress is required for mechanical ventilation-induced protease activation in the diaphragm. Journal of applied physiology (Bethesda, Md : 1985). 2010;108(5):1376-82. doi:10.1152/japplphysiol.00098.2010.

61. McClung JM, Judge AR, Talbert EE, Powers SK. Calpain-1 is required for hydrogen peroxide-induced myotube atrophy. American journal of physiology Cell physiology. 2009;296(2):C363-71. doi:10.1152/ajpcell.00497.2008.

62. Powers SK, Morton AB, Ahn B, Smuder AJ. Redox control of skeletal muscle atrophy. Free radical biology & medicine. 2016;98:208-17. doi:10.1016/j.freeradbiomed.2016.02.021.

63. Li YP, Chen Y, Li AS, Reid MB. Hydrogen peroxide stimulates ubiquitin-conjugating activity and expression of genes for specific E2 and E3 proteins in skeletal muscle myotubes. American journal of physiology Cell physiology. 2003;285(4):C806-12. doi:10.1152/ajpcell.00129.2003.

64. O'Loghlen A, Perez-Morgado MI, Salinas M, Martin ME. N-acetyl-cysteine abolishes hydrogen peroxide-induced modification of eukaryotic initiation factor 4F activity via distinct signalling pathways. Cellular signalling. 2006;18(1):21-31. doi:10.1016/j.cellsig.2005.03.013.

65. Reggiani C. Regulation of muscle mass: a new role for mitochondria? The Journal of physiology. 2015;593(8):1761-2. doi:10.1113/jp270216.

66. Borgia D, Malena A, Spinazzi M, Andrea Desbats M, Salviati L, Russell AP et al. Increased mitophagy in the skeletal muscle of spinal and bulbar muscular atrophy patients. Human molecular genetics. 2017. doi:10.1093/hmg/ddx019.

67. Muscaritoli M, Rossi Fanelli F, Molfino A. Perspectives of health care professionals on cancer cachexia: results from three global surveys. Annals of Oncology. 2016;27(12):2230-6. doi:10.1093/annonc/mdw420.

68. von Haehling S, Morley JE, Coats AJ, Anker SD. Ethical guidelines for publishing in the Journal of Cachexia, Sarcopenia and Muscle: update 2015. Journal of cachexia, sarcopenia and muscle. 2015;6(4):315-6. doi:10.1002/jcsm.12089.

Chapter 4

Protein Imbalance in the Development of Skeletal Muscle Wasting in Tumor-Bearing Mice.

Jacob L. Brown[1], David E. Lee[1], Megan E. Rosa-Caldwell[1], Thomas A. Blackwell[1], Lemuel A. Brown[2], Richard A. Perry[2], Wesley S. Haynie[2], Kendra Huseman[4], Kavithalakshmi Sataranatarajan[4], Holly Van Remmen[4], Michael P. Wiggs[3], Tyrone A. Washington[2], Nicholas P. Greene[1]

[1] Integrative Muscle Metabolism Laboratory, Exercise Science Research Center, Department of Health, Human Performance and Recreation, University of Arkansas, Fayetteville, AR 72701

[2] Exercise Muscle Biology Laboratory, Exercise Science Research Center, Department of Health, Human Performance and Recreation, University of Arkansas, Fayetteville, AR 72701

[3] Integrated Physiology and Nutrition Laboratory, Department of Health and Kinesiology, University of Texas at Tyler, TX 75799

[4]Aging and Metabolism Research Program, Oklahoma Medical Research Foundation, 825 N.E. 13th Street, Oklahoma City, OK 73104, United States; Oklahoma City VA Medical Center, Oklahoma City, OK, United States.

Corresponding Author: Nicholas P. Greene

Exercise Science Research Center

University of Arkansas

155 Stadium Dr, 321Q HPER

Fayetteville, AR 72701

E-mail: npgreene@uark.edu

Phone: 479-575-6638

Fax: 479-575-2853

Running Title: Cancer cachexia induced by dysregulated protein turnover.

Abstract

Cancer cachexia occurs in approximately 80 percent of cancer patients and is a key contributor to cancer-related death. The mechanisms controlling development of tumor-induced muscle wasting are not fully elucidated. Specifically, the progression of cancer-cachexia is underexplored. Therefore, we examined skeletal muscle mass throughout the progression of cancer-cachexia. Lewis Lung Carcinoma (LLC) was injected into the hind-flank of C57BL6/J mice at 8 wks age with tumor allowed to develop for 1, 2, 3, or 4 wks and compared to PBS injected control. Tumor-induced muscle wasting was evident at 4 wks following LLC-implantation. Muscle cross sectional area decreased ~40% and collagen deposition increased 3-fold 4 wks following tumor implantation. Myogenic signaling was altered in tumor-bearing mice when compared to control animals. Protein synthesis did not change throughout the progression of cancer-cachexia. FOXO1/3 mediated ubiquitin proteasome system was induced 4 wks following tumor implantation. Moreover, there was an increase in autophagy machinery after 4 wks of tumor growth. Apoptosis mediated DNA damage did not change throughout the progression of cancer-cachexia. Finally, MAPK signaling was altered in cachectic muscle. These data show dysregulation of controllers of skeletal muscle mass throughout a time-course progress of cancer-cachexia and give insight to potential therapeutic mechanisms.

Key Words: protein synthesis, LLC, ubiquitin, MAPK, ERK, p38

Introduction

Cancer is one of the leading causes of death worldwide with over half of the people affected by cancer dying as a result of the condition [1, 2]. Cancer-cachexia is a wasting syndrome that occurs in approximately 80% of cancer patients [3-5]. In fact, cancer-cachexia is the primary cause of death for 20%-40% of cancer deaths [3-5]. Cancer-cachexia is defined as a multifactorial syndrome which displays an ongoing loss of skeletal muscle mass (with or without loss of fat mass) that cannot be fully reversed by conventional nutritional support and leads to progressive functional impairment [3, 5]. As efforts to reverse cancer-cachexia have been largely unsuccessful, recent suggestions in the literature have emphasized needs to focus on prevention of the condition [6]. However, few efforts have been placed toward understanding the early stage development of cancer-cachexia. We recently demonstrated that muscle mitochondrial health is impaired well before onset of measurable muscle wasting in cancer-cachexia in Lewis Lung Carcinoma (LLC) tumor-bearing mice using a time course model [7]. Those data suggest early onset derangements in muscle health. Therefore, it may become critical to define the early alterations that may trigger the onset of the cachectic phenotype to best define mechanisms of cancer-induced muscle wasting. However, skeletal muscle atrophy occurs primarily by an imbalance of protein turnover favoring protein degradation over protein synthesis [8, 9]; yet, the underlying mechanisms of muscle loss in the development of cancer-cachexia have not been fully elucidated. Therefore, a critical need remains to define alteration of muscle protein turnover processes in the development of cancer-cachexia induced muscle wasting.

From prior literature, it is clear cancer-cachexia is associated with decreased rates of muscle protein synthesis, and increased rates of protein degradation [10-13]. We also know that protein turnover is regulated by a series of anabolic processes including myogenesis and protein

synthesis [14-16] [17, 18] [19, 20] [21, 22] [10-13], and catabolic processes including the ubiquitin proteasome system, autophagy, and apoptosis [23] [24] [13] [8, 25] [26-28]. Each of these processes may present significant dysregulation during cancer-cachexia; however, the nature by which this negative protein balance develops in cancer-cachexia remains largely unknown. The initial development of cancer- induced muscle wasting is understudied in scientific literature despite the need to consider measures to prevent the condition. Therefore, the purpose of this study was to examine regulation of protein turnover in skeletal muscle throughout a time course progression of cancer-cachexia in tumor-bearing mice. By examining a comprehensive measurement of protein turnover regulation throughout the progression of cancer-cachexia we provide key information about the pathogenesis of this condition.

Methods

Animals and Interventions

Animal experiments were performed at the University of Arkansas, Fayetteville. All procedures were approved by the Institutional Animal Care and Use Committee of the University of Arkansas. We have previously reported on several aspects of these animals regarding body and tissue masses and mitochondrial health [7].

Tumor Implantation and Tissue Collection. Male C57BL/6J mice were purchased from Jackson Laboratories. The mice were kept on a 12:12-h light-dark cycle with *ad libitum* access to normal rodent chow and water. $1X10^6$ LLC cells suspended in sterile PBS were implanted to the hind flank of mice at 8 weeks of age [7]. The tumor was allowed to develop for 1, 2, 3 or 4 weeks as previously described [7]. To allow measure of protein synthesis, a bolus of deuterium oxide (~20 µL/g body weight) was injected intraperitoneally in the mouse approximately 24 hours before tissue collection. Drinking water was thereafter supplemented with 4% deuterium oxide in order to maintain the plasma pool of deuterium oxide [29-31]. Animal tissues were quickly collected under isoflurane anesthesia prior to euthanasia. Tissues were quickly weighed and snap-frozen in liquid nitrogen for further processing and stored at -80°C.

Histology

Tibialis Anterior (TA) muscles were imbedded in optimal cutting temperature (OCT) compound and frozen for sectioning. Sections were cut at 10 µm using a Leica CM1859 cryostat (Leica Biosystems, Buffalo Grove, IL) and stained with Hematoxylin & Eosin (H & E) for cross sectional area analysis. Muscle fibers were circled using Nikon Basic Research Imaging Software (Melville, NY). Roche Diagnostics (Indianapolis, IN) *In Situ* cell death detection

Fluorescein (11684795910) was used to detect damaged DNA. Manufacturer's protocols were used. Slides were mounted with DAPI mounting media. Nikon Ti-S inverted epiflourescent microscope with LED-based light source was used to image total nuclei (DAPI) and TUNEL + nuclei (FITC). Total nuclei and TUNEL + nuclei were then counted using Nikon Basic Research Imaging Software.

24-Hour Protein Synthesis In-Vivo

A detailed description of this method for measuring protein synthesis has previously been published [32]. 15 mg and 35 mg of gastrocnemius muscle were powdered and homogenized in a 10% TCA solution for mixed and myofibrillar FSR, respectively. In order to isolate the myofibrillar fraction, homogenate was centrifuged at 600 G for 15 minutes. The supernatant containing cytosolic proteins was then discarded. Mixed and myofibrillar fractions were then washed 3 times with 10% TCA solution by centrifugation to eliminate cytosolic amino acids and subsequently placed in 6 M HCL. The solution was then heated at 100˚C for 24 hours in order to break down proteins into their amino acid building blocks. An aliquot of the hydrolysate was dried down and derivatized with a 3:2:1 solution of methyl-8, methanol, and acetonitrile to determine ^{2}H-labeling of alanine on its methyl-8 derivative. The solution was then placed in a GC-MS capillary column (Agilent 7890A GC HP-5 ms capillary column) and positioned in the GC-MS. 1 µL of solution was ran on the Agilent GC-MS at an 80:1 split. GC-MS settings have previously been described [32, 30]. A ratio of deuterated alanine over alanine was employed to assess protein synthesis. In order to normalize results based on the precursory pool of ^{2}H2O, plasma was reacted with 10 M NaOH and a 5% solution of acetone in acetonitrile for 24 h in order to conjugate the free ^{2}H2O to acetone. The solution was extracted by adding Na_2SO_4 and chloroform, and placed in capillary columns to be analyzed on the GC-MS to detect acetone at

an 80:1 split. FSR of mixed and myofibrillar proteins were calculated using the equation EA × [EBW × 3.7 × t (h)]−1 × 100, where EA represents amount of protein-bound [2H]alanine (mole% excess), EBW is the quantity of $^{2}H2O$ in body water (mole% excess), 3.7 represents the exchange of 2H between body water and alanine (3.7 of 4 carbon-bound hydrogens of alanine exchange with water) and t(h) represents the time the label was present in hours.

RNA isolation, cDNA synthesis, and quantitative real-time PCR

Adult gastrocnemius muscles were collected and frozen in liquid nitrogen at time of harvest. 20-30 µg of powdered gastrocnemius muscle was homogenized into a 1 mL TRIZOL solution, and RNA was isolated using a commercially available kit (Ambion, Life Technologies). Isolated RNA purity and concentration was confirmed using Bio-Tek (Winooski, VT) Power Wave XS plate reader with Take3 microvolume plate and Gen5 software. After which, 1 µg of RNA was reverse transcribed into cDNA using previously described methods and Vilo SuperScript (11755050, Invitrogen, Carlsbad, CA) reagents cDNA was diluted to 1:100 (10 ng/µL) and Ct values analyzed using TaqMan reagents and commercial Step-One real-time RT-PCR instrumentation (Applied BioSystems, Foster City, CA). Assessment of 18s (Mm03928990_g1), *Pax7* (Mm01354484_m1), *MyoD* (Mm00440387_m1), *MyoG* (Mm00446194_m1) and *Igf1* (Mm00439561_m1) were performed using TaqMan probes (Life Technologies) and corresponding TaqMan reagents. No differences were seen in 18s among experimental conditions for experiments presented. Final quantification of gene expression was calculated using the ΔΔCT method. Relative quantification was calculated as $2^{-\Delta\Delta CT}$.

Immunoblotting

Gastrocnemius muscle was homogenized in a buffer containing 0.23 M Tris-HCL, pH 6.8, 4.5% w/v SDS, 45% glycerol, 0.04% w/v Bromophenol Blue, 80 mM dithiothreitol, 0.57mM 2-mercaptoethanol, complete, mini protease inhibitor cocktail (Roche, Indianapolis, IN), and phosphatase inhibitor cocktails (Sigma-Aldrich) and denatured at 95°C. Concentrations were determined using the RC/DC assay (500-0119, BioRad, Hercules, CA) and 40 μg total protein was resolved by SDS-PAGE, transferred to a PVDF membrane and blocked in 3% w/v Bovine Serum Albumin in Tris-buffered saline with 0.2% Tween 20 (TBST). Membranes were probed overnight for primary antibodies specific to p-AKT (Cell Signaling 9271), AKT (Cell Signaling 9272), p-4EBP1 (Cell Signaling 9644), 4EBP1 (Cell Signaling 9452), p-p70s6k (Cell Signaling 9205), p70s6k (Cell Signaling 9202), p-FOXO1 (Cell Signaling 9464), FOXO1 (Cell Signaling 2880), p-FOXO3 (Cell Signaling 9464), FOXO3 (Cell Signaling 2497), p-FOXO4 (Cell Signaling 9471), FOXO4 (Cell Signaling 9472), Beclin1 (Cell Signaling 3738), p62 (Sigma p0067) and LC3 (Cell Signaling 4108) isolated from rabbit and mouse. Antibodies were diluted in TBST with 5% milk. Licor secondary antibodies conjugated with HRP (animal experiments) or Infared (IR) Dye (cell culture experiments) were used according to manufacturers protocols. For animal experiments, membranes were imaged on Protein Simple FluorChem (Minneapolis, MN) with Licor WesternSure Premium Chemiluminescent substrate (926-95000) and analyzed using Alpha View software. For cell culture experiments membranes were imaged on Licor Odyssey FC using IR detection. All bands were normalized to the 45 kDa Actin band of Ponceau S stain as a loading control.

Statistical Analysis

For animal experiments, independent factors were PBS and number of weeks tumor progressed. A One-Way ANOVA was employed as the global analysis for each dependent variable. Where significant F-ratios were found, differences among means were determined by Student Newman-Keuls post hoc test. For all experiments, the comparison-wise error rate, α, was set at 0.05 for all statistical tests. All data were analyzed using the Statistical Analysis System (SAS, version 9.3, Cary, NC, USA), figures were compiled using GraphPad Prism (La Jolla, CA, USA) and data expressed as mean ± SEM.

Results

Characterization of the progression of LLC-induced cancer-cachexia. Phenotypic characteristics of these mice including body and tissue masses have previously been reported [7]. Most importantly, muscle wet weights were ~15-20% lower 4 wks following tumor implantation when compared to PBS control mice [7]. Here, we report that mean CSA of TA muscle fibers were ~15% smaller 3 wks following tumor implantation and ~40% smaller by 4 wks of tumor growth compared to PBS control mice (Figure 1B). Furthermore, there were a larger number of small fibers (200μM^2-600μM^2 area) and a smaller number of large fibers (>1400 μM^2) when comparing 4 wks of tumor burden to PBS control mice (Figure 1C). Finally, we assessed mRNA content of putative markers of muscle denervation. We observed that while mRNA of Acetylcholine Receptor (AchR) α, Gad45A, RUNX1 and MusA were not significantly altered (Figure S1). AchR δ and AchR ε were downregulated by ~35% and 45% 2 wks and 3 wks following tumor implantation, respectively (Figure S1).

Myogenic signaling is impaired 1 wk following tumor implantation. To determine the impacts of the tumor-bearing state on anabolic functions in the muscle we assessed aspects of myogenesis and protein synthesis. Briefly, myogenesis is the formation of muscular tissue which is necessary for repair of injured muscle. Satellite cells are labeled with Pax7 [33]. Upon activation, satellite cells express MyoD and subsequently Myogenin which is responsible for proliferation and differentiation of satellite cells, respectively [21, 22]. From these assessments we observed that *Pax7* mRNA content was ~35% lower 1 wk following tumor implantation when compared to PBS control mice, and did not recover throughout the progression of cancer-cachexia (Figure 2A). *MyoD* mRNA content was ~50% lower in both 1 wk and 2 wk tumor-bearing groups when compared to PBS control mice (Figure 2B). mRNA content of *MyoD* recovered 3 wks following tumor implantation. In tumor-bearing mice, *CyclinD1* mRNA content was ~45% lower than PBS control mice in all tumor-bearing groups (Figure 2C). *Myogenin* mRNA was ~50% lower than PBS control mice 1 wk following tumor implantation, but recovered by 3 and 4 wks following tumor implantation (Figure 2D).

Mixed protein synthetic rate is lower in cachectic muscle. Next, in our assessment of anabolic function we determined 24-h FSR and assessed mTOR signaling components. Mixed muscle FSR was ~40% lower than the PBS control group 4 wks following tumor implantation with no other significant differences among experimental conditions (Figure 3A). In contrast, there was no significant change in myofibillar FSR during the progression of cancer-cachexia (Figure 3B); however, there was a mean decrease in the 3 and 4 wk groups when compared to PBS. To examine mTOR related signaling we assessed the upstream marker Akt, mTOR Complex component and negative regulator of mTOR – Deptor, and downstream mTOR targets p70S6K1 and 4EBP-1 [34] [17, 18]. We observed that content and phosphorylation of Akt,

p70s6k and 4EBP1 did not change throughout the progression of cancer-cachexia (Figure 3 C,E,F). However, Deptor protein content was ~40% greater 3 wks following tumor implantation when compared to other experimental groups (Figure 3D).

Protein breakdown is upregulated in cachectic muscle. To investigate the contributions of putative catabolic processes we assessed markers of the ubiquitin-proteasome system, autophagy and apoptosis. With regards to the ubiquitin-proteasome system, FOXO1 and FOXO3 signaling are important regulators of the atrogenes: Atrogin1 and MuRF1 [23]. These are important E3 ligases known to promote skeletal muscle wasting [23]. We observed that total FOXO1 protein content was ~50% greater than PBS control mice 4 wks following tumor implantation (Figure 4A). Phosphorylation of FOXO1^{T24} and FOXO4^{T28} did not change as tumor growth progressed; however, there was a non-significant ~50% mean increase in FOXO3^{T32} phosphorylation relative to total protein content 4 wks following tumor implantation when compared to other experimental groups (Figure 4B). Furthermore, Atrogin1 mRNA content was 3 fold greater than PBS control mice 4 wks after tumor implantation (Figure 4C), while MuRF1 mRNA content was 2 and 4 fold greater than PBS control mice at 3 and 4 wks following tumor implantation (Figure 4D), respectively. Muscle protein ubiquitination was ~50% higher than PBS control mice 4 wks following tumor implantation (Figure 4E).

To provide insight into the potential contributions of autophagy, a process involved in the formation of an autophagosome in order to facilitate lysosomal clearance of proteins and organelles [26-28], we examined upstream regulator Beclin1, as well as LC3 (involved in the closing of the autophagosome) and p62 (a linker protein between the autophagosome and cargo that is degraded by the lysosome upon completion of autophagy). Beclin1 protein content was ~80% greater than PBS control mice 4 wks post tumor implantation (Figure 4F). Furthermore,

total LC3 protein content was ~60% higher than PBS control mice after 4 wks of tumor growth (Figure 4G). By contrast, there was no change in the LC3 II:I ratio (an indicator of autophagy initiation) throughout the progression of cancer-cachexia (Figure 4H) nor in protein content of p62 (marker of autophagy resolution, Figure 4I).

Apoptosis is not altered in progression of LLC-induced cancer-cachexia. To examine apoptosis in cachectic muscle, we used TUNEL staining, and Caspase 3 protein content. Loss of myonuclei may limit the muscles' ability to increase in size. There was no significant difference in the number of TUNEL positive nuclei throughout the progression of cancer-cachexia (Figure 5A). Moreover, total Caspase 3 was not different between the PBS, 1 wk, 2 wk, 3 wk and 4wk groups (Figure 5B). Cleaved Caspase 3 was not detectable by immunoblot.

MAPK phosphorylation is induced in tumor-bearing mice. MAPKs are key controllers of both anabolic and catabolic signaling within skeletal muscle [35, 36], therefore in order to assess MAPKs in cachectic muscle we examined p38 and ERK phosphorylation status. $ERK^{T202/Y204}$ and $p38^{T180/Y182}$ MAPK phosphorylations relative to respective total protein contents were 4 fold and 3 fold greater than PBS control mice 4 wks following tumor implantation, respectively (Figure 6A/B).

Discussion

Loss of muscle mass occurs largely from an imbalance of protein turnover favoring protein degradation [37], which is commonly observed in late stage cancer-cachexia [11, 10, 38]; however, we are the first to measure modalities of protein turnover throughout a time course development of LLC-induced cancer-cachexia. We recently demonstrated that impaired mitochondrial health develops well prior to onset of muscle wasting [7]. Those data suggest

impaired myocellular health prior to measurable muscle wasting. Here, we have shown alterations in cellular programing necessary for the maintenance of muscle mass as soon as 1 wk following tumor implantation with impaired signaling for satellite cell proliferation and myogenesis. Interestingly, through additional assessments of muscle protein synthesis and degradative pathways including autophagy, ubiquitin-proteasome system and apoptosis, it appears primary decrements contributing to the negative protein balance occur via activation of the ubiquitin-proteasome system and reduced mixed muscle protein synthesis which develop concurrent to the onset of phenotypic muscle wasting. The data presented in this study provides a comprehensive overview of machinery responsible for the maintenance of muscle mass throughout the progression of cancer-cachexia in tumor-bearing mice.

Cross Sectional Area is altered in tumor-bearing mice. In the current study cachectic muscle mass loss developed at 4 wks post tumor implantation, which is commonly observed in this model [39, 16, 40, 7]. These mice display a degree of muscle mass loss (~15% smaller muscle wet weights [7], and a ~40% decrease in mean CSA) that would be considered a negative prognosis clinically and greatly increase mortality among cancer patients. However, the reductions in total muscle mass are smaller than many prior reports and without significant loss in tumor free body mass suggesting that 4 wk tumor-bearing mice displayed mild/moderate cachexia. We have demonstrated that *AchR* δ and ε are downregulated in cachectic muscle; however, at this point we cannot conclude that functional denervation is occurring. In fact, AChR density is often higher than needed for efficient capture of the acetylcholine released [41]; therefore, functional denervation is not likely occurring at this stage in the development of cancer-cachexia.

Satellite Cells and Myogenic Signaling. In cancer-cachexia, the sarcolemma becomes damaged due to factors secreted by the tumor, which elicits a repair response [19]. Our data indicates *Pax7* mRNA, a satellite cell marker, content decreased as soon as 1 wk following tumor implantation, implying the satellite cell pool may be diminished thus impairing regenerative capacity shortly after the onset of the tumor-bearing state [42]. Intriguingly, these results appear to contradict findings from He et al. [20] in which an increase in Pax7 protein content was noted in response to tumor burden in both C26 and LLC models of cancer-cachexia. These contradictions may be due to methodology differences to measure Pax7 expression. It is possible that reduced *Pax7* mRNA here coupled with increased Pax7 protein previously reported [20] indicates altered turnover of Pax7 and accumulation of dysfunctional satellite cells, at current though this speculation requires further testing to resolve. Moreover, our data shows that both MyoD (important for satellite cell proliferation [22]), MyoG (important for satellite cell differentiation [22]) and Cyclin D1 mRNAs content are decreased 1 wk following tumor implantation. Dysregulation of *MyoD* and *MyoG* mRNA expression corroborates recent findings outlining impaired myogenesis in response to tumor burden in mice [20]. Taken together the aberrant myogenic signaling we observe suggests a potential limit on muscle regrowth potential post cancer treatment suggesting a need to determine means impairing myogenic potential in early tumor-bearing states to prevent this effect.

Mixed muscle protein synthesis is reduced concurrent to muscle wasting in tumor-bearing mice. In cancer cachexia literature, there is an ongoing debate as to whether a decrease in protein synthesis, upregulated protein degradation or both play a bigger role in the onset of cancer-induced muscle wasting [43]. There appears to be discrepancies based on both the type of model used and the methodology for measuring protein synthesis [43, 44, 38, 16, 45]. Our

protein synthesis data showed a decrease in the mixed muscle fraction with no change in the myofibrillar fraction (despite a ~25% mean decrease in FSR) measured over a 24 hour time period. These results corroborate studies such as Toledo et al. [44] which describes a ~50% reduction in protein synthesis in the gastrocnemius muscle in LLC tumor bearing mice. We are the first to measure protein synthesis in LLC tumor-bearing mice utilizing deuterium oxide for a 24 hour time period, a validated measurement of protein synthesis [29], in LLC tumor-bearing mice. This approach, may provide a specific advantage in the ability to assess protein synthetic function over the course of a full light/dark cycle and thus a potentially more accurate reflection of basal protein synthetic rates. In regards to myofibrillar protein synthesis, we should note that most reports measuring muscle protein synthesis in a cachectic phenotype have more severe wasting with greater losses in muscle masses and losses in total body mass than this study [16, 44, 46, 47]. It is likely that development of a more severe phenotype would alter protein synthetic signaling and induce a more severe loss of myofibrillar FSR comparable to other studies. These data suggest that decrements in mixed-muscle protein synthesis is a significant contributor to muscle wasting in LLC tumor-bearing mice.

Induction of skeletal muscle protein degradation systems in tumor-bearing mice. Our data indicates that there is increased protein breakdown 4 wks after tumor implantation which in the absence of impairments in protein synthesis likely explains muscle mass losses at this stage of cachectic development. We note upregulation of E3 ligases *Atrogin1* and *MuRF1* 4 wks following tumor implantation with concomitantly increased protein ubiquitination. This increase in the ubiquitin-proteasome system likely occurs through enhanced FOXO1 content and a mean increase FOXO3 phosphorylation 4 wks following tumor-implantation.

Autophagy is another key controller of protein breakdown [26-28]. Our data indicates an increase in Beclin1 and LC3 protein content 4 wks following tumor-implantation. Based on current data it appears that rates of autophagy are not significantly enhanced in the cachectic state; however, autophagy machinery (Beclin1 and LC3) appears to be upregulated suggesting greater capacity for protein degradation through this system in cachectic muscle. Finally, we observed no significant induction of apoptosis in the muscle of cachectic mice, suggesting that at this stage of mild/moderate cachectic wasting apoptosis is not a primary contributor to muscle protein degradation.

Therefore, in our assessments of muscle anabolic and catabolic functions in tumor-bearing mice we observe early onset decrements to myogenic signaling, followed by reduced mixed muscle protein synthesis, increased ubiquitin-proteasome function, increased atrogene expression and an upregulation of autophagy machinery. Loss of protein synthesis and the promotion of protein breakdown occur concomitantly with cancer-mediated muscle loss.

MAPK signaling is altered in tumor-bearing mice. To identify potential mechanisms leading to impaired protein anabolism and enhanced protein ubitination we next examined MAPK signaling in tumor-bearing mice. Our data shows that both ERK and p38 MAPK phosphorylation's increase by 4 fold and 3 fold, respectively 4 wks following tumor implantation. Prior literature shows an increased phosphorylation of these MAPKs can lead to both impaired muscle regeneration and increased protein breakdown [48, 35, 36, 49-52]. The next chapter in this dissertation further explores MAPKs role in the promotion of cancer-mediated muscle loss.

Summary and conclusions. In this study, we have analyzed muscle size, myogenesis, protein turnover and apoptosis throughout the progression of cancer-cachexia. Based on our data, loss of mixed protein synthetic rates along with increased protein breakdown via the ubiquitin-proteasome system are likely the major contributors for the onset of cancer-cachexia in LLC tumor-bearing mice. Furthermore, there appears to be early alterations in myogenic signaling potentially contributing to the irreversibility of cancer-cachexia. Future research should continue to examine MAPKs role in cancer-induced muscle wasting. These data will provide novel information for the development of therapies to prevent and treat cancer-cachexia.

Acknowledgements

Support for LLC experiments has been provided in part by the Arkansas Biosciences Institute, the major research component of the Arkansas Tobacco Settlement Proceeds Act of 2000 and National Institutes of Health under Award Number R15AR069913 from the National Institute of Arthritis And Musculoskeletal And Skin Diseases and the National Institute Of General Medical Sciences. Contents of this publication are solely the responsibility of the authors and do not necessarily represent the official views of the ABI, NIGMS or NIH. The authors would like to thank Drs. Sami Dridi, Elizabeth Greene and Jeffrey Wolchok (U. Arkansas), as well as Mr. Connor Benson (UT Tyler), Ms. Haley McCarver and Mrs. Katie Stephenson-Brown for their contributions to the experiments presented here and editing. We would like to thank the Cell and Molecular Biology program at the University of Arkansas, Fayetteville for supporting Jacob L. Brown's graduate education. We would also like to extend our gratitude to the numerous other faculty, Exercise Science Research Center at the University of Arkansas.

Figures

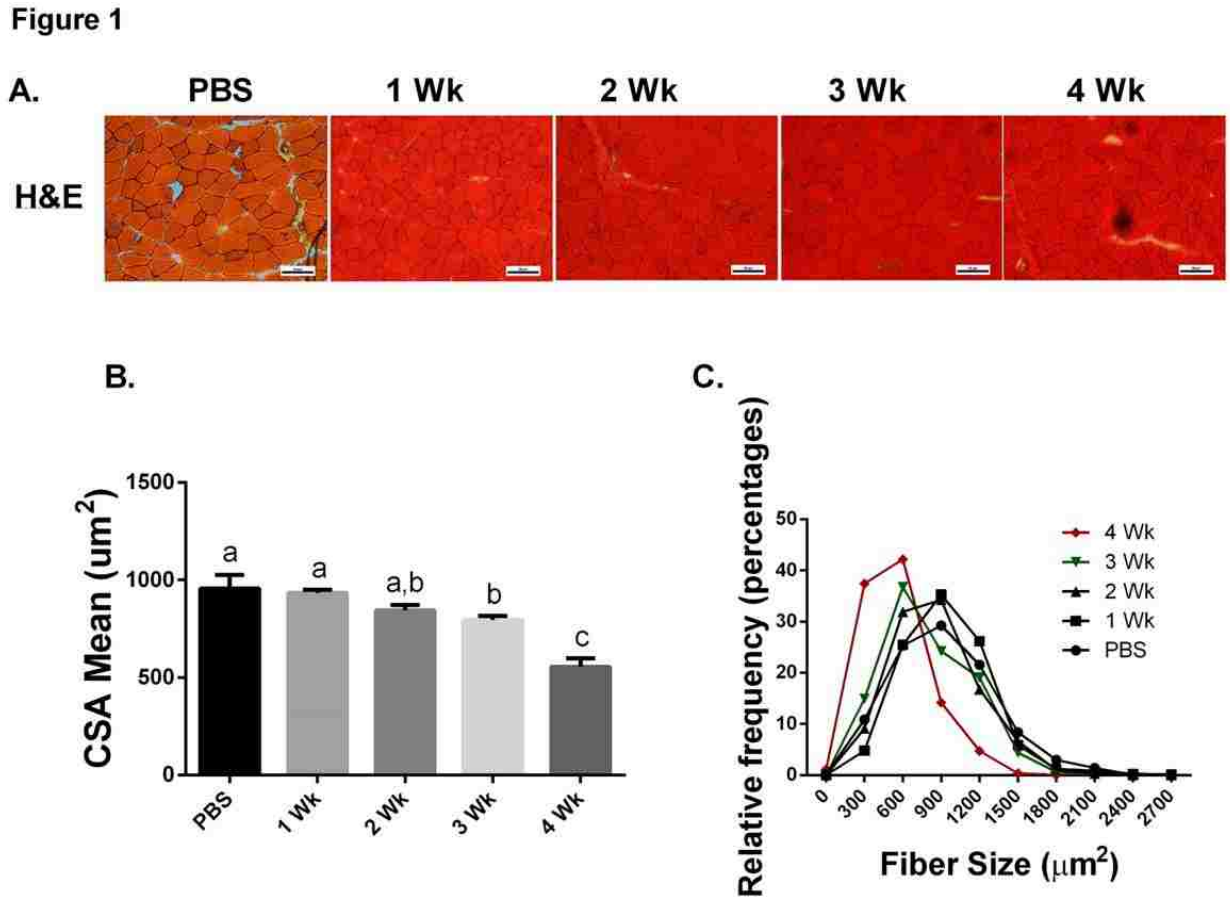

Figure 1. Cross sectional area throughout the progression of cancer-cachexia. A: Hematoxylin and Eosin staining sample images (scale 50 μM). B. Mean CSA of TA muscle fibers throughout the progression of cancer-cachexia. C. Histogram of fiber sizes throughout the progression of cancer-cachexia. N of 7-8 was utilized for each group. Lettering denotes statistical significance at an alpha set at $p<0.05$.

Figure 2

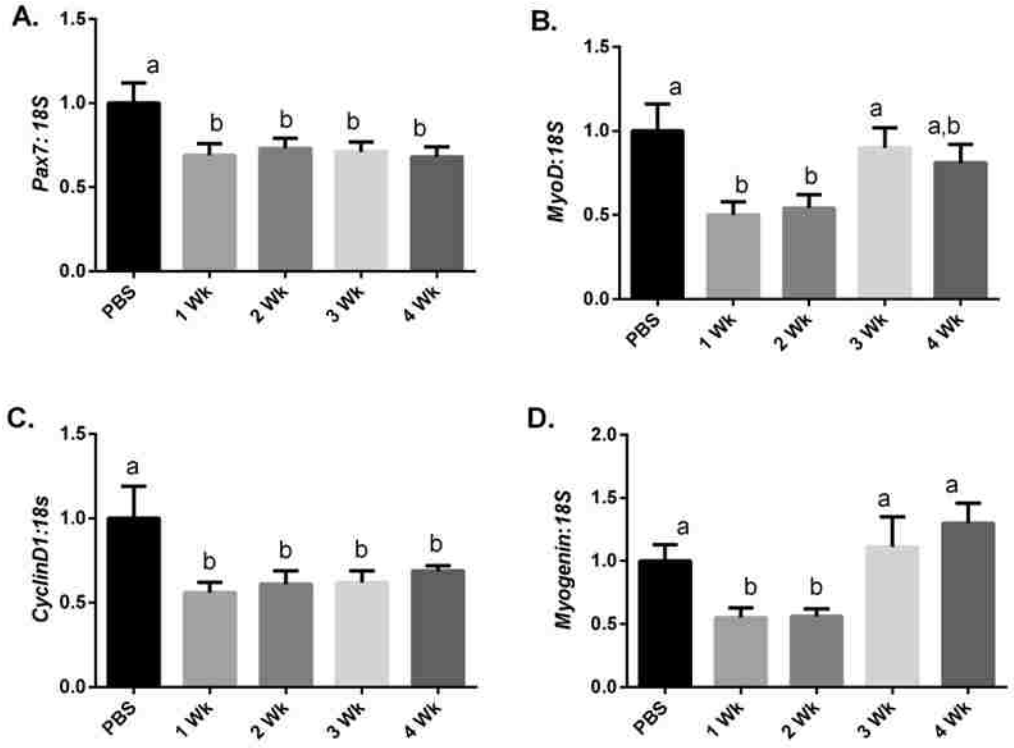

Figure 2. Myogenic signaling throughout the progression of cancer-cachexia. A. *Pax7* mRNA content throughout the progression of cancer-cachexia. B. *MyoD* mRNA content throughout the progression of cancer-cachexia. C. *CyclinD1* content throughout the progression of cancer-cachexia. D. *MyoG* content throughout the progression of cancer-cachexia. N of 7-8 was utilized for each group. Lettering denotes statistical significance at an alpha set at $p<0.05$.

Figure 3

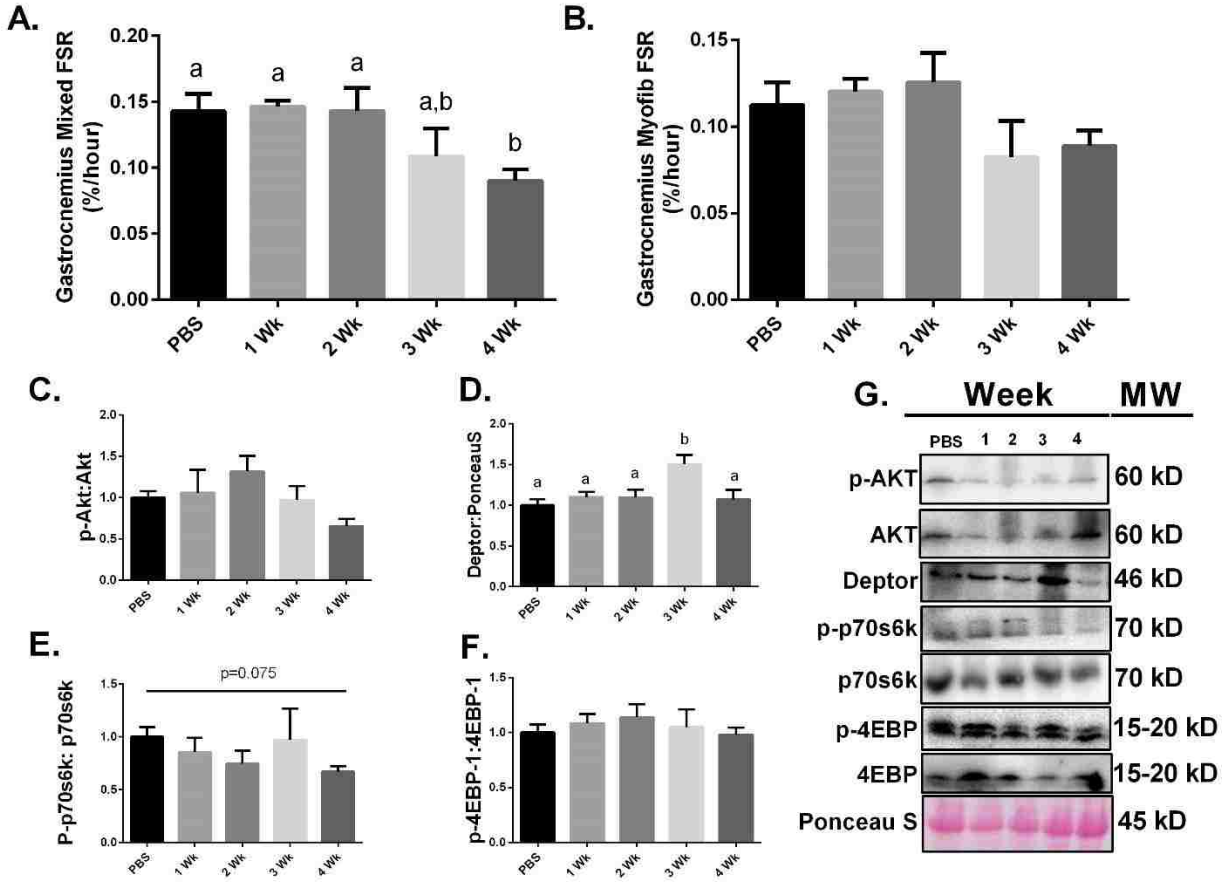

Figure 3. Protein synthesis throughout the progression of cancer-cachexia. A. Mixed FSR throughout the progression of cancer-cachexia. B. Myofibrilar FSR throughout the progression of cancer-cachexia. C. AKT phosphorylation relative to total protein. D. Deptor protein content throughout the progression or cancer-cachexia. E. 4EBP1 phosphorylation relative to total protein content. F. p70s6k phosphorylation relative to total protein content. G. Sample images for immunoblot analysis. N of 7-8 was utilized for each group. Lettering denotes statistical significance at an alpha set at $p<0.05$.

Figure 4

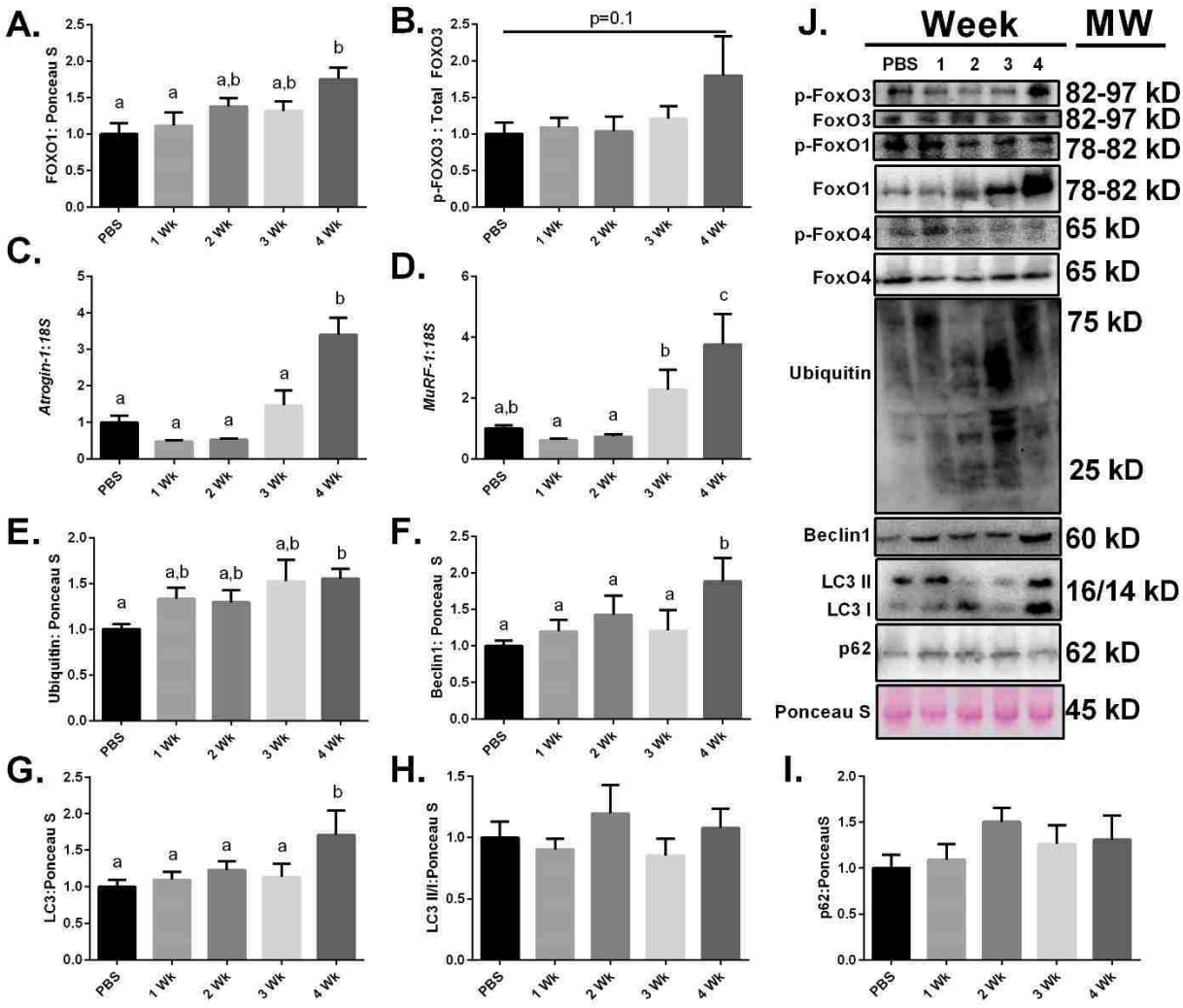
A.
FOXO1: Ponceau S
B.
p-FOXO3 : Total FOXO3
p=0.1
C.
Atrogin-1:18S
D.
MuRF-1:18S
E.
Ubiquitin: Ponceau S
F.
Beclin1: Ponceau S
G.
LC3:Ponceau S
H.
LC3 II/I:Ponceau S
I.
p62:PonceauS
PBS
1 Wk
2 Wk
3 Wk
4 Wk
J.
Week
MW
PBS 1 2 3 4
p-FoxO3
FoxO3
p-FoxO1
FoxO1
p-FoxO4
FoxO4
Ubiquitin
Beclin1
LC3 II
LC3 I
p62
Ponceau S
82-97 kD
82-97 kD
78-82 kD
78-82 kD
65 kD
65 kD
75 kD
25 kD
60 kD
16/14 kD
62 kD
45 kD

Figure 4. Protein breakdown throughout the progression of cancer-cachexia. A. FOXO1 protein content throughout the progression of cancer-cachexia. B. Phosphorylation of FOXO3 relative to total protein content throughout the progression of cancer-cachexia. C. *Atrogin1* mRNA content throughout the progression of cancer-cachexia. D. *MuRF1* mRNA content throughout the progression of cancer-cachexia. E. Ubiquitinated proteins throughout the progression of cancer-cachexia. F. Beclin1 protein content throughout the progression of cancer-cachexia. G. Total LC3 protein content throughout the progression of cancer-cachexia. H. LC3 II/I ratio throughout the progression of cancer-cachexia. Immunoblot sample image of ubiquitin. I. p62 protein content throughout the progression of cancer-cachexia. J. Representative immunoblot images. N of 7-8 was utilized for each group. Lettering denotes statistical significance at an alpha set at $p<0.05$.

Figure 5

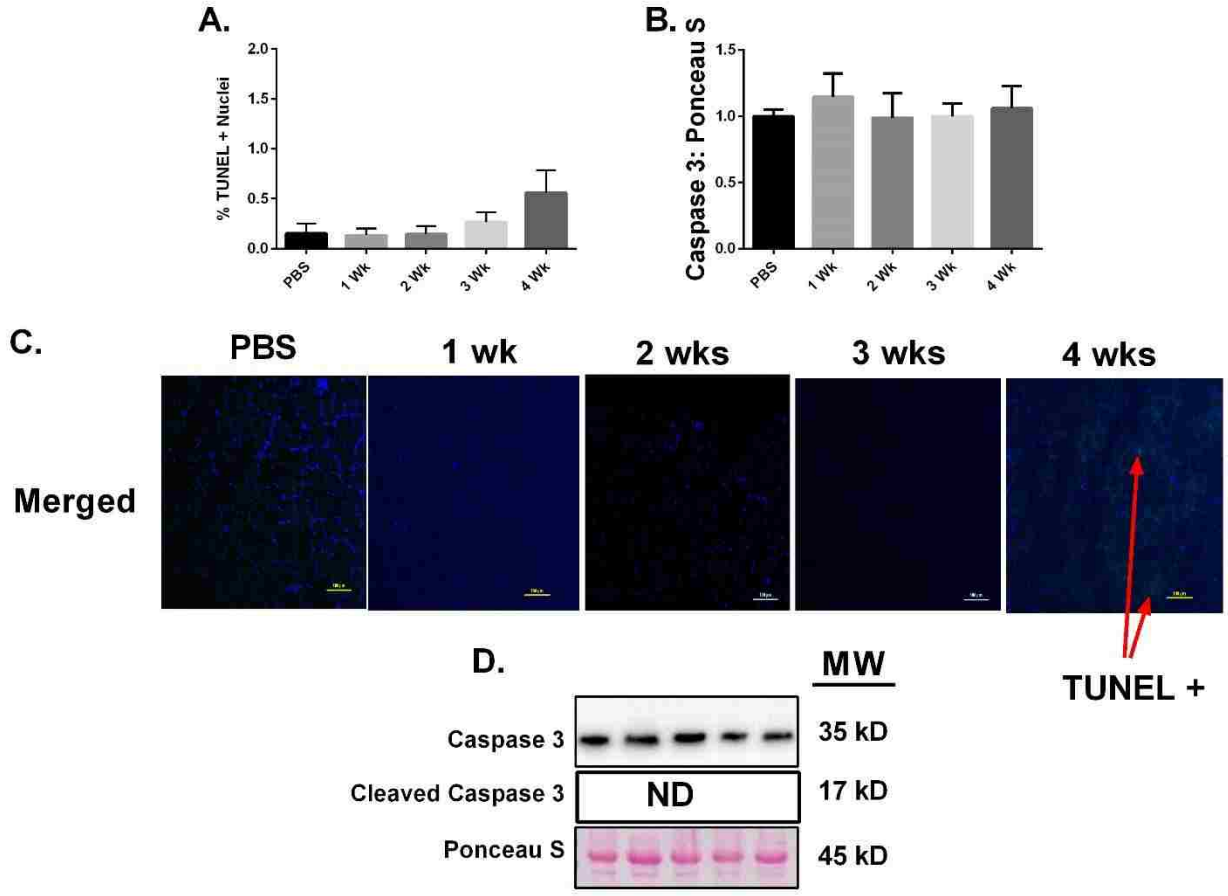

Figure 5. Apoptosis throughout the progression of cancer-cachexia. A. Percent TUNEL + nuclei throughout the progression of cancer-cachexia. B. Total caspase 3 protein content throughout the progression of cancer-cachexia. D. Sample images for the TUNEL assay including a positive control image. E. Representative immunoblot images. N of 7-8 per group was utilized. Lettering denotes statistical significance at an alpha set at $p<0.05$.

Figure 6

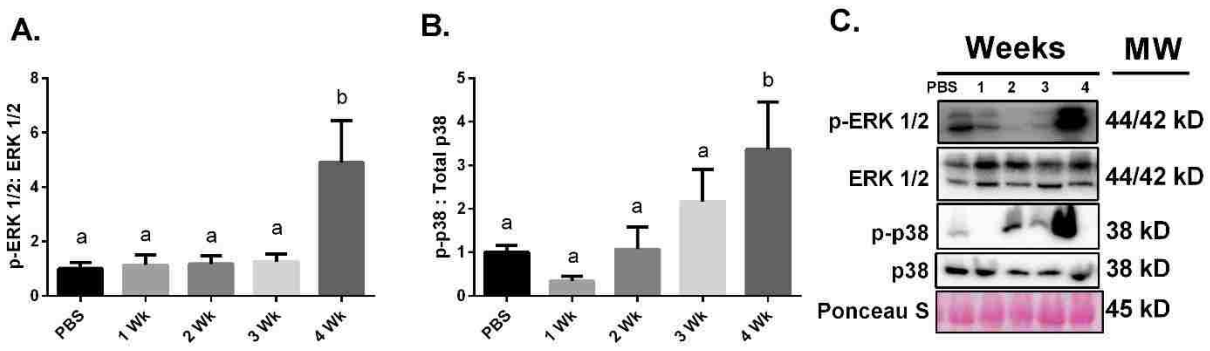

Figure 6. MAPK signaling throughout the progression of cancer-cachexia. A. ERK MAPK phosphorylation relative to total protein content. B. p38 MAPK phosphorylation relative to total protein content. C. Representative immunoblot images. N of 7-8 per group was utilized. Lettering denotes statistical significance at an alpha set at $p<0.05$.

Figure S1

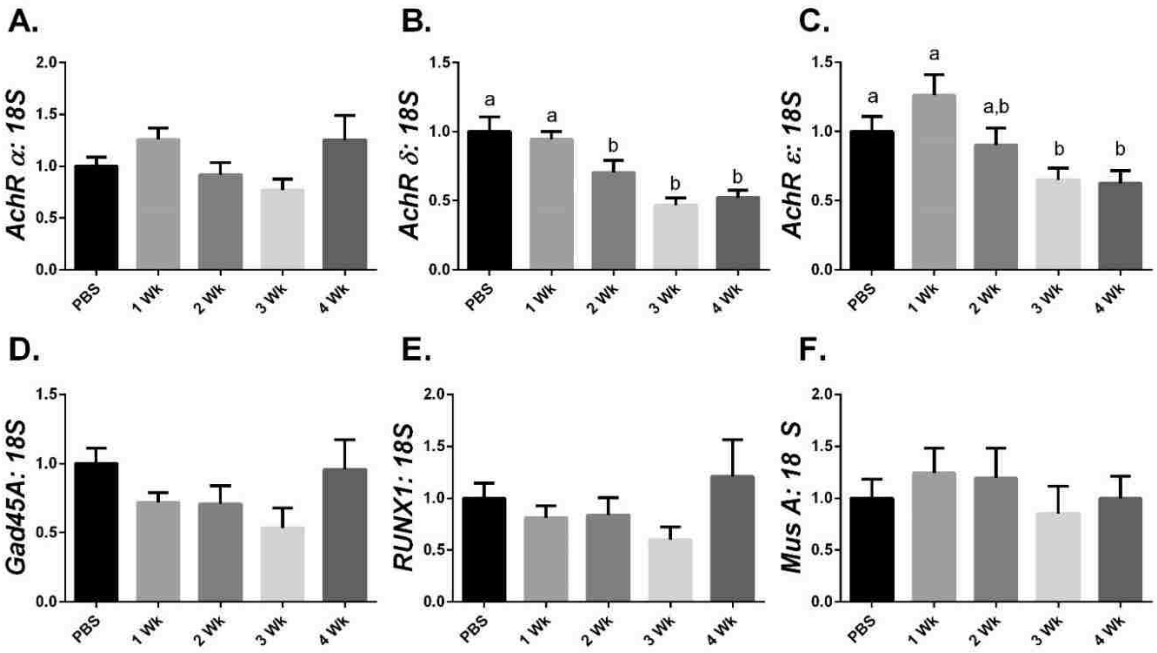

Figure S1. Denervation markers throughout the progression of cancer-cachexia. A. *AchR α* mRNA content throughout the progression of cancer-cachexia. B. *AchR δ* mRNA content throughout the progression of cancer-cachexia. C. *AchR ε* mRNA content throughout the progression of cancer-cachexia. D. *Gad45A* mRNA content throughout the progression of cancer-cachexia. E. *Runx1* mRNA content throughout the progression of cancer-cachexia. F. *Mus A* mRNA content throughout the progression of cancer-cachexia. N of 7-8 was utilized for each group. Lettering denotes statistical significance at an alpha set at $p<0.05$.

References

1. Ferlay J, Soerjomataram I, Dikshit R, Eser S, Mathers C, Rebelo M et al. Cancer incidence and mortality worldwide: sources, methods and major patterns in GLOBOCAN 2012. International journal of cancer. 2015;136(5):E359-86. doi:10.1002/ijc.29210.

2. Fitzmaurice C, Dicker D, Pain A, Hamavid H, Moradi-Lakeh M, MacIntyre MF et al. The Global Burden of Cancer 2013. JAMA oncology. 2015;1(4):505-27. doi:10.1001/jamaoncol.2015.0735.

3. Fearon Kenneth CH, Glass David J, Guttridge Denis C. Cancer Cachexia: Mediators, Signaling, and Metabolic Pathways. Cell metabolism. 2012;16(2):153-66. doi:http://dx.doi.org/10.1016/j.cmet.2012.06.011.

4. Onesti JK, Guttridge DC. Inflammation based regulation of cancer cachexia. Biomed Res Int. 2014;2014:168407. doi:10.1155/2014/168407.

5. Fearon K, Strasser F, Anker SD, Bosaeus I, Bruera E, Fainsinger RL et al. Definition and classification of cancer cachexia: an international consensus. The Lancet Oncology. 2011;12(5):489-95. doi:10.1016/s1470-2045(10)70218-7.

6. Fearon K. Cachexia: Treat wasting illness on multiple fronts. Nature. 2016;529(7585):156. doi:10.1038/529156b.

7. Brown JL, Rosa-Caldwell ME, Lee DE, Blackwell TA, Brown LA, Perry RA et al. Mitochondrial degeneration precedes the development of muscle atrophy in progression of cancer cachexia in tumour-bearing mice. Journal of cachexia, sarcopenia and muscle. 2017. doi:10.1002/jcsm.12232.

8. Narsale AA, Puppa MJ, Hardee JP, VanderVeen BN, Enos RT, Murphy EA et al. Short-term pyrrolidine dithiocarbamate administration attenuates cachexia-induced alterations to muscle and liver in ApcMin/+ mice. Oncotarget. 2016. doi:10.18632/oncotarget.10699.

9. Oliveira AG, Gomes-Marcondes MC. Metformin treatment modulates the tumour-induced wasting effects in muscle protein metabolism minimising the cachexia in tumour-bearing rats. BMC cancer. 2016;16:418. doi:10.1186/s12885-016-2424-9.

10. Suzuki H, Asakawa A, Amitani H, Nakamura N, Inui A. Cancer cachexia—pathophysiology and management. Journal of Gastroenterology. 2013;48(5):574-94. doi:10.1007/s00535-013-0787-0.

11. Miyamoto Y, Hanna DL, Zhang W, Baba H, Lenz HJ. Molecular Pathways: Cachexia Signaling-A Targeted Approach to Cancer Treatment. Clinical cancer research : an official journal of the American Association for Cancer Research. 2016;22(16):3999-4004. doi:10.1158/1078-0432.ccr-16-0495.

12. Tisdale MJ. The ubiquitin-proteasome pathway as a therapeutic target for muscle wasting. The journal of supportive oncology. 2005;3(3):209-17.

13. Aversa Z, Pin F, Lucia S, Penna F, Verzaro R, Fazi M et al. Autophagy is induced in the skeletal muscle of cachectic cancer patients. Scientific reports. 2016;6:30340. doi:10.1038/srep30340.

14. White JP, Puppa MJ, Gao S, Sato S, Welle SL, Carson JA. Muscle mTORC1 suppression by IL-6 during cancer cachexia: a role for AMPK. American Journal of Physiology - Endocrinology and Metabolism. 2013;304(10):E1042-E52. doi:10.1152/ajpendo.00410.2012.

15. Washington TA, White JP, Davis JM, Wilson LB, Lowe LL, Sato S et al. Skeletal muscle mass recovery from atrophy in IL-6 knockout mice. Acta physiologica (Oxford, England). 2011;202(4):657-69. doi:10.1111/j.1748-1716.2011.02281.x.

16. Puppa MJ, Gao S, Narsale AA, Carson JA. Skeletal muscle glycoprotein 130's role in Lewis lung carcinoma-induced cachexia. FASEB journal : official publication of the Federation of American Societies for Experimental Biology. 2014;28(2):998-1009. doi:10.1096/fj.13-240580.

17. Gingras AC, Raught B, Gygi SP, Niedzwiecka A, Miron M, Burley SK et al. Hierarchical phosphorylation of the translation inhibitor 4E-BP1. Genes & development. 2001;15(21):2852-64. doi:10.1101/gad.912401.

18. Burnett PE, Barrow RK, Cohen NA, Snyder SH, Sabatini DM. RAFT1 phosphorylation of the translational regulators p70 S6 kinase and 4E-BP1. Proceedings of the National Academy of Sciences of the United States of America. 1998;95(4):1432-7.

19. Penna F, Costamagna D, Fanzani A, Bonelli G, Baccino FM, Costelli P. Muscle wasting and impaired myogenesis in tumor bearing mice are prevented by ERK inhibition. PloS one. 2010;5(10):e13604. doi:10.1371/journal.pone.0013604.

20. He WA, Berardi E, Cardillo VM, Acharyya S, Aulino P, Thomas-Ahner J et al. NF-κB–mediated Pax7 dysregulation in the muscle microenvironment promotes cancer cachexia. The Journal of clinical investigation. 2013;123(11):4821-35. doi:10.1172/JCI68523.

21. Hettmer S, Wagers AJ. Muscling in: Uncovering the origins of rhabdomyosarcoma. Nature medicine. 2010;16(2):171-3.

22. Karalaki M, Fili S, Philippou A, Koutsilieris M. Muscle regeneration: cellular and molecular events. In vivo (Athens, Greece). 2009;23(5):779-96.

23. Attaix D, Ventadour S, Codran A, Bechet D, Taillandier D, Combaret L. The ubiquitin-proteasome system and skeletal muscle wasting. Essays in biochemistry. 2005;41:173-86. doi:10.1042/eb0410173.

24. Bodine SC, Baehr LM. Skeletal muscle atrophy and the E3 ubiquitin ligases MuRF1 and MAFbx/atrogin-1. American Journal of Physiology - Endocrinology and Metabolism. 2014;307(6):E469-E84. doi:10.1152/ajpendo.00204.2014.

25. Rom O, Reznick AZ. The role of E3 ubiquitin-ligases MuRF-1 and MAFbx in loss of skeletal muscle mass. Free radical biology & medicine. 2016;98:218-30. doi:10.1016/j.freeradbiomed.2015.12.031.

26. Kobayashi S. Choose Delicately and Reuse Adequately: The Newly Revealed Process of Autophagy. Biological & pharmaceutical bulletin. 2015;38(8):1098-103. doi:10.1248/bpb.b15-00096.

27. Chang YY, Neufeld TP. An Atg1/Atg13 complex with multiple roles in TOR-mediated autophagy regulation. Molecular biology of the cell. 2009;20(7):2004-14. doi:10.1091/mbc.E08-12-1250.

28. He C, Klionsky DJ. Regulation Mechanisms and Signaling Pathways of Autophagy. Annual review of genetics. 2009;43:67-93. doi:10.1146/annurev-genet-102808-114910.

29. Gasier HG, Riechman SE, Wiggs MP, Previs SF, Fluckey JD. A comparison of 2H2O and phenylalanine flooding dose to investigate muscle protein synthesis with acute exercise in rats. American journal of physiology Endocrinology and metabolism. 2009;297(1):E252-9. doi:10.1152/ajpendo.90872.2008.

30. Nilsson MI, Dobson JP, Greene NP, Wiggs MP, Shimkus KL, Wudeck EV et al. Abnormal protein turnover and anabolic resistance to exercise in sarcopenic obesity. FASEB journal : official publication of the Federation of American Societies for Experimental Biology. 2013;27(10):3905-16. doi:10.1096/fj.12-224006.

31. Hudson MB, Smuder AJ, Nelson WB, Wiggs MP, Shimkus KL, Fluckey JD et al. Partial Support Ventilation and Mitochondrial-Targeted Antioxidants Protect against Ventilator-Induced Decreases in Diaphragm Muscle Protein Synthesis. PloS one. 2015;10(9):e0137693. doi:10.1371/journal.pone.0137693.

32. Nilsson MI, Greene NP, Dobson JP, Wiggs MP, Gasier HG, Macias BR et al. Insulin resistance syndrome blunts the mitochondrial anabolic response following resistance exercise. American journal of physiology Endocrinology and metabolism. 2010;299(3):E466-74. doi:10.1152/ajpendo.00118.2010.

33. Buckingham M. Skeletal muscle progenitor cells and the role of Pax genes. Comptes rendus biologies. 2007;330(6-7):530-3. doi:10.1016/j.crvi.2007.03.015.

34. Pain VM. Initiation of protein synthesis in eukaryotic cells. European journal of biochemistry / FEBS. 1996;236(3):747-71.

35. Porter JD, Khanna S, Kaminski HJ, Rao JS, Merriam AP, Richmonds CR et al. A chronic inflammatory response dominates the skeletal muscle molecular signature in dystrophin-deficient mdx mice. Human molecular genetics. 2002;11(3):263-72.

36. Wilde JM, Gumucio JP, Grekin JA, Sarver DC, Noah AC, Ruehlmann DG et al. Inhibition of p38 mitogen-activated protein kinase signaling reduces fibrosis and lipid accumulation after

rotator cuff repair. Journal of shoulder and elbow surgery. 2016;25(9):1501-8. doi:10.1016/j.jse.2016.01.035.

37. Sandri M, Sandri C, Gilbert A, Skurk C, Calabria E, Picard A et al. Foxo transcription factors induce the atrophy-related ubiquitin ligase atrogin-1 and cause skeletal muscle atrophy. Cell. 2004;117(3):399-412.

38. Lima M, Sato S, Enos RT, Baynes JW, Carson JA. Development of an UPLC mass spectrometry method for measurement of myofibrillar protein synthesis: application to analysis of murine muscles during cancer cachexia. Journal of Applied Physiology. 2013;114(6):824-8. doi:10.1152/japplphysiol.01141.2012.

39. Lee DE, Brown JL, Rosa-Caldwell ME, Blackwell TA, Perry RA, Jr., Brown LA et al. Cancer Cachexia-Induced Muscle Atrophy: Evidence for Alterations in microRNAs important for Muscle Size. Physiological genomics. 2017:physiolgenomics.00006.2017. doi:10.1152/physiolgenomics.00006.2017.

40. Pin F, Busquets S, Toledo M, Camperi A, Lopez-Soriano FJ, Costelli P et al. Combination of exercise training and erythropoietin prevents cancer-induced muscle alterations. Oncotarget. 2015;6(41):43202-15. doi:10.18632/oncotarget.6439.

41. Pennefather P, Quastel DM. Relation between subsynaptic receptor blockade and response to quantal transmitter at the mouse neuromuscular junction. The Journal of General Physiology. 1981;78(3):313-44. doi:10.1085/jgp.78.3.313.

42. Kuang S, Gillespie MA, Rudnicki MA. Niche regulation of muscle satellite cell self-renewal and differentiation. Cell stem cell. 2008;2(1):22-31. doi:10.1016/j.stem.2007.12.012.

43. Johns N, Stephens NA, Fearon KC. Muscle wasting in cancer. The international journal of biochemistry & cell biology. 2013;45(10):2215-29. doi:10.1016/j.biocel.2013.05.032.

44. Toledo M, Busquets S, Penna F, Zhou X, Marmonti E, Betancourt A et al. Complete reversal of muscle wasting in experimental cancer cachexia: Additive effects of activin type II receptor inhibition and beta-2 agonist. International journal of cancer. 2016;138(8):2021-9. doi:10.1002/ijc.29930.

45. Llovera M, Garcia-Martinez C, Lopez-Soriano J, Agell N, Lopez-Soriano FJ, Garcia I et al. Protein turnover in skeletal muscle of tumour-bearing transgenic mice overexpressing the soluble TNF receptor-1. Cancer letters. 1998;130(1-2):19-27.

46. White JP, Baynes JW, Welle SL, Kostek MC, Matesic LE, Sato S et al. The regulation of skeletal muscle protein turnover during the progression of cancer cachexia in the Apc(Min/+) mouse. PloS one. 2011;6(9):e24650. doi:10.1371/journal.pone.0024650.

47. White JP, Puppa MJ, Sato S, Gao S, Price RL, Baynes JW et al. IL-6 regulation on skeletal muscle mitochondrial remodeling during cancer cachexia in the ApcMin/+ mouse. Skeletal muscle. 2012;2:14. doi:10.1186/2044-5040-2-14.

48. Wynn TA. Cellular and molecular mechanisms of fibrosis. The Journal of pathology. 2008;214(2):199-210. doi:10.1002/path.2277.

49. Shefer G, Oron U, Irintchev A, Wernig A, Halevy O. Skeletal muscle cell activation by low-energy laser irradiation: a role for the MAPK/ERK pathway. Journal of cellular physiology. 2001;187(1):73-80. doi:10.1002/1097-4652(2001)9999:9999<::aid-jcp1053>3.0.co;2-9.

50. Ding H, Zhang G, Sin KW, Liu Z, Lin RK, Li M et al. Activin A induces skeletal muscle catabolism via p38beta mitogen-activated protein kinase. Journal of cachexia, sarcopenia and muscle. 2017;8(2):202-12. doi:10.1002/jcsm.12145.

51. Quan-Jun Y, Yan H, Yong-Long H, Li-Li W, Jie L, Jin-Lu H et al. Selumetinib Attenuates Skeletal Muscle Wasting in Murine Cachexia Model through ERK Inhibition and AKT Activation. Molecular cancer therapeutics. 2017;16(2):334-43. doi:10.1158/1535-7163.mct-16-0324.

52. Li YP, Chen Y, John J, Moylan J, Jin B, Mann DL et al. TNF-alpha acts via p38 MAPK to stimulate expression of the ubiquitin ligase atrogin1/MAFbx in skeletal muscle. FASEB journal : official publication of the Federation of American Societies for Experimental Biology. 2005;19(3):362-70. doi:10.1096/fj.04-2364com.

Chapter 5

Mitochondrial Oxidative Stress and p38 MAPK signaling is Responsible for LLC-Mediated Loss of Myotube Diameter *In-Vitro*

Jacob L. Brown[1], Tyrone A. Washington[2], Nicholas P. Greene[1]

[1] Integrative Muscle Metabolism Laboratory, Exercise Science Research Center, Department of Health, Human Performance and Recreation, University of Arkansas, Fayetteville, AR 72701

[2] Exercise Muscle Biology Laboratory, Exercise Science Research Center, Department of Health, Human Performance and Recreation, University of Arkansas, Fayetteville, AR 72701

Corresponding Author: Nicholas P. Greene

Human Performance Laboratory

University of Arkansas

155 Stadium Dr, 321Q HPER

Fayetteville, AR 72701

E-mail: npgreene@uark.edu

Phone: 479-575-6638

Fax: 479-575-2853

Running Title: Oxidative Stress and MAPK signaling responsible for cancer-cachexia.

Abstract

Cancer-cachexia contributes to as much as 40% of cancer related deaths. The underlying mechanisms behind tumor-induced muscle wasting are not fully elucidated. In this dissertation I have shown that oxidative stress and enhanced MAPK phosphorylation is present in cachectic muscle; therefore, I have elected to use Lewis Lung Carcionoma conditioned media (LCM) to mimic cancer-cachexia in an *in-vitro* system to examine the roles of oxidative stress, p38 MAPK and ERK 1/2 MAPK in muscle atrophy *in vitro*. To do so, myotubes were treated with either Control or LCM concurrently with either MitoTEMPO (MitoT, a mitochondrial specific antioxidant), SB202190 (inhibitor of p38 MAP kinase) or PD98059 (MEK1/2 inhibitor preventing ERK 1/2 activity). MitoT and inhibition of p38 MAPK, but not ERK-MAPK, ameliorated LCM-induced loss of myotube diameter by ~30 and 20% respectively. Inhibition of p38 MAPK protected against LCM-mediated upregulation of total ubiquitin, and p38 MAPK inhibition downregulated the mRNA content of *Atrogin-1* and *MuRF-1* by ~40 and 50%, respectively. Also, LCM reduced puromycin incorporation by ~50%, while long term (18 hour) inhibition of both p38 and ERK MAPK increased puromycin incorporation by ~75% despite no change in protein synthetic signaling. These data indicate oxidative stress and p38 MAPK signaling may be key promoters of cancer-induced muscle loss.

Key Words: MAPK, p38 ERK, mitotempo, LLC, cancer, cachexia, conditioned, media

Introduction

Cancer-cachexia is a co-morbidity of cancer that is defined as an ongoing loss of skeletal muscle mass and function that cannot be fully reversed by conventional nutritional support [1, 2]. Cancer-cachexia occurs in approximately 80% of cancer patients and is the primary cause of death for 20%-40%, depending on type of cancer, of the estimated 8.2 million cancer related deaths globally [3, 1, 4, 2]. Furthermore, loss of muscle mass increases chemotherapy toxicity leading to increased suffering for cancer patients [5-7]. Cancer-cachexia is a major global health care problem that is often overlooked and underestimated; therefore, more effort is needed to understand underlying mechanisms of cancer-mediated muscle loss in efforts to then develop efficacious treatment modalities.

Skeletal muscle wasting is primarily caused by an imbalance of protein turnover favoring protein degradation over protein synthesis; however, mechanisms behind this imbalance of protein turnover vary depending on the (patho)physiological circumstance [8, 9]. Cancer-cachexia is a complex wasting syndrome which is not fully understood; however, we recently demonstrated that oxidative stress in skeletal muscle occurs well before cancer-induced muscle wasting [10]. Therefore, oxidative stress may be a key contributor of cancer-cachexia [11], however more research is needed to further validate this observation.

Reactive oxygen and nitrogen species (ROS/RNS) exhibit pleotropic effects on skeletal muscle [12] meaning ROS is often beneficial to skeletal muscle when produced at manageable levels; however, when ROS production is elevated for extended periods of time (oxidative stress) ROS have a wide array of cytotoxic effects [12]. Oxidative stress can lead to increased rates of protein breakdown through the ubiquitin proteasome system [13], as well as decreased rates of

skeletal muscle protein synthesis [14, 15]. Considering the early onset of mitochondrial oxidative stress I have recently observed in tumor-bearing mice [10], and its likely role in generating a negative protein balance [13] [14, 15], targeting ROS may be a potentially efficacious therapeutic strategy to treat cancer-cachexia; however, antioxidant administration may increase tumor size [16].

Additionally, MAPKs are known to mediate multiple cellular events including the induction of catabolic functions, and MAPK activation and signaling are dysregulated during oxidative stress [17]. Specifically, both p38 MAPK and ERK MAPK are major regulators of proteostasis [18-21]. Inhibition of p38 MAPK signaling can attenuate ROS mediated upregulation of the ubiquitin proteasome system as well as autophagy related genes [17]. In chapter four of this dissertation I observed that phosphorylation of both p38 and ERK MAPK were elevated in cachectic muscle when compared to muscle from control mice, this event developed concurrently to the onset of muscle wasting in tumor-bearing mice. This cancer-cachexia mediated induction of MAPK signaling may therefore directly contribute to muscle loss. In fact, pharmacological inhibition of both p38 and ERK 1/2 MAPK attenuated cancer-induced muscle loss [22]. However, more research is needed to fully understand the utility of targeting MAPKs in the prevention and treatment of cancer-cachexia.

Currently, it is postulated that antioxidants may only be helpful for individuals with a compromised antioxidant defense status due to the inability to specifically target skeletal muscle ROS production [16]. Therefore, it is critical to understand the role of oxidative stress mediated muscle loss in cancer-cachexia in a controlled *in-vitro* environment. Using Lewis Lung Carcinoma conditioned media (LCM) to mimic tumor derived bloodborne factors is a well-established *in-vitro* model to study cancer-cachexia [23, 24]. Utilizing this model, I hypothesize

that LCM induces loss of myotube diameter which will be attenuated by antioxidant treatment, and that LCM-mediated loss of myotube diameter is dependent on MAPK signaling. This research will open new doors for development of targeted therapies to treat cancer-cachexia and provide mechanistic insight into pathological cellular processes behind cancer-induced muscle wasting.

Materials and Methods

Tissue Culture

C2C12 myoblasts were plated at 50,000 cells per well of a 6 well cell culture plate with 2mL DMEM (11965092, Life Technologies, Carlsbad, CA) supplemented with 20% Fetal Bovine Serum (26140079, Life Technologies) and 1% pen/strep (15140122, Life Technologies). Cell proliferation and differentiation were performed as previously described [25, 26]. Myoblasts were plated for experiments at passage 6.

LLC Conditioned Media Treatment

In order to collect LLC conditioned media (LCM), LLC cells were grown to 100% confluence as previously described [10, 27]. LLC cells were then incubated in DMEM supplemented with 10% Fetal Bovine Serum and 1% pen/strep for ~18 hours. The media was then collected and filtered to remove cell particulates. LLC conditioned media was then diluted to 25% total volume in serum free media. For the Control group, 25% total volume of 10% fetal bovine serum growth media was diluted in serum free media. C2C12 myotubes were then treated with either control or LCM for 24 hours. This method was adapted from Puppa et al. [28] and Guohua et al. [24].

Drug Treatments

To determine if neutralizing mitochondria-derived ROS may protect against LCM induced myotube atrophy MitoTEMPO (MitoT, a mitochondrial targeted antioxidant) was administered to C2C12 cells incubating in either control or LCM at a concentration of 2 μM. MitoT has a wide range of concentrations used in literature (1nM [29]-25 μM[30])

To examine the roles of p38 MAPK and ERK 1/2 MAPK in the loss of myotube diameter on myotubes treated with Control or LCM, differentiated C2C12 myotubes were treated with either PD98059 (20 μM; PHZ1164, Life Technologies) (MEK1/2 inhibitor preventing ERK 1/2 activity) or SB202190 (20 μM; S7067, Sigma Aldrich) (inhibitor of p38 MAP kinase). These concentrations of inhibitors have been previously published by Brown et al. [26].

Myotube Diameter Analysis

Myotube diameter analysis was performed as previously published [26, 25]. Briefly, C2C12 myoblasts proliferated until 80-100% confluency. The myoblasts were differentiated for 120 hours. Myotubes were then placed in control or LCM and appropriate drug treatments were added. Myotubes were imaged with 40X objective with a phase contrast filter using Nikon TiS (Nikon, somewhere, someplace). 5 lines were drawn across the diameter of each myotube representing sections across the full length of the tube in order to measure the average diameter of the myotube. This was performed on every myotube imaged in the experimental conditions. Researcher was blinded from experimental conditions for this analysis. All cell culture experiments were conducted in triplicate and repeated in order to ensure data accuracy.

MitoSox Analysis

After 18 hours incubation in control or LCM with either vehicle or MitoT treatment, 5μM MitoSOX Red (M36008, Invitrogen) in PBS was added to differentiated C2C12 cells for 10 minutes, rinsed, and cells were visualized at 510/580nm (ex/em) on Nikon TiS epifluorescent microscope (Melville, NY) to assess mitochondrial superoxide production.

RNA isolation, cDNA synthesis, and quantitative real-time PCR

RNA was isolated from cells as previously described [25, 26]. Isolated RNA purity and concentration was confirmed using Bio-Tek (Winooski, VT) Synergy HTX plate reader with Take3 microvolume plate and Gen5 software. After which, 1 μg of RNA was reverse transcribed into cDNA using previously described methods [31, 32]. cDNA was diluted to 1:100 (10 ng/μL) and Ct values analyzed using TaqMan reagents and commercial Step-One real-time RT-PCR instrumentation (Applied BioSystems, Foster City, CA). Assessment of 18s (Mm03928990_g1), *Atrogin-1* and *MuRF-1* were performed using TaqMan probes (Life Technologies) and corresponding TaqMan reagents. No differences were observed in 18s among experimental conditions for experiments presented. Final quantification of gene expression was calculated using the ΔΔCT method. Relative quantification was calculated as $2^{-\Delta\Delta CT}$.

Immunoblotting

C2C12 cells were homogenized in a buffer containing 0.23 M Tris-HCL, pH 6.8, 4.5% w/v SDS, 45% glycerol, 0.04% w/v Bromophenol Blue, 80 mM dithiothreitol, 0.57mM 2-mercaptoethanol, complete, mini protease inhibitor cocktail (Roche, Indianapolis, IN), and phosphatase inhibitor cocktails (Sigma-Aldrich) and denatured at 95°C as previously described [25]. Concentrations were determined using the RC/DC assay (500-0119, BioRad, Hercules, CA)

and 20μg total protein was resolved by SDS-PAGE, transferred to a PVDF membrane and blocked in 5% Milk in Tris-buffered saline. Membranes were probed overnight for primary antibodies specific to ERK 1/2 MAPK (Cell Signaling 4695), phosphorylated ERK 1/2 MAPK (Cell Signaling 4370, T 202/ Y204), p38 MAPK (Cell Signaling 9212), phosphorylated p38 MAPK (Cell Signaling 4511, Y 180/182),), p-4EBP1 (Cell Signaling 9644), 4EBP1 (Cell Signaling 9452), p-FOXO1 (Cell Signaling 9464), FOXO1 (Cell Signaling 2880), p-FOXO3 (Cell Signaling 9464), FOXO3 (Cell Signaling 2497), Ubiquitin (Cell Signaling 3933) and Deptor (EMDMillipore, ABS222) all isolated from rabbit. Antibodies were diluted in 50% LiCor Blocking Buffer and 50% TBS. Membranes were imaged on LiCor Odyssey Fc (Lincoln, NE) and analyzed using Image Studio software (LiCor). All bands were normalized to the 45 kDa Actin band of Ponceau S stain as a loading control.

SuNSET Protein Synthesis

Protein synthesis was measured using the SuNSET protocol [33, 34] as we have previously published [25]. Briefly, 1μM puromycin dihydrochloride (Calbiochem, Darmstadt, Germany) was added to cell culture media and incubated 30 minutes prior to protein extraction. Immunoblotting protocols were followed as described above using 1:20,000 dilution of mouse anti-puromycin IgG 2a antibody (EMD Millipore, Darmstadt, Germany) followed by 1:20,000 dilution of HRP conjugated anti-mouse IgG fragment specific 2a antibody (Jackson ImmunoResearch Labs, West Grove, PA). The entire lane was assessed for optical density and this was normalized to optical density of the entire lane of Ponceau S stain. This was used as a relative measure of the amount of actively translated proteins in the polysome prior to harvest of cells.

Statistical analysis

Independent factors included media (con or LCM) and drug treatment (Vehicle or MitoT/SB/PD as appropriate to experiment) Control (Con) Vehicle, LCM Vehicle, Con MitoT, LCM MitoT, Con MAPK inhibitors (includes PD098059 and SB202190 all administered during separate experiments) and LCM MAPK inhibitors. These independent factors were divided into three separate cell culture experiments hereafter referred to as LCM MitoT, LCM p38 inhibitor and LCM ERK 1/2 inhibitor. Data in each separate cell culture experiments were analyzed by two-way ANOVA with factors of media (Con vs LCM) and pharmacological inhibition (Vehicle vs MitoT, SB or PD). Here significant F ratios were found a Student Newman Kuels Post Hoc test was used to delineate differences among means. For all experiments, the comparison-wise error rate, α, was set at 0.05 for all statistical tests. All data were analyzed and graphed using using GraphPad Prism (La Jolla, CA, USA) and data expressed as mean ± SEM.

Results

MitoT Protects Against LCM-Mediated Loss of Myotube diameter. Myotube diameter of C2C12 myotubes treated with LCM were ~40% smaller than groups treated with control media, however, myotube diameter of cells treated with LCM+MitoT were not significantly different from myotubes treated with control media (Figure 1A). MitoSox fluorescence from C2C12 myotubes treated with LCM exhibited a ~20% greater mean red intensity from MitoSox when compared to cells treated with control media. MitoSox fluorescence of myotubes treated with MitoT was ~20% lower when compared to cells treated with vehicle (Figure 1B). LCM treatment resulted in 50% less puromycin incorporation when compared to myotubes treated with control media with no effect of MitoT (Figure 1C). Ubiquitin protein content was not

different between groups (Figure 1D); however, there was a ~40% mean increase in LCM vehicle when compared to other groups (p=0.08).

MitoTempo rescues LCM-mediated loss of myotube diameter through FOXO signaling. Neither LCM nor MitoT treatment altered the relative phosphorylations of p38 MAPK, ERK MAPK, 4EBP1or FOXO3; however, LCM+Vehicle treatment increased relative FOXO1 phosphorylation by ~50% (Figure 2A). *Atrogin-1* mRNA content was not different between experimental groups; however, MuRF-1 mRNA was ~40% greater in LCM+MitoT when compared to Control+Vehicle (Figure 2B).

Inhibition of p38 MAPK partially protects against LCM-Mediated Loss of Myotube Diameter. Myotube diameter of cells treated with LCM+Vehicle was ~40% smaller than cells treated with Control Media, while myotube diameter of cells treated with LCM+SB202190 was ~25% smaller than myotubes treated with control media and ~20% greater when compared to myotube diameter of cells treated with LCM+Vehicle (Figure 3A). Relative phosphorylation of MAPK APK was ~40 and 50% in Control+ SB202190 and LCM+ SB202190 when compared to control vehicle, respectively (Figure 3B). Puromycin incorporation was ~2 fold greater in myotubes treated with SB202190 when compared to myotubes treated with vehicle, additionally a ~50% lower mean puromycin incorporation in LCM cells compared to control media did not reach statistical significance (p=0.058) (Figure 3C). Protein ubiquitination was ~2 fold greater in LCM+Vehicle when compared to all other groups, and not different between control media and LCM+SB202190 (Figure 3D). Neither LCM nor SB202190 treatment altered the protein content or relative phosphorylations of 4EBP1, Deptor and FOXO3; however, LCM+Vehicle treatment increased relative FOXO1 phosphorylation by ~2.5 fold (Figure 3E). *Atrogin-1* mRNA content was ~50% higher in LCM+Vehicle when compared to control media groups, and 50% lower

than control media groups with LCM+SB202190 (Figure 3F). *MuRF-1* mRNA content was ~60% lower in groups containing SB202190 when compared to the vehicle counterparts (Figure 3F).

ERK 1/2 MAPK inhibition does not protect against LCM-mediated loss of myotube diameter despite promoting protein synthesis. Diameter of myotubes treated with LCM was ~35% lower than the myotube diameter of myotubes treated with Control media, regardless of ERK MAPK inhibition (Figure 4A). Phosphorylated ERK relative to total ERK was ~50% lower in groups containing PD98059 when compared to the Control Media+Vehicle group. LCM+Vehicle was ~30% lower than Control+Vehicle (Figure 4B). Puromycin incorporation was 3-fold and 2-fold greater in Control+PD98059 and LCM+PD98059, respectively when compared to Control+Vehicle (Figure 4C). Ubiquitin protein content was ~50% greater with LCM+PD98059 treatment when compared to control+vehicle treatment (Figure 4D). Protein content or relative phosphorylations of 4EBP1, Deptor, FOXO3 and FOXO1 was not different between groups. Both Atrogin-1 and MuRF-1 mRNA was decreased by ~30 and 40% with LCM+Vehicle treatment when compared to control+vehicle treatment, respectively.

Discussion

In this study, I have demonstrated treatment with both the mitochondrial ROS scavenager MitoT and p38 MAPK inhibitor SB202190 can attenuate LCM-mediated loss of myotube diameter *in vitro*. Both MitoT and SB202190 protected against the promotion of ubiquitin-mediated catabolism from LCM treatment, while p38 MAPK inhibition additionally upregulated protein synthesis in myotubes. In contrast, inhibition of ERK MAPK did not protect against LCM-mediated loss of myotube diameter. These data suggest that oxidative stress and subsequent p38 MAPK activation in the tumor-bearing state may be key developments in the

development of cachectic muscle loss. These findings help to elucidate potential mechanisms behind tumor-induced loss of myotube diameter and may provide insight to further therapeutic strategies via targeting of oxidative stress and p38 MAPK.

The use of LCM to mimic cancer-cachexia *in-vitro* is a well-established model [23, 24]; however, there are distinct differences between this model and LLC implantation *in-vivo.* Specifically, in Chapter 3 of this dissertation I established that mitochondrial ROS production doubles *in-vivo [10]*. LCM treatment of myotubes only increases mitochondrial ROS production by ~20-30% *in-vitro*. Moreover, in Chapter 4, I showed MAPK phosphorylation to be enhanced in cachectic muscle, while *in-vitro* LCM treatment had no effect on MAPK signaling. Other studies have demonstrated that LCM treatment promotes phosphorylation of both p38 and ERK MAPK; however, this may be attributed to differences in the LCM treatment protocol [23]. Gao et al. [23] used a protocol which utilized 3 days of likely less concentrated LCM media, while in this dissertation I used a more concentrated LCM for a shorter time frame. These differences among others need to be further explored in order to effectively mimic cancer-cachexia *in-vitro.*

LCM-mediated loss of myotube diameter is rescued by increased mitochondrial ROS scavenging. The loss of myotube diameter in response to LCM (~30-40% loss across experiments) mimics the cachectic phenotype observed *in-vivo* (~40% loss of cross sectional area of adult muscle). In this study, MitoT treatment ameliorated LCM-mediated loss of myotube diameter, which suggests oxidative stress will induce cancer-mediated muscle loss. In chapter 3 of this dissertation, oxidative stress increased dramatically shortly after tumor implantation. Unfortunately at this time MitoT exact mechanism of protection against LCM-mediated muscle loss is not fully understood. Also, future studies should analyze if increasing ROS scavenging *in-vivo* protects against cancer-cachexia. In fact, there is much controversy on this topic as

antioxidant administration may exacerbate tumor growth [16]. However, my data suggests specifically targeting mitochondrial ROS in the muscle may be an effective strategy to treat cancer-cachexia if targeted to skeletal muscle; therefore, future studies should be developed to examine potential means by which to specifically target mitochondrial ROS.

LCM-mediated loss of myotube diameter is rescued with p38 inhibition. In Chapter 4, p38 MAPK phosphorylation increased by 3-fold in cachectic muscle; however, LCM treatment did not alter p38 MAPK phosphorylation status. Despite this, long term p38 MAPK inhibition (~18 hours) ameliorated LCM-induced loss of myotube diameter. The mechanism behind this appears to be through a combination of inhibiting catabolic signaling (decreased protein ubiquitination as well as decreased *Atrogin-1* and *MuRF-1* mRNA content) and the promotion of protein synthesis. These data are consistent with previous literature regarding p38 MAPK's role in catabolic signaling [17]. At this point, p38 MAPK's role in the regulation of protein synthesis is not clear.

Inhibition of ERK-MAPK does not protect against LCM mediated loss of myotube diameter despite promoting protein synthesis. ERK MAPK inhibition in cancer-cachexia literature has been shown to protect stretch-induced protein synthetic response *in-vitro* [35] which is consistent with these findings. ERK-MAPK has pleiotropic roles in modulating proteostasis. In an acute manner, ERK-MAPK has been seen to promote protein synthesis following acute resistance exercise [36].However, I have previously shown that IL-6 induced chronic phosphorylation of ERK-MAPK inhibits anabolic signaling [26]. In conjunction with that previous work, these current findings suggest that longer term ERK MAPK activity may in fact repress anabolic functions and thus alleviating this ERK MAPK activity may be necessary to promote muscle protein anabolism. However, considering these discrepancies in the literature,

more research is needed to further elucidate the role of ERK-MAPK with the regulation of protein synthesis as well as the onset of cancer-cachexia.

Based on these data, the compounds which ameliorated LCM-mediated loss of myotube diameter (MitoT and p38 MAPK inhibitor) appeared down-regulate the ubiquitin proteasome system response. Inhibition of ERK MAPK promoted protein synthesis, but did not alter ubiquitin proteasome mediated catabolism. Taken together, this suggests the ubiquitin proteasome system is largely responsible for cancer-induced muscle wasting.

The current study uncovers potential mechanisms for tumor mediated loss of muscle size, and a new role of MAPK signaling in the regulation of protein synthesis, which will lead to new novel studies. Increased mitochondrial ROS scavenging and p38 MAPK inhibition ameliorated LCM-mediated loss of myotube diameter. Considering ROS induces p38 MAPK phosphorylation [17], the protective effect of MitoT and p38 inhibition against tumor derived factors may be acting through similar mechanisms. In chapters 3 and 4 of this dissertation ROS emission and p38 phosphorylation are both elevated, which suggests oxidative stress mediated p38 phosphorylation may be a potential mechanism for cancer-induced muscle wasting. These data may lead to the development of therapies to treat cachexia, and broadens the understanding of skeletal muscle plasticity.

Acknowledgements

Support for LLC experiments has been provided in part by National Institutes of Health under Award Number R15AR069913 from the National Institute of Arthritis And Musculoskeletal And Skin Diseases and the National Institute Of General Medical Sciences. Contents of this publication are solely the responsibility of the authors and do not necessarily represent the

official views of the ABI, NIGMS or NIH. The authors would like to thank Drs. Sami Dridi, Elizabeth Greene and Jeffrey Wolchok (U. Arkansas) for their contributions to the experiments presented here and editing.

Conflict of Interest

The authors claim no conflicts of interest.

Figures

Figure 1

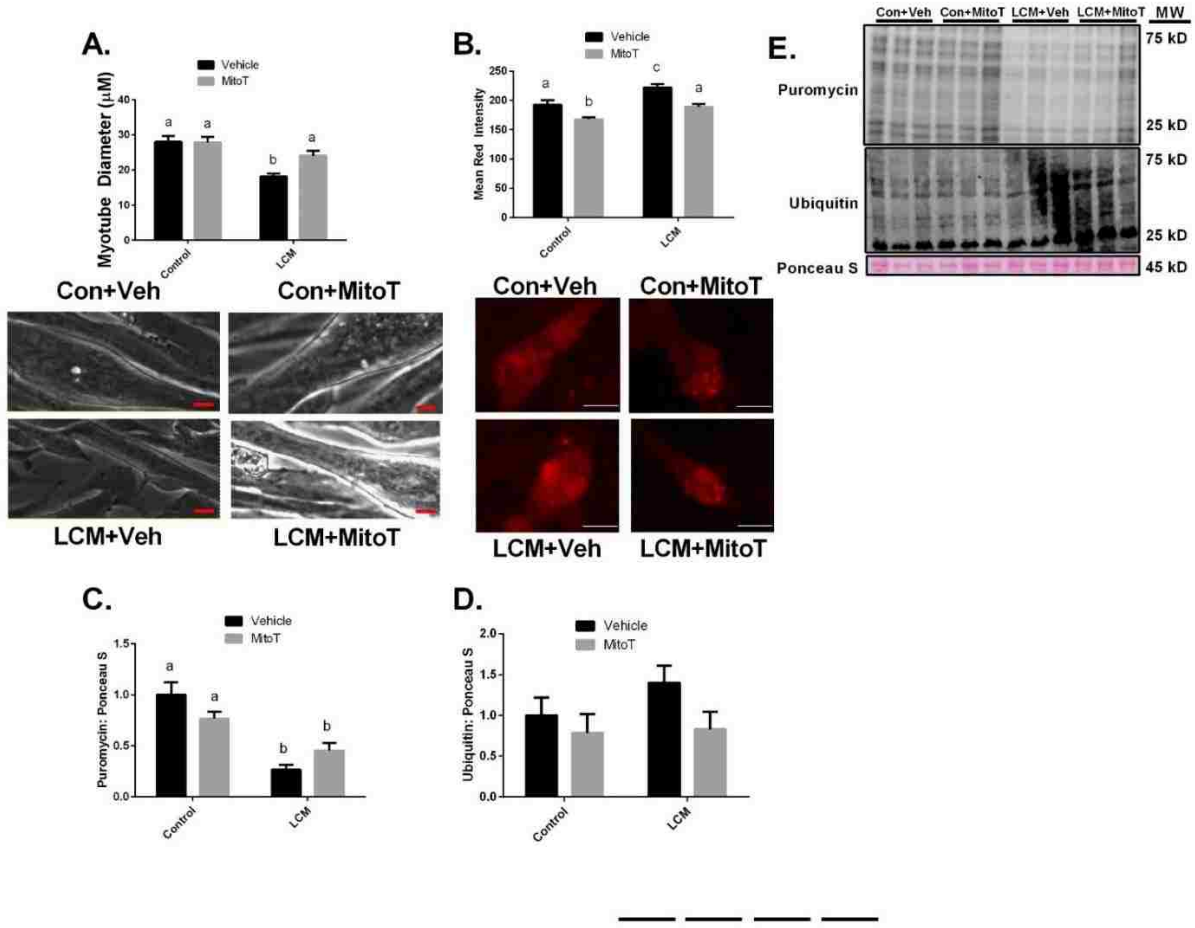

Figure 1. MitoT Protects Against LCM-Mediated Loss of Myotube diameter. A: Myotube diameter analysis of control media+vehicle, control media+MitoT, LCM+vehicle and LCM+MitoT. B. Mitosox analysis of control media+vehicle, control media+MitoT, LCM+vehicle and LCM+MitoT. C: Puromycin incorporated for groups control media+vehicle, control media+MitoT, LCM+vehicle and LCM+MitoT after 30 minutes puromycin treatment following 18 hours of treatments. D: Protein content of ubiquitin following 18 hours of control media+vehicle, control media+MitoT, LCM+vehicle or LCM+MitoT treatment. All measured in C2C12 myotubes and normalized to and Ponceau S. * $P < 0.05$ between indicated groups. Data are mean ± SEM. E: Representative immunoblot images for each protein of interest taken in order from same membrane.

Figure 2

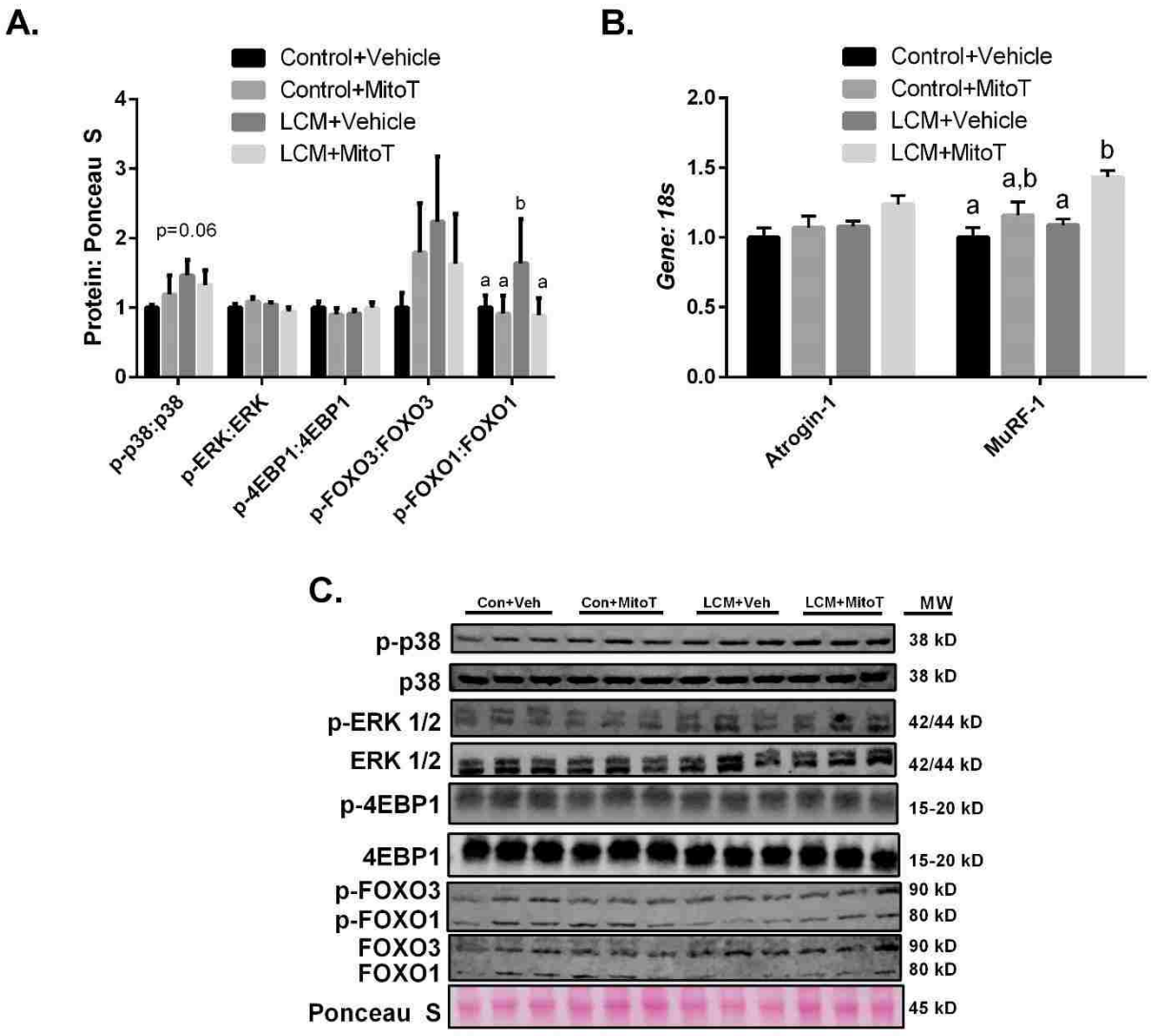
A.
Control+Vehicle
Control+MitoT
LCM+Vehicle
LCM+MitoT
Protein: Ponceau S
p=0.06
a a b a
p-p38:p38
p-ERK:ERK
p-4EBP1:4EBP1
p-FOXO3:FOXO3
p-FOXO1:FOXO1
B.
Gene: 18s
a a,b a b
Atrogin-1
MuRF-1
C.
Con+Veh
Con+MitoT
LCM+Veh
LCM+MitoT
MW
p-p38
38 kD
p38
38 kD
p-ERK 1/2
42/44 kD
ERK 1/2
42/44 kD
p-4EBP1
15-20 kD
4EBP1
15-20 kD
p-FOXO3
90 kD
p-FOXO1
80 kD
FOXO3
90 kD
FOXO1
80 kD
Ponceau S
45 kD

Figure 2. MitoTempo rescues LCM-mediated loss of myotube diameter through FOXO signaling. A: Protein content of p-p38 relative to total p38, p-ERK relative to total ERK, p-4EBP1 relative to total 4EBP1, p-FOXO3 relative to total FOXO3 and p-FOXO1 content relative to total FOXO1 following 18 hours of control media+vehicle, control media+MitoT, LCM+vehicle or LCM+MitoT treatment. B: *Atrogin-1* and *MuRF-1* mRNA content following 18 hours of control media+vehicle, control media+MitoT, LCM+vehicle or LCM+MitoT treatment. All measured in C2C12 myotubes and normalized to and Ponceau S. * $P < 0.05$ between indicated groups. Data are mean ± SEM. C: Representative immunoblot images for each protein of interest taken in order from same membrane.

Figure 3

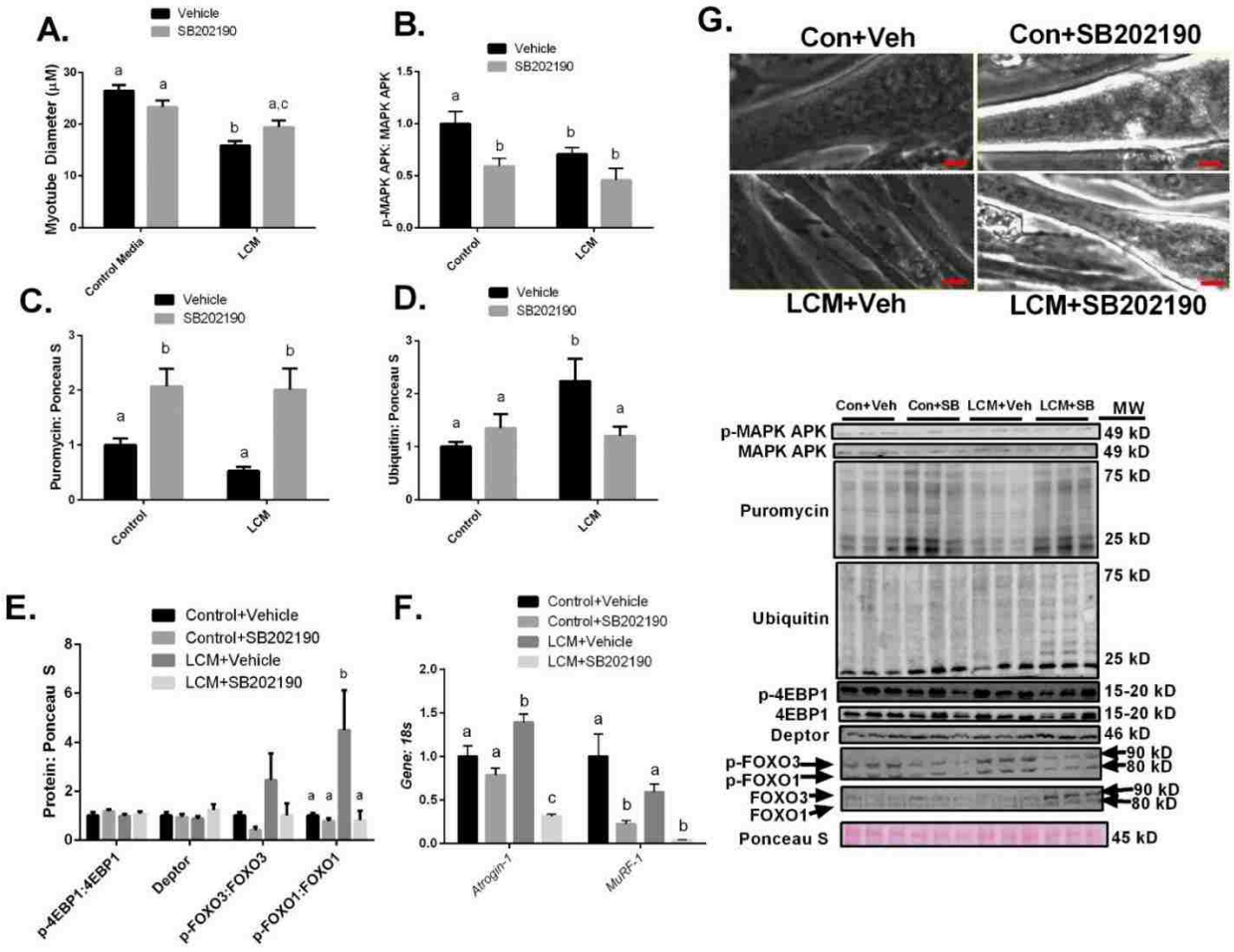
A.
Vehicle
SB202190
Myotube Diameter (μM)
Control Media
LCM
B.
Vehicle
SB202190
p-MAPK APK: MAPK APK
Control
LCM
G.
Con+Veh
Con+SB202190
LCM+Veh
LCM+SB202190
C.
Vehicle
SB202190
Puromycin: Ponceau S
Control
LCM
D.
Vehicle
SB202190
Ubiquitin: Ponceau S
Control
LCM
Con+Veh
Con+SB
LCM+Veh
LCM+SB
MW
p-MAPK APK
MAPK APK
Puromycin
Ubiquitin
p-4EBP1
4EBP1
Deptor
p-FOXO3
p-FOXO1
FOXO3
FOXO1
Ponceau S
49 kD
49 kD
75 kD
25 kD
75 kD
25 kD
15-20 kD
15-20 kD
46 kD
90 kD
80 kD
90 kD
80 kD
45 kD
E.
Control+Vehicle
Control+SB202190
LCM+Vehicle
LCM+SB202190
Protein: Ponceau S
p-4EBP1:4EBP1
Deptor
p-FOXO3:FOXO3
p-FOXO1:FOXO1
F.
Control+Vehicle
Control+SB202190
LCM+Vehicle
LCM+SB202190
Gene: 18s
Atrogin-1
MuRF-1

Figure 3. Inhibition of p38 MAPK partially protects against LCM-Mediated Loss of Myotube Diameter. A: Myotube diameter analysis of control media+vehicle, control media+SB202190, LCM+vehicle and LCM+SB202190. B. Protein content of relative MAPK APK phosphorylation following 18 hours of treatments. C: Puromycin incorporated for groups control media+vehicle, control media+SB202190, LCM+vehicle and LCM+SB202190 after 30 minutes puromycin treatment following 18 hours of treatments. D: Protein content of ubiquitin following 18 hours of control media+vehicle, control media+SB202190, LCM+vehicle or LCM+SB202190 treatment. E. Protein content of p-4EBP1 relative to total 4EBP1, Deptor, p-FOXO3 relative to total FOXO3 and p-FOXO1 content relative to total FOXO1 following 18 hours of control media+vehicle, control media+SB202190, LCM+vehicle or LCM+SB202190 treatment. F. *Atrogin-1* and *MuRF-1* mRNA content following 18 hours of control media+vehicle, control media+SB202190, LCM+vehicle or LCM+SB202190 treatment. All measured in C2C12 myotubes and normalized to and Ponceau S. * $P < 0.05$ between indicated groups. Data are mean ± SEM. G: Representative immunoblot images for each protein of interest taken in order from same membrane.

Figure 4

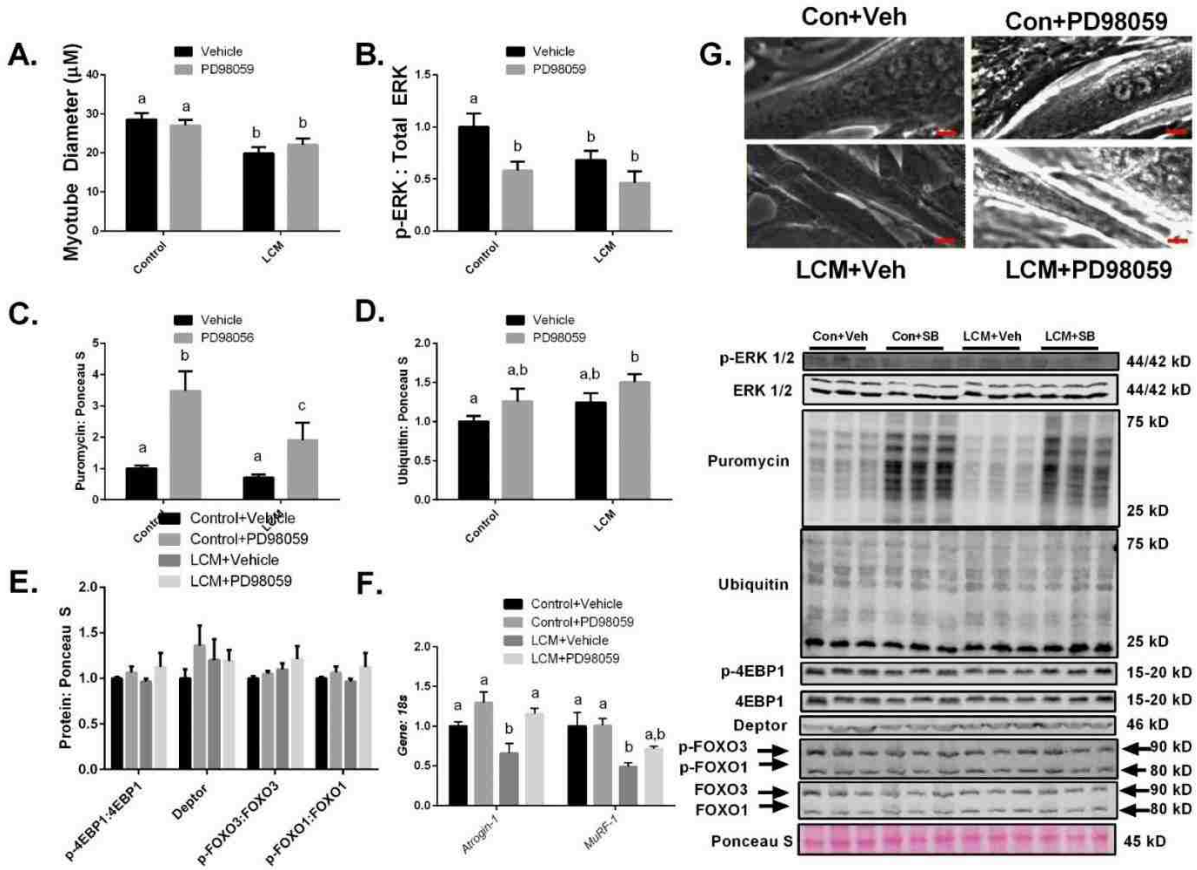
A.
Myotube Diameter (μM)
Vehicle
PD98059
Control
LCM
B.
p-ERK : Total ERK
C.
Puromycin: Ponceau S
PD98056
D.
Ubiquitin: Ponceau S
E.
Protein: Ponceau S
p-4EBP1:4EBP1
Deptor
p-FOXO3:FOXO3
p-FOXO1:FOXO1
Control+Vehicle
Control+PD98059
LCM+Vehicle
LCM+PD98059
F.
Gene: 18s
Atrogin-1
MuRF-1
G.
Con+Veh
Con+PD98059
LCM+Veh
LCM+PD98059
Con+SB
LCM+SB
p-ERK 1/2
ERK 1/2
Puromycin
Ubiquitin
p-4EBP1
4EBP1
Deptor
p-FOXO3
p-FOXO1
FOXO3
FOXO1
Ponceau S
44/42 kD
75 kD
25 kD
15-20 kD
46 kD
90 kD
80 kD
45 kD

Figure 4. Inhibition of ERK-MAPK does not protect against LCM mediated loss of myotube diameter despite promoting protein synthesis. A: Myotube diameter analysis of control media+vehicle, control media+PD98059, LCM+vehicle and LCM+PD98059. B. Protein content of p-ERK relative to total ERK following 18 hours of control media+vehicle, control media+PD98059, LCM+vehicle and LCM+PD98059 treatment. C: Puromycin incorporated for groups control media+vehicle, control media+PD98059, LCM+vehicle and LCM+PD98059 after 30 minutes puromycin treatment following 18 hours of treatments. D: Protein content of ubiquitin following 18 hours of control media+vehicle, control media+PD98059, LCM+vehicle and LCM+PD98059 treatment. E. Protein content of p-4EBP1 relative to total 4EBP1, Deptor, p-FOXO3 relative to total FOXO3 and p-FOXO1 content relative to total FOXO1 following 18 hours of control media+vehicle, control media+PD98059, LCM+vehicle and LCM+PD98059 treatment. F. *Atrogin-1* and *MuRF-1* mRNA content following 18 hours of control media+vehicle, control media+PD98059, LCM+vehicle and LCM+PD98059 treatment. All measured in C2C12 myotubes and normalized to and Ponceau S. * $P < 0.05$ between indicated groups. Data are mean ± SEM. G: Representative immunoblot images for each protein of interest taken in order from same membrane.

References

1. Fearon Kenneth CH, Glass David J, Guttridge Denis C. Cancer Cachexia: Mediators, Signaling, and Metabolic Pathways. Cell metabolism. 2012;16(2):153-66. doi:http://dx.doi.org/10.1016/j.cmet.2012.06.011.

2. Fearon K, Strasser F, Anker SD, Bosaeus I, Bruera E, Fainsinger RL et al. Definition and classification of cancer cachexia: an international consensus. The Lancet Oncology. 2011;12(5):489-95. doi:10.1016/s1470-2045(10)70218-7.

3. Ferlay J, Soerjomataram I, Dikshit R, Eser S, Mathers C, Rebelo M et al. Cancer incidence and mortality worldwide: sources, methods and major patterns in GLOBOCAN 2012. International journal of cancer. 2015;136(5):E359-86. doi:10.1002/ijc.29210.

4. Onesti JK, Guttridge DC. Inflammation based regulation of cancer cachexia. Biomed Res Int. 2014;2014:168407. doi:10.1155/2014/168407.

5. Jung HW, Kim JW, Kim JY, Kim SW, Yang HK, Lee JW et al. Effect of muscle mass on toxicity and survival in patients with colon cancer undergoing adjuvant chemotherapy. Supportive care in cancer : official journal of the Multinational Association of Supportive Care in Cancer. 2015;23(3):687-94. doi:10.1007/s00520-014-2418-6.

6. Barret M, Antoun S, Dalban C, Malka D, Mansourbakht T, Zaanan A et al. Sarcopenia is linked to treatment toxicity in patients with metastatic colorectal cancer. Nutrition and cancer. 2014;66(4):583-9. doi:10.1080/01635581.2014.894103.

7. Cespedes Feliciano EM, Lee VS, Prado CM, Meyerhardt JA, Alexeeff S, Kroenke CH et al. Muscle mass at the time of diagnosis of nonmetastatic colon cancer and early discontinuation of chemotherapy, delays, and dose reductions on adjuvant FOLFOX: The C-SCANS study. Cancer. 2017;123(24):4868-77. doi:10.1002/cncr.30950.

8. Narsale AA, Puppa MJ, Hardee JP, VanderVeen BN, Enos RT, Murphy EA et al. Short-term pyrrolidine dithiocarbamate administration attenuates cachexia-induced alterations to muscle and liver in ApcMin/+ mice. Oncotarget. 2016. doi:10.18632/oncotarget.10699.

9. Oliveira AG, Gomes-Marcondes MC. Metformin treatment modulates the tumour-induced wasting effects in muscle protein metabolism minimising the cachexia in tumour-bearing rats. BMC cancer. 2016;16:418. doi:10.1186/s12885-016-2424-9.

10. Brown JL, Rosa-Caldwell ME, Lee DE, Blackwell TA, Brown LA, Perry RA et al. Mitochondrial degeneration precedes the development of muscle atrophy in progression of cancer cachexia in tumour-bearing mice. Journal of cachexia, sarcopenia and muscle. 2017. doi:10.1002/jcsm.12232.

11. White JP, Puppa MJ, Sato S, Gao S, Price RL, Baynes JW et al. IL-6 regulation on skeletal muscle mitochondrial remodeling during cancer cachexia in the ApcMin/+ mouse. Skeletal muscle. 2012;2:14. doi:10.1186/2044-5040-2-14.

12. Di Meo S, Reed TT, Venditti P, Victor VM. Role of ROS and RNS Sources in Physiological and Pathological Conditions. Oxidative medicine and cellular longevity. 2016;2016:1245049. doi:10.1155/2016/1245049.

13. Li YP, Chen Y, Li AS, Reid MB. Hydrogen peroxide stimulates ubiquitin-conjugating activity and expression of genes for specific E2 and E3 proteins in skeletal muscle myotubes. American journal of physiology Cell physiology. 2003;285(4):C806-12. doi:10.1152/ajpcell.00129.2003.

14. O'Loghlen A, Perez-Morgado MI, Salinas M, Martin ME. N-acetyl-cysteine abolishes hydrogen peroxide-induced modification of eukaryotic initiation factor 4F activity via distinct signalling pathways. Cellular signalling. 2006;18(1):21-31. doi:10.1016/j.cellsig.2005.03.013.

15. Zhang L, Kimball SR, Jefferson LS, Shenberger JS. Hydrogen peroxide impairs insulin-stimulated assembly of mTORC1. Free radical biology & medicine. 2009;46(11):1500-9. doi:10.1016/j.freeradbiomed.2009.03.001.

16. Assi M, Rebillard A. The Janus-Faced Role of Antioxidants in Cancer Cachexia: New Insights on the Established Concepts. Oxidative medicine and cellular longevity. 2016;2016:9579868. doi:10.1155/2016/9579868.

17. McClung JM, Judge AR, Powers SK, Yan Z. p38 MAPK links oxidative stress to autophagy-related gene expression in cachectic muscle wasting. American journal of physiology Cell physiology. 2010;298(3):C542-9. doi:10.1152/ajpcell.00192.2009.

18. Morales MG, Olguin H, Di Capua G, Brandan E, Simon F, Cabello-Verrugio C. Endotoxin-induced skeletal muscle wasting is prevented by angiotensin-(1-7) through a p38 MAPK-dependent mechanism. Clinical science (London, England : 1979). 2015;129(6):461-76. doi:10.1042/cs20140840.

19. Wissing ER, Boyer JG, Kwong JQ, Sargent MA, Karch J, McNally EM et al. P38alpha MAPK underlies muscular dystrophy and myofiber death through a Bax-dependent mechanism. Human molecular genetics. 2014;23(20):5452-63. doi:10.1093/hmg/ddu270.

20. Girven M, Dugdale HF, Owens DJ, Hughes DC, Stewart CE, Sharples AP. l-glutamine Improves Skeletal Muscle Cell Differentiation and Prevents Myotube Atrophy After Cytokine (TNF-alpha) Stress Via Reduced p38 MAPK Signal Transduction. Journal of cellular physiology. 2016;231(12):2720-32. doi:10.1002/jcp.25380.

21. Barreto R, Waning DL, Gao H, Liu Y, Zimmers TA, Bonetto A. Chemotherapy-related cachexia is associated with mitochondrial depletion and the activation of ERK1/2 and p38 MAPKs. Oncotarget. 2016;7(28):43442-60. doi:10.18632/oncotarget.9779.

22. Chacon-Cabrera A, Fermoselle C, Urtreger AJ, Mateu-Jimenez M, Diament MJ, de Kier Joffe ED et al. Pharmacological strategies in lung cancer-induced cachexia: effects on muscle proteolysis, autophagy, structure, and weakness. Journal of cellular physiology. 2014;229(11):1660-72. doi:10.1002/jcp.24611.

23. Gao S, Carson JA. Lewis lung carcinoma regulation of mechanical stretch-induced protein synthesis in cultured myotubes. American journal of physiology Cell physiology. 2016;310(1):C66-79. doi:10.1152/ajpcell.00052.2015.

24. Zhang G, Jin B, Li YP. C/EBPbeta mediates tumour-induced ubiquitin ligase atrogin1/MAFbx upregulation and muscle wasting. The EMBO journal. 2011;30(20):4323-35. doi:10.1038/emboj.2011.292.

25. Lee DE, Brown JL, Rosa ME, Brown LA, Perry RA, Jr., Wiggs MP et al. microRNA-16 Is Downregulated During Insulin Resistance and Controls Skeletal Muscle Protein Accretion. Journal of cellular biochemistry. 2016;117(8):1775-87. doi:10.1002/jcb.25476.

26. Brown JL, Rosa-Caldwell ME, Lee DE, Brown LA, Perry RA, Shimkus KL et al. PGC-1alpha4 gene expression is suppressed by the IL-6-MEK-ERK 1/2 MAPK signalling axis and altered by resistance exercise, obesity and muscle injury. Acta physiologica (Oxford, England). 2016. doi:10.1111/apha.12826.

27. Lee DE, Brown JL, Rosa-Caldwell ME, Blackwell TA, Perry RA, Jr., Brown LA et al. Cancer Cachexia-Induced Muscle Atrophy: Evidence for Alterations in microRNAs important for Muscle Size. Physiological genomics. 2017:physiolgenomics.00006.2017. doi:10.1152/physiolgenomics.00006.2017.

28. Puppa MJ, Gao S, Narsale AA, Carson JA. Skeletal muscle glycoprotein 130's role in Lewis lung carcinoma-induced cachexia. FASEB journal : official publication of the Federation of American Societies for Experimental Biology. 2014;28(2):998-1009. doi:10.1096/fj.13-240580.

29. Liang HL, Sedlic F, Bosnjak Z, Nilakantan V. SOD1 and MitoTEMPO partially prevent MPTP, necrosis and mitochondrial apoptosis following ATP depletion-recovery. Free radical biology & medicine. 2010;49(10):10.1016/j.freeradbiomed.2010.08.018. doi:10.1016/j.freeradbiomed.2010.08.018.

30. He Q, Harris N, Ren J, Han X. Mitochondria-Targeted Antioxidant Prevents Cardiac Dysfunction Induced by Tafazzin Gene Knockdown in Cardiac Myocytes. Oxidative medicine and cellular longevity. 2014;2014:654198. doi:10.1155/2014/654198.

31. Greene NP, Lee DE, Brown JL, Rosa ME, Brown LA, Perry RA et al. Mitochondrial quality control, promoted by PGC-1alpha, is dysregulated by Western diet-induced obesity and partially restored by moderate physical activity in mice. Physiological reports. 2015;3(7). doi:10.14814/phy2.12470.

32. Washington TA, Brown L, Smith DA, Davis G, Baum J, Bottje W. Monocarboxylate transporter expression at the onset of skeletal muscle regeneration. Physiological reports. 2013;1(4):e00075. doi:10.1002/phy2.75.

33. Goodman CA, Hornberger TA. Measuring protein synthesis with SUnSET: a valid alternative to traditional techniques? Exercise and sport sciences reviews. 2013;41(2):107-15. doi:10.1097/JES.0b013e3182798a95.

34. Goodman CA, Mabrey DM, Frey JW, Miu MH, Schmidt EK, Pierre P et al. Novel insights into the regulation of skeletal muscle protein synthesis as revealed by a new nonradioactive in vivo technique. The FASEB Journal. 2011;25(3):1028-39. doi:10.1096/fj.10-168799.

35. Gao S, Carson JA. Lewis lung carcinoma regulation of mechanical stretch-induced protein synthesis in cultured myotubes. American Journal of Physiology - Cell Physiology. 2016;310(1):C66-C79. doi:10.1152/ajpcell.00052.2015.

36. Fluckey JD, Knox M, Smith L, Dupont-Versteegden EE, Gaddy D, Tesch PA et al. Insulin-facilitated increase of muscle protein synthesis after resistance exercise involves a MAP kinase pathway. American journal of physiology Endocrinology and metabolism. 2006;290(6):E1205-11. doi:10.1152/ajpendo.00593.2005.

Chapter 6

Overall Conclusions

This dissertation examines a novel time course progression of cancer-cachexia. These data indicate that pathological changes in muscle metabolism occur very shortly after tumor implantation into the mouse host. From a clinical standpoint, these data suggest that preventative measures to cancer-cachexia should be taken immediately upon diagnosis, at least if the cancer type is associated with cachexia. Furthermore, I have shown increased oxidative stress and aberrant MAPK signaling in skeletal muscle is at least partially responsible for the onset of cancer-cachexia through *in vitro* studies. Future studies following this dissertation should focus on the efficacy of antioxidant therapy and MAPK inhibition *in-vivo* as potential therapies for cancer-cachexia. Additionally, as characteristics of cancer-cachexia often vary across models, in order to ensure data is consistent across cancer types, these experiments should be repeated in other clinical models of cancer-cachexia.

Mitochondrial Degeneration Occurs Prior to Cancer-Induced Muscle Wasting (Chapter 3).

This was the first experiment to investigate mitochondrial degeneration and dysfunction throughout a time course development of cancer-cachexia in tumor-bearing mice. This aim provided insight into causes of skeletal muscle metabolic dysfunction beyond mitochondrial quality control (biogenesis, dynamics and mitophagy), and directly measured mitochondrial quality (MitoTimer), mitochondrial ROS emission and respiratory function (RCR). Intriguingly, mitochondrial ROS production doubled as soon as 1 wk following tumor implantation, which I hypothesize was likely instigated by tumor-derived circulating factors. These data implicated the importance of early cancer detection, as well as preventive measures for cancer-cachexia, especially since cancer-cachexia is often not treated before stage IV of cancer is reached [1].

Cancer-Induced Muscle Wasting Occurs Through a Combination of Reduced Protein Synthesis and Increased Protein Breakdown (Chapter 4).

In this study we analyzed muscle size, myogenesis, protein turnover and apoptosis throughout the development of cancer-cachexia. Based on our data, loss of mixed protein synthetic rates along with increased protein breakdown occur concurrently with muscle wasting. Furthermore, there appeared to be early alterations in myogenic signaling potentially contributing to the irreversibility of cancer-cachexia. In conjunction with my observations in chapter 3, inefficient mitochondria and oxidative stress may cause the dysregulated protein turnover we observed in this study; however, at this point we cannot definitively state the mechanism behind cancer-cachexia. We also observed elevated p38 and ERK MAPK signaling in cachectic muscle; therefore, we hypothesized pathological MAPK signaling may also be a major contributing factor in the onset of LLC-induced cancer-cachexia.

Oxidative Stress and Dysregulated MAPK Signaling Lead to Loss of Myotube Diameter *In-Vitro* (Chapter 5).

In this study I used LLC Conditioned Media (LCM) to mimic cancer-cachexia *in-vitro.* LCM induced a ~40% loss of myotube diameter when compared to control media, which was similar to the loss of muscle cross sectional area I observed *in-vivo* (Chapter 4). Based on findings of early mitochondrial oxidative stress (Chapter 3) and aberrant MAPK signaling (Chapter 4) in the development of cancer-cachexia *in-vivo,* I performed *in vitro* experiments to target these aspects to determine potential efficacy of antioxidants or MAPK inhibition in preventing cancer-induced muscle loss. Using a mitochondrial targeted antioxidant (MitoTempo, herein referred to as MitoT), I was able to partially rescue tumor-derived loss of myotube diameter. Moreover, I examined the role of MAPKs in the promotion of cancer-cachexia. In

Chapter 4 of this dissertation, ERK and p38 MAPK phosphorylation were elevated 2 fold in cachectic muscle when compared to control muscle. By using inhibitors for both ERK and p38 MAPK, I demonstrated that p38 inhibition partially rescued LCM-dependent loss of myotube diameter, while ERK inhibition appeared to have no effect.

Underlying mechanisms in which MitoT and p38 MAPK inhibition rescue myotube diameter are still not fully understood; however, it appears both MitoT and p38 MAPK inhibition prevent an upregulation of catabolic programing. Long term MAPK inhibition (~18 hours) also appeared to promote protein synthesis. Mechanisms behind MAPK involvement in protein synthesis are not fully understood. This aim uncovered potential mechanisms for tumor mediated loss of muscle size, and a new role of MAPK signaling in the regulation of protein synthesis, which may lead to potential for development of new and efficacious therapeutic strategies.

Concluding Statements

These studies give a clear overview of the changes in skeletal muscle physiology throughout a timecourse progression of cancer-cachexia. These data provide new insight into potential underlying aberrations into the root cause of cancer-cachexia, and may lead to the development of new therapeutic strategies.

Limitations and Delimitations

This dissertation has a few limitations and delimitations which should be taken into consideration. For the timecourse studies (Chapters 3 and 4), there was not an age matched control for the 1 wk, 2 wks or 3 wks tumor growth groups. It is possible that differences in age may influence dependent variable analysis; however, age differences did not appear to affect skeletal muscle size. Also, it is common that the development of cancer-cachexia occurs with hypophagia, unfortunately I was unable to collect appropriate food intake data to determine if this may have aided in the onset of cachectic muscle loss in this study.

In previous literature LCM treatment commonly occurs over 72 hour to mimic a cachectic phenotype in cells [2, 3] ; however, I obtained a significant loss of myotube diameter after only 18 hours of LCM treatment. Because of this I elected to use an 18 hour LCM treatment for my *in-vitro* studies in Chapter 5 instead of the commonly used 72 hour treatment. One difference between my methodology and prior literature may have been the confluence of LLC cells upon harvest of LCM. LLC cells were ~90% confluent before the 10% FBS growth media incubated on those cells for another 24 hours. Because of this, it is likely my LCM was more concentrated than prior studies.

For my experiments in Chapter 5 of this dissertation, I was unable to test MitoTempo treatment and MAPK inhibition *in-vivo* in order to make sure my findings are translatable to mammals. This is a worthwhile goal for future studies.

References

1. Muscaritoli M, Rossi Fanelli F, Molfino A. Perspectives of health care professionals on cancer cachexia: results from three global surveys. Annals of Oncology. 2016;27(12):2230-6. doi:10.1093/annonc/mdw420.

2. Gao S, Carson JA. Lewis lung carcinoma regulation of mechanical stretch-induced protein synthesis in cultured myotubes. American journal of physiology Cell physiology. 2016;310(1):C66-79. doi:10.1152/ajpcell.00052.2015.

3. Zhang G, Jin B, Li YP. C/EBPbeta mediates tumour-induced ubiquitin ligase atrogin1/MAFbx upregulation and muscle wasting. The EMBO journal. 2011;30(20):4323-35. doi:10.1038/emboj.2011.292.

Appendices

UNIVERSITY OF ARKANSAS

Office of Research Compliance

MEMORANDUM

TO: Nicholas Greene

FROM: Craig N. Coon, Chairman

DATE: 7/13/15

SUBJECT: IACUC Approval

Expiration Date: Jan 1, 2018

The Institutional Animal Care and Use Committee (IACUC) has APPROVED your protocol 15065: "Mitochondrial Degeneration in the Onset of Cancer-Cachexia Induced Muscle Atrophy" you may begin work immediately

In granting its approval, the IACUC has approved only the information provided. Should there be any further changes to the protocol during the research, please notify the IACUC in writing (via the Modification form) prior to initiating the changes. If the study period is expected to extend beyond Jan 1, 2018 you must submit a newly drafted protocol prior to that date to avoid any interruption. By policy the IACUC cannot approve a study for more than 3 years at a time.

The IACUC appreciates your cooperation in complying with University and Federal guidelines involving animal subjects.

CNC/aem

cc: Animal Welfare Veterinarian

Administration Building 210 • 1 University of Arkansas • Fayetteville, AR 72701-1201 • 479-575-4572
Fax: 479-575-3846 • http://vpred.uark.edu/199

UNIVERSITY OF ARKANSAS

Office of Research Compliance

July 09, 2015

MEMORANDUM

TO: Dr. Nicholas Greene

FROM: Dr. Ines Pinto
Institutional BioSafety Committee

RE: IBC Protocol Approval

IBC Protocol #: 15025

Protocol Title: "Mitochondrial Degeneration in the Onset of Cancer-Cachexia Induced Muscle Atrophy"

Approved Project Period: Start Date: July 9, 2015
Expiration Date: July 8, 2018

The Institutional Biosafety Committee (IBC) has approved Protocol 15025, "Mitochondrial Degeneration in the Onset of Cancer-Cachexia Induced Muscle Atrophy" You may begin your study.

If further modifications are made to the protocol during the study, please submit a written request to the IBC for review and approval before initiating any changes.

The IBC appreciates your assistance and cooperation in complying with University and Federal guidelines for research involving hazardous biological materials.

109 MLKG • 1 University of Arkansas • Fayetteville, AR 72701-1201 • 479-575-4572 • Fax: 479-575-6527 • http://rscp.uark.edu

UNIVERSITY OF ARKANSAS | Research & Economic Development
Research Compliance

December 15, 2017

MEMORANDUM

TO:	Dr. Nicholas P. Greene
FROM:	Ines Pinto, Biosafety Committee Chair
RE:	New Protocol
PROTOCOL #:	18018
PROTOCOL TITLE:	In Vitro Examination of Muscle Plasticity
APPROVED PROJECT PERIOD:	Start Date December 14, 2017 Expiration Date December 13, 2020

The Institutional Biosafety Committee (IBC) has approved Protocol 18018, "*In Vitro* Examination of Muscle Plasticity". You may begin your study.

If modifications are made to the protocol during the study, please submit a written request to the IBC for review and approval before initiating any changes.

The IBC appreciates your assistance and cooperation in complying with University and Federal guidelines for research involving hazardous biological materials.

MitoTimer Methodology

FDB Electroporation:

-Prepare plasmids at 2μg/μl in sterile saline and need 20μl for one FDB muscle. If co-injecting an over-expression vector with a reporter gene (i.e. pMitoTimer or pGFP3), make a ratio of 3:1 (over-expression vector:reference reporter gene).

-Prepare a solution of .36mg/ml hyaluronidase in sterile saline (Store at -20 degrees C)

1. Using an anesthetizing box, deeply anesthetize a mouse using 4% isoflurane in O2 with an anesthetic instrument. Monitor the anesthetic depth by toe pinch reflex

2. Under observation of a dissection microscope, inject 10 μL of the hyaluronidase solution under the footpads of one foot of the mouse using a 1" long insulin needle. Penetrate the skin at a point close to the heel of the foot and advance the needle subcutaneously towards the base of the toe for ¼"

3. Repeat with other foot if needed

4. Disconnect the anesthesia and place mouse in cage. Allow animal to fully recover from anesthesia

5. After 1HOUR, anesthetize the animal again. Following the same procedure described for the hyaluronidase solution, inject a total of 20 μg of the plasmid DNA. The total injection volume should be less than 20 μL/foot. Note: when 15-20 μL is needed it is advisable to close the skin at the needle entry point with tissue-glue

6. Disconnect the anesthesia and place the mouse in a cage. Allow it to fully recover from anesthesia, wait for 10-15 min

7. Anesthetize the animal for a third time, place it on a heating pad

8. Select one foot of the animal. Place one gold-platted acupuncture needle under the skin at heel and a second one at the base of the toes. Electrodes are oriented parallel to each other and perpendicular to the long axis of the foot.

9. Connect the head of the needles (electrodes) to the electrical stimulator using micro-clip connectors. Electro orate the muscles by applying 10 pulses, 20ms in duration/each, at 1Hz. Depending on the spacing of the electrodes, the pulsing voltage amplitude is adjusted (by monitoring with an oscilloscope) to yield an electric field of about 75V/cm. Note: no contractions in response to the stimuli should be observed if the level of anesthesia is adequate.

10. If needed, repeat with other foot

11. Return animal to cage, observe to make sure animal is okay, allow recovery for 10-15 days

FDB Harvest and Mounting

1. Harvest FDB. If both confocal microscopy and protein analysis is required, carefully slice the muscle in half longitudinally. Immediately homogenize half of the muscle in protein buffer and incubate the other half with 1 mL 4% PFA for 20 minutes (at room temperature) and then transfer to 1 mL PBS and incubate for 5 min. Try not to expose to tissue to bright light in order to preserve the fluorescence of the reporter if you use pMitoTimer.

2. Carefully remove the tendon running the length of the muscle. Place the tissue on a gelatin coated slide. Use tweezers to orientate the tissue and flatten it on the slide. Make sure there are no air bubbles under the tissue.

3. Allow the tissue to adhere to the slide. This typically takes 5-10 min, but it can vary on the thickness and type of tissue.

4. On one side of the slide pipette 50:50 PBS:Glycerol and place a coverslip over the slide. You want the coverslip to be as close to the slide as possible. This is easy for thin tissues, and you can push the coverslip and slide together if the tissue is deformable (press and wiggle, Be very careful with this).

5. Remove any excess 50:50 that has come out from under the coverslip with blotting paper.

6. Seal the coverslip by painting the edges with nail polish. This will prevent the 50:50 from evaporating over time.

7. Image immediately

MitoTimer Imaging

Parameters for imaging Mito-Timer on ConFocal Microscope

-Use FITC (green) and TRITC (red) channels.

-Aspect ratio: 800x800

-Green HV: 565

-Red HV: 685

-Gain: 1

-Offset: 10%

-Lazer intensity: 15%

-2 pixels/sec

-0.5 um slice

-check sequential imaging (line)

-Take at least 10 images at 100X magnification

Parameters for imaging Mito-Timer on epiflourescent microscope.

-Aspect Ratio: 800X600

-Set equal exposure times for both FITC and TRITC channels (100 ms is a good place to start). Make sure this is the same for all images taken for all groups.

-Analog Gain: 2X

-Image FITC and TRITC Channels and Merge Images.

-Save images as ND2 files.

MitoTimer Analysis.

Make a matlab folder for each sample. Inside the matlab folder make three more folders and label them 10X, 40X and 100X for the different objectives images were taken at. For your saved ND2 images, separate the channels and save each image separately as 1_Green or 1_Red depending on the filter for the image. Save as jpeg. Make sure LUTs is normalized across all images for the entire study before you save the individual images. For the next images for the sample you would save them as 2_Green or 2_Red. Save them to the appropriate folder based on the objective the images were taken at. Open the cell profiler software and make the output

folder the same folder that the images are saved in. Hit analyze in the bottom left and corner. Once the cell profiler is finished, open up the matlab code and change the destination in three different spots to the folder the images are saved in. Run the matlab program and then copy the data to an excel spreadsheet.

Protein Synthesis Methodology

Dueterium Dosages

All injections or consumption of $^{2}H_20$ should begin 24 hours before tissue harvest. For rats or mice use 20ul of 99.8% $^{2}H_20$ per gram body weight ($20ul \cdot g\ bw^{-1}$). Animals should have access to 4% $^{2}H_20$ *ad libitum* at all times after injection. Using this calculation, our lab has consistently obtained 2.5 – 3.0 atom percent excess of ^{2}H-labeling of body water, which is adequate for determining FSR. It is possible to use a higher or lower dose in order to increase or decrease enrichment, but not necessary.

Mice

Mice weigh anywhere from 20 – 35 g, so you would inject 0.4 - 0.7ml respectively of 99.8% $^{2}H_20$.

Animal Injections

All injections should be delivered via intraperitoneal (I.P.) injection.

Plasma Collection and Analysis

This assay requires 20ul of plasma to measure the concentration of 2H20 in the blood. It is recommended to draw at least 500ul of whole blood in order to have more than enough plasma for multiple attempts getting the plasma concentration.

Mice Blood Samples

Blood taken from animals should drawn from either from a cardiac puncture (if non-survival to obtain the maximal amount of blood), lateral saphenous vein, or the tail vein and placed in microcentrifuge tube. Store on ice in until plasma is separated by centrifugation. Mice have a total blood volume of approximately *1.5ml*, therefore the only way to get a large enough blood volume is cardiac puncture.

Obtaining plasma from whole blood

1. Centrifuge whole blood samples at 3,800 rpm at 4ºC for 20 min.

2. Extract plasma (liquid supernatant) with 1.0 ml pipette or transfer pipette and place into 1.5 ml microcentrifuge tubes, freeze at -80ºC until analysis.

Preparation of Plasma Samples for Analysis:

1. Remove samples from -80ºC and allow thawing for analysis.

2. Place 20ul of plasma into 2.0 ml microcentrifuge tubes.

3. Add 2.0 µl of 10N NaOH to samples.

4. Add 4.0 µl of a 5% (vol/vol) acetone (CH3Cl3) in acetonitrile (CH3CN), cap and allow settling for a minimum of 24 h.

We have found that you should do a quick spin in the centrifuge to ensure that all of the products in the reaction are in the bottom of the microcentrifuge tube.

5. Add ~0.5 g sodium sulfate (Na2SO4) to samples.

0.5 g is not an exact measurement, but it should be relatively close. Sodium sulfate acts as a drying agent in this process

6. Add 0.6 ml of chloroform (CH3Cl3) to each sample, cap and vortex vigorously.

- Chloroform stops the reaction of 2H transferring from deuterium to acetone

7. Extract 100ul from the centrifuge tube and add to a GC-MS vial containing the insert.

*The reason we use inserts in the vials is to cut down on costs. The glass vials cost ~$1 a piece, while the inserts cost only $0.25. Please do not label on or throw away the glass vials. Instead label on the screw caps and throw away both the insert and screw cap.

2. Method

a. The following temperature program is used: 60ºC initial, increase by 20°C/min to 100ºC, increase by 50ºC/min to 220ºC, and hold for 1 min. The sample was injected at a spit ratio of 40:1 with a helium flow of 1 mL/min. The mass spectrometer is operated in electron impact mode (70eV).

b. Inject 1ul sample into GC-MS

c. Selective ion monitoring of mass-to-charge ratios (m/z) 58 (M) and 59 (M + 1) was conducted using a dwell time of 10 ms per ion. 2H acetone elutes at between 1.7-1.85 min.

1. Linear Standard Curve Preparation

First Create a stock solution of 5% $^{2}H_2O$ (5.0 ml of $^{2}H_20$ + 95 ml of ultrapure diH_2O) and then make the following dilutions:

% **labeled**	**ml of stock**	**ml of diH_2O**	**total ml**
5.0	1.0	0	1.0
2.5	0.5	0.5	1.0
1.25	0.25	0.75	1.0
1.0	0.20	0.8	1.0
0.5	0.10	0.9	1.0
0.25	0.05	0.95	1.0
0.125	0.025	0.975	1.0
0	0	1.0	1.0

Standards should be prepared and ran in the same manner as the plasma samples above.

Product Numbers:

Acetone (CH_3COCH_3)	EMD, AX0120-8
Acetonitrile (CH_3CN)	Fisher, A998-4
GC-MS glass vials	Agilent, 5182-0714
GC-MS vial inserts	Agilent, 5182-0549
GC-MS vial screw top caps	Agilent, 5185-5820
Chloroform (CH_3Cl_3)	Fisher, C298
Sodium hydroxide (NaOH)	Fisher, 5612-3
Sodium Sulfate (Na_2SO_4)	Fisher, S414
Trichloroacetic acid (TCA-Cl_3CCOOH)	EMD, TX1045-5

Methyl-8 (N,N-Dimethylformamide dimethyl acetal) Sigma 394963

Analyzing Plasma Sample Data

1. Open the Enhanced Data Analysis Program that was provided by Agilent.

2. In the left window pane, find and select the data file you want to analyze. Left click on the data file and select Load.

   This will make the data file appear Bolded. All files that you have opened in the current session of Data Analysis will remain bolded

3. Along the top menu toolbar, select Chromatogram → Extract Ion Chromatogram

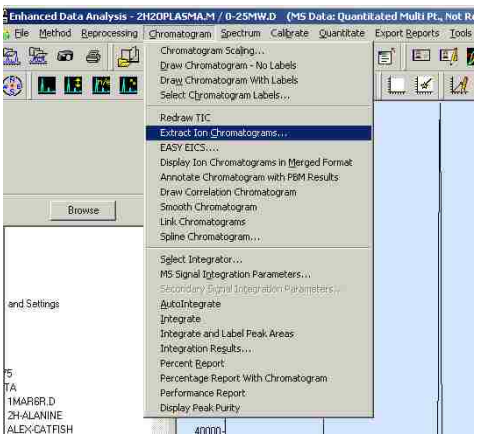

4. In the pop up box that appears Enter 1.7 - 1.85 into the Time Range fields,

   This range will change slightly based on many different factors including Column Length, Column Age, and different machines. It should be relatively close to that range.

5. Enter 58 in Ion 1, this corresponds to m, or in this case Acetone.

6. Enter 59 in Ion 2, this corresponds to m+1, or in this case ^{2}H-Acetone.

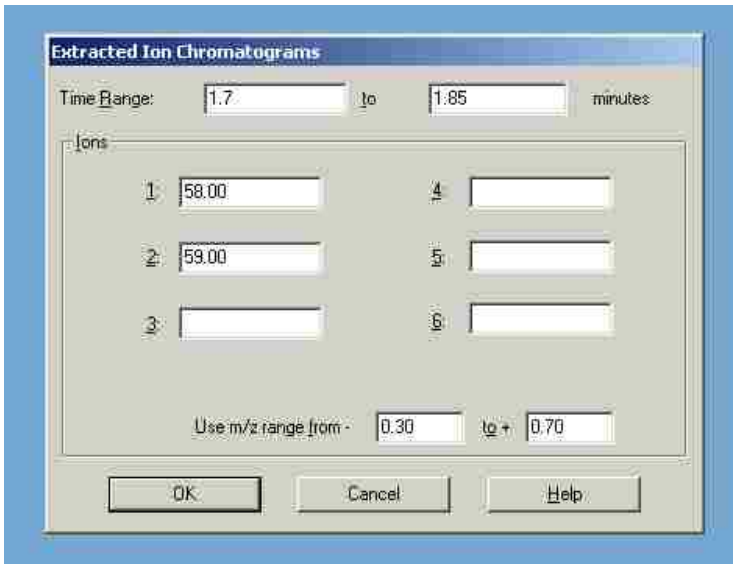

7. This creates the screen where the top peak is for M and the bottom peak is for M+1. You

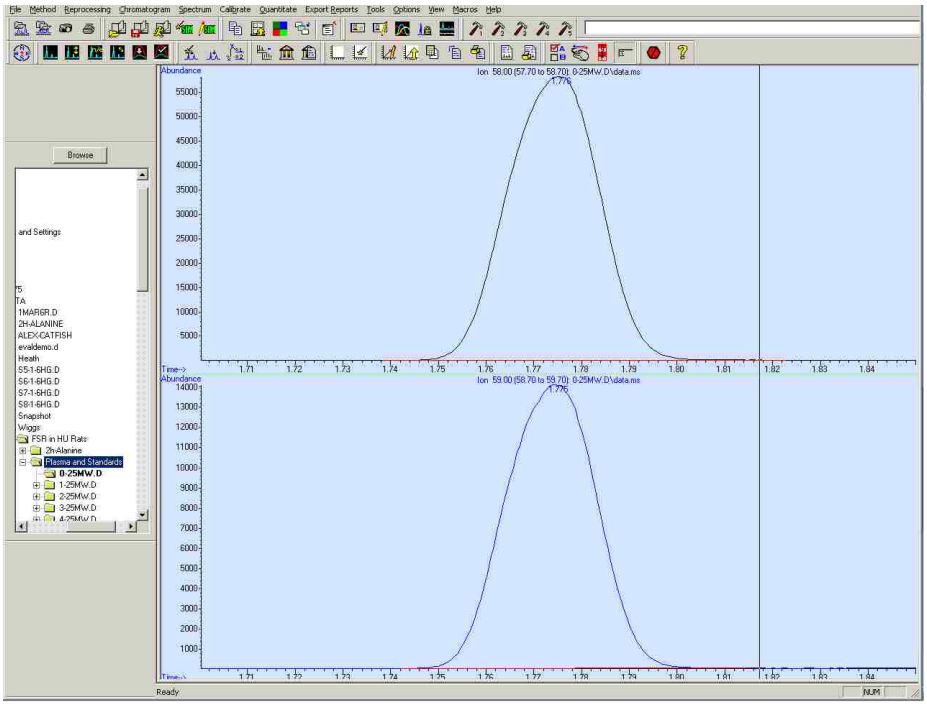

may choose to merge the peaks if you want to view just one graph.

8. The goal of this measurement is to get a ratio of M+1:M, To get this go to Chromatogram → Percent Report. This will open up a text box. Copy and Paste the Peak Heights for both of the peaks in to Excel and get a ratio of M+1:M. *Notice that time times are virtually identical in the column labeled R.T. min. Sometimes you can get multiple peak numbers for m+1.

Always take the one with the time closest to the peak for M.

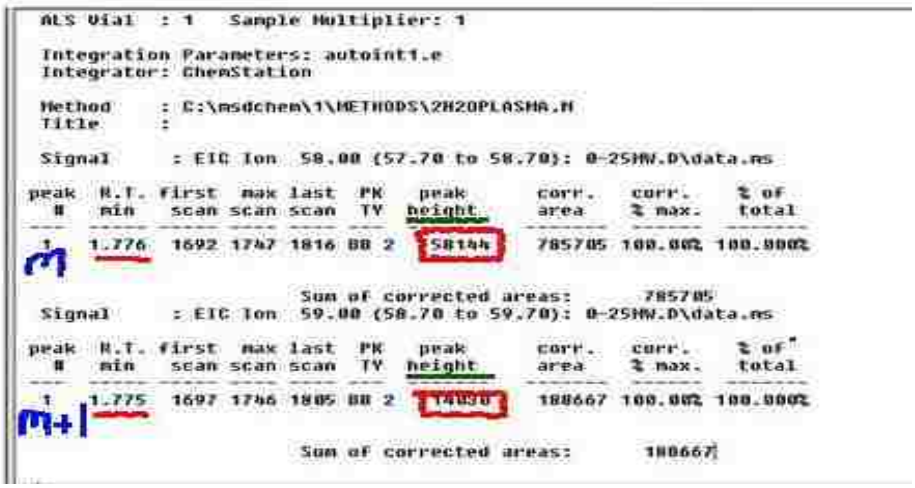

```
ALS Vial  : 1   Sample Multiplier: 1

Integration Parameters: autoint1.e
Integrator: ChemStation

Method    : C:\msdchem\1\METHODS\2H2OPLASMA.M
Title     :

Signal     : EIC Ion  58.00 (57.70 to 58.70): 0-25MW.D\data.ms

peak  R.T.  first  max  last  PK   peak      corr.    corr.    % of
  #   min    scan scan scan  TY  height     area     % max.   total
---  -----  ----- ---- ----  --  ------    -------  ------   -------
  1  1.776  1692 1747 1816  BB  2  58144    785705 100.00% 100.000%

                    Sum of corrected areas:      785705
Signal     : EIC Ion  59.00 (58.70 to 59.70): 0-25MW.D\data.ms

peak  R.T.  first  max  last  PK   peak      corr.    corr.    % of
  #   min    scan scan scan  TY  height     area     % max.   total
---  -----  ----- ---- ----  --  ------    -------  ------   -------
  1  1.775  1697 1746 1805  BB  2  14030    188667 100.00% 100.000%

                    Sum of corrected areas:      188667
```

Muscle Preparation:

1. Weight out 30 ± 5 mg of muscle 60mg if assessing myofibrillar fraction as it makes up 50% of the mixed muscle homogenate).

2. Place into 2.0 ml microcentrifuge tubes and add 0.400 ml of 10% TCA (Cl_3CCOOH) on ice.

    a. For Myofibrillar FSR:

        i. weight out ~60 mg of mixed muscle and add 400ul of Norris buffer with 1% Triton.

ii. Homogenize using a polytron homogenizer at full speed and allow settling on ice for a minimum of 1 h. Visibly check to make sure there are no large ‘chunks’ of muscle in the vial

iii. Centrifuge at 14,000 rpm for 30 min at 4ºC. Decant supernatant and add 0.3 ml of 10% TCA on ice.

iv. The remainders of the steps are the same as the mixed muscle homogenate.

v. To conserve tissue sample, it is possible to prep samples for western blotting and myofibrillar FSR. If you use the ‘unrefined’ separation of adding triton to Norris buffer and centrifuging at 14,00 rpm to obtain the cytosolic and membrane fraction, you can then use the myofibrillar pellet that we typically discard. This fraction contains more than just myofibrillar proteins. It also contains nuclear, microsomal, mitochondrial, connective tissue. Therefore, it should probably be termed myofibrillar rich fraction since that is the predominant fraction of the pellet.

3. Homogenize using a polytron homogenizer at full speed, centrifuge at 3,800 rpm, decant supernatant and add 0.3 ml of 10%TCA on ice. TCA is a weak acid that causes the proteins to fall out of solution, therefore all free amino acids should be washed out in the supernatant.

4. Repeat step 3 three additional times, always decanting TCA after centrifugation.

5. Add 0.3 ml of 6 N HCl, vortex and place into 2.0 ml **screw top tubes**.

    a. HCL and heating breaks the proteins into amino acids so we can measure alanine with the GC/MS. You must use screw tops to prevent evaporation in the sample. Snap caps will not work.

6. Incubate at 100ºC for 24 h.

    a. Vortex the samples periodically throughout the heating process to remove all the black chunks of tissue. I like to vortex about 15mins after they are first put on the heating block, then at 1hr, maybe at 2-3hrs, let samples sit for overnight and then vortex first thing in the morning and finally about 1hr before the end of the 24hrs.

    b. Hydrolysate should turn from clear at the beginning to a very dark brown after heating.

7. Pipette between 50 and 100 ul of hydrolysate into a 1.5-2.0ml microcentrifuge tube place in heating block at heat at 100ºC with top off for 1 h to allow HCL to evaporate.

a. Sample could alternatively be placed under a low stream of N_2 to dry or could be dried using a freeze drier. The MBL uses the heating block method because of its ease and relatively short time frame. Freeze the remainder of the hydrolysate in the -80° C Freezer.

b. Currently the MBL has gone to using 50ul of hydrolysate and 50 of 3:2:1 solution (below)

c. Sample Must Be Completely DRY! Check by thumping or rotating the tube to see if any liquid still remains.

8. Make a 3:2:1 solution of Methyl-8 (N,N-Dimethylformamide dimethyl acetal), methanol (CH_3OH) and acetonitrile (CH_3CN).

    a. As a rule of thumb we make a little extra than the 100ul needed for all the samples, but not too much so we are not wasting reagent. For example to run 24 samples, you need 2.4 ml of the 3:2:1 solution, but I would recommend making 2.6 ml.

    b. This is 3 parts Methyl-8, 2 parts methanol and 1 part acetonitrile

9. Pipette equal volume from step 7 (50 - 100ul) of the 3:2:1 Methyl-8, methanol (CH_3OH) and acetonitrile into the dried samples.

    a. If the sample was not completely dry, addition of the the methyl-8 solution will 'smoke' (releases visible vapors) and the methyl-8 will be inactivated. If this occurs the reaction will not occur and there will be no peaks if ran on the GC/MS.

10. Heat samples in heating block at ~70ºC for one hour, vortexing intermittently, to ensure the dried hydrolysate dissolves into solution.

11. Place sample into GC-MS vial inserts and place into the GC-MS glass vials and cap. Label the samples on the cap and place them into the auto-injection loader.

Gas Chromatography Mass Spectrometry (GC-MS)

1. System:
    a. Agilent 5973N-MSD equipped with an Agilent 6890 GC system.
    b. DB17-MS capillary column (30 m × 0.25 mm × 0.25 µm).

2. Settings:
    a. The following temperature program was used: 90ºC initial, hold for 5 min, increase by 5°C/min to 130ºC, increase by 40ºC/min o 240ºC, and hold for 5 min. The sample was injected at a spit ratio of 20:1 (5:1 for human tissue) with a helium flow of 1 ml/min. The mass spectrometer was operated in electron impact mode (70eV).

b. Selective ion monitoring of mass-to-charge ratios (*m/z*) 99 (M) and 100 (M + 1) was conducted using a dwell time of 10 ms per ion. ^{2}H alanine elutes at ~ 12 min (9 min on our system).

c. For Muscle 80:1 splitting is probably a better starting point and even then may still have to be diluted in acetonitrile (50 ul dilution will probably work).

3. Linear Standard Curve Preparation

a. **Solution A** - Stock Solution of L-alanine ($C_3H_7NO_2$):

i. Place 10 mg L-alanine into 1.0 ml of ultrapure dH_2O (Solution A).

b. **Solution B** - Stock Solution of L-alanine-2-d ($CH_3CD(NH_2)CO_2H$):

i. Place 1 mg of L-alanine-2-d into 1.0 ml of ultrapure dH_2O (Solution B).

% labeled	**Sol A (ml)**	**Sol B (ml)**	**H_2O (ml)**	**total (ml)**
2.0	1.0	0.2	0.8	2.0
1.0	1.0	0.1	0.9	2.0
0.75	1.0	0.075	0.925	2.0
0.5	1.0	0.050	0.950	2.0
0.25	1.0	0.025	0.975	2.0
0	1.0	0	1.0	2.0

c. Take 0.1 ml of each standard and place into GC-MS glass vials and dry under a low stream of N_2 (can place in heating block at heat at 100ºC with top off for 1 h). Freeze the remainder of the hydrolysate.

a. Add a 3:2:1 solution of Methyl-8, methanol (CH_3OH) and acetonitrile (CH_3CN); cap and vortex vigorously.

b. Place sample into GC-MS vial inserts and place into the GC-MS glass vials and cap.

*The goal is to have the peaks for your standards look the same as for your tissue samples, so peak heights should correspond pretty well. The goal for peak heights on samples is 200,000 – 400,000, so you would not want peak heights on your standards in the 1 million ranges. The steps above suggest 100ul of each standard, but that is assuming a split of 1:20. As you decrease your split, you should also decrease the amount of standard you use. 800,000 is typically the maximal accepted limit.

*Standards should be run with each new run on the GC-MS. They should also be analyzed exactly the same way as the tissue. In other words, if you are changing split ratios on the GC-MS, you need to re-run the standards.

Analyzing Muscle Sample Data

1. Open the Enhanced Data Analysis Program that was provided by Agilent.

2. In the left window pane, find and select the data file you want to analyze. Left click on the data file and select Load.

   This will make the data file appear Bolded. All files that you have opened in the current session of Data Analysis will remain bolded

3. Along the top menu toolbar, select Chromatogram → Extract Ion Chromatogram

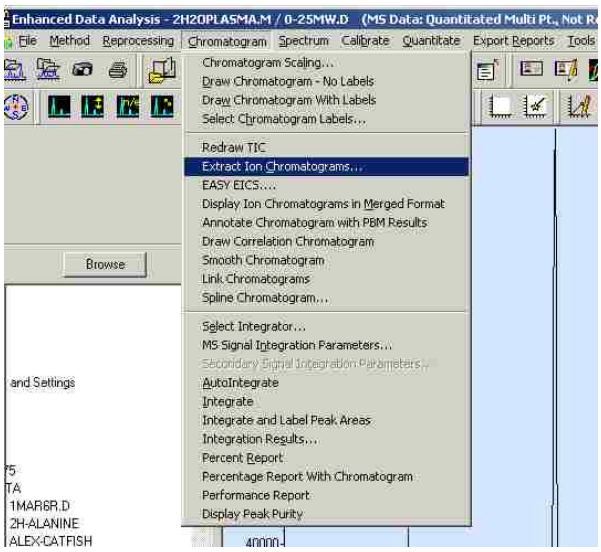

4. In the pop up box that appears Enter 8 – 12 minute into the Time Range fields,

   This range will change slightly based on many different factors including Column Length, Column Age, and different machines. It should be relatively close to that range.

5. Enter 99 in Ion 1, this corresponds to m, or in this case Alanine.

6. Enter 100 in Ion 2, this corresponds to m+1, or in this case ^{2}H-Alanine.

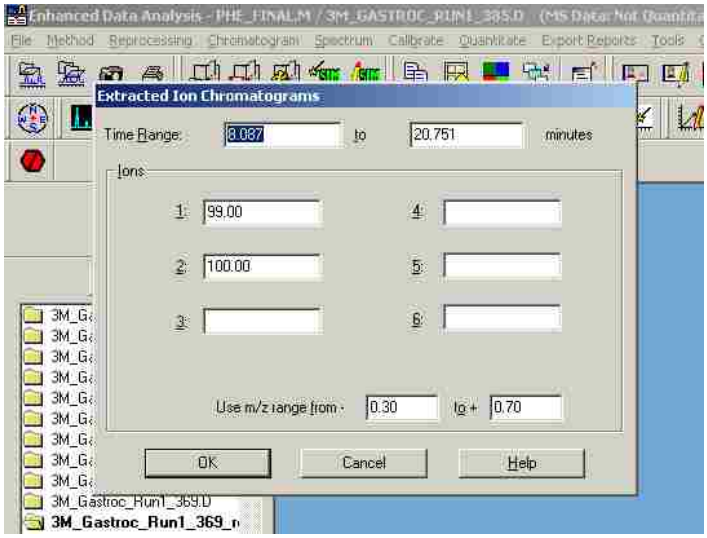

7. When analyzing muscle peak heights, we take only a small portion of the curve. We have designated that all measurements will be taken between 25 and 50% of the peak height.

    a. Peak height can be determined either by choosing peak height from the menu similar to what is done in step 8 of analyzing plasma samples. To get this go to Chromatogram → Percent Report. This will open up a text box. Copy and Paste the Peak Heights for both of the peaks in to Excel. Use a simple formula to calculate 25 and 50%.

    b. In the past, we have also chosen to get peak height by the eyeball method. Simply zoom in on the peak by left clicking and drawing a box around the top of the peak until you can get a very good opinion on the peak height

c. Don't be surprised if the two methods give different peaks; just be *CONSISTENT* in which method you choose and stick with it.

8. To get the area under the curve (AUC) between 25-50% of the peak height. Right Click and hold while your cursor is located ON THE CURVE where the value on the y-axis corresponds to the value you calculated for 25%. Drag the cursor to the value ON THE CURVE corresponding to 50% and release your click. You box should look similar to the picture below.

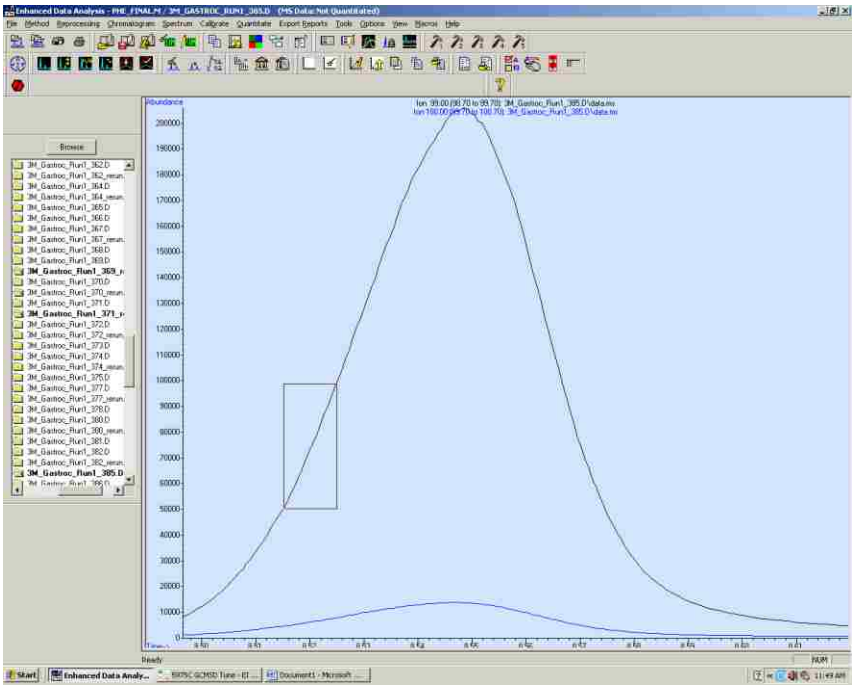

9. This will pop up a box with the 99 and 100 AUC.

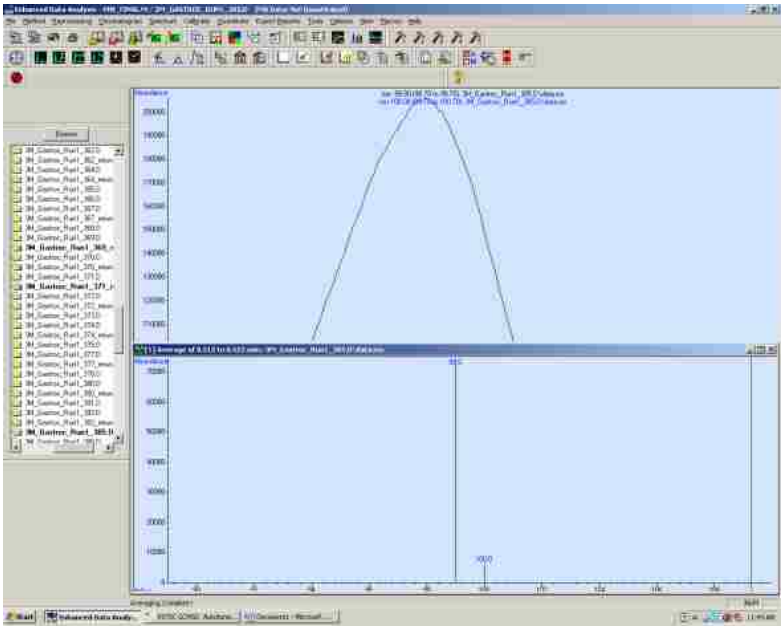

10. To get the values, go to Spectrum→Tabulate.

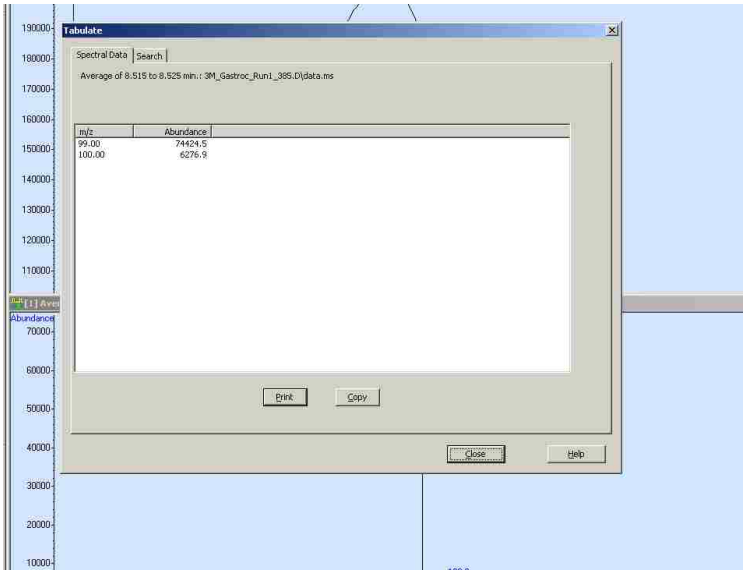

11. Copy and paste into Excel. It is up to you how you want to set up your spreadsheet but I have provided an example below.

0.7*D13

K	L	M	N	O	P	Q	R
Number	Group	25%	50%	M	M+1	Ratio	MPE
352	CC	43328	86656	64264	5332.4	0.08298	
358	CC	34784	69568	51133.5	4320.1	0.08449	
362	CC	57152	114304	82607.1	6765.3	0.08190	
369	CC	20322	40644	29430.9	2531.7	0.08602	
370	CC	70720	141440	103658	8692	0.08385	
371	CC	44304	88608	64858.4	5287.4	0.08152	
372	CC	30160	60320	44679.5	3694.9	0.08270	
378	CC	32528	65056	48713.4	4057.1	0.08329	
383	CC	27074	54148	39776.5	3414	0.08583	
386	CC	74608	149216	111097	9020.7	0.08120	
392	CC	51888	103776	77143.1	6522.9	0.08456	
365	HU	57536	115072	84776.4	6848.7	0.08079	
368	HU	57312	114624	84605.8	6682.7	0.07899	
374	HU	46544	93088	68979.1	5496.5	0.07968	
382	HU	36912	73824	55056.5	4518.4	0.08207	
394	HU	8848	17696	12935.4	1104.2	0.08536	
399	HU	84128	168256	123058	9927.5	0.08067	
404	HU	55232	110464	82057.9	6454.1	0.07865	
406	HU	90932	181864	134897	10648.6	0.07894	
346	Lun	37792	75584	55785.6	4597.7	0.08242	
354	Lun	36384	72768	52806.6	4291.9	0.08128	
366	Lun	35616	71232	52822.6	4458.3	0.08440	
367	Lun	39024	78048	58928.9	4905.2	0.08324	
385	Lun	41360	82720	60816.5	4933.6	0.08112	
388	Lun	26108	52216	39231	3248.4	0.08280	
389	Lun	21352	42704	31886.4	2675	0.08389	
397	Lun	28460	56920	43202	3590.5	0.08311	

12. MPE is determined by solving for X in your equation determined by your standard curve.

Respiration and ROS Methodology

RCR Measurements

- Vacuum out chamber and add 965 microliters of Creatine Buffer
- Hit “Go”
- Add tissue and cap. Wait for the line to stabilize.
- Mark “mito” and then add 10 microliters of malate and10 microliters of pyruvate and mark “mp”
- Adjust the cap so that the fluid is just at the well
- Wait two minutes from the mark of MP and add 5 microliters of ADP. Mark “adp”
- Wait 5 minutes from the mark of adp and then add 10 microliters of Oligo. Mark “oligo”
- Wait 10 minutes from the mark oligo and then stop the recording and save the data.
- Wash two times with dH2O and then add dH2O. Go to step one when the next tissues are ready.

Clean for Storage

- Vacuum out chambers and disconnect. Do everything like “cleaning” accept place electrodes in electrode box instead of adding a new membrane.
- Place stir rods in tube and place also in electrode box along with gaskets.
- Remove plungers from syringes and wash with dH2O unless it is the oligo syringe which needs to be washed with ET-OH. Run the plunger through with either dH2O or ET-OH depending on the syringe and then place separate in the “syringe box”.

Analyzing the RCR Data – Permeabilized Fibers

- Open the software and then open the File you want. –Click Rate- show rate cursors

- Click the red line button and adjust the start and end lines to be 30 sec apart.
- Move the lines to the ADP mark.
- Slide it slowly along the line until you find the highest number. This will be your state 3.
- For the state 4 you need to adjust your start and end line for 2 min apart then move them past the oligo mark. Search for the lowest value and this will be your state 4.
- The state 3 divided by the state 4 is the RCR.
- IN the event that the RCR is significantly lower or higher than normal (about 6-8) adjust the start and the end lines to be 1 min apart, find the middle value of the state 4 and use that. If it is still wrong find the middle between the middle and the lowest or the highest and then middle.

RCR = (state 3) / (state 4)

State 3 / 40 μL of mitochondria x [protein] = rate per unit mass

State 4 / 40 μL of mitochondria x [protein] = rate per unit mass

SOP for Mitochondria Oxygraph (Cleaning/Calibration/Measurements)

Cleaning

- Turn on surge protector to vacuum out the chambers and disconnect the line on the bottom left
- 1=4 2=2 3=3
- Unscrew the chambers by turning them to the right. Remove stir rod, black rings, and membrane.

- Wash with dH2O, get electrode polish and a Q-tip, polish the silver ring and electrode hard, wash with dH2O
- KCl made from each project 17.5g/100mL of dH2O. When a project is done, clean and put stir rod in tube and store in electrode box.
- Put 200 microliters of KCl on electrode before membrane
- To change membrane, use black tool from electrode box.
- Chem wipe. Don't touch, cut and put the rest back.
- Membrane, touch edge, flip and cut. Make sure inside is facing up.
- Use KCl 4 or 5 drops on silver with one drop on top.
- Paper first then plastic. Black O ring. Slowly place tool then quickly press.
- Replace large black O ring and replace the electrode on chamber.
- Replace wire anddH2O and stir bar.
- Turn on.

Calibration

- Check air pressure from rat room and convert to KPa
- Turn upside down to eliminate air
- Turn on surge protector to vacuum out the chambers. DON'T GO TO THE BOTTOM! Just touch stir rod!
- Add 2 ml Buffer Z (put tip on wall) replace in H2O bath.
- Open software. User, Oxigraph+, OK 3times, calibrate, liquid phase, cal, channel1, temp 37, pressure in KPa, OK 2times
- Watch for the rate. If you have rate click OK.

- Add sodium hydrosulfite wait for override to say OK. Click OK and save. Turn off stir rod.
- Wash with Et-OH 3X & then fill with dH2O
- If there is a problem, wash with Et-OH 3x & then use dH2O 3X and try again.

SOP for Mitochondrial Substrates

- 5mg of Oligomyacin (Sigma) into 5 mL of Ethanol
    - 4 mL in bottle of Oligomyacin
    - Add 1 mL and pour into 5 mL tube and vortex
- Aliquot into 10 .5 mL tubes
- Write "O" on tubes and freeze in the -20 freezer at the bottom (should last a long time!)

- Day before use, thaw buffer X and Z in the -4 glass fridge
- Make sure these three substrates are made. Usually once a week.
- Pyruvate 55mg/ 1 mL of Tris HCL Changed to 22mg -> Online protocol uses 44mg
- Malate 35.6mg/ 1 mL of Tris HCL
- ADP 21.4mg/ 1 mL Tris HCL
- 100mMol Tris HCL 1.576g in 100 mL

- 91mg/35 mL -> Creatine (made fresh daily) 13mg/5 mL buffer Z (975 microliters/chamber/tissue) Place in H2O bath for later use (e.g., 5 animals with 4 tissues each would need 20mL buffer Z and 52mg Creatine)

- Saponin (made fresh daily) .5mg/ 1mL of dH2O (Good for 2 animals) use 5m. Measure powder and then add dH2O to powder. Mix and then pour into tube. Place in white fridge.

- Need 4 2mL tubes per piece of tissue
- Add 1mL of buffer X to the first tube and then add 34 microliters directly before adding tissue for 30 min perm.
- Add 1.5mL of Z to the other three tubes for the 5 min washes.

Respiration Quick Reference

Make these Fresh Daily:

- Creatine 13mg/5mL
- Malate 22mg/ mL
- Pyruvate 35.6mg/ mL
- ADP 21.4mg/ mL
- Saponin 0.5mg/ mL

Order of Substrates:

- Add mito & lid
- Add 10 µL Malate & Pyruvate. Wait 2 min
- Add 5 µL ADP. Wait 5 min
- Add 10 µL Oligo. Wait 10 min

(1mL) Buffer X (initial pH 7.3) – Used for separating fibers and for permibilizing

Amount Need for (RCR + ROS) per animals/day

Buffer X 5 mL for separation 1.5 mL / fiber – usually 4 = 6 mL =11

Buffer Z 60 mL 1.5 mL x 3 wash x 4 fibers = 18mL

Calibration = 12mL /day

Respiration = 4 mL/animal

Amplex Red = 1mL/fiber

4 animals/day

Reagent	MW(g/mol)	Conc (mM)	200mL (g)	500mL (g)	1L (g)	Product #
K-MES	233.33	60	2.8000	6.9999	13.9998	Sigma M0895
KCl	74.56	35	0.5219	1.3048	2.6096	Sigma P4504
K2EGTA	100mM	7.23	5.54mL	13.86mL	27.7mL	
CaK2EGTA	200mM	2.77	14.45mL	36.15mL	72.3mL	
Imidazole	68.08	20	0.2723	0.6808	1.3616	Sigma 10125
Dithiothreitol (DDT)	154.1	0.5	0.0154	0.0385	0.0771	Santa Cruz sc-29089
Taurine	125.15	20	0.5006	1.2515	2.5030	Sigma T8691

ATP	551.1	5.7	0.6283	1.5706	3.1413	Sigma A2383 (order)
PCr	327.2	15	0.9815	2.4540	4.9080	Roche (order) 10621714001
MgCl 6H2O	203.3	3mM		1.4018		
pH 7.1, 295 mosmol/kg H2O initial pH 3.86 pH 3.12 (w.o KOH) pH 5.58 (w/KOH)						

K2EGTA=7.608g EGTA + 2.3g KOH in 200 mL dH2O – pH 7.4 with KOH – pH ??????

CaK2EGTA=7.608g EGTA (order) +2.002g CaCO3 in 200mL dH2O at 80° C + then add 2.3g KOH in the 200mL. pH 7.4

EGTA 0.3804 in 10mL KOH 0.115 in 10mL

CaCO3 0.1001 in 10mL

For per. RCR

Initial pH 7.5 (5/2)

(1.5 mL) Buffer Z – used for washes, respiration, base for Amplex Red

Reagent	MW (g/mol)	Conc (mM)	200mL (g)	500mL (g)	1 L (g)	Product #	1.5L
K-MES	233.33	110	2.1333	12.8332	25.6663	Sigma M0895	38.4996
KCl	74.56	35	0.5219	1.3048	26096	Sigma P4504	3.9144
EGTA	280.35	1	0.0761	0.1902	0.3804	Sigma E4378	0.5706
K2HPO4	174.18	5	0.1742	0.4355	0.8709	Fisher P380	1.3065
MgCl2 * 6 H2O	203.3	5	0.2085	0.50825	1.0165	Sigma M2670	1.5248
Glutamate	169.11	0.005				Sigma G8415 (50 µL)	75 µL
Malate	134.09	0.002				Sigma M6773 (200 µL)	300 µL
BSA		0.05%	0.1	0.25	0.5	Sigma A6003	0.75

pH 7.1, 295 mosmol/kg H2O (pH @ room temp per powers lab history)

Sigma G5889 – Glutamate 0.073g/5mL of dH2O (=0.1M x 147.13g (MW) x 0.005L) 1M stock -> 15 mL = 2.5367g Glutamate

- ➔ 0.01mL (10 µL)/200mL of Buffer Z (=10 µL/20mL of Buffer Z) – boiling when putting glutamate it should be warm or hot to get in solution pH 7.4

Sigma M7397 – Malate 0.089g/5mL of dH2O (=0.1M x 178.05g(MW) x 0.005L)

- ➔ 0.04mL (40 µL)/200mL of Buffer Z (=4 µL/20mL of Buffer Z) 1M stock -> 15mL = 2.0114g Malate – pH 7.4

Glutamate 0.5 µL in 10 mL Malate 2 µL in 10mL

Freeze Glutammate & Malate @ -20°C – Aliquot in small vials

500 mL = 600 µL 114.12 mg ECTA

Preparation of 10uM Amplex Ultra Red stock 1 (regular stock for state 4 H202 assay):

Goal: H202 assay buffer stock 1: Buffer Z <w. 0.5 mg/ml BSA) +1mM EGTA + 25µM blebbstatin + 10µM Amplex Ultra Red + 25U

1. Make 5mM Amplex Ultra Red (AUR). Add 666.6ul of DMSO to 1mg Amplex Ultra Red (Invitrogen # A36006), vortex. 5 vials 600µL in 300µL
2. Prepare 10uM Amplex Red. Add 160.6mL Buffer Z (0.5mg/ml BSA) + 325µL 5mM AUR + (3.25µL 0.5M EGTA) already in buffer Z + 406µL 10mM Bleb
3. Prepare in black tubes. 1.05ml Aliquot in the dark. Store in -80.

Typically only run state 4

Preparation of 10uM Amplex Ultra Red stock 2 (for state 3 H202 assay with ADP clamp):

Goal: H202 assay buffer stock 2: Buffer Z (w/ 0.5mg/ml BSA) + 20mM Cr + 1mM EGTA + 25µM blebbstatin + 10µM Amplex Ultra Red + 25U/ml CuZn-SOD + 5mM DOG + 2U/ml HK

1. Prepare 10uM AUR stock. Add 80.3 mL Buffer Z (0.5mg/ml BSA) + 0.24237g of creatine monohydrate + 0.0667mg 2-DOG + 406.25µL of 400U/ml HK + 162.5µL 5mM AUR + 162.5µL 0.5M EGTA + 406.25µL 5000 IU/ml SOD + 203µL 10mM Bleb
2. Prepare in black tubes. 1.05ml Aliquot in the dark. Store in -80.

Preparation of Amplex Red (used for PDN 58)

1. Remove 1 vial from freezer. As of 11/09, one vial contains 154ug of Amplex Red. DOUBLE CHECK THE CONTENT LISTING ON THE LABEL AS THESE AMOUNTS CAN BE CHANGED BY THE MANUFACTURER!
2. Make 10mM Stock. The MW of Amplex Red is 257.25g/mol. Dissolve in DMSO. This requires 59.864 ul of DMSO, or simply 59.9 ul, added directly to the vial. Vortex well but not too much as vigorous vortexing can denature certain compounds.

3. Dilute stock to 10uM and store in separate aliquots. This is a 1000 fold dilution, therefore the final volume will be 59.864 ml. Dilute using 0.5mg/ml BSA in Buffer Z (double check that the pH of Z is at 7.40). DO NOT USE PURE WATER!

   TIP: The vial will hold approximately 700 ul volume. Add ~500 ul of Buffer Z to vial, pipette up and down to ensure proper mixing, and then transfer to small beaker or 50 ml plastic tube. Add another 500 ul and repeat. Do this at least 4 times to ensure that ALL Amplex red has been removed from vial. DO NOT SIMPLY PIPETTE OUT AMPLEX RED DISSOLVED IN DMSO AS THE SMALLEST DROP MISSED CAN AFFECT YOUR FINAL CONCENTRATION – especially considering the 1000 fold dilution!

4. Add 120 ul 0.5M EGTA final concentration.
5. Bring final volume up to 59.864 ml, or whatever is appropriate for the mass in your original vial.

   TIP: If using a 50 ml plastic tube, bring final volume up to 25-30 ml (RECORD WHAT FINAL VOLUME IS!) and add the remaining Z to the 2nd tube, so long as the total volume in both tubes is 59.864 including the original 59.864 ul of DMSO/AMPLEX RED. Then pour some of the solution from the 1st tube into the 2nd and then back and forth. Do so several times to get complete mixing. Otherwise just use a small beaker!

6. Aliquot in 925 ul volumes into black 1.5 ml Eppendorf tubes. This volume permits 3 experiments of 300ul each, with a bit of extra to ease pipetting for the 3rd experiment. You may have to spin it down. In general, do not aliquot any more than you need – this saves money in the long run.

Succinate (sodium succinate dibasic hexahydrate)

Make stock solution of 0.5 m succinate = 2.026g in 15 mL of Buffer Z. Add 20ul to ROS chamber for final concentration of 10mM.

HRP buffer

Sigma P8375 – 1KU

To make 300u/mL, dissolve contents of both in 3.33 mL of Buffer Z.

You will be adding 3.33uL into the ROS chamber per sample so aliquot this into small amounts 30-50uL or smaller.

Protocol 5 – Max Succinate				
Substrate	Event Code	STOCK	Titration Volume (ul)	Final Concentration in Chamber
AmplexRed Assay Buffer		10mM	1000	25uM
HRP		300U/ml	3.33	1U/ml
ADD FIBER AND GET BACKGROUND FOR 8 MINUTES				
Succinate	S	0.5M	20	10mM
Auranofin	AF	1m M	1	1uM

Reagent	#	Supplier
Amplex Red	A36006	Thermofisher
HRP	P8375	Sigma
Auranofin	A6733	Sigma

1 KU = 1000

300u/m

H2O2 Standard Curve Protocol

1. Make H2O2 standards via serial dilution:

Make H2O2 stock by serial dilution			
Vial	Vol. of ddH2O added in uL	3% (v/v) Vol. of [H2O2] added in uL	[H2O2] stock. uM
A	4310	100	20000
B	3980	20 uL of A	100
C	3200	800 ul of B	20
D	2000	2000 ul of C	10

E	2000	2000 ul of D	5

2. Perform H2O2 titration in buffers containing all substrates/inhibitors

[H2O2] stock uM	[H2O2] stock pmol/ul	Vol. of [H2O2] added in uL	Total pmol of H2O2 added (ul)
E 5	5	3	15
E 5	5	3	30
D 10	10	3	60
D 10	10	4	100
C 20	20	3	160
C 20	20	5	260
C 20	20	8	420

583uM

Stir Bar 6 Setting for Ocean Optics Device

Setup – Integration Time – 500mSec

Strip Chart – Update every 10 scans

Integrate 583 -> 587 581-587

Make sure Cuvette is facing correct way… Slotted side facing LED.

Strip Chart Wiz – Update every scan integrate 581-587

Stir speed – 6/10

*In order to lengthen time of acquisition on strip chart, go to "schematic Window" tab, and double-click "Trend_#" icon. Default Buffer size = 1,000 (about 10 minutes). Can increase this value to increase acquisition duration.